STRUCTURE AND FUNCTION OF ER CLASS 1 ALPHA MANNOSIDASE

by

KHANITA KARAVEG

(Under the Direction of Kelley W. Moremem)

ABSTRACT

Mammalian class 1 α1,2-mannosidases play critical roles in the maturation of Asn-linked glycoproteins in the endoplasmic reticulum (ER) and Golgi complex as well as influencing the timing and recognition for disposal of terminally misfolded glycoproteins during ER-associated degradation. Despite several recent reports of X-ray structures of class 1 mannosidases, the proposed catalytic mechanism has not yet been experimentally investigated. As a potential target for therapeutic intervention in ER storage disorders, human ER mannosidase I was chosen to investigate the impacts of single and double mutants of three putative catalytic and two glycone binding residues. The kinetics of binding for a D463N mutant to $Man_9GlcNAc_2$ was analyzed by surface plasmon resonance indicating that this residue is mainly responsible for substrate binding, but not catalysis. The optimum pH and pK_a shift observed in the E330Q/A mutants strongly indicate that E330 is the general acid catalyst. A proton inventory study gave a DIE of 1.8±0.2, but did not resolve the involvement of a second water residue previously proposed from X-ray structure studies. The presumed general base catalyst is E599 based on X-ray structure determination of a co-complex between an α1,2-mannobiose thiodisaccharide substrate analog and human ER mannosidase I resolved to 1.4 Å. The uncleaved thiodisaccharide co-complex bridges the enzyme +1 and -1 subsites and reveals a unique $^{3}S_{1}$ sugar ring conformation for the -1 subsite residue. This information, in combination with prior X-ray structure data of human ER mannosidase I in a co-complex with the glycone mimic, 1-deoxymannojirimycin, suggests that the class 1 mannosidases employ a novel $^{3}H_{4}$ sugar conformation in the -1 subsite at the catalytic transition state. Potential roles for additional residues adjacent to the catalytic carboxyl side chains are also proposed to influence the ionization state during acid/base catalysis.

INDEX WORDS: α-mannosidase, glycosylhydrolase, conformation itinerary,

thiodisaccharide, crystallography, mechanism.

STRUCTURE AND FUNCTION OF ER CLASS 1 ALPHA-MANNOSIDASE

by

KHANITA KARAVEG

B.S., Chulalongkorn University, Thailand, 1995

M.S. University of Louisville, 1997

A Dissertation Submitted to the Graduate Faculty of The University of Georgia in Partial Fulfillment of the Requirements for the Degree

DOCTOR OF PHILOSOPHY

ATHENS, GEORGIA

2005

STRUCTURE AND FUNCTION OF ER CLASS 1 ALPHA-MANNOSIDASE

by

KHANITA KARAVEG

Major Professor:	Kelley W. Moremen
Committee:	Michael Pierce
	Bi-Cheng Wang
	Marcus Fechheimer
	William N. Lanzilotta

Electronic Version Approved:

Maureen Grasso
Dean of the Graduate School
The University of Georgia
May, 2005

DEDICATION

To Mrs. Thanom Karaveg, my mother and Mr. Jinda Karaveg, my father, who gave me the talent and allowed me to choose my own path and have been very supportive. To my sisters, Ms. Sopid Karaveg and Mrs. Mayuree Soitong, who have been so understanding and cheerful from afar for many years. To my niece and nephew who always look up to her/his aunt.

Most of all, I wishfully grant my achievement to my beloved daughter Cheyenne R. Webb.

ACKNOWLEDGEMENTS

Firstly, I would like to express my gratitude and appreciation to my major professor, Dr. Kelley W. Moremen for his support, guidance, encouragement, patience and understanding, especially for giving me the opportunity and believing in my ability during the difficult time and through out. I am also truly grateful for his kind effort to ensure the quality of my dissertation during writing and revision process.

Secondly, I would like to thank my committee, Dr. Michael Pierce, Dr. Bi-Cheng Wang, Dr. Marcus Fechheimer, and Dr. William N. Lanzilotta for their great insightful direction and much enthusiasm.

Thirdly, I would like to thank many colleagues who have contributed their time and effort directly and indirectly to the work presented in this dissertation. Their names and their affiliates are listed as following: Dr. Zhi-Jie Liu, Dr. Wolfram Tempel, Dr. Lirong Chen and Ms Doowon Lee, all are the members of Dr.Wang's crystallography lab; Dr. Aloysius Siriwardena, Department of Chemistry and Biochemistry,University of Mississippi; Dr. Kumar Kolli and Dr. John Glushka, members of complex carbohydrate research center, University of Georgia, and Dr. Eric Roush, Research scientist, BIAcore AB, Inc.

Fourthly, I would also like to thank all the members of the Moremen lab, especially, Ms. Trisha Sheahan, Dr. Alison V. Narin, Dr. Lu Meng, and Dr. Steve Mast for their kind friendship and assistance. My acknowledgement also extends to the former members of the Moremen lab, Dr. Daniel S. Gonzalez and Dr. Anita Lal.

Lastly, I would like to thank Dr. Srinivas Kidambi for his personal assistance for the past few years, especially for providing me the security and stability with love and care.

TABLE OF CONTENTS

Page

LIST OF TABLES

Page

LIST OF FIGURES

Page

CHAPTER 1

INTRODUCTION

1.1 Glycoside hydrolase

Glycosyl hydrolases (GH) (EC 3.2.1.-) are a group of enzymes which hydrolyze the *O*-glycosidic bond between two or more carbohydrates or between a carbohydrate and a non-carbohydrate moiety. To date, more than 12,600 amino acid sequences have been identified and classified as glycosidases [1]. A classification of glycosyl hydrolases into families based on the sequence similarities, substrate specificity, mechanism of action, mode of action, and 3D structure results in 97 families, which are continuously updated and listed at the Carbohydrate-Active Enzymes (CAZy) server (http://afmb.cnrs-mrs.fr/CAZY). This section will be a brief introduction to Family 47 glycosylhydrolases. A more complete description including figures will follow this section

Family 47 glycohydrolases (GH47) are also known as class 1 α1,2-mannosidase and can be subcategorized into four main subclasses; 1) ER class 1 α1,2-mannosidase (ERManI); 2) Golgi class 1 α1,2-mannosidase A/B/C (GManIA/IB/IC); 3) the fungal secreted enzymes and; 4) ER degradation enhancing α-mannosidase-like (EDEM) proteins [2]. The members of ERManI and GManIA/IB/IC subclasses are key enzymes involved in N-linked glycan biosynthesis in both the endoplasmic reticulum (ER) and Golgi complex (Figure 1) [2-4]. The enzymes of the GH47 hydrolyze specific α1,2-mannoside linkages on N-linked oligomannose structures by an inverting mechanism to produce specific trimmed N-glycan isomer structures. The members of ERManI subclass prefer to hydrolyze a single α1,2-mannose of the middle branch of the $Man_9GlcNAc_2$ precursor structure to generate $Man_8GlcNAc_2$ isomer B while the Golgi enzymes

(GManIA/IB/IC) prefer to hydrolyze α1,2-mannoside linkages on the alternate terminal branches of $Man_9GlcNAc_2$ producing mainly $Man_8GlcNAc_2$ isomers A or C. The members of the EDEM subclass are catalytically inactive. The members of EDEM and ERManI subclasses play a major role in glycoprotein folding quality control and targeting the misfolded glycoprotein for degradation via the ER associated degradation (ERAD) pathway [5, 6]. The presence of the $Man_8GlcNAc_2$ isomer B glycan structure on misfolded glycoproteins is important for the recognition of those glycoproteins by EDEM subfamily members prior to targeting these molecules for disposal. The rate of catalytic removal of the specific central branch α1,2-mannose residue on the N-linked oligomannose structures is controlled by the action of ERManI [5, 6]. Thus $Man_8GlcNAc_2$ isomer B structure is not only an intermediate product of the N-linked glycan maturation process, but also serves as a molecular marker for targeting the misfolded glycoproteins for degradation.

The action of ERManI not only results in the processing of high mannose N-glycans, but it also determines the timing and fate of improperly folded glycoproteins in the lumen of the ER. The functional relationship between the members of both ERManI and EDEM subclasses of GH47 proteins in targeting the misfolded glycoproteins for ER disposal are of interest since they could potentially serve as targets for therapeutic intervention for several ER storage disorders such as such as α1-antitrypsin deficiency leading to emphysema [7, 8] and mutant forms of cystic fibrosis transmembrane conductance regulator (CFTR) leading to cystic fibrosis [9].

In order to understand the mechanism for catalysis and substrate recognition of class 1 α1,2-mannosidases, several class 1 α1,2-mannosidase homologues have been cloned and expressed in the Moremen laboratory, including human (*Homo sapiens*) ERManI (*Hs*ERManI) [10], murine (*Mus musculus*) Golgi Mannosidase IA (*Mm*GManIA) [11], rabbit (*Oryctolagus*

cuniculus) Golgi mannosidase IB (*Oc*GManIB) [11] and the human (*Homo sapiens*) and yeast (*Saccharomyces cerevisiae*) EDEM homologues [12, 13]. *Hs*ERManI is the main subject of this dissertation, which includes the various methods and strategies used to investigate the structural and biological aspects of enzyme function as well as mechanistic details of catalysis and substrate recognition.

The body of this dissertation work can be broken down into 4 stages (Figure 1). Stage I involves cloning, expression, characterization and purification of *Hs*ERManI. Stage II describes the structural analysis of class 1 mannosidase members, two of which were done in collaborations with the Howell [14] and the Wang [15] laboratories. As a result of the structural studies, stage II led to the proposal of a catalytic mechanism for class 1 α1,2-mannosidases that is unconventional in regard to the standard acid/base glycosidase mechanism including 1) the utilization of a second water residue for indirect, through-water protonation of the glycosidic bond, 2) ambiguous assignment of the amino acids involved catalysis, 3) a unique coordination of a Ca^{2+} ion in the active site suggesting the involvement of Ca^{2+} in catalysis and/or substrate binding, 4) the co-complex structure of *Hs*ERManI and class 1 mannosidase inhibitors, 1-deoxymannojirimycin (dMNJ) or kifunensine (Kif) suggesting that the transition state involves the formation of an energetically unfavorable $^{1}C_{4}$ sugar ring conformation, and 5) the X-ray structures of five members of class 1 mannosidase that are similar in protein fold and active site geometry suggesting that they utilize the same set of catalytic residues and mechanism, regardless of their substrate/product specificity. X-ray structural analysis in stage III allowed the further investigation of the enzyme catalytic mechanism. The goal of stage III was to address the functions and identify the roles of specific amino acid residues in active site. This stage involved the mutagenesis of the potential catalysis-related amino acids and the detailed analyses of enzyme kinetics and substrate binding by surface plasmon resonance (SPR) and comparison with the wild

type enzyme. Stage IV involved the X-ray structural analysis of a co-complex of *Hs*ERManI and the nonhydrolyzable thiodisaccharide substrate analogue of Manα1,2 Man. The results of stage III and stage IV provided the experimental data as well as the structural evidence to answer the questions which the previous structural analysis was unable to provide. As the results of this dissertation work 1) the general acid and general base catalysts were unambiguously assigned to E330 and E599, respectively, 2) the roles of D463, F659, and Ca^{2+} were addressed, and 3) a novel $^{3}H_{4}$ sugar conformation was identified as the transition state intermediate for class 1 α1,2-mannosidases. However, the investigation on solvent deuterium isotope effects was unable to address the involvement of water in the protonation of the glycosidic oxygen. The function of T688 is also remained unclear due to an unanticipated set of data indicating that this residue contributes to both substrate binding and catalysis. Besides addressing the function of amino acid residues in the active site and catalytic mechanism of class 1 α1,2-mannosidases, this dissertation also demonstrated the use of specific mutation, E330Q of *Hs*ERManI, as tool for mapping the interactions between oligosaccharide substrates and the recombinant mutant enzyme by SPR. This approach was used to calculate the contribution of mannose residues in substrate binding and can also be used to map the contributions of individual amino acids in the glycan binding cleft both in the *Hs*ERManI, as well as other GH47 proteins.

1.2 The N-linked oligosaccharide biosynthesis and maturation

The majority of proteins synthesized in the ER are glycoproteins. About 90% of these are predicted to carry N-linked glycans with an average of 1.9 N-linked glycans per polypeptide chain [16]. The core oligosaccharide is synthesized independently as a lipid-linked oligosaccharide precursor, $Glc_3Man_9GlcNAc_2$-P-P-dolichol [17, 18], by the stepwise addition of monosaccharides to dolichol pyrophosphate, a polyisoprenoid lipid carrier that anchors the

oligosaccharide to the membrane. After the polypeptide is synthesized and translocated into the ER lumen, the core oligosaccharide is co-translationally transferred onto a newly synthesized polypeptide to form N-linked glycoproteins by the action of the oligosaccharyl transferase (OST) [19]. The OST is a multimeric complex enzyme [20], which efficiently catalyzes the formation of glycosidic bond between the transferred oligosaccharide, $Glc_3Man_9GlcNAc_2$, and the amide nitrogen atom of the asparagine residues within the Asn-X-Ser/Thr sequon, where X can be any amino acid except proline. Immediately after $Glc_3Man_9GlcNAc_2$ is transferred to the nascent polypeptide, the oligosaccharide undergoes maturation and modification which is takes place in the ER and Golgi-apparatus (Figure 2). The enzymes involved in N-linked glycan maturation and its action in relation to the glycan structure are shown in Figure 3. The oligosaccharide structures and isomers generated during the maturation process were summarized in Table 1.

In the ER, N-linked oligosaccharide maturation involves the removal of a terminal α1,2-glucose by the action of α-glucosidase I (GDI) and two inner α1,3-glucose residues by α-glucosidase II (GDII) (Figures 2 and 3). The presence of the inner most glucose residue on the oligosaccharide (Figure 4) is required for calnexin (CNX)/calreticulin (CRT) recognition and retention of the unfolded glycoprotein [21]. The inner-most glucose residue can be reglucosylated to the original linkage by the action of (UDP)-glucose:glycoprotein glucosyltransferase (GT). Reglucosylation of the glycan allows the glycoprotein to reenter the CNX/CRT folding cycle and obtain a proper folding prior to anteriograde transport to the Golgi complex.

The removal of glucose can also be accomplished by the action of endo α-mannosidase. The endo α-mannosidase catalyzes the cleavage of an internal Manα1,2 Man glycosidic linkage in $Glc_{1\text{-}3}Man_9GlcNAc_2$ producing $Man_8GlcNAc_2$ isomer A [22] (Figures 2 and 3). The enzyme is also capable of removal the same linkage on oligosaccharides with truncated mannose branches, $Glc_1Man_{8\text{-}4}GlcNAc_2$. The endo α-mannosidase does not respond to α-glucosidase or α-

mannosidase inhibitors [23]. The enzyme does not share homology with α-mannosidases and no other related proteins have been identified [24]. Beside the endo α-mannosidase, the mannose trimming is catalyzed by various branch-specific exo-α-mannosidases which are either ER or Golgi resident enzymes.

In *S. cerevisiae*, the mannose trimming step is initiated in the ER by the action an exo-α1,2-mannosidase I termed ERManI (*Sc*ERManI) which removes a single terminal mannose residue of the $Man_9GlcNAc_2$ to produce a specific $Man_8GlcNAc_2$ isomer B (Figures 2 and 3). This is the last oligosaccharide trimming step in yeast prior to transport from leaving the ER to the Golgi complex where mannan structures are synthesized by the action of several mannosyltransferases [25].

In mammalian systems, the mannose trimming can be achieved by one of the following mannosidase activity: 1) endo α-mannosidase which cleaves $Glc_{3-1}Man_9GlcNAc_2$ to produce $Man_8GlcNAc_2$ isomer A [22]; 2) ER α1,2-mannosidase I (ERManI), a homolog of *Sc*ERManI, which hydrolyzes $Man_9GlcNAc_2$ to produce $Man_8GlcNAc_2$ isomer B ; 3) ER mannosidase II (ERManII) which cleaves $Man_9GlcNAc_2$ to produce $Man_8GlcNAc_2$ isomer C and smaller oligosaccharides [26] (Figures 2 and 3).

In contrast to endo α-mannosidase and ERManII, the action of ERManI serves not only as a step for mannose trimming, but also a step which allows the presentation of $Man_8GlcNAc_2$ isomer B glycan structure on the glycoprotein to the ER-associated degradation (ERAD) machinery (Figure 4). Presenting this glycan structure on proper folded glycoproteins is presumed to have no significant impact other than processing of the glycan. In contrast, the presence of the $Man_8GlcNAc_2$ isomer B glycan structure on an unfolded or misfolded glycoprotein allows the glycoprotein to be recognized by members of the EDEM subfamily [27, 28] which target the glycoprotein for ER disposal via the ERAD pathway [5, 6].

Unlike ERManI, ERManII is a class 2 α-mannosidase (glycosyl hydrolase family 38) and is not inhibited by Kif, an inhibitor of class 1 α-mannosidases. ERManII is related to a cytosolic α-mannosidase involved in oligosaccharide catabolism. Besides generating the $Man_8GlcNAc_2$ isomer C, ERManII can also trim other mannose residues producing $Man_{7\text{-}6}GlcNAc_2$ oligosaccharides. Reduction in the number of mannose residues on the oligosaccharide affects the efficiency of the GT in reglucosylation [29, 30]. Inefficiency in reglucosylation of the N-linked glycan ultimately results in an accelerated dissociation of the glycoprotein from the CNX/CRT cycle, similar to the action of endo α-mannosidase.

In higher eukaryotes, the mannose trimming of N-linked oligosaccharide is continued in the Golgi complex (Figure 2). The remaining α1,2-mannosyl residues on the oligosaccharide are removed by the action of Golgi α1,2 mannosidases (GMan) namely IA, IB and IC to generate a $Man_5GlcNAc_2$ structure. These enzymes are distinguished by the $Man_8GlcNAc_2$ isomer product intermediates generated using $Man_9GlcNAc_2$ as substrate and the order of specific α1,2-mannosyl residues being removed (Figure 5). *In vitro,* all of these enzymes catalyze the less efficient removal of the middle branch α1,2-mannosyl residue when is presented with $Man_9GlcNAc_2$ as a substrate. However, *in vivo* these enzymes act after ERManI and therefore cleave a $Man_8GlcNAc_2$ isomer B structure to $Man_5GlcNAc_2$. The $Man_5GlcNAc_2$ is then modified by addition of β1,4-GlcNAc residue onto the terminal α1,3-mannosyl residue on branch A of the glycan. This step is catalyzed by GlcNAc transferase I and is a committing step in glycan processing into complex and hybrid structures (Figure 2).

The removal of the α1,3- and α1,6-mannosyl residues on the α1,6-mannosyl branch of N-linked glycans is catalyzed by Golgi mannosidase II (GManII) following GlcNAc transferase I action to produce the $GlcNAcMan_3GlcNAc_2$ core of complex type oligosaccharides. This is the last mannose trimming step in N-linked glycan biosynthesis. Further extension of the

$GlcNAcMan_3GlcNAc_2$ core by glycosyltransferases is continued in the Golgi complex (Figure 2). The process requires the action several Golgi glycosyltransferases to catalyze the maturation, branching and extension of glycan structures into the diverse array of complex glycans found on cell surface and secreted glycoproteins.

1.3 ER quality control, ERAD and diseases

Upon the translocation of the nascent polypeptide into the ER lumen, the polypeptide can be subjected to various post-translational modifications. Beside signal sequence cleavage, membrane insertion, disulfide bond formation and oligomerization, the polypeptide can also be subjected to N-linked glycosylation. The details of N-linked glycosylation and maturation processes were described in previous section. The purposes of post-translational modifications on the polypeptide are to assist in the proper folding of the polypeptide and the formation of a stable and functional proteins. In the case of N-linked glycosylation, not only are the N-linked complex glycan structures important for the folding into biologically functional polypeptides, but they also promote protein solubility, stabilization, and also play significant roles in ER quality control by serving as molecular markers that allow glycoproteins to interact with various chaperons and lectins in the ER [21].

1.3.1 ER quality control process: Unlike *S. cerevisiae*, whose quality control of glycoprotein biosynthesis is not critical [31], in mammalian systems, the folding of glycoproteins being synthesized and modified in the ER is periodically checked by a process termed "quality control" [32, 33]. The ER quality control process involves three important events: 1) folding and retention of incompletely folded glycoproteins via the CNX/CRT cycle and deglucosylation/reglucosylation by the glycosidase II/GT activities, 2) the action of ERManI to

produce the specific N-linked glycan structure ($Man_8GlcNAc_2$ isomer B) by removal of a single α1,2 mannosyl residue of the middle branch of the N-linked $Man_9GlcNAc_2$ structure, and 3) recognition and targeting of the unfolded glycoprotein for degradation by the molecular machinery of the ERAD pathway, such as proteins of the EDEM subfamily, ER associated lectins, the SEC61 translocon complex, and proteosome complex components among others (Figures 6 and 7).

The folding and retention of the incompletely folded glycoproteins takes place early in the ER (Figure 6). The presence of monoglucosylated N-linked oligosaccharides ($GlcMan_{7-9}GlcNAc_2$) and the presence of hydrophobic peptide patches on the glycoprotein are the molecular markers for this process. The monoglucosylated glycan structures associated with glycoproteins are the ligands for CNX and CRT, the homologous ER luminal (CNX) and membrane-associated (CRT) lectin chaperones [34, 35]. There are also several lines of evidence suggesting that the CNX/CRT interact with the nascent polypeptides associated with the glycoprotein [33, 34]. As a result, the interaction between CNX/CRT and N-linked glycoprotein ligand facilitates the folding process of the glycoprotein through protein-protein interactions and through the action of other recruited proteins such as ERp57 [33, 36].

Upon the dissociation of the glycoprotein from the CNX or CRT complex, the monoglucosylated N-linked glycan is exposed to the deglucosylation catalyzed by the action of glucosidase II (GDII), a membrane anchored enzyme, which removes the last α1,3 glucosyl residue. The lack of a terminal glucose residue on the N-linked glycan releases the correctly folded glycoprotein from the CNX/CRT cycle and allows the glycoproteins to be packaged into anteriograde transport vesicles by association with mannose-specific lectins such as ERGIC-53 and transported to the ER-Golgi intermediate compartment [37] or by directly fusion of the ER and Golgi vesicular-tubular clusters (VTCs) [38, 39].

In the situation where the glycoprotein has not yet reached a stable folding state, the dissociation of the glycoprotein ligand from CNX or CRT and subsequent deglycosylation by GDII exposes the N-linked glycan for reglucosylation by the action of UDP-Glc:glycoprotein glucosyltransferase (GT). GT is a soluble protein found in the lumen of the ER. It recognizes the exposed hydrophobic patches of the unfolded glycoprotein and catalyzes the addition of α1,3-glucosyl residue to N-linked $Man_9GlcNAc_2$ structures at the same mannose residue (M8) from which a glucose was removed by the GDII. The action of GT allows the unfold glycoprotein to reacquire the terminal glucosylated N-linked structure and re-enter the CNX/CRT cycle in an attempt to complete the folding process.

Incompletely folded glycoproteins may be subjected to several cycles of CNX/CRT binding, deglucosylation, and reglucosylation until the glycoprotein obtains complete folding. During the association/dissociation of the glycoprotein ligand with CNX or CRT the glycoprotein folding intermediate is exposed not only to GDII, but also the membrane bound processing hydrolases such as ERManI, ERManII, and endo α-mannosidase. After several rounds of release and reentry into the CNX/CRT cycle, the N-linked glycans of the unfolded glycoproteins are eventually modified by these latter enzymes and result in N-linked glycan structures that are no longer the preferred substrates for reglucosylation by GT. In general, this event can indirectly improve the rate of glycoprotein production by releasing CNX/CRT from futile attempts at re-folding terminally misfolded proteins and making them available for assisting in the folding of new glycoproteins. On the other hand, it may directly decrease the net production of misfolded glycoprotein by preventing the continued engaging of the chaperone machinery before folding is complete. Therefore, the rate at which the N-linked glycans associate with nascent unfolded glycoproteins are subjected to mannosidase activity will determine the rate and net efficiency of biosynthesis and transport of correctly folded forms of a given glycoprotein from the ER.

Unlike ERManII and endo α-mannosidase enzymes with unclear, contributions to the disposal of the unfolded glycoproteins, the action of ERManI is particularly important in quality control and disposal of incorrectly folded glycoproteins preventing them from accumulating in the ER lumen. In the quality control process, ERManI facilitates the release of glycoproteins from the folding and retention cycle by catalyzing the removal of the middle branch α1,2-mannosyl residue from $Glc_{0-1}Man_9GlcNAc_2$ to produce $Glc_1Man_8GlcNAc_2$ or $Man_8GlcNAc_2$ isomer B glycans. Several lines of evidences suggest that the Man8B structure is a presumed ligand for EDEM proteins in the targeting misfolded glycoproteins carrying this glycan for degradation [5, 6]. In mammalian cell lines, treatment of 1-deoxymannojirimycin (dMNJ), a class 1 α-mannosidase inhibitor, results in the accumulation of incorrectly folded T cell receptor CD3-δ subunit [40], pro/pre α factor [34], tyrosinase [41], α_2-plasmin inhibitor [42] and α1-antitrypsin (α1-AT) [43, 44]. In *S. cerevisiae* strains whose α-glucosidase or ERManI genes were disrupted, a mutant misfolded form of carboxypeptidase Y (CPY^*), a common reporter glycoprotein used to follow the ERAD process, was found to accumulate in the ER [45, 46]. These results indicate that the formation of the Man_8B structure by ERManI is essential for glycoprotein degradation.

The relationship between ERManI and EDEM in targeting misfolded glycoproteins for degradation was demonstrated by the overexpression of EDEM1 and/or ERManI in the mammalian cell lines co-expressing α1-AT variants. The results demonstrated that co-expression of ERManI and EDEM1 in HEK293 cells accelerated on the degradation of α1-$AT_{Hong\ Kong}$ (α1-AT_{NHK}) variant compared to the expression of ERManI or EDEM1 alone [47]. Moreover, the co-immunoprecipitation and time course studies showed that the EDEM1 directly interacts with misfolded α1-AT_{NHK} and accelarates its degradation via the ERAD [48]. Although, the direct interaction of EDEM with a Man8B structure has not yet been reported, the conclusion that

targeting misfolded of glycoproteins for disposal via ERAD requires ERManI activity and EDEM function are conclusive [5, 6].

1.3.2 ERAD: The term ERAD (ER-associated degradation) refers to the mechanism of removal of terminally misfolded proteins from the ER. ERAD is comprised of three events: substrate selection, transport of the substrate to the cytoplasm, and proteasome-mediated proteolysis (Figure 7).

The substrate selection event is a part of the ER quality control process that is responsible for distinguishing abnormally folded proteins from the pool of correctly folded proteins (Figure 6). There are two models involving the action of ER lumenal chaperones in recognizing the ERAD substrates [49]. The first model utilizes the ordinary chaperones such as BiP [50], an ER lumenal Hsp70 chaperone, which recognizes the solvent exposed hydrophobic amino acid patches in unfolded proteins and facilitates the folding of the polypeptide. Binding to the chaperones prevents the misfolded protein from aggregation and also facilitates the retro-translocation of the misfolded protein through an ER membrane chanel. The retro-translocation is assisted by co-chaperones such as Scj1p/Jem1p and Sls1p [50]. The second model utilizes a selection process specialized for N-linked glycoproteins. The misfolded glycoproteins which are recognized as the ERAD substrates present the specific glycan structures of $GlcMan_8GlcNAc_2$ or $Man_8GlcNAc_2$ isomer B as a result of ERManI activity. The incorrectly folded glycoproteins carrying the $GlcMan_8GlcNAc_2$ structure can re-enter the CNX/CRT cycle in an attempt to reach a properly folded state. Inefficient removal of terminal glucose of $GlcMan_8GlcNAc_2$ by glucosidase II results in prolonged association of the unfolded glycoprotein with the CNX or CRT and triggers the ERAD process. The incorrectly folded glycoproteins carrying the $Man_8GlcNAc_2$

isomer B structure is recognized as an ERAD substrate by the ER lectin known as EDEM [27, 51] (Figure 4).

Transport of the ERAD substrates across the ER membrane by retro-translocation appears to require the tranlocation channel, Sec61p, which is the same channel used for import of the polypeptide during translation [52]. The direction of the transport by Sec61p may be determined by the driving force associated with the presence of ERAD substrates, but the molecular mechanism is not clear [49]. It has been suggested that the force may be derived from four sources (Figure 7): chaperone-mediated extraction, (poly)ubiquitin-mediated ratcheting, AAA ATPase action (p97 in mammalian systems). Chaperone-mediated extraction requires cytoplasmic chaperones such as Hsp70 and Hsp90 in order to maintain the solubility of the cytoplasmic domains, which is important for retro-translocation of integral membrane proteins into the cytosol by the ERAD process. Upon retro-translocation via the Sec61p channel, the ERAD substrates are subjected to polyubiquitination by the action of three enzymes: ubiquitin activating enzymes (E1), ubiquitin conjugating enzymes (E2) and ubiquitin ligases (E3). The polyubiquitination marks the ERAD substrate for degradation via the proteasome-mediated proteolysis. The AAA ATPase protein complex has been shown to interact with the polyubiquitin chain and the NpI1p/Ufd1p proteins [53] and is associated with the 19S domain of proteosome [54]. The function of AAA ATPase protein was proposed to act as an intermediate chaperone that brings the translocated ERAD substrates to the proteosome for degradation. The proteasome (26S) complex is comprised of two domains; the multicatalytic 20S core and the 19S cap. The 20S core of the proteasome is also comprised of AAA ATPase proteins [55]. It is also possible that the proteasome complex is positioned near the Sec61p and can facilitate the ATP-dependent retro-translocation of an ERAD substrate [49].

The degradation of ERAD substrates is carried out by the 20S core of the proteasome complex. The domain contains three proteolytic activities, namely trypsin, chymotrypsin and peptidyl-glutamyl-like activities [55]. The N-linked glycan of the ERAD substrate can be removed by cytosolic peptide:N-glycanase [56, 57] and the released oligosaccharide can be hydrolyzed by various glycosyl hydrolase such as the cytosolic mannosidase [58].

1.3.3 Diseases: Cells normally are able to clear the proteins that fail the ER quality control process and dispose of the proteins via ERAD. In several cases, the ERAD pathway may become inefficient as a result of overwhelming the disposal machinery by an excessive expression of misfolded proteins. Diseases related with ER quality control usually result from the aggregation of incorrectly folded proteins in intracellular compartments and/or the reduction in the production of functional protein (Table 2). For example, inhibition of proteasome degradation or overexpression of wildtype (PrP^{c}) or mutant forms (PrP^{sc}) of secreted prion proteins result in the accumulation of the proteins in the cytosol [59]. The accumulation of the prion proteins in the cytosol results in spontaneous aggregation, which is toxic to the cell and leads to cell degeneration. The aggregated mutant form of rhodopsin, a rod visual pigment, is also a common cause of the retinitis pigmentosa as the result of inherited retinal degeneration [60].

One of the common ERAD-associated disease caused by the loss of protein function is cystic fibrosis (CF). The pathogenesis of CF results from the absence of the cystic fibrosis transmembrane conductance regulator (CFTR) in the plasma membrane of the lung epithelial cells. The most commonly inherited form of CF results from a trinucleotide deletion to result in the loss of a phenylalanine at position 508 (ΔF508). The ΔF508 mutant of CFTR can fold slowly, however it is predominantely targeted for degradation via ERAD. Only a small amount of ΔF508

CFTR can escape ER quality control disposal and reach the plasma membrane in a functional form [61].

Another example of an inherited disease associated with ERAD is α1-antitrypsin (α-AT) deficiency [62, 63]. α-AT is an elastase inhibitor synthesized in the liver and secreted into the bloodstream where it circulates to the lung and protects the tissue from being attacked by proteolytic activity of elastase. The patients carrying the gene encoding the mutant form of α-AT known as the Z variant (α-AT_Z) often develop early onset emphysema as the result of proteolytic attack in lung tissues and in serum. Besides the effects of the reduction in function of α-AT in peripheral tissues, the production of mutant α-AT_Z can also cause liver disease due to the accumulation and aggregation of the misfolded α-AT_Z in the liver.

1.4 Glycosyl hydrolase family 47

The members of the class 1 mannosidases or glycosyl hydrolase family 47 are divided into 4 main subfamilies (Figure 8) based on sequence similarities and preference toward specific branches of α1,2 mannoside linkages on $Man_9GlcNAc_2$ substrates [2]. The 4 subfamilies are 1) ER mannosidase I; 2) Golgi mannosidase I; 3) the fungal secreted enzymes and; 4) ER degradation enhancing α-mannosidase-like (EDEM) proteins. The detailed molecular biology, enzymatic, characteristics, structure and function of the selected members of these subclasses are further described below.

1.4.1 ER mannosidase I subfamily: The ERManI subfamily members are characterized by the specific hydrolysis of a single α1,2-mannosyl residue on the non-reducing end of branch B, which extends from the 1,3-mannosyl residue (M7) (Figure 3) when it is presented with the $Man_9GlcNAc_2$ substrate and generate the $Man_8GlcNAc_2$ isomer B as a major product. With

longer incubation or using higher concentration of purified recombinant enzyme, the enzyme was able to cleave other α1,2-mannoside linkages on the $Man_8GlcNAc_2$ isomer B structure to produce smaller oligosaccharides ($Man_{5-7}GlcNAc_2$) [31]. The members of this subgroup are found strictly in ER, termed ER α-mannosidase I (ERManI). ERManI has been identified and characterized in *S. cerevisiae* and mammalian systems and sequences with high similarity have been identified in several other organisms.

S. cerevisiae ERManI (*Sc*ERManI) is transcribed from the *MNS1* gene (chromosome X) and encodes a 63 kDa protein [64]. The enzyme is a type II transmembrane protein with a single transmembrane domain of 20 amino acids and no significant cytoplasmic tail [65]. The catalytic domain, comprised of ~510 amino acids, is located at COOH-terminus of the enzyme facing the lumenal side of ER. The protein contains three N-glycosylation sites. *Sc*ERManI is the first enzyme of class 1 α-mannosidases whose X-ray structure has been determined [66], and revealed an enzyme-product interaction through the docking of the N-linked oligosaccharide in the glycan binding cleft of the adjoining protein in the crystal lattice. The structural analysis is discussed in detail in the next section.

The human ERManI (*Hs*ERManI) gene is located on chromosome 9 and encodes a 76 kDa protein [10, 67]. The protein is predicted to be a single type II transmembrane protein with a 22 amino acid membrane spanning domains, an cytoplasmic tail of 85 amino acids and a stem region of 137 amino acids [10]. The catalytic domain is comprised of the COOH-terminal 460 amino acids. *Hs*ERManI is 43% identical (54% similar) to *Sc*ERManI [10, 67]. The cDNA encoding the catalytic domain of *Hs*ERManI has been cloned and expressed in *Pichia pastoris* as a 55 kDa protein [14, 67]. Detailed biochemical characterization, expression, and purification of *Hs*ERManI and analysis of several site-directed mutants are described in this dissertation. The structure of the recombinant enzyme is very similar to that of yeast enzyme. The co-crystal

structure of *Hs*ERManI with the mannose mimic inhibitors, dMNJ and Kif, were also obtained, revealing the possible mechanism of catalysis and inhibition of this enzyme [14], and by extension all of the catalytically active class 1 α-mannosidases [14, 15, 66, 68, 69].

Two putative open reading frames for ERManI were also identified in the *C. elegans* genome (Figure 8) that have a high degree of sequence similarity to the yeast and human enzyme [2]. The activity of ERManI was also reported to be detected in the microsomal preparation from the filamentous fungi, *Aspergillus oryzae* [70] and *Candida albicans* [71].

1.4.2 Golgi mannosidase I subfamily: The second subfamily of GH47 enzymes is comprized of a collection of Golgi class 1 α-mannosidases, named Golgi Man IA, IB and IC [2]. The enzymes exhibit some differences in their respective orders of α1,2-mannose removal from $Man_{8-9}GlcNAc_2$ but all three subfamily members very slowly hydrolyze the nonreducing terminal α1,2-mannosyl residue on branch B to generate a final product of $Man_5GlcNAc_2$ (Figures 2 and 3) [72-74]. The expression of Golgi Man IA transcripts on Northern blots is constant throughout embryonic development while Golgi Man IB transcripts are relatively high in early embryonic stages and decrease after 15 days of embryonic development [4]. Golgi Man IC transcripts are found to be highly expressed in most tissues, but the expression pattern differs from that of IA and IB [74]. In humans, Golgi IA, IB, and IC genes are found on chromosomes 6q22, 1p13, and 1p35–36 [74, 75]. Despite the fact that these enzymes are derived from different genes on different chromosomal locations, they are likely related by gene duplication occurring late in evolution, as indicated by similar positions of the intron and exon boundaries within the respective genes [76].

All three of the Golgi α-mannosidase subfamily members are type II transmembrane proteins of ~71-73 kDa, with short cytoplasmic tails and long stem regions of ~100 amino acids.

The catalytic domains are found on the COOH-terminal regions similar to that of class 1 α-mannosidase ERManI subfamily. Within a species, the catalytic domain of the Golgi ManIA shares 71% and 65% identity with that of Golgi Man IB and IC, respectively. The catalytic domain of Golgi α-mannosidase subfamily members share about 30-36% identity with *Hs*ERManI [12, 13].

Representative members of Golgi mannosidase I subfamily have been isolated from various sources, including filamentous fungi, insects and mammalian systems including human, mouse, rabbit and pig (Figure 8). Sequence analysis indicated that there are two homolog genes in *C. elegans*. There is no report of Golgi α-mannosidase found in *S. cerevisiae*, whose N-linked glycan biosynthesis involves only one mannose trimming step catalyzed by ERManI [3]. The X-ray structure of Golgi ManIA isolated from *Mus musculus* has been determined [15]. Golgi ManIA [72] is characterized by the ability to hydrolyze α1,2-mannoside linkages from the nonreducing termini of branches A (90%) and C (10%) when presented with a $Man_9GlcNAc_2$ substrate [72]. The recombinant enzyme was expressed in *P. pastoris* as a secreted protein containing one N-linked glycosylation site, which was found to occupy the active site of the adjacent enzyme molecule in the crystal lattice to facilitate crystal packing. The structure of Golgi ManIA resembles an enzyme-product complex which reveals the structural basis of substrate branch preference on high mannose N-glycans and contrasts with the structure of the enzyme-product complex for *Sc*ERManI. Structural details are discussed in next section.

1.4.3 Fungal secreted mannosidase subfamily: The members of the fungal secreted mannosidase subfamily are initially encoded as type II transmembrane proteins, but the proteins are presumed to function in a soluble form [2]. The secreted forms of the enzymes are about 53-55 kDa in size and are optimally active at relatively low pH (4-5). The representative members of

this subfamily were isolated from *Aspergillus saitoi* [77], *Pennicilium citrinum* [78] and *Trichoderma reesei* [79]. The X-ray structure of the enzymes from *P. citrinum* [69] and *T. reesei* [68] have been determined using the recombinant proteins expressed in *P. pastoris.* The former enzyme hydrolyzes α1,2-mannoside linkage on branch A and C similar to the Golgi ManIA and Golgi ManIC, but its amino sequence is 33% identical to Golgi Man IA and IC [80]. The substrate specificity of the latter enzyme has not yet been identified. Sequence comparison indicates that the *T. reesei* enzyme is about 50% identical to the enzymes from *P. citrinum* and *A. saitoi* [79].

1.4.4 EDEM subfamily: The EDEM (ER degradation enhancing α-mannosidase-like protein) subfamily of proteins was defined by sequence homology to the catalytic domain of ER α-mannosidase I, but appear to have no catalytic activity for hydrolysis of α1,2-mannosidic linkages [2]. The lumenal domain of the members of the EDEM subfamily are about 40% similar and 30% identical to ER α-mannosidase I subfamily members. Blast searches against EST sequence databases using the coding region of class 1 α-mannosidase resulted in identification three human homologs named EDEM1, EDEM2 and EDEM3 [2, 12, 13]. EDEM1 is proposed to be a type II membrane-bound protein similar to ERManI and Golgi ManIA, IB and IC, while the EDEM2 and EDEM3 appear to function as the soluble proteins because their NH_2-terminal domains are proposed to contain a cleavable NH_2-terminal signal sequence. The EDEM1 and EDEM2 proteins contain an extended COOH-terminal sequence of 70-100 amino acids beyond the mannosidase-homology domain. The EDEM3 protein contains a significantly longer COOH-terminal domain of 434 amino acids, which appears to contain a protease-associated domain. There are two EDEM-related proteins identified from *S. cerevisiae* named HTM1/MNL1 and YLR057w. The former protein is predicted to function as soluble protein similar to EDEM2 and

EDEM3. The latter is a membrane bound protein similar to that of EDEM1. The function of EDEM proteins in ER quality control was elucidated by the overexpression of the recombinant protein in host cells expressing a misfolded reporter protein to monitor the effect of EDEM expression on the ERAD of the reporter protein [5, 12, 13, 28, 51, 81].

1.5 Glycosyl hydrolase family 38

The class 2 α-mannosidases or glycosyl hydrolase family 38 are a group of enzymes that hydrolyze a collection of mannosyl glycosidic bonds on high mannose-glycan substrates. The class 2 α-mannosidases can be distinguished from class 1 α-mannosidases in many ways. Class 1 and 2 enzymes can be distinguished primarily based on their significant differences in protein sequence and their differences in substrate specificity [2]. Unlike the class 1 α-mannosidases which catalyze the hydrolysis of α1,2-mannosidic linkages, the class 2 enzymes can catalyze the hydrolysis of α1,2, α1,3, or α-1,6 mannosidic linkages. While class 1 enzymes can be inhibited by the pyranose analogue inhibitors such as dMNJ or Kif, class 2 enzymes can be effectively inhibited by the furanose analogue inhibitors such as swainsonine (Sw) and poorly inhibited by the pyranose analogues [82]. Class 2 enzymes require cations such as Zn^{2+} or Co^{2+} for catalytic activity, while class 1 enzymes require Ca^{2+} for catalytic activity. Class 2 enzymes catalyze the hydrolysis of glycosidic bonds by a retaining mechanism, while class 1 enzymes employ an inverting mechanism for catalysis.

The representative members of class 2 α-mannosidases found in the mammalian cells are Golgi α-mannosidase II (GManII), Golgi α-mannosidase IIx (GManIIx), lysosomal α-mannosidase (LAM), ER α-mannosidase II (ERManII) and the cytosolic α-mannosidase (CytMan). As described above, the ERManII and GManII/IIx are involved in N-linked glycan maturation in the ER and the Golgi complex, respectively. GManII is a Zn^{2+}-dependent enzyme

which hydrolyzes the terminal α1,3- and α1,6-mannosyl residues of the $GlcNAcMan_5GlcNAc_2$ processing intermediate to generate the $GlcNAcMan_3GlcNAc_2$ structure [83]. The GManIIx is a Co^{2+}-stimulated enzyme that may hydrolyze the terminal α1,3- and α1,6-mannosyl residues of $Man_5GlcNAc_2$ to generate a $Man_3GlcNAc_2$ structure [84]. While mannose trimming by GManII is a common path of N-linked glycan maturation, the action of GManIIx serves as an alternative pathway for complex glycan biosynthesis for specific tissues, such as testis [85].

LAM and CytMan function in the catabolism of the mannose-containing glycans generated from the disposal of misfolded glycoproteins through ERAD or the catabolism of endocytosed glycoproteins. LAM activity is stimulated by addition of Zn^{2+} ions and may contain tightly bound Zn^{2+} in the active site of the enzyme. The enzyme can hydrolyze all of the alpha mannosidic linkages, α1,2-, α1,3-, and α1,6, associated with high mannose glycan substrates to produce the $ManGlcNAc_{2\text{-}1}$ as the enzymatic end product [86]. The cytosolic α-mannosidase requires Co^{2+} for its catalytic activity and can remove 4 of the terminal α1,2-, α1,3-, and α1,6-mannosyl residues of branches B and C of the oligosaccharide substrate resulting in an oligosaccharide product containing an intact α1,2 mannosyl chain on branch A [58]. The LAM is a lysosomal enzyme and active at pH ~4.5 compared to GManII/IIx and cytosolic α-mannosidase which are active at neutral pH.

The X-ray structures of GManII isolated from *Drosophia melanogaster* (*Dm*GManII) [87] and LAM from bovine sources(*Bos taurus*) (*Bt*LAM) [88] are similar despite the low level of sequence identity between them. The enzyme structure comprises of three main domains: NH_2-terminal α/β-domain, a three-helical bundle and an all-β COOH-terminal domain. The domains are connected by disulfide bonds and stabilized by a zinc-binding site forming an oval shaped molecule (Figure 9). The catalytic domain resides within the NH_2-terminal α/β domain where coordination of Zn^{2+} is found.

1.6 Catalytic mechanisms of glycosyl hydrolase

The glycosidic bond, particularly the linkage between two glucose residues is the most stable bond within naturally occurring biopolymers, with half-lives of approximately 5 million years [89]. In contrast, the hydrolysis of glycosidic linkages can be accomplished by the action of various glycosyl hydrolases with the rate constants up to 1000 s^{-1}. These enzymes catalyze the same reaction to hydrolyze an acetal linkage via an acid-base catalytic mechanism [90-92]. Enzymatic hydrolysis of a glycosidic bond requires two critical components: a proton donor which protonates the glycosidic oxygen and a nucleophile or base which attacks the anomeric carbon (Figures 10 and 11). The hydrolysis of a glycosidic bond can occur with one of two possible stereochemical outcomes for the non-reducing residue of the substrate (Figures 10 and 11). The mechanism which gives rise to an overall retention of anomeric configuration of the released glycone is known as a retaining mechanism, and the other which results in an inversion of anomeric configuration of the released glycone is known as an inverting mechanism. Details of these mechanisms are described below.

1.6.1 The enzyme-substrate binding site: The active site nomenclature used in this dissertation follows the convention proposed by Davies, *et al* [93] and is illustrated in Figure 12. The active sites of glycosyl hydrolases are comprised of two main subsites. The subsites are labeled as +*n* and -*n* in relation to the bond that is being hydrolyzed. The +*n* subsites define the active site that binds the reducing end portion of the glycan substrate. The -*n* subsites define the active site that binds the non-reducing end portion of the glycan substrate. The portion of the glycan that binds to +*n* subsite was previously termed aglycone. This term was used to define the non-carbohydrate moiety for synthetic substrate analogues that were used to investigate the catalytic mechanisms of the enzymes. In contrast, the portion of the glycan substrate that binds to –*n* subsite is termed the

glycone. The term also refers to the carbohydrate part of the substrate that contributes the C1 acetal linkage to the glycosidic bond.

To investigate the catalytic mechanism utilized by glycosyl hydrolase family 47 enzymes, several compounds and substrates are used. For example, the inhibitors of class 1 mannosidase such as dMNJ and Kif are found to bind to the enzymes at the glycone binding site or -1 subsite based on the X-ray structures of co-complexes of these compounds with the *Hs*ERManI [14]. The substrates for the ER, Golgi, and fungal secreted class 1 mannosidases are the oligosaccharide substrates ($Man_{9\text{-}6}GlcNAc_2$) and the disaccharide substrates such as mannopyranosyl-α-(1,2)-α-mannopyranoside (mannobiose; Manα1,2Man) and methyl-O-α-mannopyranosyl-α-(1,2)-α-mannopyranoside (Manα1,2Man-*O*-Me). As a result of the exo-glycosidase action by these enzymes, the terminal mannose residue on the non-reducing end (glycone or -1 mannose) of the substrate is cleaved from the remaining part of the glycan (aglycone or $\geq$+1 mannose residue).

1.6.2 Inverting mechanism: Enzymes that cleave glycosidic bonds with an inverting mechanism use of two carboxyl side chains, usually a Glu or Asp, which serve as general acid and general base catalysts (Figure 11a). The pair of carboxylic acids are located approximately 10 ± 2 Å apart [94]. The reaction occurs via a single-displacement mechanism where the general acid catalyst directly protonates the glycosidic oxygen while the general base activates a water nucleophile for the attack of the anomeric carbon atom (Figure 6a). To date, there are 26 glycosidase families, consisting of >2,660 members (~20% of all of the known glycosyl hydrolases, including members of glycosyl hydrolase family 47), employ an inverting mechanism for catalysis. Two representative members are summarized in Table 3.

1.6.3 Retaining mechanism: Glycosidases which employ a retaining glycosidase mechanism generally catalyze the cleavage of a glycosidic linkage using a pair of carboxyl groups which are located approximately 5.5 Å apart using double-displacement mechanism involving the formation of a transient covalent glycosyl-enzyme intermediate (Figure 11b) followed by a deglycosylation step catalyzed by an incoming water molecule. In the first step, a carboxyl group of a Glu or Asp side chain functions as a general acid catalyst, protonating the glycosidic oxygen, and inducing the bond cleavage, while the other carboxylate group serves as a nucleophile, forming a covalent bond with the released glycone. In the second step, the transient enzyme-linked intermediate is attacked an incoming general base-activated water molecule at the anomeric center to result in a released glycone that regenerates the anomeric configuration of the original glycosidic linkage. The majority of the known glycosyl hydrolases (44 families, with >10,700 members) employ a retaining mechanism for catalysis. A representative set of enzymes utilizing an inverting (I) and a retaining (R) mechanism with the conformations of their respective transition intermediates information are summarized in Table 3.

1.6.4 Sugar conformational itinerary: Both inverting and retaining mechanisms have been proposed to require the formation of an oxocarbenium ion transition state with charge delocalization between the anomeric center (C1) and the ring oxygen (O5) [95-97]. The resulting partial double bond character of the C1-O5 bond results in a ring-flattened co-planarity of C5, O5, C1 and C2 at or near the transition state. Among the potential pseudorotational conformational itineraries for sugar pyranose ring interconversions, there are four potential conformations where the planarity of C5, O5, C1 and C2 is satisfied (Figure 13: $^{2,5}B$, $B_{2,5}$, $^{4}H_{3}$, and $^{3}H_{4}$) [95]. Recent data have suggested that three of these potential transition state conformations are employed among the known GH families (GH families 6, 8, 11, 67 are

proposed to use $^{2,5}B$, GH families 26 and 38 are proposed to use $B_{2,5}$, and GH families 5, 7, 18, and 20 are proposed to use $^{4}H_{3}$) [95, 98-107]. These key transition state conformations have generally been identified either by trapping covalent intermediates using fluorinated glycone analogs (for retaining glycosidases) or co-crystalization with thioglycoside substrate mimics, substrate analog inhibitors, or natural substrates in combination with active site mutants. Of the four possible coplanar oxocarbenium ion transition states, only the $^{3}H_{4}$ conformation has not yet been identified for any known glycosidase.

1.7 Structure and function of glycoside hydrolase family 47

Family 47 α-mannosidases have been extensively studied from a variety of species in regard to enzyme kinetics, substrate specificity, and structure [2, 3, 14, 15, 66, 68, 69, 108]. Two classes of co-complexes have been characterized by X-ray diffraction. Putative enzyme-glycan product co-complexes have been isolated for both ER and Golgi family 47 hydrolases revealing the structural basis for branch specificity for these enzymes [14, 15, 66, 69]. In addition, co-complexes between ERManI and glycone monosaccharide mimics, kifunensine and 1-deoxymannojirimycin (dMNJ), have revealed several unprecedented aspects of glycone binding and hydrolysis by this family of enzymes [14]. The sources of X-ray structures of class 1 α-mannosidase and their important features are summarized in Table 4.

1.7.1 Overall protein structures

The overall protein structures of the family 47 glycosidases are very similar. The enzyme catalytic domain structures consist of about 400-470 amino acids which form an $(\alpha\alpha)_7$ barrel, which is composed of 14 α-helices that form two 7-stranded concentric antiparallel barrel layers.

The barrel helices are connected alternately from the inside barrel to the outside barrel (Figure 14). The inner helices form a parallel array of 7 helices designated as α2, α4, α6, α8, α10, α12 and α14. The outer helices are also composed of a parallel arrangement of 7 helices designated as α1, α3, α5, α7, α9, α11 and α13. Each helix is connected by a set of β-sheets perpendicular to the central axis of the barrel at the long connection (LC side) and a set of short loops on the opposite side of the barrel forming a short connection (SC side). The β-sheets at the LC side can be separated into 6 groups of 3 antiparallel β-sheets forming a layer of β-sheets resembling petal-like arrangement of an "open flower" [66]. At the SC end of the structure, the barrel is plugged by a β-hairpin at the C-terminus. A calcium ion, essential to the class 1 enzyme activity, is found coordinated with the carbonyl and hydroxyl groups of the threonine at the apex of the β-hairpin and 6 additional water residues forming an 8-fold pentagonal bipyramidal coordination. The overall structure is about 50 × 50 × 50 Å. The pocket cavity (~15 Å deep and ~10 Å wide) in the middle of the barrel contains the enzyme active site. The pocket varies from 15-35 Å wide at the funnel opening [15, 109]. The barrel structure may be stabilized by a single disulfide bond found between Cys residues bridging helices α10 and α11, with the exception of the α1,2-mannosidase isolated from *T. reesei* which does not contain the equivalent disulfide.

The protein sequence similarity of the catalytic domain of GH family 47 and the superimposition of the C_α backbone structures of the known GH47 enzymes indicate an RMS of ~1.0 Å in the helical regions, especially within the residues of the active site. Thus, these protein structures are highly conserved, while the β-sheets of LC side are highly variable (Figure 15) [15].

1.7.2 Oligosaccharide-Protein Complex Structures

A high mannose oligosaccharide of an adjoining protein monomer was found to bind in the active site of both *Sc*ERManI [66] and *Mm*GManIA [15] crystal structures assisting the crystal lattice formation. The oligosaccharide of *Mm*GManIA is a $Man_6GlcNAc_2$ structure which resembles the $Man_5GlcNAc_2$ enzymatic aglycone product with an additional α1,6-mannose residue linked to M5 (Figure 16A). The oligosaccharide rotates the glycosidic bond around M3-α1,6-M4 linkage in presenting the M6-α1,2-M9 linkage into the binding pocket (see Figure 3 for mannose residue nomenclature). The oligosaccharide of *Sc*ERManI is a $Man_5GlcNAc_2$ structure (Figure 16B) that presents the M7-α1,2-M10 linkage into the binding site. In both enzymes the -1 mannose residues was cleaved and no sugar was detected in the -1 subsite. Therefore, the structures resemble the respective enzyme-product complexes where the oligosaccharide-protein interactions at ≥+1 subsites can be observed.

The positions and interactions between the M6 residue in the +1 binding site of *Mm*GManIA and M7 in the equivalent site in *Sc*ERManI are virtually superimposable. The sugar at +1 subsite directly interacts with the D415 (D275 in *Sc*ERManI) via hydrogen bonds between carboxyl O-γ2 and the O3' hydroxyl, the carboxyl O-γ1 and the O4' hydroxyl. In addition, the O4' hydroxyl of the +1 mannose also forms a hydrogen bond with the peptide nitrogen of L413 (R273 in *Sc*ERManI) while the O-6' hydroxyl has a hydrogen bond with the carboxyl O-ε1 of E351 (E207 in the *Sc*ERManI).

The binding interaction at the +2 subsite and beyond are distinct between *Sc*ERManI and *Mm*GManIA enzyme. The interactions between the oligosaccharide and the ≥ +2 binding site residues for *Mm*GManIA involve nine indirect hydrogen bonds through bridging water molecules and direct interactions via hydrogen bonds between the O2' hydroxyl of M4 and the carboxyl O-ε2 of Glu^{524}, as well as the O3' hydroxyl of M5 and the Oγ serine. The flattened sugar ring of

core the NAG2 is stacked adjacent to W341 indicating the role of hydrophobic interaction at the base of the glycan structure [15]. In the *Sc*ERManI enzyme, the dominant interaction in the ≥ +2 binding sites are five hydrogen bonds from R273 to residues M7, M4 and M3, and the direct hydrogen bonds between the protein and glycan residues M5, M4, and M6 [66]. In addition, steric hindrance for the oligosaccharide at M5 can be clearly observed when the oligosaccharide found in the *Sc*ERManI structure is aligned into the active site of *Mm*GManIA (Figure 17E). These data indicate that the substrate specifities of these enzymes are defined by the binding cleft topology which constrains the specific orientation and conformation of the oligosaccharide substrate to present distinctive linkages to the active site machinery.

Comparing the binding cleft among the class 1 α-mannosidase shows that the substrate specificity is also conveyed by the dimensions of the binding cleft (Figure 18). The binding cleft topology appears as a funnel where the opening is larger and narrowing toward the bottom of the active site. The binding cleft opening of *Mm*GManIA (22.3 ×14.5 $Å^2$) is narrower compared to the *Pc*ManI (36.7 ×22.1 $Å^2$) and *Hs*ERManI (33.1× 17.6 $Å^2$). In the *Sc*ERManI enzyme, mutating R273 to Leu resulted in broader the cleft opening and altered the specificity to result in a poor-efficiency enzyme with a substrate specificity partially between ERManI and the corresponding Golgi mannosidase enzymes [110].

1.7.3 Co-crystal structures with the inhibitors

The co-crystal structures between the mannose analog inhibitors (Figure 19) and human ERManI [14] and the *P. penicilium* α-mannosidase [69] revealed the glycone conformation in the -1 subsite at the core of the enzyme $(\alpha\alpha)_7$ barrel catalytic domain. Upon binding of the inhibitor, two water residues which form the pentagonal bipyramidal coordination with calcium ion in the

barrel active site are replaced by two hydroxyls (O2' and O3') of the inhibitors (Figure 20A). Both kifunensine and 1-deoxymannojirimycin adopt an unusual high free energy $^{1}C_{4}$ conformation (Figure 20) facilitated both by a direct coordination of the inhibitor O2' and O3' hydroxyls with an enzyme-associated Ca^{+2} ion and by a matrix of hydrogen bonds and hydrophobic interactions via F659 (residue numbering from human ERManI) and C5-C6 arm of the ligands. The O6' hydroxyl of the inhibitors also interacts with the carboxyl group of E599 and the side chain nitrogen of R597.

1.7.4 Proposed catalytic mechanism

The superimposition of the co-complex structure of *Hs*ERManI with dMNJ and the oligosaccharide found in the active site of *Sc*ERManI structure led to the proposal of a novel inverting glycosidase mechanism for these enzymes, where the water nucleophile was one of the water ligands directly coordinated with the enzyme-bound Ca^{+2} ion and the catalytic acid, E330 was proposed to act indirectly through a water molecule in the protonation of the glycosidic oxygen (Figure 21) [14]. Unambiguous identification of the catalytic acid and base residues was not possible because of the unusual nature of the catalytic mechanism. Further evidence supporting the proposed mechanism was found in the computational analysis of ligand docking using various sugar ring conformations [109]. The docking of Man-E_4-1,2-Man and the two water residues corresponding to W1 and W5 at the optimal position suggested that E330 is the catalytic proton donor and E599 is the catalytic base acting through the respective water residues. W5 appears to mediate proton donation via a Grotthus-type proton hopping mechanism [14], because E330 is not within hydrogen bonding distance of the O2 atom of Man7. E330 is unlikely to move around to be able to form hydrogen-bond with the O2 atom of the -1 mannose residue because it is anchored in place by a salt bridge with R334 that restricts its motion. This observation is the

first case of a water molecule mediating proton donation from a carboxylic acid. The only water that can be activated by the nucleophile and attack the C1 anomeric carbon is W1 which is also coordinated by the Ca^{2+} ion. This suggests that the Ca^{2+} has a more important role in catalysis than merely stabilizing the $^{1}C_{4}$ conformation of the -1 sugar. Given the above mechanism, D463 is not within hydrogen-bonding distance of W1 and is ruled out as the catalytic base. The simulated docking of disaccharide suggested that the nonreducing-end mannosyl residue might adopt an E_{4} conformation in mimicking the transition state [109].

Figure 1: The project outline. The work decribed in this dissertation comes from four stages of research. Stage I decribes the cloning, characterization, expression, and purification of human ER mannosidase I (*Hs*ERManI). Stage II decribes the X-ray structure analysis of class 1 α-mannosidases. Stage III decribes the mutagenesis studies and the characterization of the kinetics and binding properties of the mutants. Stage IV described the co-complex structure of *Hs*ERManI and the thiodisaccharide substrate analogue.

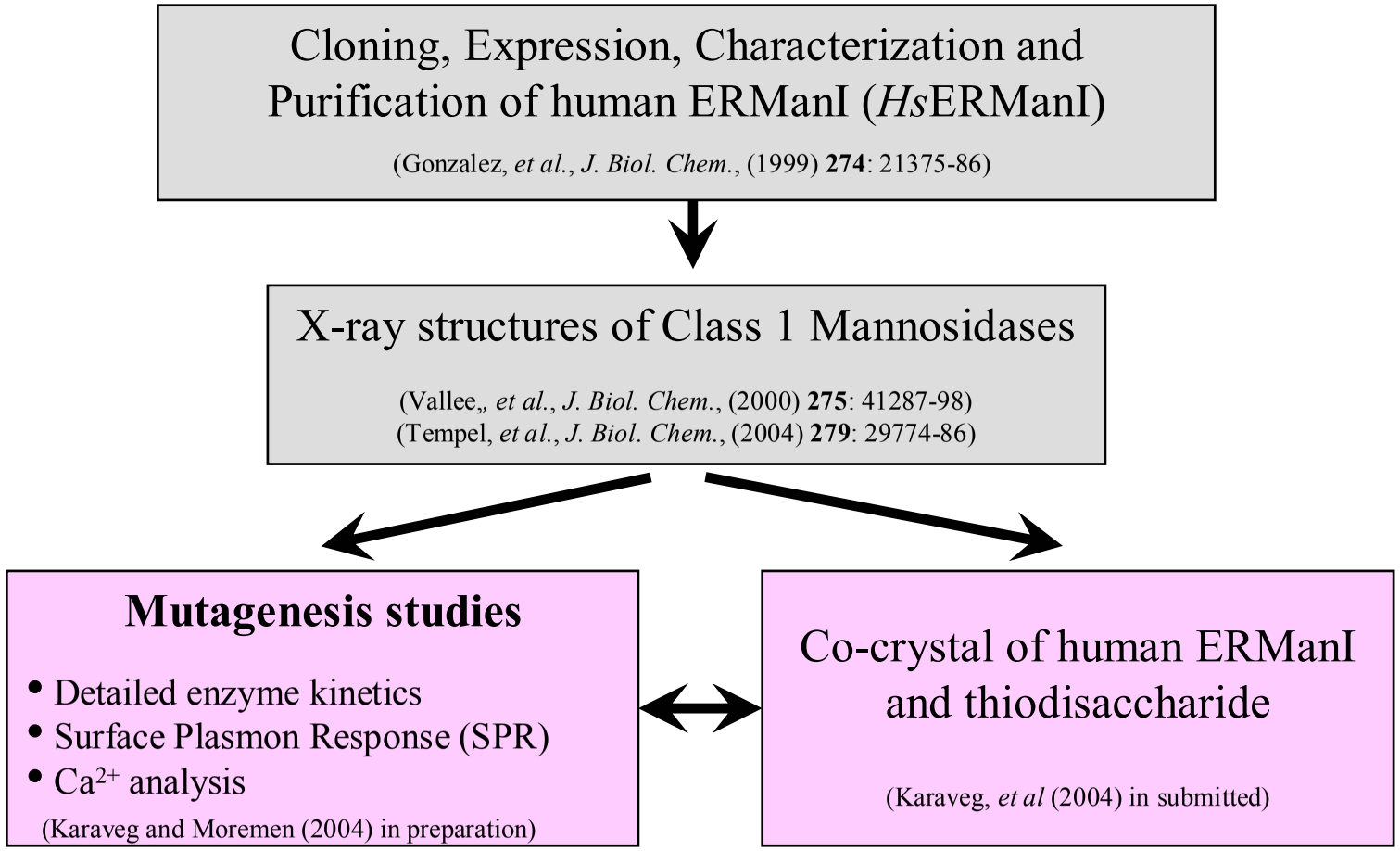
Cloning, Expression, Characterization and Purification of human ERManI (*Hs*ERManI)
(Gonzalez, *et al.*, *J. Biol. Chem.*, (1999) **274**: 21375-86)
X-ray structures of Class 1 Mannosidases
(Vallee,, *et al.*, *J. Biol. Chem.*, (2000) **275**: 41287-98)
(Tempel, *et al.*, *J. Biol. Chem.*, (2004) **279**: 29774-86)
Mutagenesis studies
• Detailed enzyme kinetics
• Surface Plasmon Response (SPR)
• Ca^{2+} analysis
(Karaveg and Moremen (2004) in preparation)
Co-crystal of human ERManI and thiodisaccharide
(Karaveg, *et al* (2004) in submitted)

Figure 2: The main pathway of N-linked oligosaccharide modification in mammalian glycoprotein biosynthesis. The dolicol pyrophosphate oligosaccharide precursor of N-linked glycans is transferred to a newly synthesized polypeptide as it passes through the ER membrane. This step is catalyzed by the oligosaccharyl transferase (OST). The oligosaccharide is then subjected to modication by a series of the ER enzymes, namely glucosidase I (Glc I); glucosidase II (Glc II); UDP-Glc:glycoprotein glucosyltransferase (Glc T); ER mannosidase I (ERManI); ER mannosidase II (ERManII); endo α-mannosidase (Endo α-man). The N-linked glycans on correctly folded glycoproteins are processed further by a series of the Golgi enzymes, namely Golgi mannosidase IA and IB (Golgi ManIA/B); GlcNAc transferase I (GnTI); and either α-mannosidase III or Golgi mannosidase IIx (Golgi Man III/IIx). The complex glycan structures are completed in the Golgi complex by a series of glycosyl transferase such as GlcNAc transferase II (GnTII). Positions where processing inhibitors can act to block enzyme reactions are indicated by a thin arrow with the following abbreviations: dMNJ, 1-deoxymannojirimycin; Kif, kifunensine; Sw, swainsonine. The legend for the oligosaccharide structure displayed in the figure is indicated in the lower right.

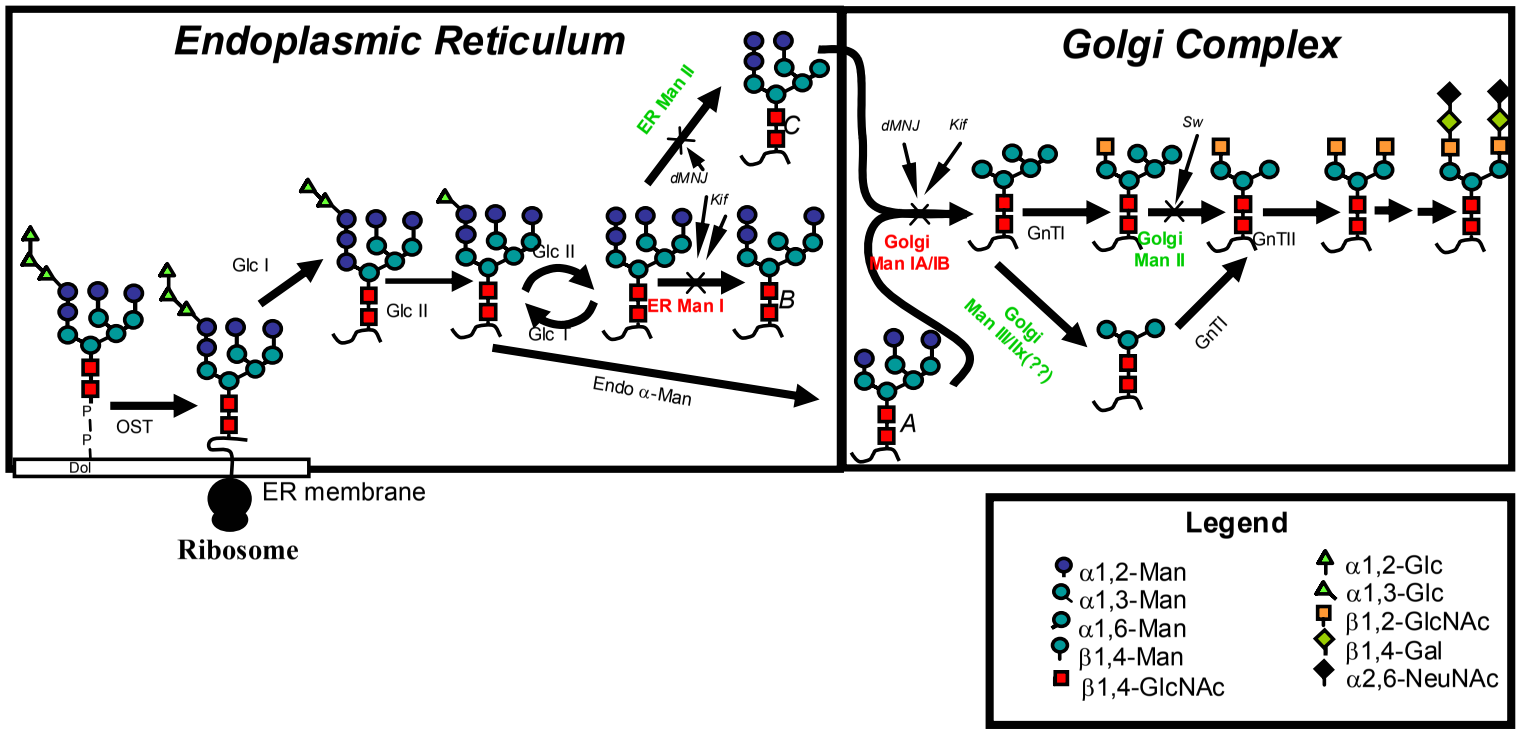

Modified from Moremen, K.W. (2000) in *A Comprehensive Handbook: Carbohydrates in Chemistry and Biology*, p. 81-117.

Figure 3: The N-linked oligosaccharide attached to nascent polypeptides and the enzymes that modify the glycan. The nascent polypeptide moiety is shown as a red hexagon. The oligosaccharide comprises of chitobiose core (two GlcNAc residues shown in purple rectangles), nine mannose residues shown in green ovals and three glucose residues shown in blue diamonds. Note that the non-reducing ends of the glycan structure is separated into three branches namely A, B and C indicated by solid black arrows above the figure. The enzymes and their sites of action are shown:(a) glucosidase I, (b) glucosidase II, (c) UDP-glc:glycoprotein glucosyltranferase, (d) ER mannosidase I, (e) ER mannosidase II, (f) endo α-mannosidase, (e–g) Golgi mannosidases. The arrows with dash lines in red indicate the hydrolysis activities. The arrow with solid line in blue indicates the transferase activity.

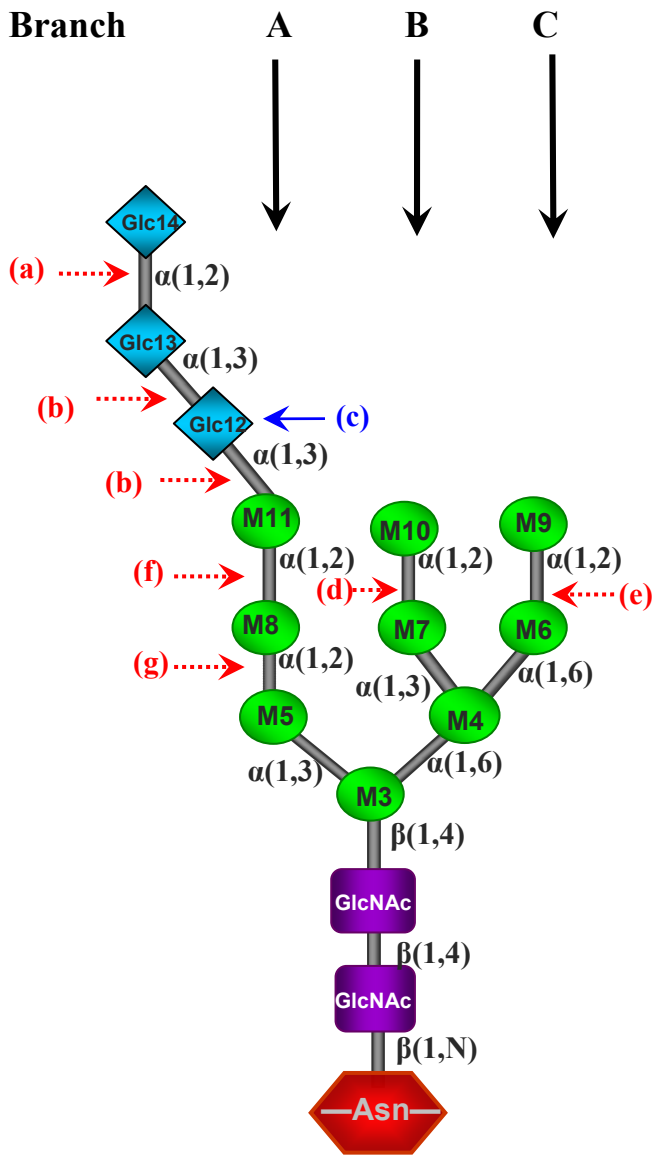

Modified from Cabral, et al. (2001) *Trends Biochem. Sci.* 26:10, 619-624

Table 1. Nomenclature for the oligosaccharide structures produced by the sugar processing enzymes of the N-linked glycoprotein maturation and biosynthesis pathway.

Oligosaccharide	Structure/oligomers/isomers				Alias
	A	B	C	D	
Glucosylated glycan ($Glc_{0-3}Man_{8-9}GlcNAc_2$)	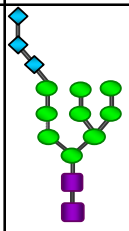	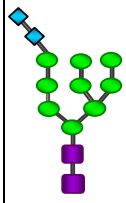	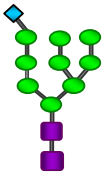	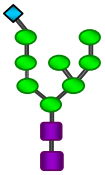	Glc(1-3)Man9 (D=GlcMan8)
$Man_9GlcNAc_2$	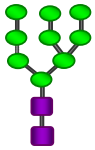				Man9
$Man_8GlcNAc_2$	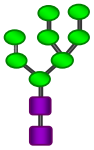	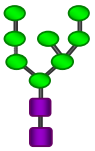	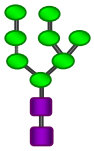		Man8
$Man_7GlcNAc_2$	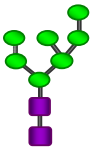	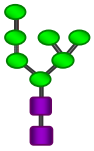	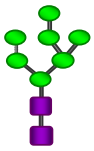	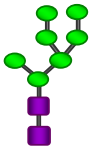	Man7
$Man_6GlcNAc_2$	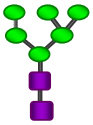	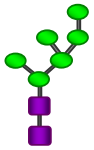	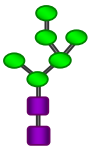		Man6
$Man_5GlcNAc_2$	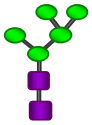				Man5
$GlcNAcMan_5GlcNAc_2$	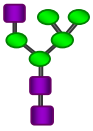				GlcNAcMan5
$GlcNAcMan_3GlcNAc_2$	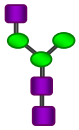				GlcNAcMan3

Figure 4: The oligosaccharide structures recognized by the ER quality control machinery and ERAD. The core oligosaccharide ($Glc_3Man_9GlcNAc_2$) is covalently linked to the side chain amide nitrogen of asparagines in the consensus Asn-X-Ser/Thr sequence on proteins in the secretory pathway. The terminal glucose residues are removed by the glucosidase I and II. The inner-most glucose residue of the incompletely folded glycoprotein can be reglucosylated by the UDP-glucose:glycoprotein glucosyl transferase (GT) resulting the $Glc_1Man_9GlcNAc_2$ structure which is the molecular marker for binding of calnexin/calreticulin(CNX/CRT) to facilitate the folding and retention of the glycoprotein. The deglucosylation of this glucose residue is catalyzed by the glucosidase II resulting in the $Man_9GlcNAc_2$ structure which allows the correctly folded glycoprotein to dissociate from the CNX/CRT cycle and continue to the secretory pathway. Removal of the terminal mannose on the middle branch of $Glc_{1-0}Man_9GlcNAc_2$ by the action of ERManI results in the formation of $Glc_1Man_8GlcNAc_2$ or $Man_8GlcNAc_2$ structures, which allows the misfolded glycoprotein to be recognized by EDEM as an ERAD substrate and targeting for degradation.

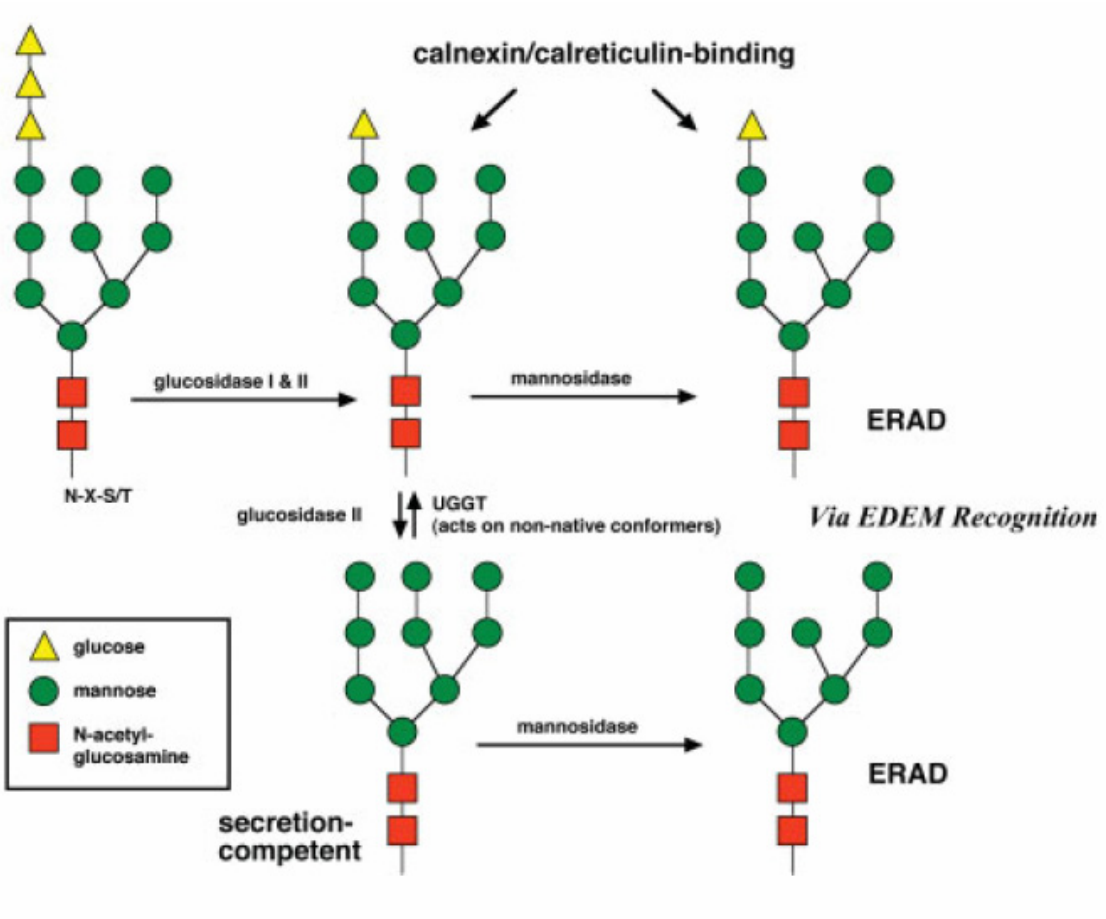

From McCracken, A.A., and Brodsky, J.L. (2003). Bioessays *25*, 868-877.

Figure 5: Comparison of $Man_9GlcNAc_2$ and $Man_8GlcNAc_2$ isomer B trimming by mammalian ER and Golgi α1,2-mannosidases. Enzymes highlighted in *black above* the *arrows* represent the major pathway(s), whereas those *beneath* the *arrow* indicate a minor pathway (<30% of product); ●, α1,2-linked mannose residues; ○, α1,3-and α1,6-linked mannose residues;□, $GlcNAc_2$. IA, IB and IC are the Golgi Class 1 α-mannosidases. ER here refers to ERManI. The number of mannose residues on substrates or product are indicated as Man_{9-5} at the bottom of the figure.

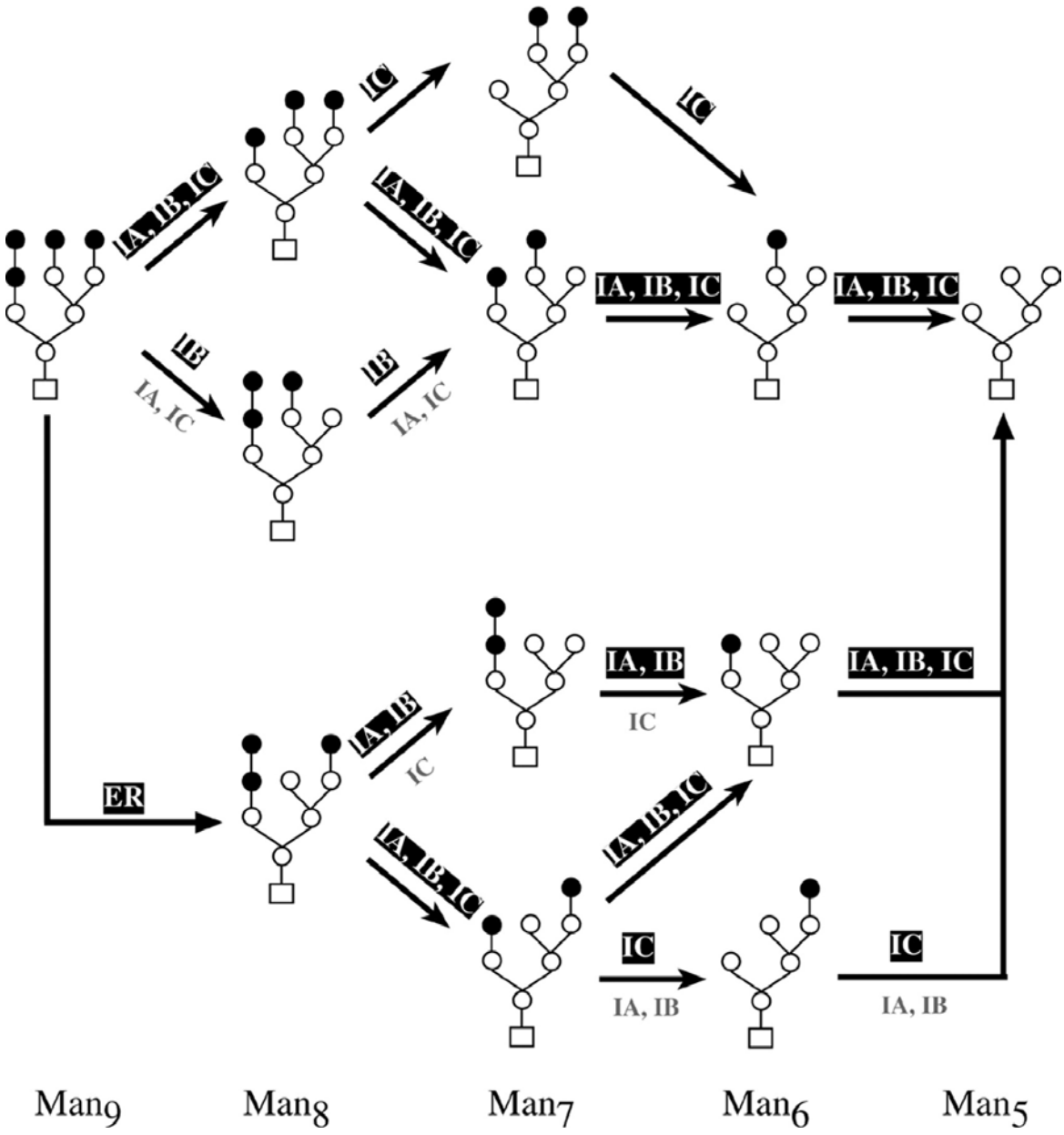

From Tremblay, L.O. and A. Herscovics (2000) *J. Biol. Chem.* **275**: 31655-60.

Figure 6: ER quality control and glycoprotein protein biosysthesis. Shown are the ER quality control processes in conjuntion with the early steps in N-linked glycan maturation. Immediately after addition of the core glycan, the outermost of the two glucose residues (m, n) are removed by glucosidase I and glucosidase II resulting in the monoglucosylated core glycan structure. The terminal glucose associated with the N-linked glycan allows the recognition of the glycan intermediate by calnexin (CNX) and calreticulin (CRT). In addition to binding by CNX and CRT, the folding of the glycoprotein is facilitated through protein-protein interaction with the chaperones and the association with ERp57, a thiol-disulfide oxidoreductase that provides assistance during disulfide bond formation. Upon the release from CNX or CRT, the N-linked glycan is exposed to glucosidase II (GDII) which removes the inner most glucose (l). Incompletely folded glycoproteins can re-enter the CNX/CRT cycle by addition of a terminal glucose by the action of the UDP-Glc:glycoprotein glucosyltransferase (GT) which will add a glucose back to the glycan at the same position and linkage which was removed by GDII. The glycoprotein can exit and enter the CNX/CRT as many times as is required to achieve the stable and functional folding of the polypeptide, or until the terminal central branch mannose of the N-linked glycan is removed by the action of the ER α-mannosidase I (ERManI). ERManI removes the terminal α1,2-mannosyl residue on branch B resulting a $Man_8GlcNAc_2$ isomer B (Man8B). Incompletely folded glycoproteins carrying the Man8B structure are then recognized by the EDEM proteins and targeted for degradation via ERAD by retrotranslocation through the translocon complex. For correctly folded glycoproteins, the removal of terminal glucose by GDII allows the glycoprotein to be transported to the Golgi complex for further modicafication. Also shown in the diagram are the mannose specific lectins, such as ERGIC-53, VIP36, and VIPL which may assist in the packing and transporting of glycoproteins between ER and Golgi complex. The UDP-glucose transported into the lumen of the ER and the UDP-glucose/UMP

exchanger are also included in the figure as the process which supplies the UDP-Glc from the cytosol to reglucosylate the high-mannose glycans on incompletely folded glycoproteins by the action of GT. Abbreviations used are EDEM, ER degradation-enhancing α-mannosidase-like protein; VIP36, vesicular integral protein 36; VIPL, VIP36-like protein; ERAD, ER-associated protein degradation; ERGIC, ER-Golgi intermediate compartment; and ERp57, ER protein 57.

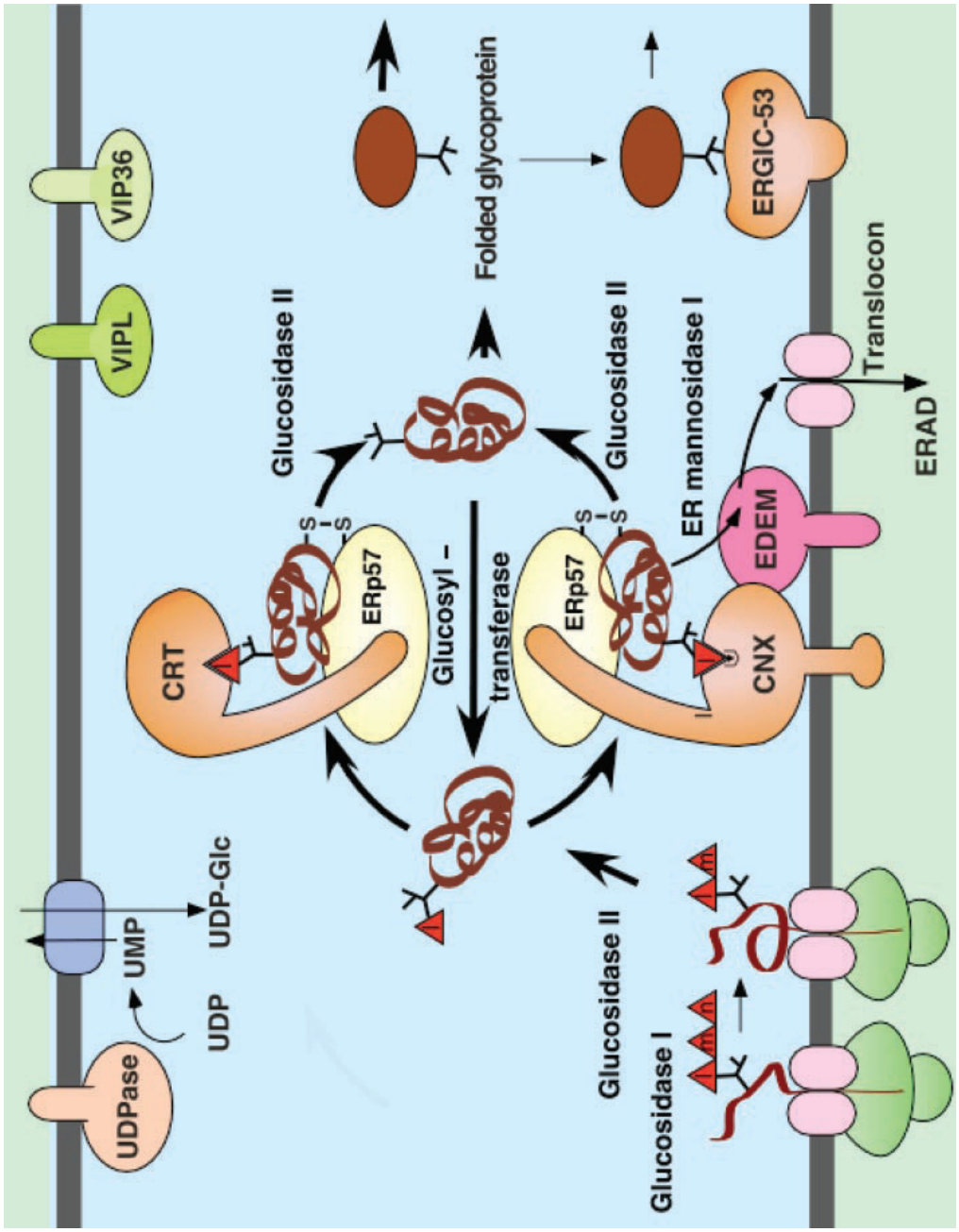

From Helenius, A. and M. Aebi (2004) *Annu. Rev. Biochem.*, **73**: 1019-49

Figure 7: The ERAD pathway. The newly synthesized polypeptide enters the ER lumen through the Sec61p translocon during translation and immediately undergoes afolding process assisted by various ER chaperones. Association with BiP facilitates the binding and translocation of the polypeptide. The proteins that fail in the ER quality control are subjected to ERAD. The terminally misfolded proteins are ERAD substrates and must be retro-translocated through the ER membrane utilizing the Sec61p channel. The retro-translocation of the ERAD substrate is facilitated by chaperones such as BiP, and co-chaperones (Scj1p/Jem1p, Sls1p). For misfolded N-linked glycoproteins, recognition as an ERAD substrate is accomplished by exposure of specific glycan structures (Figure 4) following release from the specialized chaperones calnexin/calreticulin and subsequent binding by the lumenal lectin EDEM proteins that target them for retro-translocation to the cytosol. On the cytosolic site of the ER membrane, the polypeptide interacts with various cytosolic chaperones (Ssa1p/Hsp70, Hsp90, Hdj2, Cdc48p/p97) to facilitate the retro-translocation of the polypeptides and prevent them from aggregation. The ERAD substrate is modified by the ubiquitination machinery (Hrd1/Der3p, Rsp5p, SCFFbx2, CHIP, Ubc1/6/7p, Cue1p) to add polyubiquitin chains which serve as recognition markers for proteolysis by the proteasome. The Ufd1p and Npl4p proteins are the mediators which recognize the polyubiquitin chain on the ERAD substrates and deliver them to the proteasome or recruit the proteasome to the retro-translocation site. Several chaperones and factors required for ERAD, such as EDEM and Sec61p can be upregulated in their expression expressed via the unfolded protein response (UPR) which is activated by the accumulation of misfolded proteins in the ER. The dashed line is the partition between the pathway for protein folding and maturation versus the ERAD pathway.

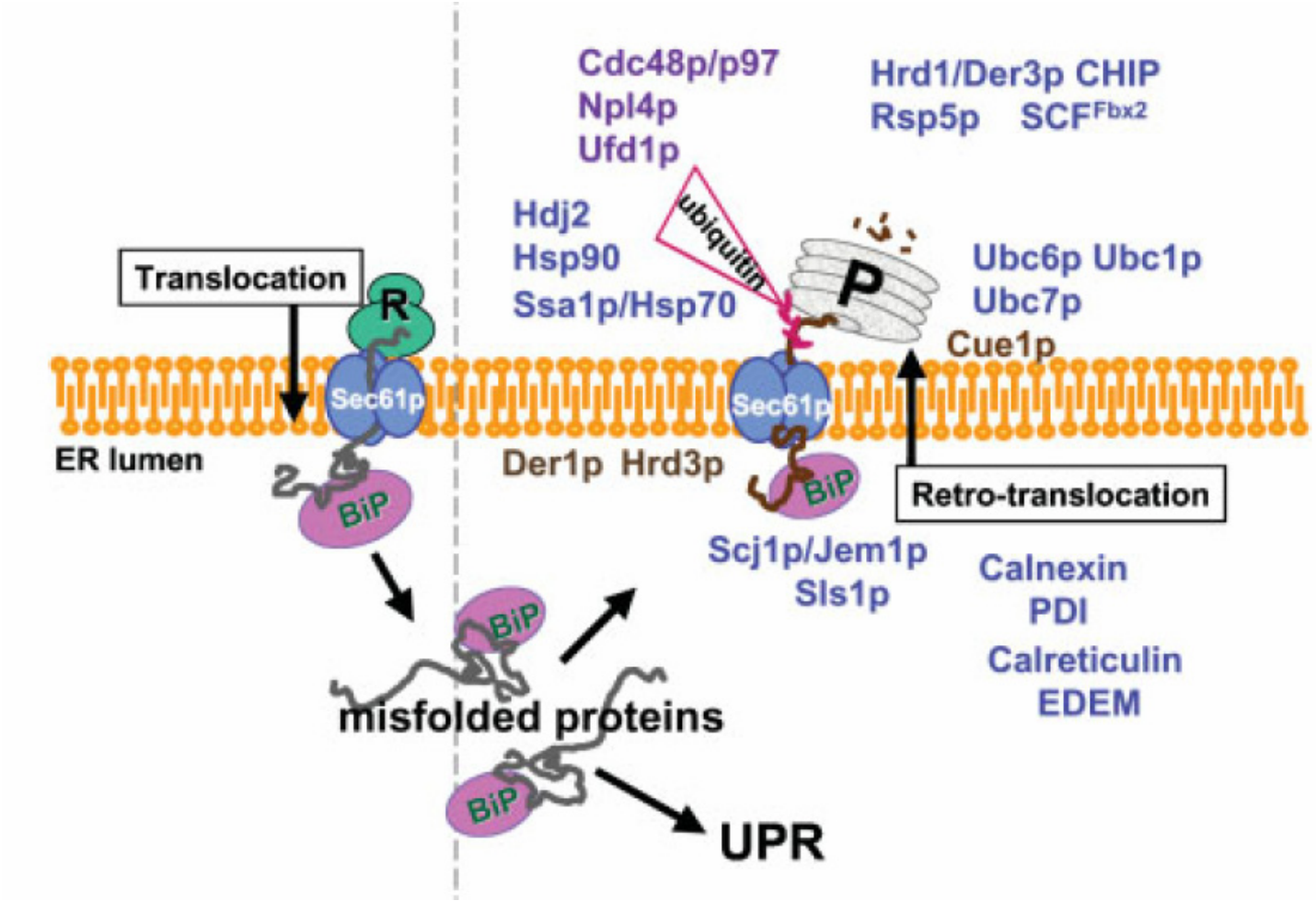

From McCracken, A.A., and Brodsky, J.L. (2003). *Bioessays* **25,** 868-877.

Table 2. Select ERAD substrates of medical relevance

ERAD substrate	**Associated disease**
a1-protease inhibitor	Emphysema and liver disease
Aquaporin-2	Nephrogenic diabetes insipidus
Beta-hexosaminidase	Tay-Sachs disease
CD4	AIDS
Collagen	Osteogenesis Imperfecta
Connexin	Charcot-Marie-tooth disease
DF508 CFTR	Cystic fibrosis
Fibrinogen Familial	hypofibrinogenemia
HMG-CoA reductase	Heart disease
Insulin receptor mutants	Type A insulin resistance
LDL receptor class II mutants	Hypercholesterolemia
MHC class I; HEF	Infantile (CMV) hepatitis
	Hereditary hemochromatosis
MPO Y173C	Myeloperoxidase deficiency
Pael-R	Parkinson's Disease
Pro-PTHrP	Hypercalcemia associated malignancy
Rhodopsin	AD retinitis pigmentosa
Thyroglobulin	ongential hypothyroid
Tyrosinase	Amelanotic melanomas
Wilson protein	Wilson disease

From McCracken, A.A., and Brodsky, J.L. (2003) *Bioessays* **25**, 868-877.

Figure 8: Dendrogram of selected members of the class 1 mannosidase family from human, Drosophila, *C. elegans*, Arabidopsis and selected fungal sources. Sequences of the conserved α-mannosidase catalytic domains were compared. The four subgroups of class 1 mannosidases, including ER mannosidase I, Golgi mannosidase I, fungal secreted mannosidase, and EDEM are shown and labeled. The GenPept numbers are noted in parentheses. The enzyme that is the subject of this dissertation is showed in pink.

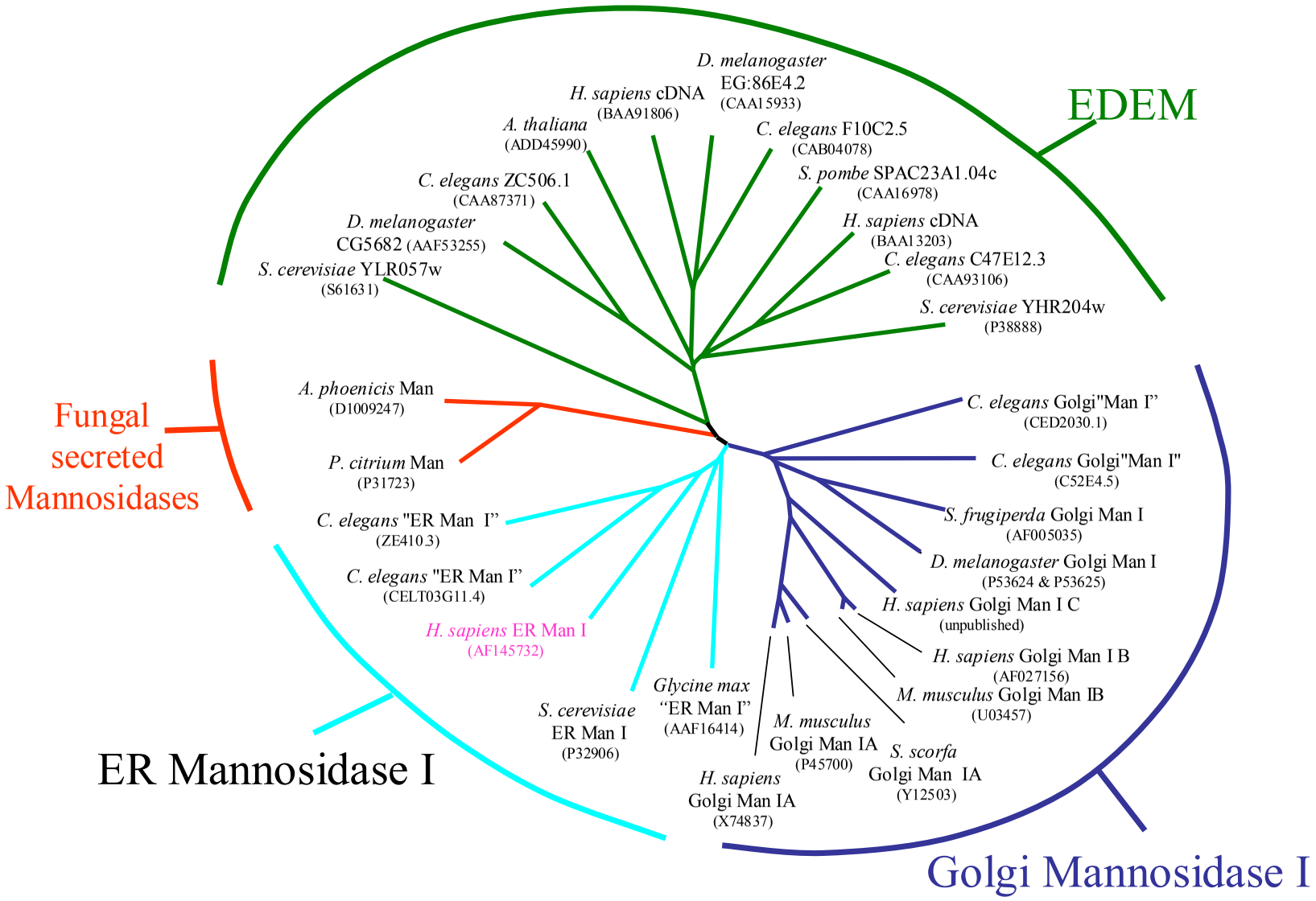

Modified from Moremen, K.W. (2000), in *A Comprehensive Handbook: Carbohydrates in Chemistry and Biology*, p. 81-117.

Figure 9: The ribbon representation of the X-ray structures of class 2 α-mannosidases. Shown are top views onto the planar surface (A and C) and the side views (C, D) of the crystal structures of Golgi mannosidase II (A and B) isolated from *Drosophia melanogaster* (*Dm*GManII; PDB:1HTY, figures from [87]) and the lysosomal α-mannosidase (C and D) from bovine sources (*Bos taurus*) (*Bt*LAM; PDB:1O7D, figures from [88]). The structures of the enzymes are similar, forming an oval shaped protein. The structures are comprised of three main domains: an NH_2-terminal α/β-domain, a three helical bundle, and an all-β COOH-terminal domain (Ig-like domain). The Zn^{2+} required for catalytic activity is found coordiated between the NH_2-terminal α/β-domain and the three helical bundle domain.

A

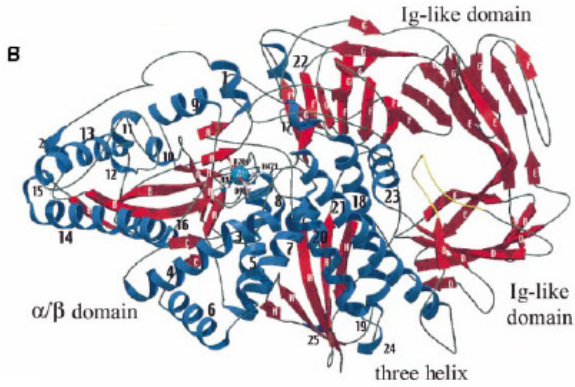
Ig-like domain
α/β domain
Ig-like
domain
three helix
bundle

B

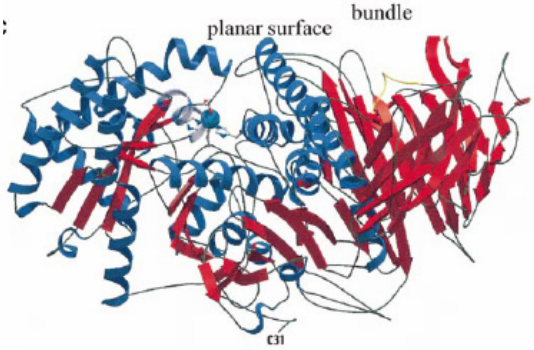
planar surface

C

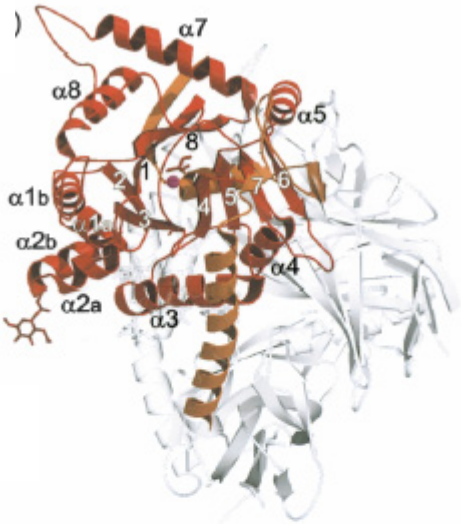
α7
α8
α5
α1b
α2b
α4
α2a
α3

D

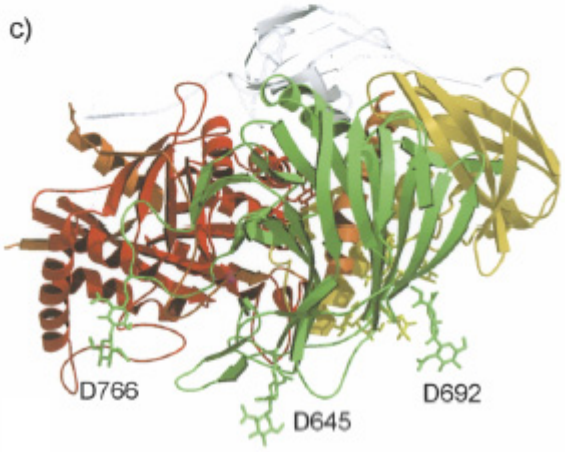
c)
D766
D645
D692

Figure 10: Catalytic mechanisms of glycosyl hydrolases. Glycosyl hydrolases catalyze the cleavage of glycosidic bonds by an acid-base hydrolysis mechanism resulting in two potential stereochemical outcomes of the released glycone as determined by the changes in anomeric configuration (a = axial, e = equatorial or α, β). The process by which the product of catalysis retains its anomeric configuration is called a retaining mechanism. The process by which the product of catalysis changes its anomeric configuration is called an inverting mechanism. The change in anomeric configuration without the enzyme catalyst, via a chemical reaction is called mutarotation.

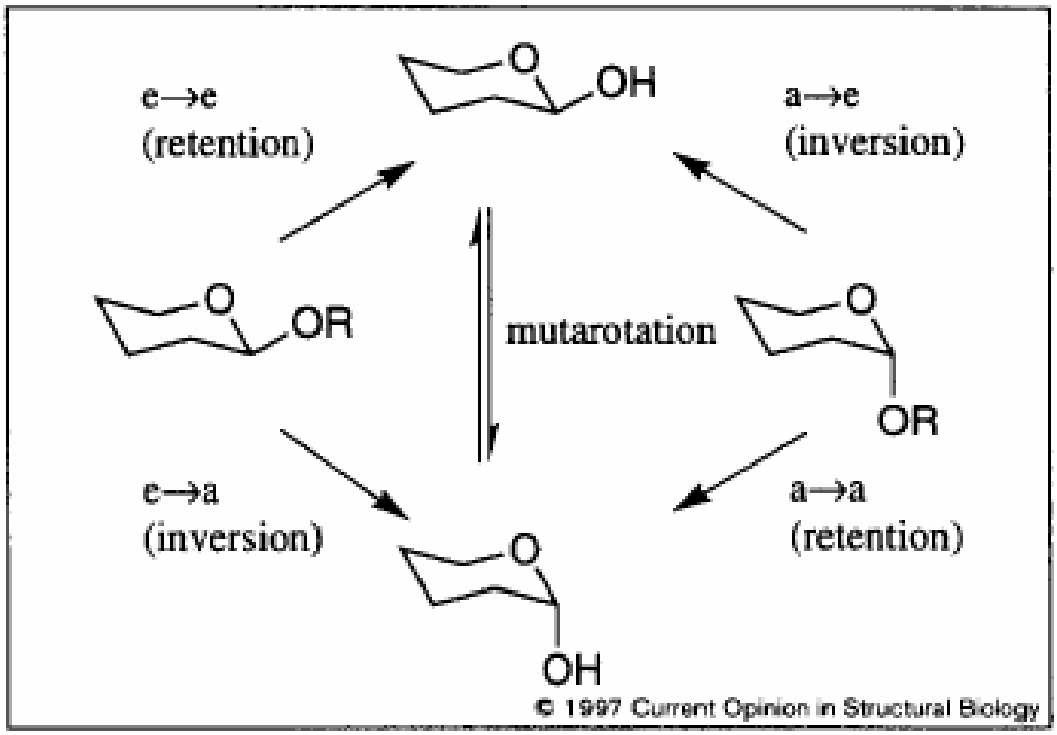

From Davies, G. and B. Henrissat (1995) *Structure*, **3**: 853-9

Figure 11: General mechanisms for inverting (a) and retaining (b) glycosidases. The hydrolysis of glycosidic bonds involves alterations in the conformation of the glycone sugar ring to allow the formation of an oxocarbenium ion followed by a bond cleavage reaction which is induced by two carboxylate side chains and a water molecule in the enzyme active site. The inverting mechanism is carried out in asingle step by protonation of the glycosidic oxygen via a carboxyl group of the general acid catalyst and an attack of the C1 position by a nucleophilic water residue which is activated by the carboxylate side chain of the general base catalyst. The retaining mechanism occurs in two steps. The first step involves the carboxyl group of the general acid/base catalyst, which protonates the glycosidic oxygen with a simultaneous nucleophilic attack of the anomeric carbon by the carboxylate side chain of the nucleophile amino acid to form a covalent bond with the glycone and the elimination of the aglycone. The second step is the deglycosylation of the covalent intermediate between the glycone and the nucleophile amino acid by the assistance of an incoming water residue, which is activated by the carboxylate group of the general acid/base catalyst, resulting in the release of the free glycone. The inverting mechanism results in the formation of a single transition state intermediate, while the retaining mechanism results in two transtion state intermediates and a transient covalent intermediate with the glycone.

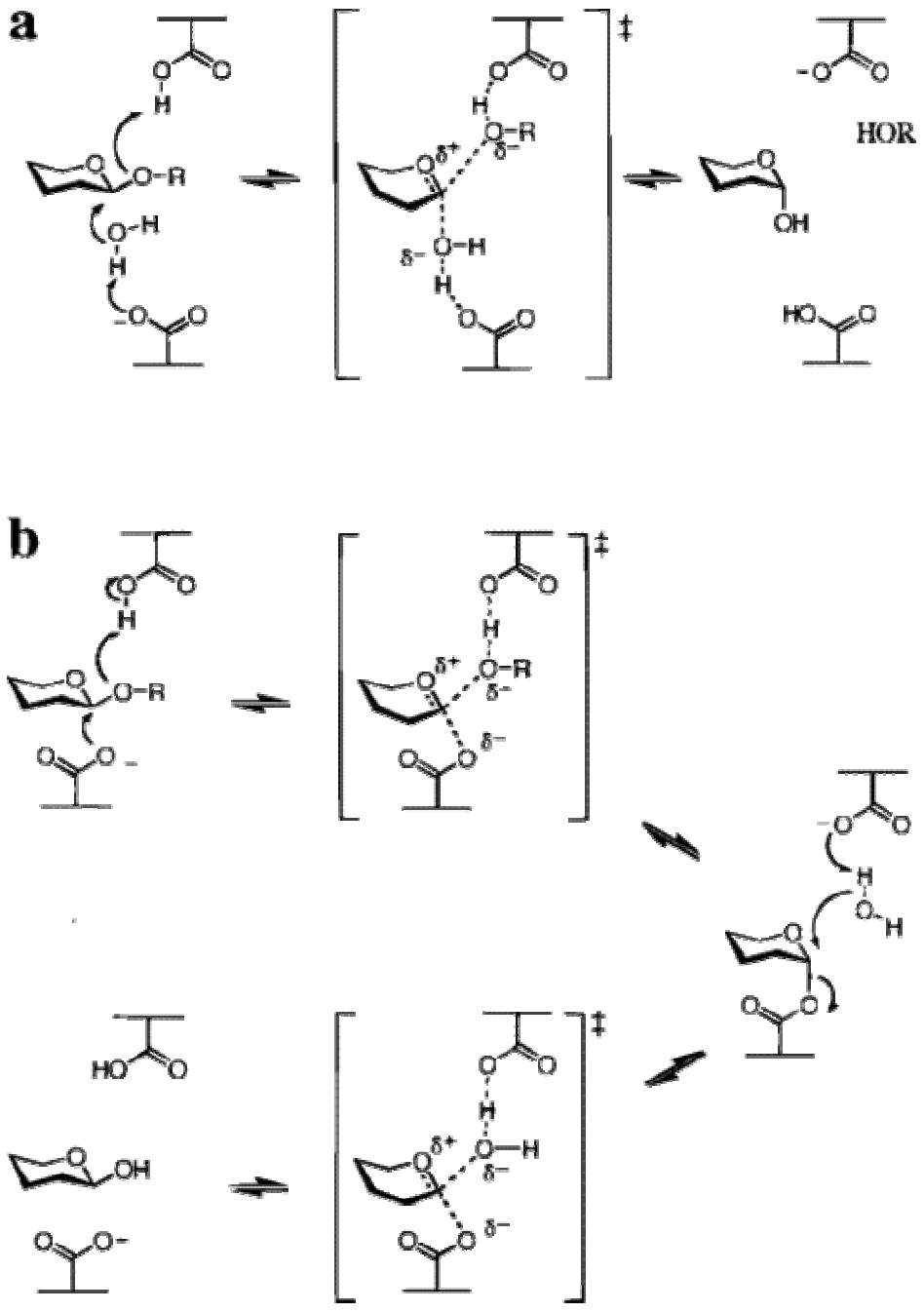

From Zechel and Withers (2000) *Acc. Chem. Res*. **33**:11-18

Figure 12: The nomenclature for the sugar-binding subsites and anomeric sugar configurations. (A) The terminology convention for the reducing and non-reducing ends of glycan substrates (trisaccharide of α1,2 mannose in Panel A) is drawn showing the non-reducing end on the left and the reducing end on the right of the trisaccharide. (B) The *+n,-n* nomenclature applied to the cleavage of a monosaccharide from the non-reducing end of a disaccharide or an oligosaccharide substrates is indicated. The point of cleavage is indicated by an arrow. Upon cleavage of the glycosidic bond, two types of products are formed. The aglycone is the product of the reducing end of the substrate, while the glycone is the product of the non-reducing end of the substrate. For the oligosaccharide substrate of the ERManI, the aglycone product is the $Man_8GlcNAc_2$ isomer B and the glycone product is a free mannose monosaccharide (shown at the bottom).

A.

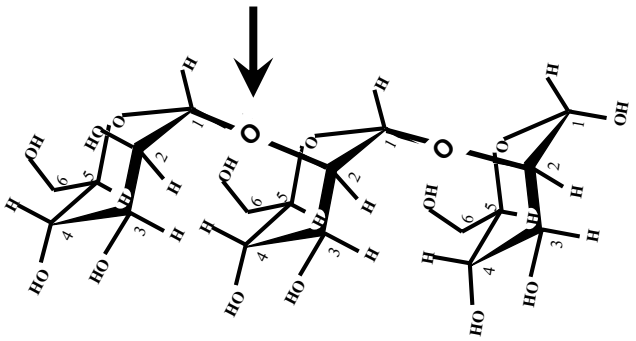

B. Nonreducing ⟷ Reducing

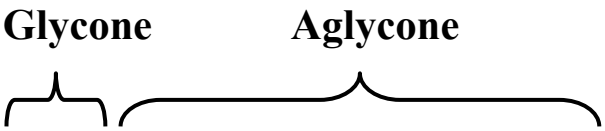

Disaccharide

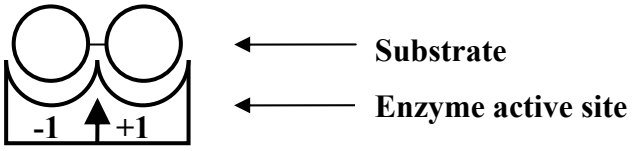

Oligosaccharide

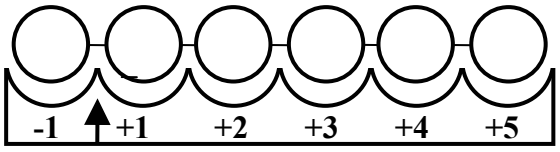

ERManI Products

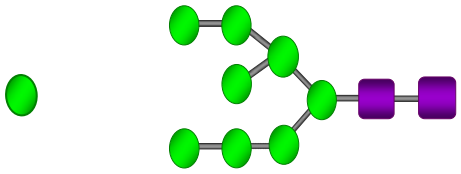

Mannose **$Man_8GlcNAc_2$**

Table 3. Selected glycoside hydrolase and the ligand in -1 subsite

Family	Mechanism[#]	Glycosidase	Ligand	conformation
GH-1	R (e→e)	*S. alba* myrosinase	D-*glucono*-1,5- lactone	$^{4}H_{3}$
			Gluco-tetrazole (*K*i = 0.7 μM)	$^{4}H_{3}$
			Gluco-hydroximolactame (*K*i = 0.6 μM)	$^{4}H_{3}$
			2-F-α-D-*glcp*-enzyme intermediate*	$^{4}C_{1}$
GH-3	R (e→e)	Barley β-D-glucan-gluc'ase	4′,4″,4^{v}-*S*-trithiocellohexaose	$^{4}C_{1}$
			Cyclohexitol-enzyme intermediate	$^{4}C_{1}$
			2-F-α-D-*glcp*-enzyme intermediate	$^{4}C_{1}$
			B-D-glucose	$^{4}C_{1}$
GH-5	R (e→e)	*B. agaradhaerens* Cel5A	2′,4′-dinitrophenyl 2-F-β-cellobioside	$^{1}S_{3}$
			2-F-α-cellotriosyl-enyzme intermediate	$^{4}C_{1}$
			Cellotriose	$^{4}C_{1}$
			Methyl 4″,4‴-*S*-dithio-α-cellobiosyl-β-cellobioside	$^{4}C_{1}$[‡]
			Methyl 4′,4″,4‴,4^{IV}-*S*-tetrathio-α-cellopentaoside	$^{4}C_{1}$
GH-6	I (e→a)	*T. reesei* Cel6A	Methyl 4″-*S*-thio-β-cellotetraoside	$^{2}S_{O}$
GH-7	R (e→e)	*F. oxysporum* Cel7B	Methyl 4′,4″,4‴-*S*-trithio-α-cellotetraoside	$^{1}S_{3}$
GH-10		*C. fimi* Cex	*xylobio*-isofagomine (*K*i = 130 nM)	$^{4}C_{1}$
			xylobio-deoxynojirimycin (*K*i = 5800 nM)	$^{4}C_{1}$
			xylobio-lactame oxime (*K*i = 370 nM)	^{4}E
			xylobio-imidazole (*K*i = 150 nM)	^{4}E
GH-11	R (e→e)	*B. agaradhaerens* Xyl11	2-F-α-xylobiosyl-enzyme intermediate	$^{2,5}B$
GH-11	R (e→e)	*B. agaradhaerens* Xyn11	2-F-α-xylobiosyl-enzyme intermediate	$^{2,5}B$
		B. agaradhaerens Xyn11 (E93A)	α-Xylotriose	$^{2,5}B$
GH-11	R (e→e)	*B. circulans* Xyl11	2-F-α-xylobiosyl-enzyme intermediate	$^{2,5}B$
GH-18	R (e→e)	*S. marcescens* ChiA (D313A)	Octa-*N*-acetylchitooctaose	$^{1,4}B$
		S. marcescens ChiA (E315Q)	Octa-*N*-acetylchitooctaose	$^{1,4}B$
		S. marcescens ChiA (Y390F)	Hexa-*N*-acetylchitohexaose (cleaved)	$^{1,4}B$
GH-18	R (e→e)	*S. marcescens* ChiB	Allosamidine	^{4}E
		S. marcescens ChiB (E144Q)	Penta-*N*-acetylchitopentaose	$^{1,4}B$
GH-20	R (e→e)	*S. marcescens Sm*CHB	Di-*N*-acetylchitobiose	^{4}E
		*S. marcescens Sm*CHB (D539A)	Di-*N*-acetylchitobiose	$^{1,4}B$
		*S. marcescens Sm*CHB (E540D)	Di-*N*-acetylchitobiose	$^{1,4}B$
GH-20	R (e→e)	*S. plicatus* SpHEX	GlcNAc-thiazoline	$^{4}C_{1}$
			GalNAc-isofagomine (*K*i = 2.7 μM)	$^{4}C_{1}$
GH-22	R (a→a)	Hen egg-white lysozyme (E35Q)	2-F-α-chitobiosyl-enzyme intermediate	$^{4}C_{1}$
GH-26	R (e→e)	β-D mannanase	2′,4′-dinitrophenyl 2-F-β-D-mannotrioside	$^{1}S_{5}$
			2-F-α-D-mannotriosyl-enzyme	$^{2}S_{O}$
GH-27	R (a→a)	Chicken α-*N*Ac-galactosaminidase	α-*N*-acetylgalactosamine	$^{4}C_{1}$
GH-47	I (a→e)	Human ER α-1,2-mannosidase I	Kifunensin	$^{1}C_{4}$
			1-Deoxymannojirimycin	$^{1}C_{4}$

[#]R stands for retaining and I stands for inverting. *2-F stands for 2-deoxy-2-fluoro. [†] The –1 α-D-glucopyranosyl unit mimics a distorted β-D-glucopyranosyl residue. [‡]The substrate does not bind in the 'true' –1 subsite. [§]Ca^{2+} coordinates to OC(2) and OC(3) and stabilises the $^{1}C_{4}$ conformation. R

Modified from Vasella, *et al* (2002) *Curr. Opin. Chem. Biol*. 6:619-629.

Figure 13: Interconversion of sugar ring conformations highlighting the proposed transition states employed by glycosidases. Pyranose ring sugar conformational interconversions are shown with nomenclature for the reference plane of four ring atoms (shaded blue) as per IUPAC-IUB rules [111]. Routes are noted for the interconversion between conformers from the low free energy $^{4}C_{1}$ chair conformation through various half chair (*H*), boat (*B*), and skew-boat (*S*) conformations. Only four of the conformations have a co-planarity at C5-O5-C1-C2 (red shading in $B_{2,5}$, $^{4}H_{3}$, $^{2,5}B$, and $^{3}H_{4}$) [95]. Overlap of the nomenclature reference plane and the C5-O5-C1-C2 plane is indicated by brown shading. The blue boxed regions illustrate the proposed transition state conformations for $B_{2,5}$, $^{4}H_{3}$, and $^{2,5}B$ bracketed by conformations that have been identified based on the isolation of trapped intermediates in various co-crystal studies with inverting and retaining enzymes. The red boxed region illustrates the potential $^{3}H_{4}$ transition state for Class 1 (family 47) α-mannosidases bracketed by the $^{4}C_{1}$ chair conformation found for the ERManI-dMNJ complex and the $^{3}S_{1}$ conformation described in this dissertation.

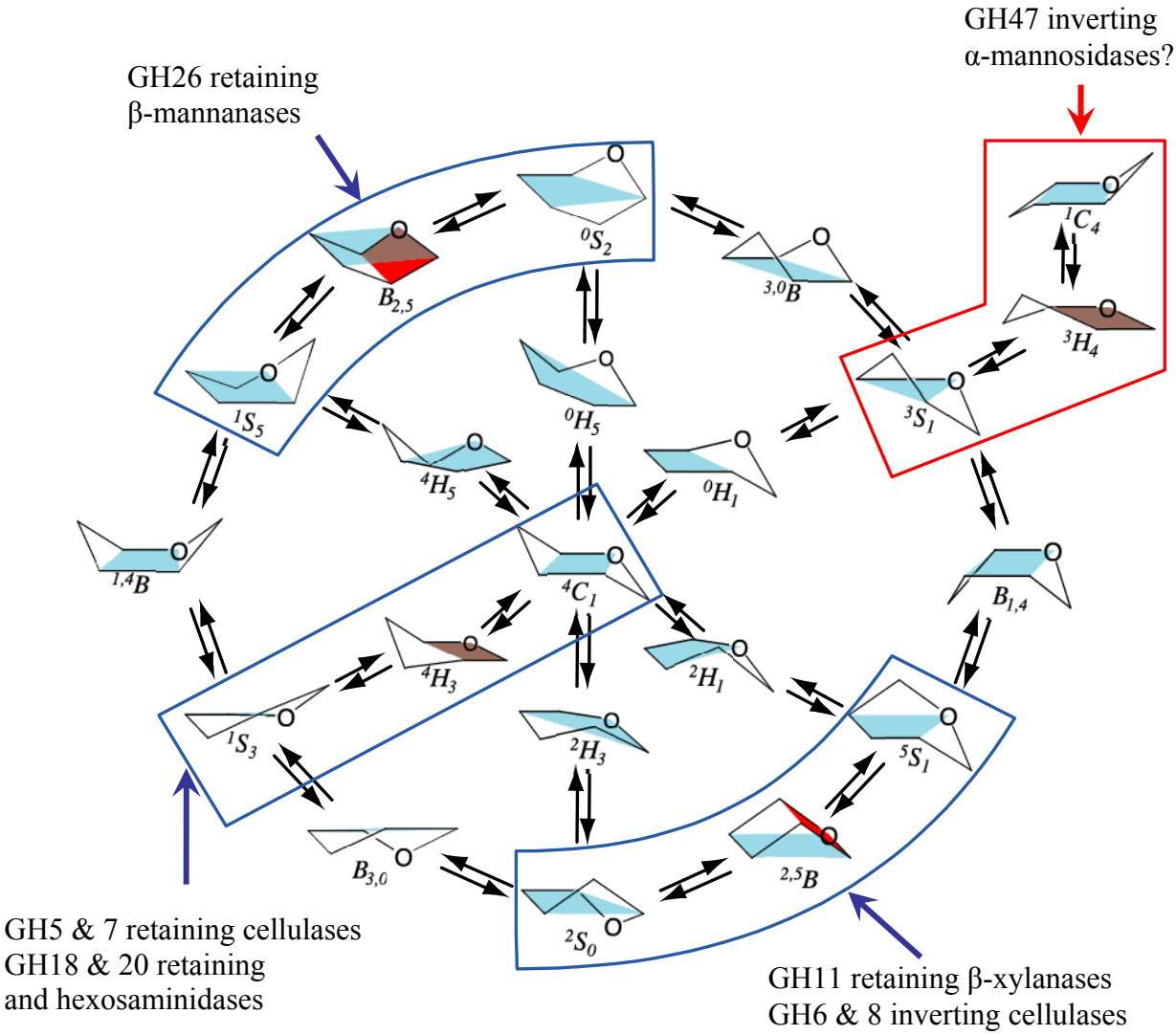

Created by Moremen, KW (2004)

Table 4. Crystal structures of Class 1 mannosidases

Subfamily	**ER Mannosidase**		**Golgi Mannosidase**	**Fugal secreted Mannosidase**	
Source of enzyme	Yeast (*S. cerevisiae*)	Human (*H. sepien*)	Mouse (*M. musculus*)	Pennidilium (*P. citrinum*)	Trichoderma (*T. Reesei*)
Name	*Sc*ERManI	*Hs*ERMan	*Mm*GManIA	*Pc*ManI	*Tr*ManI
Catalytic domain amino acids	34-539	239-697	178-644	36-510	7-494
Crystal structures					
Native					
PDB	1DL2	1FM1	1NXC	1KKT	1HCU
Resolution (Å)	1.54	1.90	1.51	2.2	2.37
Space group	$P3_121$	$P3_121$	$P2_12_12_1$	$P12_11$	$P12_11$
dMNJ					
PDB	1G6I	1FO2		1KRE	
Resolution (Å)	1.59	2.38		2.2	
Space group	$P3_121$	$P3_121$		$P12_11$	
KIF					
PDB		1FO3		1KRF	
Resolution (Å)		1.75		2.2	
Space group		$P3_121$		$P12_11$	
Catalytic residues					
General acid	E132	E330	E282	E100	E122
General basic	E435	E599	E549	E409	E393
Ca^{2+} coordination	T525	T688	T635	T501	T485
Substrate binding (M7)	D275	D463	D415	D267	D245
Glycone hydrophobic interaction	F499	F659	F607	F468	F452
H-bonding to M3	R273	R461	L413	G625	L243
Chiobiose hydrophobic Interaction[a]	N196, A198	T394, A396	**W339, W341**	H186, N188	A170, S172

[a] The residues in bold were found to form stacked hydrophobic interactions with the chitobiose core of the oligosaccharide substrate at the opening of the binding cleft of the *Mm*GManIA structure. The residues found at the equivalent positions for the other class 1 α-mannosidases are indicated, although there is no indication that these residues interact with the respective oligosaccharide substrates.

Figure 14: Class 1 α1,2-mannosidase X-ray structures. Schematic ribbon representation viewed down the $(\alpha\alpha)_7$-barrel (the left column) and at 90° to the first orientation (right column). The calcium ion (Ca) is represented as a dark green sphere. Shown in A and B is the structure of *S. cerevisiae* ER mannosidase I (*Sc*ERManI; Protein Data Bank 1DL2) [66]; C and D is the structure of human ER mannosidase I (*Hs*ERManI; Protein Data Bank 1FM1) [14]; E and F is the structure of *T. reesei* α-mannosidase (*Tr*ManI; Protein Data Bank 1HCU) [68]; G and H is the structure of *P. citrinum* α-mannosidase (*Pc*ManI;Protein Data Bank 1KKT) [69]; I and J is the structure of mouse Golgi mannosidase IA (*Mm*GManIA; Protein Data Bank 1NXC) [15]. The long connection (LC side) and the short connect (SC side) are indicated. The stick form represents the N-linked glycan associated with the *Sc*ERManI, *Pc*ManI or *Mm*GManIA structures.

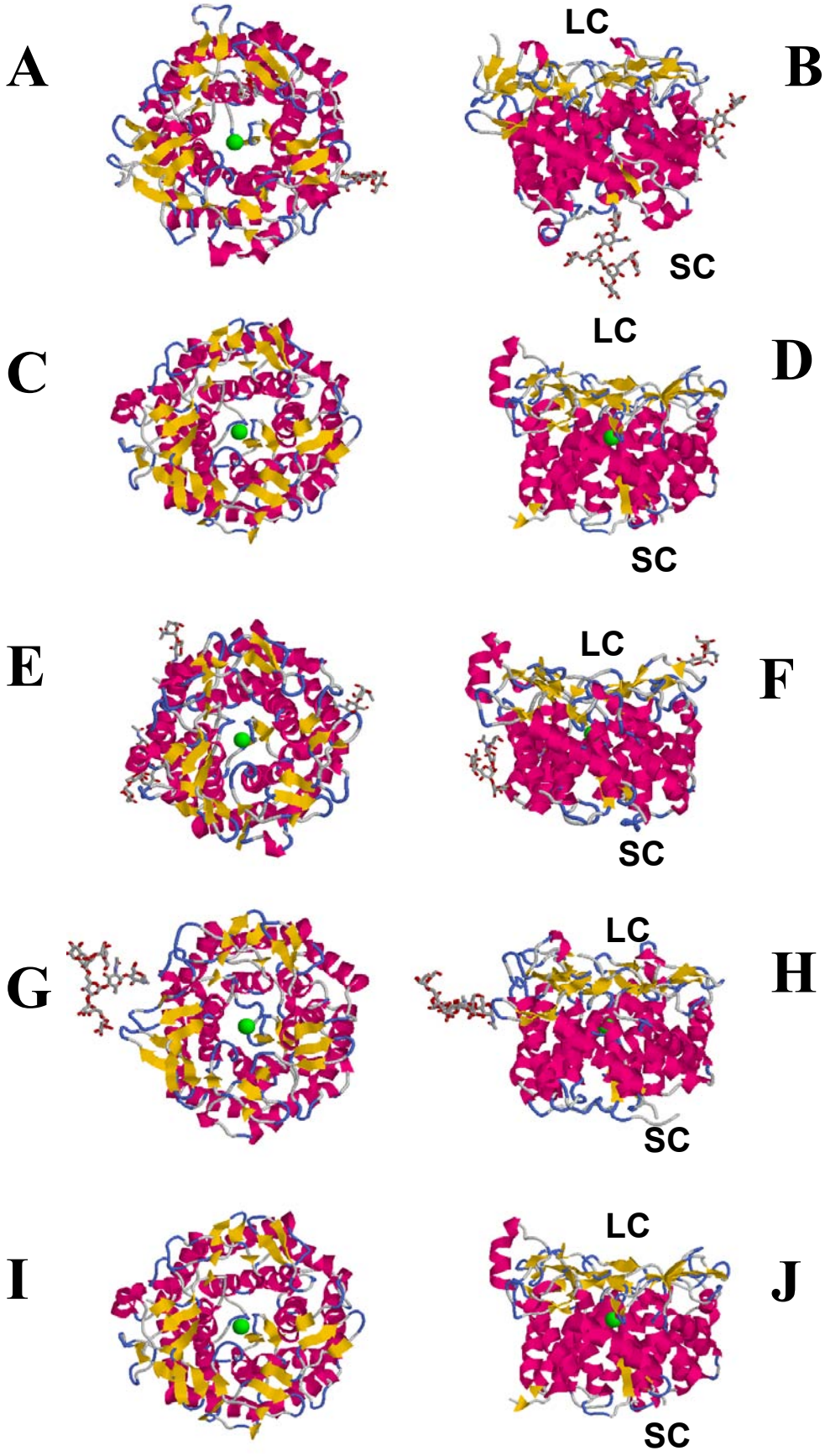
A
B
LC
SC
C
D
LC
SC
E
F
LC
SC
G
H
LC
SC
I
J
LC
SC

Figure 15: Alignment of class 1 α1,2- mannosidase catalytic domain protein sequences.

The sequence of the catalytic domain of murine Golgi mannosidase IA is compared with the catalytic domain sequences of other Class 1 mannosidases. (A) Sequence data include human ER mannosidase I (*Hs*ERManI; Protein Data Bank 1FO2), *S. cerevisiae* ER mannosidase I (*Sc*ERManI; Protein Data Bank 1DL2), *P. citrinum* α-mannosidase (*Pc*ManI; Protein Data Bank 1KKT), *T. reesei* α-mannosidase (*Tr*ManI; Protein Data Bank 1HCU), and mouse Golgi mannosidase IA (*Mm*GManIA; Protein Data Bank 1NXC). Sequences are numbered from the NH_2 terminus of the intact protein. The coloring of the sequence labels is the same as the coloring of the C_α backbone and carbon atom coloring in Panels B and C, respectively. The *spiral sketches* indicate segments of helical structure and the *arrows* indicate segments of β-sheet structure. Secondary structure is shown for *Hs*ERManI (above the sequence) and *Mm*GManIA (below the sequence). *Green* Asn residues with an *asterisk* in the sequence alignments are sites of *N*-glycosylation within the respective protein in the crystal structure. B, a stereo view of the aligned C_α backbone representation of *Mm*GManIA (*orange*), *Hs*ERManI (*magenta*), *Tr*ManI (*gray*), and *Pc*ManI (*green*), demonstrating the similarity in backbone position in the core of the barrel but deviation in structure in the periphery of the barrel. *C*, a stereo view of the positions of amino acid side chains in the -1 glycone binding site for the aligned Class I mannosidases (within 5 Å of dMNJ in the aligned structures). Protein structures were aligned for *Mm*GManIA (*orange*), *Hs*ERManI (*magenta*), *Sc*ERManI (*cyan*), *Pc*ManI (*green*), and the *Tr*ManI (*gray*), and the amino acid side chains are shown in *stick form* and the associated calcium ion is shown in a *space-fill representation* in the *color* of the respective protein structure. The structure of dMNJ in the -1 glycone binding site was derived from the *Hs*ERManI structure (Protein Data Bank 1FO2) and is shown in *white stick form.* Residue numbering is based on the residues from *Mm*GManIA.

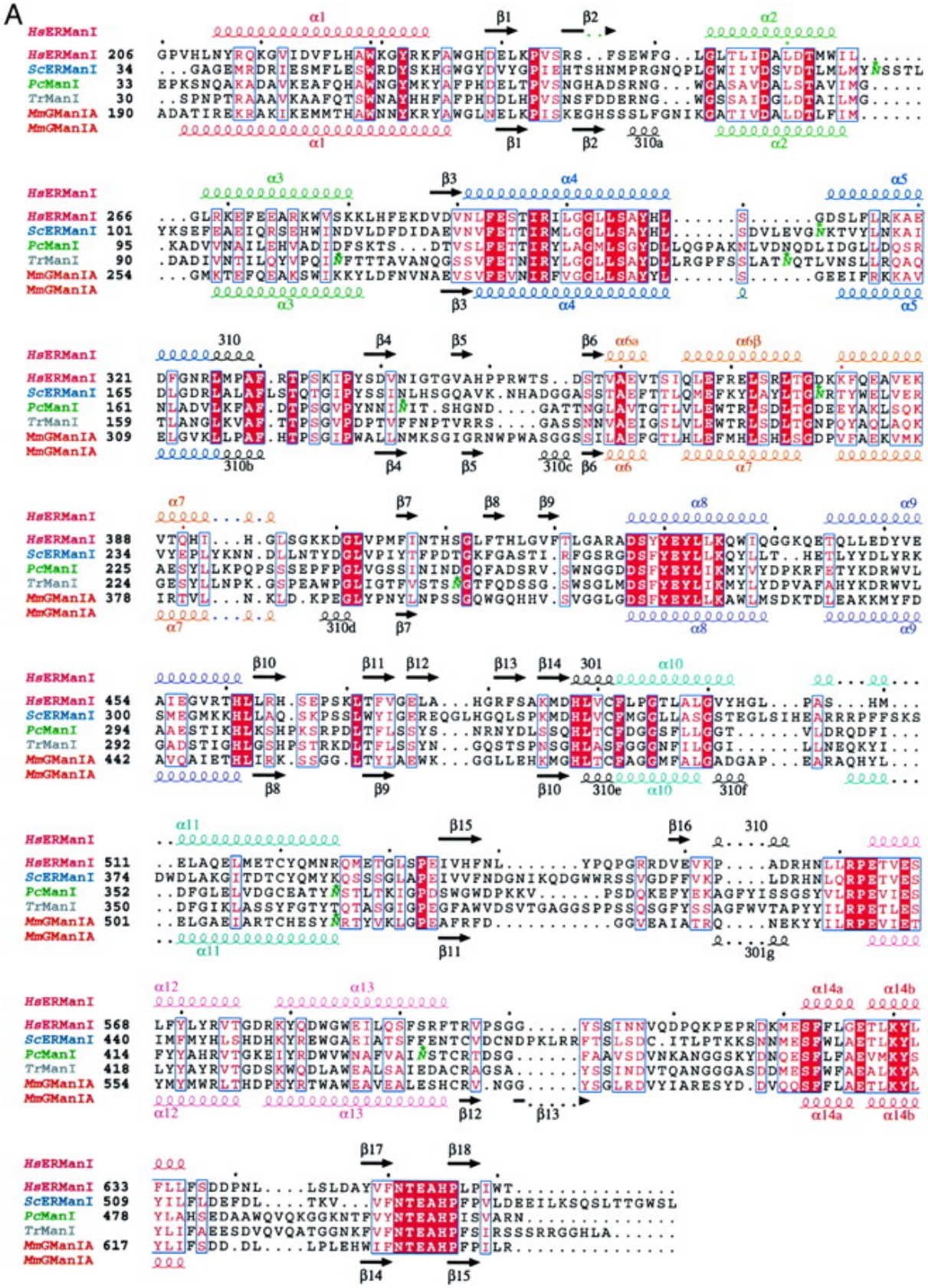
A
HsERManI
ScERManI
PcManI
TrManI
MmGManIA
α1
β1
β2
α2
α3
β3
α4
α5
310
β4
β5
β6
α6a
α6β
310b
310c
α6
α7
β7
β8
β9
α8
α9
310d
β10
β11
β12
β13
β14
301
α10
β8
β9
β10
310e
310f
α11
β15
β16
310
301g
α12
α13
α14a
α14b
β12
β13
β17
β18
β14
β15

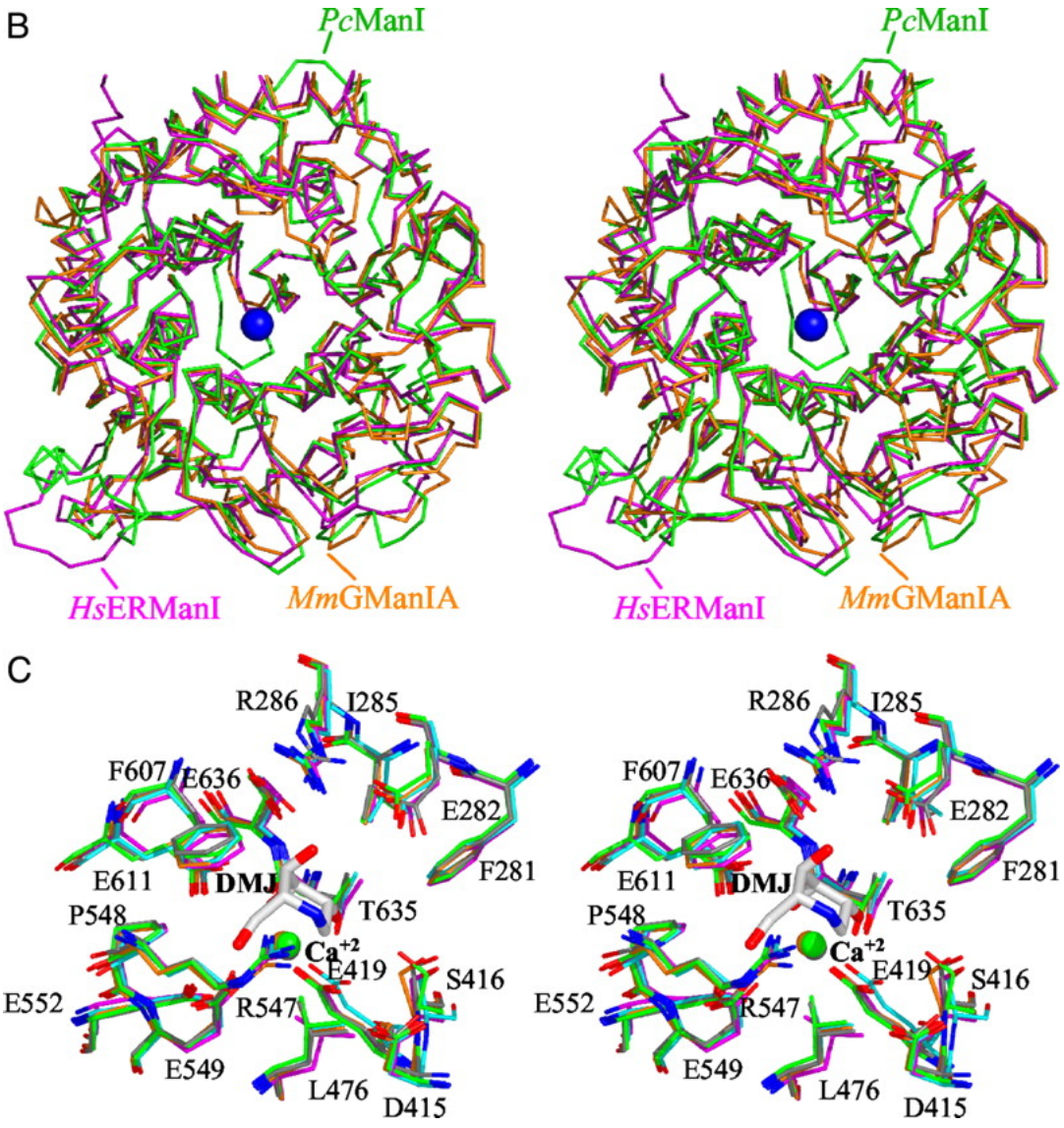

FromTempel, W., K. Karaveg*, et al.* (2004) *J. Biol. Chem.* **279**: 29774-86.

Figure 16: The crystal packing of *S. cerevisiae* ER mannosidase I (*Sc*ERManI) (A) and mouse Golgi mannosidase IA (*Mm*GManIA) (B). The N-linked oligosaccharide associated with each enzyme was found extended into the enzyme active site of an adjacent molecule in the crystal lattice, which is related by crystallographic symmetry. The N-linked glycan found in the active site of *Mm*GManIA (Protein Data Bank 1NXC, figure from [15]) resembles the $Man_5GlcNAc_2$ product. The N-linked glycan found in the active site pocket of *Sc*ERMan (Protein Data Bank 1DL2, figure from [66]) resembles the binding of the $Man_8GlcNAc_2$ isomer B product (the oligosaccharide chain indicated as HM1).

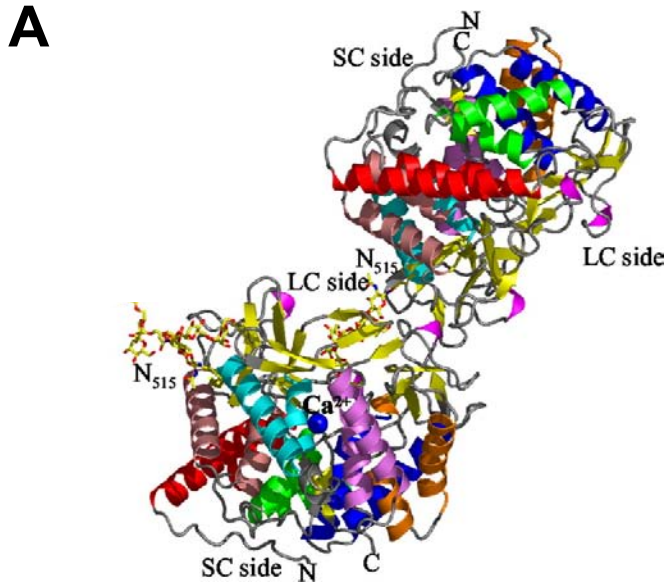
A
N
C
SC side
LC side
N_{515}
LC side
N_{515}
Ca^{2+}
SC side
N
C

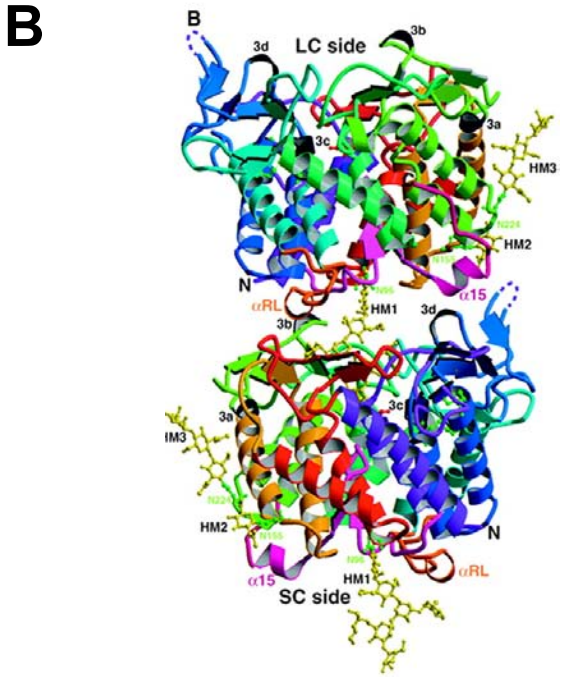
B
3d
LC side
3b
3a
3c
HM3
HM2
N
αRL
HM1
α15
3b
3d
3c
3a
IM3
HM2
N
α15
HM1
αRL
SC side

Figure 17: Comparison of the oligosaccharide conformations found in the active sites of (A) mouse Golgi mannosidase IA (*Mm*GManIA) and (B) *S. cerevisiae* ER mannosidase I (*Sc*ERManI). Shown are the schematic diagrams of the conformations of the bound oligosaccharides relative to the active site calcium (*blue sphere*) and the glycone residue in the -1 binding site (*green hexagon*, missing in the crystal structure). The *arrow* indicates the position of the glycosidic bond that is cleaved by the enzyme. C and D, the respective oligosaccharides in *stick form colored* as in the corresponding schematic diagrams in A and B respectively. Orientation of the glycans was based on a similar positioning of the residue in the -1 site (residue M6 for *Mm*GManIA and residue M7 for *Sc*ERManI). The positioning of the glycone in the equivalent of the -1 binding site (*green* sugar) was attained by using the positioning of 1-deoxymannojirimycin (dMNJ) in the active site of human ER mannosidase I (Protein Data Bank 1FO2) after aligning the latter enzyme with either the *Mm*GManIA or *Sc*ERManI structures (Protein Data Bank 1NXC and 1DL2, respectively). The monosaccharide shown in *gray* is an α1,6-mannose added to the trimmed oligosaccharide during secretion in *P. pastoris*. The *arrows around* the M3-α1,6-M4 linkage in A and B indicate that the major differences in position of distal residues in the glycan structure within the glycan binding site result from a rotation around this linkage. Also shown are the spacefill representations of (E) *Mm*GManIA and (F) *Sc*ERManI peptide structures with the oligosaccharides associated with each respective active site. The stick form of oligosaccharides shown in *magenta* and *blue* were derived from the *Mm*GManIA and *Sc*ERManI structures, respectively, after structural alignment (RMS = 1.14 Å). The calcium ion was shown in green in panel E and F and the dMNJ (Protein Data Bank 1G6I) was shown in blue stick form. The red circles indicate the steric hindrance that prevents the *Mm*GManIA to bind inappropriate terminal branches of the oligosaccharide (for this instance, the branch B) in the wrong orientation. This steric hindrance explains the enzyme branch specificity for α1,2

mannoside cleavage. In particular, GManIA cleaves branches A and C much more efficiently than that of branch B, whereas ERManI cleaves branch B more efficiently than branches A and C.

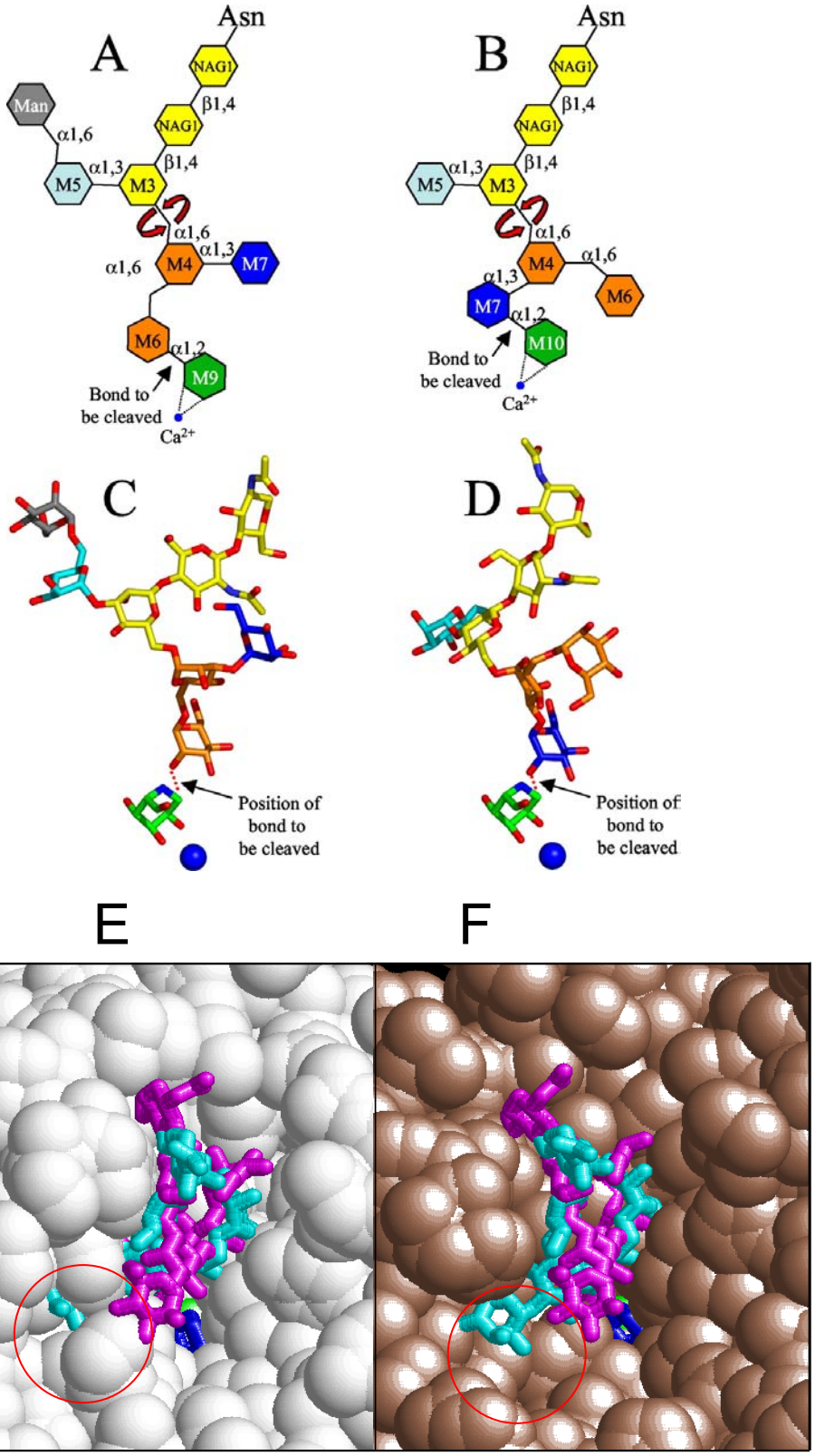

Modified from Tempel, W., K. Karaveg*, et al.* (2004) *J. Biol. Chem.* **279**: 29774-86.

Figure 18: Cross-section views of the active sites and glycan binding clefts of representative class 1 mannosidases. Three representative Class 1 α-mannosidase structures (mouse Golgi mannosidase IA (Mouse Golgi Man IA) (A and B), *P. citrinum* α-mannosidase (P. citrinum Man I) (C and D), and human ER mannosidase I (Human ER Man I) (E and F)) were aligned. The residues within 8 Å of the glycan associated with the *Mm*GManIA oligosaccharide binding site were selected for surface rendering. Two cross-sectioned enzyme surface representations were rendered at right angles from each other for each of the enzymes (*gray surface*). For reference, the glycan from the *Mm*GManIA structure is shown in *yellow stick form* in each of the respective enzyme surface structures. dMNJ bound in the -1 glycone site (*green stick form*) and the calcium ion (*blue space-filling representation*) bound at the base of the active site pocket are also shown and were obtained from the *Hs*ERManI structure (Protein Data Bank 1FO2). Measurements across the +1 binding site were made using the nearest equivalent atoms spanning each of the respective cross-sections (*lower* indicated angstrom measurements in each respective *panel*). Similarly, measurements were made across the upper portion of the glycan binding clefts at approximately similar positions and orientations (*upper* angstrom measurements in each respective *panel*). Significant differences in the structures and residues flanking the glycan binding clefts in each of the enzymes made it impossible to measure identical spans for each enzyme, but the residues used in the respective measurements are indicated and shown in *stick form* in each *panel.* A, C, and E are all in identical orientations, and B, D, and F are all in identical orientations.

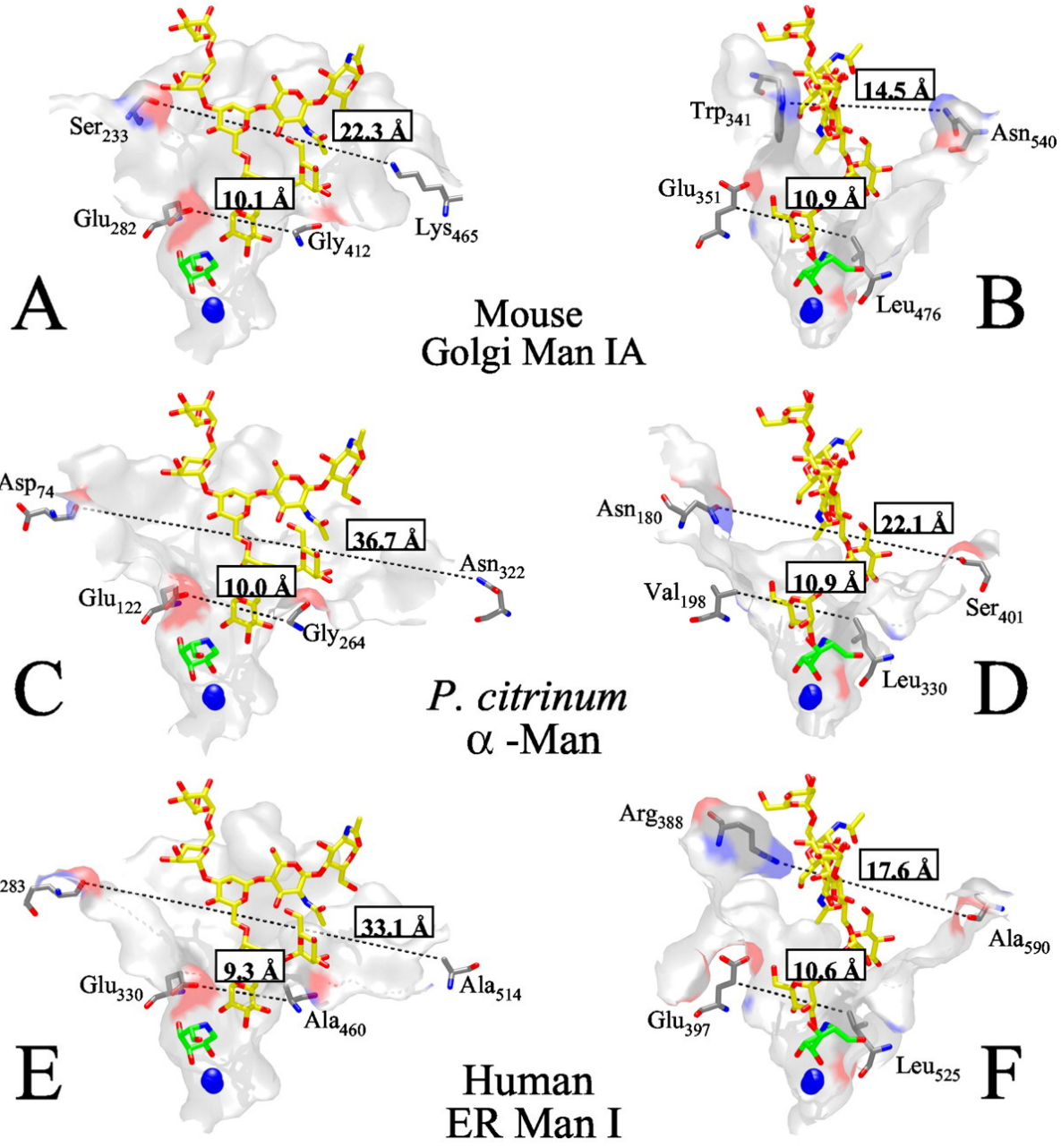

From Tempel, W., K. Karaveg, *et al.* (2004) *J. Biol. Chem.* **279**: 29774-86.

Figure 19: Binding of 1-deoxymannojirimycin and kifunensine to *Hs*ERManI. A, Location of kifunensine or 1-deoxymannojirimycin in the center of the $(\alpha\alpha)_7$-barrel. *Short* and *long dashed lines* represent hydrogen bond interactions and van der Waals contacts, respectively. Only hydrogen bonds between the protein, water, and inhibitor molecules are represented. Water-water hydrogen bonds are not represented. Interactions between ERManI and kifunensine (Panel B) or ERManI and 1-deoxymannojirimycin (Panel C) , respectively. D, surface representation of the catalytic cavity of *Hs*ERManI in the vicinity of the kifunensine-binding site. The surface is colored according to its electrostatic potential. Kifunensine is shown in stick representation. The contour level is at ±20 kT.

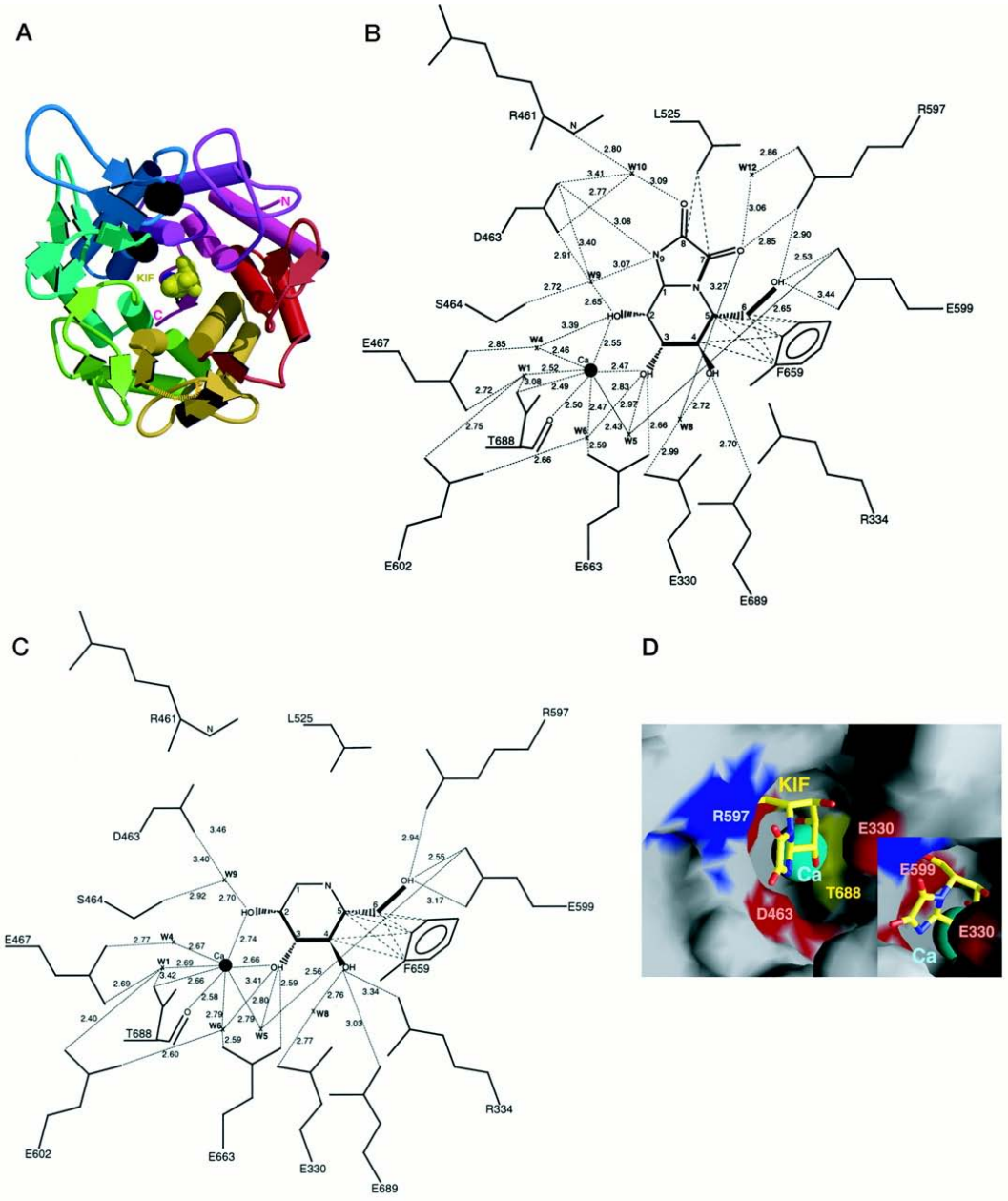

From Vallee, F., K. Karaveg*, et al.* (2000) *J. Biol. Chem.* **275**: 41287-98.

Figure 20: The *Hs*ERManI active site geometry. (A) The stick representation of kifunensine (Kif), a mannose analog is shown relative to the positon of key active site residues in the glycone binding site (-1 subsite) of human ERManI (*Hs*ERManI, Protein Data Bank, 1FO3). The putative catalysts (E330, D463 and E599), critical amino acid residues (F659 and T688), waters (W1-6) and calcium (green) were shown. The distances between E330-D463, E330-E599 and D463-E599 are shown as 9.65, 10.34, and 7.69 Å, respectively. The water residues shown in pink (W1 and W5) are proposed to have a direct role during catalysis, while the water residue shown in yellow (W6), also postulated as a possible nucleophile assisted by D463, is shown to not provide an appropriate geometry for catalysis. Also shown are 3D structures and chemical structures of mannose (Man) (B), 1-deoxymannojirimycin (dMNJ) (C) and kifunensine (Kif) (D). Mannose is shown in the $^{4}C_{1}$ conformation, while dMNJ and Kif are shown in $^{1}C_{4}$ conformation as found in association with the *Hs*ERManI -1 subsite in Protein Data Bank files 1FO2 and 1FO3, respectively.

A.

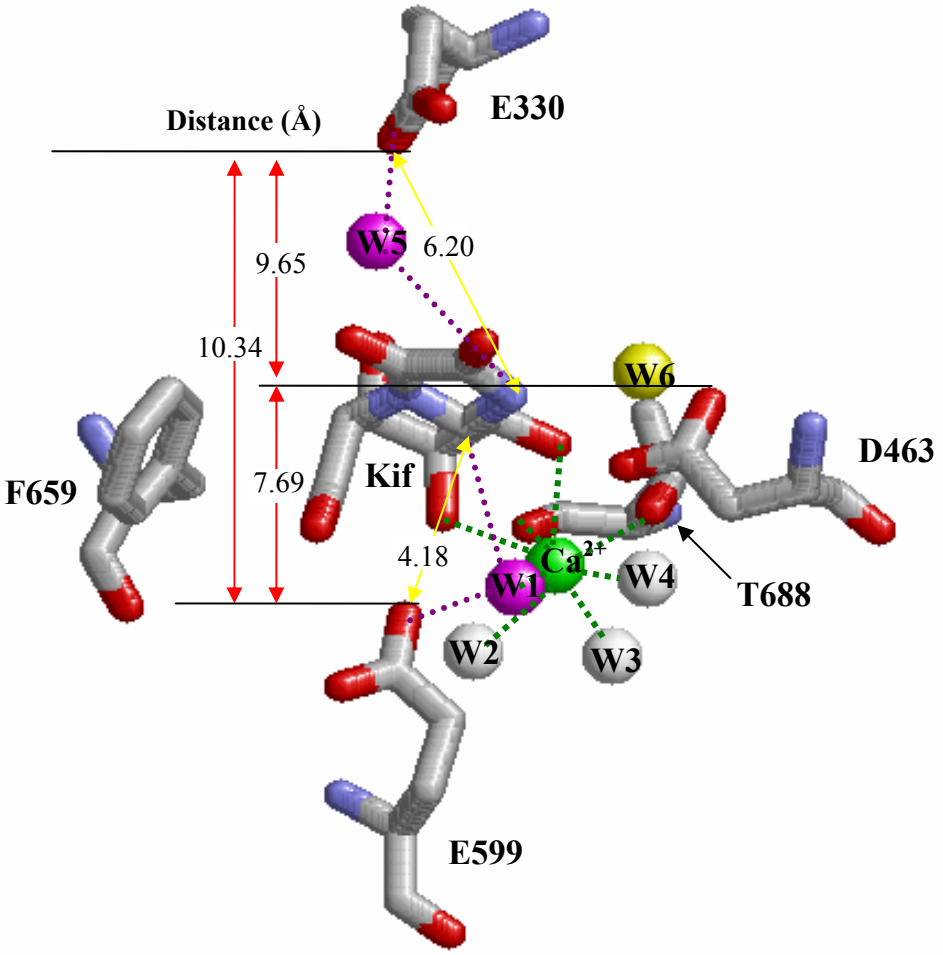

B.

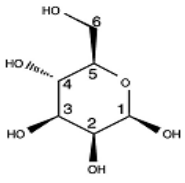

α-Mannose
(Man)

C.

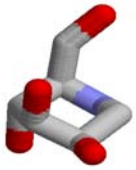

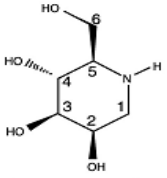

1-deoxymannojirimycin
(dMNJ)

D.

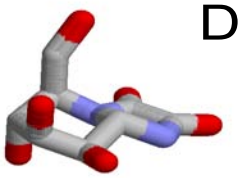

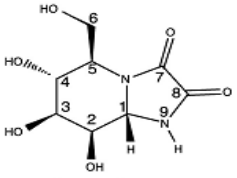

Kifunensine
(Kif)

Figure 21: Proposed mechanism of class 1 α1,2-mannosidase. A, close-up of the putative linkage between the O-2' atom of Man7 in *S. cerevisiae* ER mannosidases I (*Sc*ERManI) (Protein Data Bank, 1DL2) and the C-1 atom of in the dMNJ structure. The atom colored *red* lies in the plane defined by the nitrogen, C-2, C-3, and C-5 atoms and represents the putative deformation of the ring during catalysis. *B*, proposed catalytic mechanism.

A.

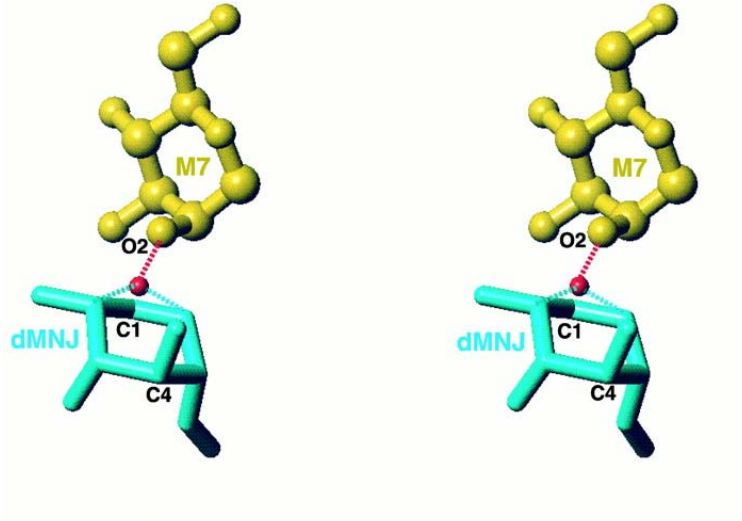

B.

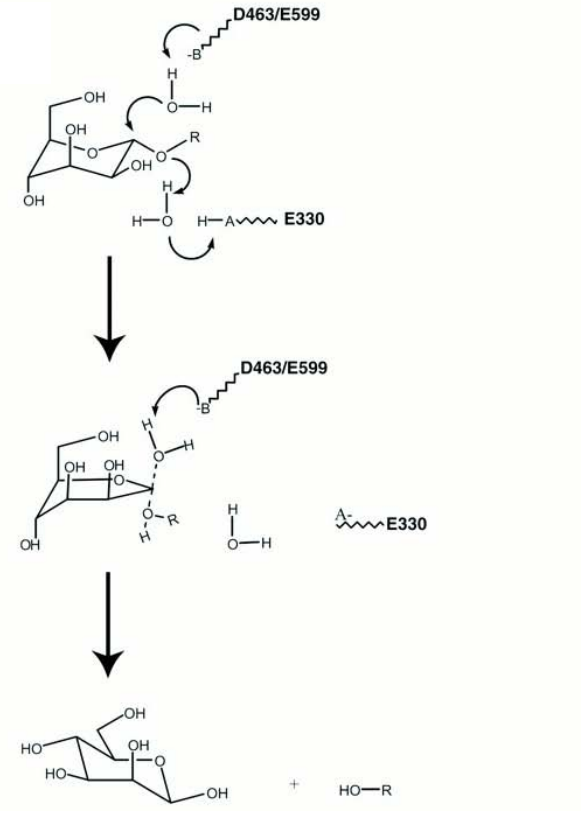

From Vallee, F., K. Karaveg, *et al.* (2000) *J. Biol. Chem.* **275**: 41287-98.

CHAPTER 2

MATERIALS AND METHODS

2.1 Cloning and expression of human ERManI

The wild type cDNA encoding *Hs*ERManI was cloned [10] and expressed as previously described [14]. Briefly, the putative cDNA encoding *C. elegans* and yeast mannosidase class 1 homologues were used to identify the mannosidase coding regions in the human cDNA database. The partial cDNA clone encoding the catalytic domain of a human coding region with greatest similarity to yeast ERManI was extended using the 5′-RACE approach with a poly(A) tail-containing EST (R55729) and human placenta cDNA as template. The final 2679-bp PCR amplimer was then subcloned into the pPROTA fusion vector at an *Eco*RI site to generate a human ERManI homolog-protein A fusion (pPROTA-ERManI). The construct was transformed into *E. coli* IQH5′.

2.2 Expression and isolation of the fusion protein containing the *Hs*ERManI linked to protein A:

The fusion protein encoding the human ERManI homolog linked to protein A was expressed by transient transfection of the pPROTA-ERManI plasmid in COS-7 cells. COS-7 cells were grown in Dulbecco's modified Eagle's minimal medium supplemented with 0.1 μg/ml penicillin, 0.1 μg/ml streptomycin, and 10% fetal calf serum (DMEM/10% FCS) to 60% confluence in T-175 flasks and transfected with a mixture of 50 μg of pPROTA-ERManI and 150 μl of Dosper liposomal transfection reagent (Roche Molecular Biochemicals, Mannheim,

Germany) for 6 h at 37 °C. Following this incubation, the transfection medium was removed, and the cultures were maintained in fresh DMEM/10% FCS and grown at 37 °C for 36 h. The growth medium was collected, 160 µl of a 50% suspension of IgG-Sepharose beads were added per 10 ml of culture medium, and the suspension was incubated at 4 °C overnight with constant shaking. The beads were collected by centrifugation at 1700 × *g* for 15 min, washed three times by resuspension and centrifugation in 15 ml of PBS. The bead were stored in MES buffer (20 mM MES (pH 7.0), 150 mM NaCl, 5 mM $CaCl_2$) and used directly in enzyme assays.

2.3 Expression of the catalytic domain of *Hs*ERManI in *Pichia pastoris*:

The catalytic domain of *Hs*ERManI (amino acids 172-689) was excised from the pPROTA-ERManI construct by digestion with *Eco*RI and ligated into the *Eco*RI site of the *Pichia* expression vector pPICZαA (Invitrogen, La Jolla, CA). The ligation mixture was transformed into *E. coli* TOP10F′. Digestion of the plasmid DNA with *Bam*HI and *Pst*I was used to verify the correct ligation. Ten µg of expression vector containing the sense-orientation construct (pPICZαA-ERManI) was linearized by digestion with *Hind*III and transformed into *Pichia pastoris* X-33 and SMD168H by the lithium chloride transformation method as described in the *Pichia* expression manual (Invitrogen). The transformants were selected on YPD agar plates (10 g/l yeast extract, 20 g/l peptone, 2% w/v dextrose and 2% w/v agar) containing 100 µg/ml of Zeocin (Invitrogen). The colonies were isolated following 3 days of growth at 30 °C.

The expression of the recombinant *Hs*ERManI enzyme activity was screened by inoculation of Zeocin resistant colonies into 5 ml BMY (10 g/l yeast extract, 20 g/l peptone, 3.4 g/l YNB (yeast nitrogen base) (DIFCO, cat. no. 233520), 10 g/l ammonium sulfate, 0.1 M phosphate buffer pH 6.0 and 4 µg/l d-biotin) containing 1% v/v glycerol in 50 ml conical tubes.

Overnight cultures were grown in a horizontal shaker at 200 rpm incubated at 30 °C. The cells were collected by centrifugation at 3000×g at 25 °C for 10 min and resuspended in 10 ml of BMY containing 0.5% v/v methanol. The cultures were continuously shaken at 200 rpm for 3 days with daily addition of 100 µl of 50% v/v of methanol. The expression of wild type recombinant enzyme was monitored by specific α-mannosidase activity toward natural substrate ($Man_9GlcNAc_2$).

2.4 Site-directed mutagenesis and expression:

The cDNA encoding ERManI in the pPICZαA vector (Invitrogen, La Jolla, CA) was used to perform site-directed mutagenesis using the QuikChange™ mutagenesis kit from Stratagene (La Jolla, CA). The sense and antisense primers for each mutant were designed based on the sequence of *Hs*ERManI (GenBank accession no. AF145732) and were synthesized by IDT (Integrated DNA Technologies, Inc.) or MGIF (Molecular Genetic Facility, University of Georgia). The pPICZαA-ERManI plasmid in (10 ng in 1 µl) and 10 pmole of sense and antisense primers (in 2 µl) were added into 49 µl of PCR mixture supplied by manufacturer (1 µl of 100 U *Pfu* polymerase, 5 µl 10× buffer, 10 µl of 100 µM dNTP, 33 µl H_2O). The PCR was carried using a thermocycle control unit (MJ Research, Cambridge, MA). The PCR was programmed as follows: 1 cycle of initial denaturation for 2 min at 95 °C, followed by 20 cycles of annealing for 1 min at 50°C followed by elongation for 15 min at 68°C and denaturation for 1 min at 95°C. The DNA template was digested by the addition of 1 µl *Dpn*I (100U/ml, supplied by manufacturer) and incubated for 2 h at 37°C. An aliquot of 1-2 µl of *Dpn*I digested mixture was transformed into *E. coli* TOP10F′.

The full coding region of each mutant was fully sequenced to confirm that only the desired mutation was generated. Confirmed mutant cDNAs were then used as a template to create the double mutations by the same procedure as used in the single amino acid mutagensis.

The mutant cDNA expression construct was transformed into *Pichia pastoris* X-33 and screened as described above. The expression of catalytically defective mutant enzymes was monitored by the Western Blot analysis. After 3 days of methanol induction, the culture media (20 μl) was separated on 10% SDS-PAGE (sodium dodecyl sulfate polyacrylamide gel electrophoresis) [112] and then transferred on to a PVDF (polyvinylidene difluoride) membrane (Milipore, Bedford, MA). The recombinant proteins were detected by immunoblotting using anti-*Hs*ERManI antibody (raised in rabbit, 1:1000) and alkaline phosphatase conjugated anti-rabbit IgG secondary antibody (1:5000) (Promega, Madison, WI). The recombinant enzyme was visualized by immersion the membrane into 5-bromo-4-chloro-3-indolylphosphate/nitroblue tetrazolium (BCIP/NBT) solution (SIGMAFAST™ BCIP/NBT, Sigma-Aldrich Corp. St. Louis, MO).

2.5 1-liter shaker flask expression and purification:

The *Pichia* transformant expressing highest level of secreted enzyme was inoculated from a single colony or frozen glycerol stock into 5 ml YPD. The culture was grown overnight at 30 ºC prior to transfer into 100 ml BMY containing 1% glycerol. After 2 days of incubation at 30 ºC, the culture (100 ml) was inoculated into 1L BMY containing 0.5% v/v methanol. Additional methanol (10 ml of 50% v/v methanol) was added to the culture daily for 5 days.

A culture media was clarified by centrifugation at 6000×g for 15 min followed by filtration through 0.45 μm membrane prior to concentration over YM-30 using Amicon Stirred

Ultrafiltration Cells (Amicon, Inc., Beverly, MA). One liter of clarified media was concentrated to 100 ml and diluted twice with 100 ml of 10 mM sodium succinate pH 6.0. Alternatively, 2L of dH_2O was added to 1L clarified media prior to cation-ion exchange chromatrography.

The final concentrated conditioned media was loaded onto a pre-equilibrated SP-Sepharose^{TM} Fast Flow media column (15×200 mm) at 2-10 ml/min. The column was pre-equilibrated and washed with 10 mM sodium succinate (pH 6.0) for at least 5 column volumes after the application of the sample. The protein was subsequently eluted with 100 ml of linear gradient of 0-1.0 M NaCl in the same buffer at a flow rate of 2 ml/min. The column was regenerated by flushing with 2 column volumes of 1 M NaCl and followed by one column volume of 0.1 M NaOH. The enzyme containing fractions were pooled and used for tests on the solubility and stability for long-term storage as well as for antibody production.

2.6 100-liter fermentor expression and purification of wild type enzyme:

The enzyme expression was scaled-up by growth of the culture in a 100-liter fermentor (New Brunswick Scientific, Edison, NJ) at the Fermentation Research Facility of the University of Georgia. The fermentor, containing 100L of BMGY (BMY medium containing 1% v/v glycerol) was inoculated with a 5L overnight culture of the *Hs*ERManI *Pichia* transformant in BMGY. The culture was maintained at 30 °C with agitation at 180 rpm and an air flow of 100 liters/min for 48 h until the glycerol in the culture was consumed. *Hs*ERManI enzyme expression was then induced by the daily addition of methanol (50% v/v stock solution) to a final concentration of 0.5%. After 5 days of induction, the medium was harvested using a Sharples Model AS-16P continuous centrifuge at 15,000 rpm for 5 h, followed by filtration using a 0.45-

μm filter. Attempts to concentrate the culture medium by ultrafiltration resulted in >50% loss of enzyme activity and the appearance of *Hs*ERManI as a precipitate on the ultrafiltration filter.

As a result, the clarified culture medium was not concentrated, but was applied in 20L batches directly or following dilution with dH_2O (1:3 ratio) onto an SP-Sepharose^{TM} Fast Flow column (50 ×130 mm; Amersham Pharmacia Biotech, Piscataway, NJ) at a flow rate of 16 ml/min. The column was washed with 500 ml of column buffer containing 10 mM sodium succinate (pH 6.0) and 1 mM $CaCl_2$. The column was eluted with a 1L linear gradient of 0-0.5 M NaCl in the same column buffer at a flow rate of 16 ml/min. The fractions containing enzyme were pooled and concentrated by ultrafiltration through a YM-10 membrane (Amicon, Inc., Beverly, MA). The solubility of the concentrated protein was maintained by the addition of NDSB201 (Calbiochem) to 0.75 M. After concentration, an EDTA-free protease inhibitor mixture (Roche) was added to prevent protease degradation.

The concentrated enzyme preparation was applied at 1 ml/min onto a Superdex 75 gel filtration column (1.6×65 cm, Amersham Pharmacia Biotech) pre-equilibrated with 20 mM MES (pH 7.0), 150 mM NaCl, 5 mM $CaCl_2$ and 0.75 M NDSB201. Fractions containing *Hs*ERManI were pooled and concentrated to 1.8 mg/ml and stored at 4 °C until the crystallization trials. EDTA-free protease inhibitor mixture (Roche) was added to the final protein solution to prevent protease degradation.

2.7 NH_2-terminal sequencing:

An aliquot of the purified enzyme (50 μg) was subjected to SDS-PAGE and transferred to a PVDF membrane (Millipore) as described previously [72, 113]. The blot was stained using Coomassie R-250 and destained by submerging the blot in 50% v/v methanol. The band

corresponding to ERManI was excised and NH_2-terminal protein sequencing was performed by the Molecular Genetics Instrumentation Facility (University of Georgia) using an Applied Biosystems 494 protein sequencer.

2.8 Rabbit antibody production:

The rabbit immunization was performed by the Animal Resources Facility, University of Georgia. The purified *Hs*ERManI in the absence of NDSB201 or protease inhibitor was provided for injection into New Zealand white rabbit (rabbit #448 and #449). Booster immunizations were given 21 days after the initial injection, with subsequent injections given at 3-6 weeks. Serum was tested by Western blot analysis and immunoprecipitation of recombinant protein. The pre-immune serum and antibody raised against *Mm*GManIA was used as the negative control.

2.9 Solubility of purified recombinant enzyme in the presence of non-detergent sulfobetaines (NDSBs):

A series of solubility tests were performed to investigate the effects of salts, detergents, glycerol, and NDSBs [114, 115] on the solubility of the enzyme. To test conditions for maintaining soluble enzyme during the crystallization trials, the purified enzyme (0.14 mg/ml) was concentrated in the presence of either 0.75 or 0.25 M NDSB256, NDSB201, or NDSB195 (Calbiochem) [114, 115], 2% octylglucoside, 1% urea, or 1% glycerol using a Centricon-10 concentrator (Amicon, Inc.) to obtain a final protein concentration of ~4 mg/ml. The concentrated samples were stored at 4 °C for 5 days. Aliquots were removed daily after centrifugation at 16,000 × *g* for 1 min. The protein concentration and enzyme activity of the supernatant was determined as described below.

2.10 Reverse phase and NH_2-HPLC:

Reverse phase HPLC was performed using either an analytical (4.5×150 mm) or a preparative (10×250 mm) Comosil C_{18} column. The column was regenerated with 80% methanol for 1 column volume and equilibrated with starting buffer for least 3 columns volumes. The pump delivered the solvent at 0.5 ml/min for the analytical column and 3 ml/min for the preparative column. Buffer A was 2% acetonitrile. Buffer B was 50% acetonitrile. Buffer C was 20 mM ammonium acetate pH 4.0. Buffer D was 5% acetonitrile in buffer C. Buffer E was 0.5% n-butanol in buffer C.

NH_2-HPLC was carried out on Hypersil APS-2 NH_2 column (4.5×250 mm). The pump delivered the solvent (50-60% of acetonitrile in 60 mM sodium phosphate buffer pH 4.0) in isocratic mode at 0.7-1.2 ml/min to maintain at least 1 min resolution of the PA-oligosaccharides.

All components of the HPLC systems were from Shimadzu Scientific Inc. The solvent delivery was either using LC-600 or LC-10AT. The LC-10AT was equipped with a SCL-10A controller and SIL-10AXL autoinjector. The fluorescence of PA-oligosaccharides was detected using a RF-535 fluorescence detector and UV detection was performed using SPD-6A UV monitor. The chromatograms were recorded and integrated using Shimadzu software Class-VP version 4.2 or 7.1.

2.11 Enzyme assays:

2.11.1 Assay of fusion proteins bound IgG-Sepharose beads —After 36 h of transient expression of the pPROTA-ERManI construct, the protein A fusion with *Hs*ERManI was harvested from the culture media of COS-7 cells by immunoprecipitation with the IgG-Sepharose beads. The IgG-Sepharose of beads (10-20µl) were washed in assay buffer and suspended in a

total assay volume of 50 µl buffer (100 mM MES (pH 7.0), 150 mM NaCl, 5 mM $CaCl_2$) and 1 µM pyridylamine-tagged $Man_9GlcNAc_2$ ($Man_9GlcNAc_2$-PA) as substrate. The reaction was stopped by heating to 100 °C for 5 min. Beads were removed by filtration through a 0.22-µm filter (Millex GV4, Millipore) prior to analysis of the α1,2-mannosidase digestion products by NH_2-HPLC as described below.

To examine the effects of cation addition on *Hs*ERManI activity, the fusion protein bound to the IgG-Sepharose beads, (10-20 µl bead volume), was washed and suspended in 50 µl buffer containing 100 mM MES (pH 7.0), 150 mM NaCl, 200 µM EDTA (ethylenediaminetetraacetic acid). The beads were then incubated with 1 mM of the indicated cations prepared as either chloride (Ca^{2+}, Mg^{2+}, Mn^{2+}, Co^{2+}, Ba^{2+}, Ho^{3+}, Yb^{3+}) or sulfate (Cu^{2+}, Fe^{2+}, Ni^{2+}, Zn^{2+}) salts. The enzyme assays were carried out using the $Man_9GlcNAc_2$-PA substrate as described above.

2.11.2 Assays for soluble recombinant enzyme — The purified wild type and mutant enzymes were assayed for α1,2-mannosidase activity using $Man_9GlcNAc_2$-PA as substrates. The enzyme reactions (20 µl) were carried out in 96-well plates by adding 10 µl of enzyme prepared in 2× Na/Ca solution (300 mM NaCl and 10 mM $CaCl_2$) to a mixture of 5 µl of 4x universal buffer (80 mM succinic acid, 80 mM MES, 80 mM HEPBS, 80 mM HEPES, and 80 mM CHES adjusted to pH with 5 M NaOH) and 5 µl of substrate. The reactions were performed at 37ºC for the indicated times and stopped by the addition of 20 µl 1.25 M Tris-HCl (pH 7.6) to the reaction mixture. The enzymatic products were resolved as described above.

2.11.3 Substrates — The substrate used in routine assays were the disaccharide substrates, methyl-*O*-α1,2-mannobiose, or α1,2-mannobiose, or the oligosaccharide substrate $Man_9GlcNAc_2$-

PA. Mannose released from disaccharide substrate was quantitated using glucose oxidase/horseradish peroxidase and *o*-dianisidine dihydrochloride as described previously [72, 116]. Briefly, the reaction mixture was incubated with 250 µl of developing solution containing glucose oxidase (55 U/ml), horseradish peroxidase (1 purpurogallin unit/ml), and *o*-dianisidine dihydrochloride (70 µg/ml) for 1-3 h at 37 ºC. The final color intensity was measured at 450 nm on a Bio-Tek (Winooski, VT) microtiter plate reader. Free mannose was used as a standard.

For natural substrate assays, $Man_{9\text{-}5}GlcNAc_2$-PA oligosaccharides were resolved by using an NH_2-HPLC column as described above. The isomers of $Man_8GlcNAc_2$-PAs were generated by digestion of $Man_9GlcNAc_2$-PA with ERManI or GolgiManIA and resolved by reverse phase HPLC on a Cosmosil C-18 column [72, 117].

One unit of enzyme activity is defined as the amount of enzyme that generates 1 µmol of $Man_8GlcNAc_2$ from $Man_9GlcNAc_2$ or free mannose in 1 min at 37 °C and pH 7.0. Protein concentration was determined using the BCA protein assay reagent (Pierce Biotechnology Inc., Rockford, IL) as described by the manufacturer. Concentration of oligosaccharide was determined by phenol-sulfuric acid assay [118].

2.11.4 Enzyme kinetic analyses — Initial rates (v) for the enzymes were determined at various substrate concentrations ranging from 10-300 µM. The catalytic coefficient (k_{cat}) and Michaelis constant (K_m) values were determined by fitting initial rates to Michaelis-Menten function (eq. 1) by non-linear regression analysis using SigmaPlot (Sigmaplot Users Manual (1993) Jandel Scientific, San Rafael, CA).

$$v_i = \frac{k_{cat} \cdot [E_t] \cdot [S]}{K_m + [S]} \qquad \text{eq. 1}$$

where E_t is total enzyme concentration.

k_{cat}/ K_m values were derived from reciprocal plots of v and [S] where needed. The K_m and k_{cat} was determined from the initial rate (v_i) using 5-8 substrate concentrations, by non-linear regression of the Michaelis-Menten equation (eq. 1) using Sigma plot 8.0.

2.11.5 pH-rate dependence analysis — The k_{cat}/K_m values were determined from initial rates of enzyme reactions at pH values ranging from 4.0-10.0 using the 1x universal buffer described above. Plots of log k_{cat}/K_m versus pH were fitted to the appropriate bell-shaped equation [119] to estimate the pK_a values of possible amino acid residues involved in substrate binding or catalysis [119].

2.11.6 Temperature dependence of catalysis—Values for k_{cat} were obtained at 5, 10, 15, 20, 25, 30, 35, 40 ºC and were used to calculate the activation energy (E_a) from the slope ($-E_a/R$) of the Arrhenius plots (ln k_{cat} as a function of $1/T$). Enthalpy at 25 ºC ($\Delta H^{\ddagger}$**)** was calculated from eq. 3 using the calculated E_a determined from the Arrhenius plot. Gibb's free energy at 25 ºC ($\Delta G^{\ddagger}$**)** was calculated from eq. 2 using k_{cat} values determined at 25 ºC. The entropy at 25 ºC ($\Delta S^{\ddagger}$**)** was calculated using eq. 4 and the values calculated for $\Delta G^{\ddagger}$ and $\Delta H^{\ddagger}$**.** The thermodynamic activation parameters were described by the following relationships [120, 121]:

$$\Delta G^{\ddagger} = RT \times (\ln \frac{k_B T}{h} - \ln k_{cat}) \qquad \text{eq. 2}$$

$$\Delta H^{\ddagger} = E_a - RT \qquad \text{eq. 3}$$

$$\Delta S^{\ddagger} = (\Delta H^{\ddagger} - \Delta G^{\ddagger})/T \qquad \text{eq. 4}$$

Errors on $\Delta G^{\ddagger}$ were calculated from

$$(\Delta G^{\ddagger})_{Err} = RT \times (k_{cat})_{Err} / k_{cat} \qquad \text{eq. 5}$$

2.12 Proton inventory study:

The deuterium isotope effect of wild type enzyme was carried out as follows. The 2× universal buffer containing NaCl and $CaCl_2$ was made in 100% H_2O or 99.8% D_2O (Sigma) and adjusted pH to 7.0 with NaOH or NaOD (Sigma), respectively. The pH curve of enzyme activity in either 100% H_2O and 99.8% D_2O buffers resulted in the same pH optimum; therefore pH correction was unnecessary for the D_2O buffer.

The appropriate ratio of D_2O and H_2O buffer were mixed to obtain 0-1 molar fraction of deuterium at 0.1 unit increments. The purified enzyme (2×) was prepared in each of molar fraction of deuterium buffer. A 10 µl aliquot of enzyme solution was carefully dispensed into a flat bottom microtiter plate containing a 20-300 µM $Man_9GlcNAc_2$-PA or 5-20 mM α-(1,2) mannobiose, which was freeze-dried and rehydrated in the appropriate 1× deuterium buffer. The reaction was allowed to proceed for 15-30 min at 37 °C. The reaction products were analyzed as described above. The catalytic rate constant (k) was to fit to a modified Gross-Butler equation (eq. 6) [122, 123].

$$k_\chi = k_0 \frac{\prod_{i=1}^{n}(1-\chi+\chi\phi_i^T)}{\prod_{j=1}^{n}(1-\chi+\chi\phi_j^R)} \qquad \text{eq. 6}$$

where k_χ is the rate constant in mole fraction D_2O (χ), k_0 is the rate constant in H_2O, and ϕ_i^T , ϕ_i^R are the isotopic fractionation factors [122, 124].

2.13 Calcium equilibrium analysis:

2.13.1 Recombinant enzyme solution preparation — The purified proteins were incubated with 200 mM EGTA (ethylene glycol bis(2-aminoethyl ether)-N,N,N'N'-tetraacetic acid) for 2h at 4 ºC

prior to desalting over the Sepharose G25 column (1 × 40 cm), which was pretreated with 0.5 M EGTA followed by pre-equilibrating in calcium-free buffer (20 mM MES, pH 7.0, 150 mM NaCl). The calcium free protein solution was concentrated to 1 mg/ml using YM-10 membrane. The calcium content of the protein solutions, confirmed by ICP-MS, was below 50 ppb.

2.13.2 Calcium buffer preparation — The total amount of calcium chloride required to generate 0-500 μM free Ca^{2+} in EGTA containing buffer (20 mM MES, pH 7.0, 150 mM NaCl, 5 mM EGTA) was calculated using WEBMAXCLITE v1.15 [125] available through http://www.stanford.edu/~cpatton/maxc.html. The calcium buffer solutions (2×) were then prepared by mixing a specific amount of $CaCl_2$ stock solution (50 mM), to 5× EGTA (25 mM) containing buffer and distilled water. The pH of the mixture was monitored and adjusted to pH 7.0 by addition of 1 M NaOH. All stock solutions were prepared in the EDTA treated plasticware. Total calcium ion concentrations in each solutions was confirmed by atomic absorption and used to recalculate the free calcium ion concentration at the analysis condition [126].

2.13.3 Enzyme assay — The calcium free enzyme solution was diluted in calcium-free buffer to obtain a stock solution of 80 μg/ml for wild type and 140 μg/ml for the T688A mutant. Aliquots of the enzyme solution (5 μl) were added into each of the calcium buffers (10 μl) before addition of 5 μl of 80 μM $Man_9GlcNAc_2$-PA. The reactions were allowed to proceed at 37 ºC and stopped by adding 20 μl of 1.25 M Tris-HCl pH 7.6 at the appropriate time course. The reaction mixture was analyzed on an NH_2-HPLC column as described below.

2.14 Preparation of Oligosaccharides and their derivatives:

2.14.1 Isolation of oligosaccharides from soybean agglutinin — $Man_9GlcNAc_2$ oligosaccharides were isolated from soybean agglutinin (SBA). Crude extracts of soybean agglutinin (2g) were prepared by ammonium sulfate precipitation [127-129]. Briefly, 1 kg of untoasted soybean flour (Arrow Head Mill, AR) was hydrated in 3.5L and acidified using concentrated HCl to pH 4.6. The insoluble matter was removed by centrifugation at 10000×g for 20 min. Ammonium sulfate (300g) was added to each liter of supernatant. After 4h of precipitation at 4°C, the precipitate was removed by centrifugation at 15000×g for 30 min. An additional 270g of ammonium sulfate was added to 1L of the supernatant and the ammonium sulfate precipitate was collected by centrifugation at 15000×g for 30 min and resuspended in 150 ml dH_2O followed by excessive dialysis against dH_2O using a 12000 MWCO dialysis bag at 4 °C. The dialyzed soybean extract was then dried by lyophilization.

Two grams of dry powder of SBA crude extract was dissolved in 10 ml of 8 M guanidine-HCl, 0.1 M Tris-HCl, pH 8.0, and reduced by the addition of 0.28 g of DTT (Sigma) for 1h at 55°C followed by addition of iodoacetamide (1.28 g) (Sigma) for 30 min at room temperature [130]. The mixture then was exhaustively dialyzed against dH_2O.

The reduced SBA was collected by centrifugation at 10000×g for 25 min followed by resuspension in 20 ml of 0.1 M Tris-HCl, pH 8.0, 20 mM $CaCl_2$. Trypsin (20 mg, Sigma) was added to the suspension and was incubated for 4h at 37 °C. The trypsin was inactivated by heating to 65°C for 1 h prior to addition of 20 mg of elastase type III (Sigma) [131]. After 24 h incubation at 37 °C with elastase, the soluble material was clarified by centrifugation at 15000×g for 25 min followed by fractionation over a Sepharose G50 column (25×300 mm) at flow rate 5 ml/min of 20 mM ammonium acetate, pH 4.0, 1% butanol. The $Man_9GlcNAc_2$ containing

glycopeptide fractions were detected by phenol-sulfuric acid assay [118] and were pooled and dried using a SpeedVac. The glycopeptides were further isolated over a C_{18} SepPak column (Alltech Associates Inc., Deerfield, IL) prior to liberation of the N-linked oligosaccharides by digestion with N-glycanase (A gift of Dr. J. Michael Pierce, University of Georgia, Athens, GA) [132].

2.14.2 $Man_9GlcNAc_2$ linked glycopeptide preparation —$Man_9GlcNAc_2$ glycopeptides were further isolated by *Concanavalin A* (ConA) affinity chromatography and preparative C_{18} chromatography as described [133]. Briefly, ConA (Sigma) was immobilized on Affigel-10 (BioRad Lab. Hercules, CA) according to manufacturer instruction. A batch of approximately 10 μmole of glycopeptide was dissolved in binding buffer (50 mM Tris-HCl, pH 7.4, 500 mM NaCl, 1 mM $CaCl_2$, 1 mM $MnCl_2$ 1 mM $MgCl_2$) and applied onto the ConA column (2.5 × 15 cm) at 2 ml/min followed by washing with at least 200 ml of binding buffer. Elution buffer (40 ml of 1 M methyl-α-mannopyranoside in binding buffer) was applied onto the column at 5 ml/min and allowed to incubate on the column without flow for 30 min. The bound glycopeptide was then eluted with an additional 10 ml of elution buffer followed by 100 ml of binding buffer at 5 ml/min. The eluted fractions were pooled and adjusted with concentrated acetic acid to obtain a final concentraton of 5% (*v/v*) acetic acid prior to passage over a prewashed C_{18} SepPak (Alltech). For a C_{18} SepPak with 5 g resin, the column was prewashed and regenerated with 10 ml 100% isopropanol followed by 20 ml 5% (*v/v*) acetic acid. The glycopeptide was applied to the column and washed with at least 15 ml of 5% acetic acid prior to elution from the C_{18} SepPak using 30% (*v/v*) isopropanol in 5% (*v/v*) acetic acid solvent. The glycopeptide eluted from the C_{18} SepPak was then dried and resuspended in dH_2O followed by application onto a preparative Comosil C_{18}

column (10 × 250 mm), which was equilibrated with buffer A (described above) and eluted with a linear gradient to 100% buffer B (described above) for 50 min at a flow rate of 2 ml/min.

2.14.3 Pyridylamine oligosaccharide preparation — Pyridylamination was carried out as described previously [134-136]. An aliquot of 2 μmole of unreduced oligosaccharide was heated at 90 °C for 1h in 100 μl of pyridylamine (PA) solution (110 mg PA in 40 μl glacial acetic acid). The reaction mixture then was reduced by adding 140 μl of a freshly prepare borane-dimethylamine (Sigma) solution (200 mg in 80 μl of acetic acid and 50 μl of water). The reduction was carried out at 80°C for 35 min. Excess PA was removed by phenol:chloroform (1:1) extraction three times prior to desalting using a Toyopearl HW40 (Tosoh Co.,Tokyo, Japan) column (1×40 cm) in 20 mM ammonium acetate buffer pH 6.0.

The PA-oligosaccharide was isolated on a preparative Comosil C_{18} (10 × 250 mm). A 200-500 μl sample containing 0.5-1 μmole PA-oligosaccharide was injected onto the column equilibrated in buffer C. The gradient was 0-35% of buffer D for a total of 70 ml, at a flow rate of 2 ml/min. $Man_9GlcNAc_2$-PA was monitored using an in-line fluorescence detector with an excitation of 310 nm and emission of 420 nm. An aliquot of each oligosaccharide containing fraction was analyzed for contamination by NH_2-HPLC chromatography (4.5 ×100 mm) before combining all fractions containing the $Man_9GlcNAc_2$-PA oligosaccharide.

Isomers of $Man_8GlcNAc_2$-PA were generated by digestion with either ERManI or Golgi ManIA and isolation by reverse phase HPLC as described above [72, 117].

2.15 Surface plasmon resonance study:

2.15.1 Instrument and sensor chip preparation — The biosensor assays were performed on a BIACORE 3000 instrument and data analyses were manipulated and fit using the BIAevaluation 3.1 software (Biacore AB, Piscataway, NJ). Prior to beginning a binding assay session, the liquid handling portion of the instrument was routinely cleaned utilizing the automated subroutines. The system was first subjected to DESORB subroutine, which allows the system to be flushed with 0.5% SDS and 50 mM glycine pH 9.5, followed by the SUPERCLEAN subroutine, which flushes the system with of 1% acetic acid, 10 mM HCl, 6 M guanidine HCl, and 0.2 M $NaHCO_3$, and finally another DESORB subroutine. New biosensor chips were docked into the instrument and were subjected to preconditioning by applying two consecutive pulses (20 μl) of 50 mM NaOH, followed by one pulse of 10 mM HCl and one pulse of 0.1% SDS followed by a normalization using NORMALIZE command, which allows the calibration of the sensor chip surface using a 70% glycerol solution.

2.15.2 Sensor chip surface preparation —The amine coupling kit (1-ethyl-3-(dimethylamiopropyl)carbodiimide, EDC), (N-hydrozysuccinimide, NHS) and ethanolamine), HPB-EP (20 mM HEPES, pH 7.4, 150 mM NaCl, 3.4 mM EDTA, 0.01% polysorbate P20) and research-grade CM5 sensor chips were supplied by the manufacturer. Recombinant ERManI immobilized chip surfaces were prepared at 25 ºC by an amine-coupling method using the automated Application Wizard (BIAcore 3000 control software, BIAcore AB). The flow cells were activated by injecting a mixture of 50 mM NHS and 200 mM EDC over the CM5 sensor chips surface for 7 min at 5 μl/min. The recombinant proteins (30 μg/ml) prepared in 10 mM sodium succinic acid (pH 6.0) and passed through 0.2 μm PVDF filter (Millipore, Billerica, MA)

were diluted in the same buffer to obtain a concentration of 5 μg/ml prior to injection onto the activated surface. The desired immobilization level was achieved by specific contact time. The remaining reactive groups were blocked by injection of 1 M ethanolamine-HCl at pH 8.5 for 7 min at 5 μl/min. The immobilization efficiency for ERManI was about 2,500 RU/min at a flow rate of 5 μl/min and 25 ºC using HPB-EP as running buffer. Mock derivatized flow cells served as reference surfaces.

2.15.3 Binding kinetic/affinity analysis — The binding analyses were performed at 10ºC with continuous flow (30 μl/min) of running buffer (10 mM MES pH 7.0, 300 mM NaCl and 5 mM $CaCl_2$). The analysis cycle was composed of 5 sections: A- a wait segment of 60s with a flow of running buffer at 30 μl/min, B- a blank KINJECT segment (a command that allows an injection of sample for kinetic analysis consisting of a sample injection phase and dissociation phase) using running buffer for 60s at a flow rate of 30 μl/min followed by a 1s dissociation phase using running buffer, C- a wait segment of 120s with a flow of running buffer at 30 μl/min, D- a KINJECT segment of analyte injection for 60s at a flow rate of 30 μl/min, E- 120-300s of dissociation phase in running buffer at a flow rate of 30 μl/min, and F- a wait segment of 60s with a flow of running buffer at 30 μl/min. An EXTRACLEAN procedure, which allows the injection port and needle to be flushed with excess running buffer was included at the end of each injection. The PRIME (a command that allows the sensorchip surface and IFC (Integrated Fluid Channel) to be thoroughly purged by the running buffer for 7 min and NORMALIZE subroutines were included at the beginning of each analysis method.

Analytes were prepared in running buffer by 2-fold serial dilution to obtain an appropriate concentration range. A concentration series of $Man_9GlcNAc_2$ glycopeptide (0.39-400 μM), Man_5-

$_9$GlcNAc$_2$-PA (0.39-100 μM) was analyzed over the low density protein chip surface of 3000 RU. Disaccharides (15.6-1000 μM), thiosaccharide (15.6-1000 μM), dMNJ (1.96-1000 μM) and Kif (1.96-1000 μM) were analyzed over the high density protein chip surface of 10000 RU. Each concentration of each sample was analyzed in duplicate utilizing the KINJECT command for 1 min followed by at least 3 min of dissociation phase. The baseline returned to the original response in 5 min for all analytes described here without a further regeneration procedure, except for analyses using Kif as the analyte, which did not dissociate from the chip surface.

The temperature dependent interaction studies were analyzed at 5, 10, 15, 20, 25, 30 and 35ºC consecutively in an automated method. The surfaces were subjected to the PRIME subroutine three times, followed by the NORMALIZE subroutine, prior to the binding analysis once the instrument became stable at each temperature. In all cases, 20 mM MES/NaOH, pH 7.0, 300 mM NaCl, 5 mM $CaCl_2$ was used as running buffer at flow rate of 30 μl/min, except in calcium-dependent binding studies, where the surface was subjected to overnight treatment of 20 mM MES/NaOH pH 7.0, 300 mM NaCl, 5 mM EGTA at a flow rate of 5 μl/min, prior to binding analysis using 20 mM MES/NaOH pH 7.0, 300 mM NaCl, 200 μM EGTA as running buffer.

The sensorgrams were recorded at 2-5 Hz wherever possible. The sensorgrams of the active surfaces were automatically subtracted from blank surface to remove bulk refraction and random noise. Report points on the sensorgram were recorded at six time locations: (a) 10s prior the injection start, (b) 20s after injection start, (c) 50s after injection start, (d) 10s after dissociation started, (e) 50s after dissociation started, (f) 60s after injection finished. The report points (a) and (f) were used to follow baseline stability. Points (b), (c), (d) and (e) were used for evaluating the binding event and affinity analysis.

2.15.4 Determination of kinetic parameters — All the sensorgrams were processed using a double-referencing method [137] and were globally fit to one of the available models in the Biaevaluation 3.1 software [138, 139]. For the fast on- and off-rate system, the dissociation constant K_D was determined by steady-state affinity; otherwise, K_D was calculated as k_d/k_a. K_D values measured at different temperatures were used to calculate thermodynamic parameters [137, 140] of binding using van't Hoff equation (eq. 7) and Gibbs free energy change (ΔG) was calculated from equation (eq. 8). The van't Hoff equation allows the calculation of thermodymanic parameters using the linear relationship of $y = \ln(K_D)$ versus $x = 1/T$ which gives a slope of $\Delta H / R$ and an intercept of $-\Delta S / R$.

$$\ln K_D = \Delta H/(RT) - \Delta S/R \qquad \text{eq. 7}$$

$$\Delta G = -RT\ln(1/K_D) \qquad \text{eq. 8}$$

Transition state analysis was also carried out using the Eyring equation (eq. 9) under conditions where k_a and k_d were available. Similar to the van't Hoff analysis, the Eyring equation allows the variables be determined from linear relationship where $y = R\ln(hk/k_bT)$ and $x = 1/T$. The slope and the intercept of Eyring plot are $-\Delta H^{\ddagger}$ and $\Delta S^{\ddagger}$, respectively.

$$k = (k_BT/h)\exp(\Delta S^{\ddagger}/R)\exp(-\Delta H^{\ddagger}/RT) \qquad \text{eq. 9}$$

R is the gas constant (8.314 J $mol^{-1}K^{-1}$), k_B is the Boltzmann constant (1.3805 $\times 10^{-23}$) $J{\cdot}K^{-1}$) and h is the Planck constant (6.6256 $\times$ 10^{-34} Js).

2.16 Isothermal calorimetric study:

Titration calorimetry measurements were performed with a 4200-ITC calorimeter (Calorimetry Sciences Corp., Lindon, UT) as described using procedure guideline given by M.M. Pierce [141] and T. Wiseman [142]. Protein solutions for ITC analysis were dialyzed overnight

against buffer containing 20 mM MES (pH 7.0), 150 mM NaCl, 5 mM $CaCl_2$ and 0.75 M NDSB201 at 4 ºC. The ligand solutions of kifunensine and 1-deoxymannorijimycin were prepared by diluting the compound with the buffer used for protein dialysis. Aliqouts (5-10 µl) of the ligand solution (1-5 mM) were automatically delivered into 1.3 ml of protein solution (1-2 mg/ml) in the reaction cell. The ITC was allowed to return to equilibrium for 4 min prior to the next injection. The heat of dilution was determined to be negligible. The data analysis was performed using DataWork and BindWork software provided by manufacturer.

2.17 Error propagation:

The standard deviation of the reported values were calculated using appropriate formulas for propagation of error as suggested by H. Ku [143], except the thermodynamic calculation from k_{cat}, which was calculated using equation (eq. 5) [120, 121].

2.18 Co-crystallization:

The catalytic domain of *Hs*ERManI was expressed and purified as described above. The recombinant protein was concentrated to 10 mg/ml in 20 mM MES/NaOH, pH 7.0, 150 mM NaCl, 5 mM $CaCl_2$ and 0.75 M NDSB-201 (3-(1-pyridino)-1-propane sulfonate). The recombinant protein was stored at 4°C in the absence of protease inhibitor. The solution was passed through a 0.2 µm filter membrane immediately prior to crystallization.

2.18.1 Crystallization screening and optimization — A sparse-matrix screen [144] with the Crystal Screen HT™ from Hampton Research was carried out using Oryx 6 crystallization robot (Douglas Instruments) in Nunc HLA plates. The crystallization drop was prepared by mixing

equal volumes (0.5 µl) of the protein and the screening solutions and sealed with paraffin oil (15 µl). The plate was then overlaid with a 4 ml mixture of silicone and paraffin oils (30:70) [145, 146] and kept at 18 °C. Crystal formation was monitored after three days. Additive screening was carried out by mixing equal volumes (0.5 µl) of the protein solution, the optimized crystallization solution (24% (*w*/*v*) PEG 4000, 100 mM MES/NaOH pH 6.0 and 50 mM ammonium sulphate), and 3× additive screen components (Hampton Research, Cat. No. HR2-428).

2.18.2 Co-crystallization of recombinant *Hs*ERManI with the thiodisaccharide substrate analogue — The thiodisaccharide analogue of Man-α1,2-Man-O-CH_3 (methyl-2-S-(α-D-mannopyranosyl)-2-thio-α-D-mannopyranoside), was synthesized by a modification of a previously published procedure [147] by Dr Aloysius Siriwardena (Univ of Mississipi) and characterized for its authenticity by NMR. For co-crystallization, the thiodisaccharide (100 mM in H_2O) was added to the protein solution to achieve a final concentration of 10–50 mM and incubated for 2 h at room temperature prior to crystallization. A hanging drop was prepared over 1 ml of mother liquor containing 24% (*w*/*v*) PEG 4000, 100 mM MES/NaOH, pH 6.0, 50 mM ammonium sulfate, 10% (*v*/*v*) 1,4 butanediol. The crystallization drop contained 1.5 µl protein/ligand solution and 1 µl of mother liquor. The crystals were grown at 25°C and harvested one day after they were first observed by flash-freezing on a cryo-loop using 10% (*v*/*v*) glycerol in mother liquor as cryoprotectant.

A diffraction quality crystal of native protein was grown by vapor diffusion at 25°C. A hanging drop was prepared over 1 ml of mother liquor containing 24% (*w*/*v*) PEG 4000, 100 mM MES/NaOH pH 6.0, 50 mM ammonium sulfate, 10% (*v*/*v*) 1,4 butanediol. The crystallization drop contained 1.5 µl protein solution and 1 µl of mother liquor. The crystals were harvested one

day after they were first observed and flash-frozen [148] on a cryo-loop [149] (Hampton Research) using 10% (*v*/*v*) glycerol in mother liquor as cryoprotectant.

2.18.3 X-ray diffraction and analysis — Diffraction data were collected at beam line 22-ID of the Advanced Photon Source, Argonne National Laboratory using a MAR Research 225 CCD detector and 1.0 Å wavelength X-rays. At a crystal-to-detector distance of 130 mm, 360 1° oscillation images were recorded with an exposure time of 2 seconds. Data processing, integration and scaling were performed with the HKL software suite [150] The structure was solved by molecular replacement using the program EPMR [151] and PDB entry 1FMI [14] as a search model. Rebuilding (Xfit [152]) was repeatedly iterated with refinement (Refmac5 [153-155] and validation (MOLPROBITY [156])**.**

CHAPTER 3

RESULTS

3.1 Recombinant protein expression in COS-7 cells and characterization of the enzyme activity of the fusion protein:

To demonstrate a catalytic activity associated with the putative human mannosidase (*Hs*ERManI) cDNA expression product, a construct encoding the COOH-terminal end of the coding region of the human mannosidase homolog (corresponding to amino acids 178-663) was generated as a fusion protein in-frame and downstream from the coding region for protein A. This construct contains an NH_2-terminal signal sequence that would target the fusion protein for translocation into the ER lumen [157]. Constructs of this type have previously been used to generate secreted forms of the catalytic domains of ER and Golgi glycoprotein processing enzymes in mammalian cells [158-165] where they can be recovered from the culture media by binding to IgG-Sepharose. When the medium from COS cells transfected with this expression construct was incubated with IgG-Sepharose beads, the fusion protein bound to the beads was tested for mannosidase activity using a variety of substrates. Incubation of the beads containing the immobilized recombinant fusion protein with a pyridylamine-tagged $Man_9GlcNAc_2$ substrate resulted in the release of a single mannose residue (Figure 22, left panels). This cleavage was linear with time and concentration of culture media (data not shown), and prolonged incubation resulted in no further cleavage of the substrate. No substrate cleavage was detected when assays were performed using medium from control transfections with a vector without an insert (data not shown). The $Man_8GlcNAc_2$ product of the reaction was identified as the Man8B isomer (Figure 23B), using C_{18}-HPLC, by comparison with the elution positions of standards that were

previously identified by NMR [72]. When the recombinant fusion protein bound to the IgG-Sepharose beads was tested with either *p*NP-α-Man or the disaccharide substrate, Manα1,2Manα-O-CH_3, no substrate cleavage was detected. As positive controls, a recombinant form of the human lysosomal α-mannosidase [113] was shown to cleave the *p*NP-α-Man substrate, and a recombinant form of murine Golgi α-mannosidase IA (*Mm*GManIA) [72] hydrolyzed the disaccharide substrate (data not shown).

The catalytic characteristics of the recombinant enzyme were determined using $Man_9GlcNAc_2$-PA as the substrate. The enzyme was active between pH 6.0 and 8.0 with an optimum at pH ~7.0. Kifunensine, dMNJ, EDTA and EGTA, a specific chelator of Ca^{2+}, inhibited the mannosidase activity (Figures 24 and 25 and Table 7), but swainsonine did not show inhibition at a concentration of 10 mM (Table 7). The enzyme inhibition by EDTA or EGTA could be reversed by the addition of Ca^{2+} (Figure 24E) and to a lesser extent by Fe^{2+} and Mn^{2+}. Other cations tested were unable to reverse the EDTA inhibition and were inhibitory in the absence of prior incubation with EDTA (Figure 25), suggesting that they compete with Ca^{2+} for binding to the enzyme. Experiments testing the effects of Ca^{2+} on the recovery of enzyme activity revealed that the enzyme bound to the IgG-Sepharose beads had been partially stripped of bound Ca^{2+} during washing with buffer (data not shown). Enzyme assays without added Ca^{2+} gave variable but lower activity than assays in the presence of added Ca^{2+}.

3.2 Comparison of the activity of the *Hs*ERManI with the activity of *Mm*GManIA:

To determine whether the human mannosidase homolog had an activity that was complementary with Golgi ManIA, a digestion time course of $Man_9GlcNAc_2$-PA were performed with the *Hs*ERManI alone, *Mm*GManIA alone, or the two recombinant enzymes mixed together in approximately equal proportions based on their rate of cleavage of $Man_9GlcNAc_2$-PA (Figure

22). The *Hs*ERManI progressively cleaved $Man_9GlcNAc_2$-PA to the Man8B isomer (Figure 22, left panels, and Figure 23), whereas the recombinant *Mm*GManIA partially cleaved this substrate to $Man_6GlcNAc_2$-PA and several larger intermediates over the same 60-min time course (Figure 22, middle panels). In contrast, a mixture of similar quantities of the two enzymes resulted in a rapid and efficient cleavage of the Man_9 $GlcNAc_2$-PA substrate to $Man_5GlcNAc_2$-PA in 60 min (Figure 22, right panels). These data indicate that the recombinant product of the *Hs*ERManI cDNA encodes an enzyme activity that is complementary to the activity of Golgi Man IA and that the combination of the two enzymes provides an efficient cleavage route for the processing of $Man_9GlcNAc_2$ oligosaccharides to the $Man_5GlcNAc_2$ structures that are necessary for further oligosaccharide maturation.

3.3 Relative inhibition by dMNJ of the *Hs*ERManI in comparison with Golgi Man IA:

Since both ERManI and *Mm*GManIA are sensitive to inhibition by dMNJ (Figure 24 and Ref. [72]), we tested the relative sensitivity of the two enzymes to inhibition by dMNJ in a reaction where both enzymes were present (Table 5). As a measurement of the relative contributions of the two enzymes in the cleavage reaction, we isolated the $Man_8GlcNAc_2$ intermediates from an enzymatic time course and determined the ratios of the $Man_8GlcNAc_2$ isomers. *Hs*ERManI was shown to exclusively produce the Man8B isomer (Figure 23B), while the recombinant *Mm*GManIA produces predominantly Man8A with small amounts of the Man8C isomer during the progress of digestion to smaller structures (Figure 23C and Ref. [72]). The combination of the two enzymes produced a mixture of the $Man_8GlcNAc_2$ isomers A, B, and C with a ratio of Man8B to Man8A + Man8C of ~0.4. This isomer ratio indicates that the ratio of the enzyme activity of the *Hs*ERManI to *Mm*GManIA was ~0.4:1 at each of the time points tested (Table 5). In contrast, when identical samples were incubated in the presence of 5 μM dMNJ, the

cleavage beyond $Man_8GlcNAc_2$ was significantly reduced, and the ratio of the $Man_8GlcNAc_2$ isomers was shifted toward the formation of the Man8B structure (Man8B/(Man8A + Man8C) = 2.14). These data indicate that there was a significantly greater inhibition of the *Mm*GManIA at this inhibitor concentration than *Hs*ERManI.

3.4 Expression and purification of recombinant *Hs*ERManI:

The cDNA encoding the catalytic domain of *Hs*ERManI was subcloned into pPICZαA at an *Eco*RI site and transformed into the *P. pastoris* X-33. The catalytic domain of the recombinant enzyme was expressed as secreted soluble protein into the culture media, which can be induced by addition of methanol to the *Pichia* culture. The level of expression of the recombinant enzyme was monitored by enzyme specific activity toward $Man_9GlcNAc_2$-PA. The α1,2-mannosidase activity from the expression culture media was detected after 6h of methanol induction and became saturated after 5 days of induction (Figure 26B). The recombinant enzyme was also detectable after 24h of induction via immunoblotting using rabbit raised *Hs*ERManI antibody (Figure 26A). The enzyme activity in the induced media started to decline shortly after 5 days of induction indicating that the secreted recombinant enzyme was being degraded faster than it was being secreted into the media. Minor bands corresponding to degradation fragments of *Hs*ERManI were observed by immunoblotting as soon as day 2 of induction (Figure 26A).

As a result, the soluble form of the catalytic domain of *Hs*ERManI was harvested from 1L cultures after 5 days of induction and purified to homogeneity by cation exchange chromatography using SP-Sepharose followed by gel filtration using Superdex-75. The recombinant enzyme was eluted as a single sharp peak at ~400 mM of NaCl solution. The SP-Sepharose purified materials were resolved by SDS-PAGE showing the co-elution of four protein fragments with molecular weight of ~55 kDa, ~42 and ~35 kDa and a small amount of ~ 86 kDa

material (Figure 27). The recombinant enzyme was separated from other fragments by gel filtration. The material in the fraction containing α1,2-mannosidase activity eluted from gel filtration appeared on SDS-PAGE as a single band at ~55 kDa franked by the minor bands of slightly larger and smaller molecular mass (Figure 28A). The purification procedure is summarized in Table 6. From 1-liter of conditioned *Pichia* media, the purification yielded 5.4 mg of recombinant ERManI at 2.86 μunit/mg representing 65% recovery after a 780-fold purification.

NH_2-terminal sequencing of the purified protein yielded a single amino acid sequence of AEVP. This corresponds to an NH_2 terminus at amino acid 226 and indicates that, in addition to the cleavage of the vector-encoded α-factor signal sequence, an additional 54 NH_2-terminal amino acids (residues 172-225) were excised by proteolytic cleavage during either the expression or purification of the protein. The purified protein encompasses amino acids 226-699.

3.5 Solubility of purified recombinant enzyme in the presence of Non-detergent Sulfobetaines (NDSBs):

During purification, the recombinant protein was found to rapidly precipitate when stored at 4°C, even at low protein concentrations (<0.1 mg/ml). A series of solubility tests were performed to investigate the effects of salts, detergents, glycerol, and NDSBs [114, 115] on the solubility of the enzyme (Figure 29). To test conditions for maintaining soluble enzyme during the crystallization trials, the purified enzyme (0.14 mg/ml) was concentrated in the presence of either 0.75 or 0.25 M NDSB256, NDSB201, NDSB195 or 1% glycerol or 2% octylglucoside to a final protein concentration of ~4 mg/ml. In the absence of additive or 1% glycerol, only 18% and 20% of starting enzyme material remained soluble after concentration and storage, respectively. In contrast, samples containing the NDSB compounds resulted in recovery of up to ~65% of the

enzyme activity in a soluble form after concentration and 25-40% remaining soluble after 9 days (Figure 29). NDSB201 was as effective a solubilizing agent as NDSB256, however, the recombinant enzyme remained fully active in NDSB201, but retained only 37% of the initial activity in NDSB256. Octylglucoside appeared to be the least effective solubilizing agent and resulted in the least amount of soluble material after 9 days of storage and the enzyme was largely inactive. There was considerable amount of degradation of the recombinant protein observed after nine days for the samples containing either NDSB256, glycerol, or the sample in the absence of solubilizing agent. As a result of the solubility studies, the pooled enzyme preparation after the SP-Sepharose step was concentrated in the presence of 1.0 M NDSB201 prior to its application to the Superdex 75 column, and the gel filtration column was run with a buffer containing at least 0.25 M NDSB201.

The solubility of the recombinant enzyme was improved greatly when the concentration step was immediately followed by the gel filtration chromotography. For instance, right after the the SP-Sepharose purification step, the recombinant *Hs*ERManI concentrated in the absence of the solubilizing agent or in the presence of 0.25 M NDSB201 improved the recovery of soluble enzyme to as high as 50% or 60% after concentration and 40% or 65% after storage at 4 ºC for 9 days respectively (data not shown).

3.6 Substrate for ERManI

The observed k_{cat} and K_m of *Hs*ERManI toward alternate substrates were shown in Figure 30. Recombinant *Hs*ERManI enzyme was used in relatively large quantities (50-100 μg/ml compared to 1 μg/ml when $Man_9GlcNAc_2$-PA was used as substrate) to follow the hydrolysis of α1,2-mannosides using, Manα1,2Man, Manα1,2Manα-O-CH_3, and $Man_8GlcNAc_2$-PA (isomer B) as substrates. The enzyme can hydrolyze each of the above substrates, but with less efficiency

than when $Man_9GlcNAc_2$-PA is used as substrate by ~120, 250 and 180-fold, respectively. The hydrolysis of these substrates displayed hyberbolic Michaelis-Menten kinetics and no product or substrate inhibition was observed**.**

3.7 *Hs*ERManI inhibition analysis:

The chemical structures of various known α-mannosidase inhibitors are shown in Figure 31 and their IC_{50} values were determined for *Hs*ERManI and are summarized in Table 7. As expected, the Class 1 mannosidase inhibitors, 1-deoxymannojirimycin (dMNJ) and kifunensine (Kif) inhibited *Hs*ERManI with IC_{50} values of 20 and 0.2 μM respectively (Figure 24B and C). The inhibition of *Hs*ERManI by dMNJ and Kif were shown in Figure 32. The plot of K_m/k_{cat} versus the inhibitor concentration, [I] appeared as a sigmoidal curve (Figure 32B and D) instead of the more standard linear relationship. This indicated that the binding of these inhibitors was not a conventional competitive or uncompetitive inhibition. Therefore, the K_i of the Kif and dMNJ were derived from nonlinear fit to eq. 10, which has been used to calculate the K_i for tight binding inhibitors[166].

$$K = \frac{[I] - [E](1 - v/v_0)}{v_0/v - 1} \qquad \text{eq. 10}$$

The K_i of Kif and dMNJ were calculated to be 0.13±0.01 and 11±0.2 μM, respectively. The binding affinity for Kif and dMNJ obtained by SPR (Figure 39B and O and Table 11) and ITC (Figure 33) binding analyses were also included in Table 7. The tight binding of Kif to *Hs*ERManI observed by SPR (Figure 39O) supported the tight binding inhibition model suggested by the inhibition study. The class II α-mannosidase inhibitor, 1,4-dideoxy-1,4-imino-D-mannitol poorly inhibited *Hs*ERManI with an IC_{50} of 1,500 μM. The other inhibitors did not inhibit *Hs*ERManI even at a concentration of > 10 mM.

3.8 Isothermal titration calorimetry study

The binding constants of *Hs*ERManI and the class 1 mannosidase inhibitors, dMNJ and Kif, were also obtained from isothernal titration calorimetry (ITC). The ITC analysis of *Hs*ERManI and dMNJ interaction (Figure 33B) and *Hs*ERManI interaction with Kif (Figure 33D) were endothermic, absorbing the heat during complex formation. The binding parameters for each inhibitors were determined by fitting the heat absorbed accross the titration curve to a 1:1 binding model available within the Bindwork analysis software version 1.1 (Calorimetry Sciences Corp.). For the interaction of *Hs*ERManI and dMNJ, the binding constant (K_A) was determined to be $0.12 \pm 0.02 \times 10^6$ M with an $n = 1.39$. For the interaction of *Hs*ERManI and Kif, the binding constant (K_A) were determined to be $13 \pm 7.5 \times 10^6$ M with an $n = 1.22$. The dissociation constants, a reciprocal of binding constant included in Table 7, were derived from duplicate ITC experiments carried out at constant temperature of 25 ºC, showing similar magnitude the inhibition (K_i) and the IC_{50} analyses. The binding stoichiometries were calculated to be close to 1, indicating that each enzyme molecule was more likely to bind to one molecule of the inhibitor, which is consistent with the observation of a single molecule of dMNJ or Kif in the active site of the *Hs*ERManI enzyme [14].

3.9 Proton inventory study

The α1,2-mannosidase specific activity for *Hs*ERManI was maximal at pD 7.0, the same as the pH maximum in protium water using 20 μM $Man_9GlcNAc_2$-PA as substrate (Figure 34). Therefore, the proton inventory study was performed at pH 7.0 without a pH correction factor. Under conditions of saturated substrate concentration, the deuterium isotope effects (DIEs) measured using $Man_9GlcNAc_2$-PA and Man-α1,2-Man as substrate were 1.76 ± 0.06, and 1.82 ± 0.03, respectively. The plot of experimental $k_{(\chi)}/k_{(O)}$ versus molar fraction of D_2O (χ) for

Manα1,2Man is shown in Figure 35A and the equivalent plot for $Man_9GlcNAc_2$-PA is shown in Figure 35B. The experimental data did not fit to the simple models [123] for single (eq. 9), two (eq.10), or many protons (eq. 11) involved in the catalysis, or a single proton (eq. 12) involved in reactant state (Figure 35 and Table 9). Despite the large standard deviation in experimental data for $Man_9GlcNAc_2$-PA, the experimental fit for $k_{(\chi)}/k_{(O)}$ of both Man-α1,2-Man and $Man_9GlcNAc_2$-PA were improved by inclusion of a polynomial function (eq. 13), which described a single reactant and transition state reaction using multiple protons. For the polynomial function, the number of protons involved was determined by the lowest power (n) which gave the best fit. The correlation coefficients (R^2) of polynomial function fitting were summarized in Table 8. The DIEs of Manα1,2Man gave a best fit at n=5 and only slightly improved when n=6, while that of $Man_9GlcNAc_2$-PA were fit best at n=6. However, the large standard deviation for the data with the $Man_9GlcNAc_2$-PA substrate might greatly affect the interpretation of the experiment.

On the other hand, when the reciprocal, $k_{(O)}/k_{(\chi)}$, were plotted against χ, the result was in a linear relationship (Figure 36), which allowed interpretation using the eq. 14 (Table 9). This model describes the situation where multiple protons are involved in the reaction, but only single proton affects the reactant state [123]. Using the relationship described in equation eq.14, the fractionation factor of reactant state (ϕ^R) was calculated from the slope yielding values of 0.71 for Manα1,2Man and 0.74 for $Man_9GlcNAc_2$-PA. These results agree with the reported values of an acid-base catalysis, in which the solvent isotope effect was between 1.5-3 and the fractionation factors ranged from 0.3-0.7 [123, 124].

3.10 Mutagenesis, expression, and purification of the enzymes

To determine the contribution of protein sidechain residues to glycone binding within the -1 subsite of *Hs*ERManI, T688 and F659 were subjected to site-directed mutagenesis as described in Chapter 2 to generate a T688A and F659A mutants. For the > +1 subsite binding pocket, the R461 was chosen for mutagenesis study. The putative catalysts, E330, D463, and E599 [14], and the potential auxiliary catalyst, H524 and R334, were also altered by mutagenesis in order to further investigate their impact on catalysis and binding of the inhibitors and oligosaccharide substrates. R597 was also mutated to Ala to monitor the effect of the side chain change.

Each of these residues was individually altered by mutagenesis (D463N, E330Q, E599Q, R334A, and H524A) along with some of the combinations of double mutants followed by expression in *Pichia pastoris* X-33 as secreted catalytic domains [14, 15]. The mutated forms of the enzyme were expressed as efficiently as the wild type enzyme, with the exception of the R334A mutant which was not detected in the culture media and was not characterized further.

The mutant enzymes behaved similarly to the wild type enzyme and could be purified by cation-exchange chromatography [14], after which each protein showed greater than 90% purity by SDS-PAGE with a molecular mass of about 53 kDa, the same as the native enzyme (data not shown). These enzymes were stored at 4 ºC and used for enzyme kinetic and binding analyses without further purification. In cases where greater purity was required, the proteins were further enriched by chromatography on a Superdex 75 column as described in the Methods section.

3.11 Analysis of enzyme kinetics

The α1,2-mannosidase specific activity toward $Man_9GlcNAc_2$-PA catalyzed by the wild type and mutant enzymes were assayed at pH 7.0 in 20 mM MES, 150 mM, 5 mM $CaCl_2$. Relative specific activities are shown in Figure 37. The enzyme activity of the mutant forms of

*Hs*ERManI in the proposed catalytic residues, E330, D463, E599, varied from 10^3-10^5-fold less than that of the wild type enzyme. The mutation of T688, F659 and H524 to Ala resulted in 10-100-fold reduction in enzyme specific activity.

All of the mutants had diminished k_{cat} values relative to wild type ERManI (Table 10), but the mutations had a relatively minor impact on K_m (variation of <4.6-fold). The H524A mutant had the least change in k_{cat} (4.3-fold reduction), while the other mutants varied from a 44-fold reduction (E330Q) to 10^5-fold reduction (E599Q) (Table 10). Double mutants of E599Q with either E330Q or D463N resulted in a significant reduction in k_{cat} and a slight increase in K_m consistent with the dominant effect of the E599Q single mutant. pH-rate analysis indicated that there was no significant change in pH optimum (<0.5 pH units) for the any of the mutants except for E330Q, which reduced the pH optimum by 1.8 units (Table 10). A plot of log k_{cat}/K_m versus pH revealed that the E330Q mutant had a major shift of the basic limb of plot by ~3.3 pH units when the curve was fit for single macroscopic dissociation constants on the acidic and basic limbs of the plot (Figure 38, dotted lines). More effective fitting of the data was found using two microscopic dissociation constants for each limb of the curve (Figure 38, solid lines). Analysis of the microscopic dissociation constants revealed changes in each value, but the greatest shift was a ~3.7 pH unit drop in pKa3 on the basic limb of the curve. These data indicate that E330 plays a direct role in establishing the pH optimum of the enzyme by acting as a catalytic acid that must be protonated for the enzymatic reaction to proceed effectively.

R461 and R597 were mutated to R461A, R461L and R597A to investigate the substrate binding and specificity. The detailed enzyme kinetic parameters for hydrolysis and binding of $Man_9GlcNAc_2$-PA were summarized in Table 10. The R461L exhibited the ability to readily hydrolyze α1,2-mannoside residues from $Man_9GlcNAc_2$-PA to $Man_{8\text{-}6}GlcNAc_2$-PA products. In contrast, the R461A or R597A were unable to cleave beyond $Man_8GlcNAc_2$. The catalytic rate of

R461L was ~9-fold faster than that of R461A and ~8-fold slower than that of wild type. In addition, the K_m values for R461A, R461L and R597A were increased 3-5-fold compared to that of the wild type enzyme.

The pH optima of wild type ERManI and the E330Q, T688A and F659A mutants were determined to be 7.0, 5.3, 6.5, and 6.8, respectively, in 20 mM MES, 150 mM and 5 mM $CaCl_2$, (Table 10). The k_{cat} and K_m for wild type enzyme were determined to be 3.7 ±1.6 s^{-1} and 110 ± 8 μM, respectively. The efficiency (k_{cat}/K_m)of $Man_9GlcNAc_2$ cleavage by T688A and F659A was 20% and 0.7% of that of the wild type enzyme respectively. The K_m was reduced by 5 times in T688A, but remained unaffected in the F659A mutant, while k_{cat} was reduced by about 30 and 100-fold in T688A and F659A, respectively. Briefly, the k_{cat}/K_m of E330Q was 0.6% of wild type at pH 7.0, but increased to 3.5% at its optimum pH 5.3. This suggested that E330Q might play a role of general acid catalyst.

3.12 Surface Plasmon Resonance (SPR) Analysis

3.12.1 Glycan binding affinity measurements to *Hs*ERManI — In addition to kinetic analysis, the binding affinity of high mannose oligosaccharides, an uncleavable thiodisaccharide analog, and an equivalent *O*-disaccharide substrate to recombinant wild type and mutant forms of ERManI were also examined by surface plasmon resonance (SPR) (Figures 39 and 40). The on- and off-rates for binding of the $Man_9GlcNAc_2$-glycopeptide ligand to the wild type enzyme and the E599Q, and F659A mutants were too fast for accurate measurement by SPR, but K_D values could be derived from equilibrium binding sensogram measurements (Figures 39A, G, and M inset plots). In contrast, the E330Q mutation significantly slowed the on- and off-rates for all of the ligands, allowing their measurement independently from both kinetic and equilibrium binding data. The resulting data (Table 11) indicate that the E599Q mutant had a 4-fold weaker binding

affinity than the wild type enzyme for $Man_9GlcNAc_2$-glycopeptide and an ~1000-fold reduction in binding affinity to dMNJ. In contrast, the E330A mutant had a ~100-fold increase in binding affinity for the $Man_9GlcNAc_2$-glycopeptide ligand with a virtually unchanged affinity for dMNJ. These values, in combination with slowed on- and off-rates and the decreased k_{cat} for the E330Q mutant, indicate that the reduced catalytic turnover and replacement of the catalytic acid with an uncharged isosteric amide facilitates slower binding kinetics, higher binding affinity for the substrate, and no change in affinity for the glycone residue. The binding of Kif to the wild type enzyme resulted in no significant off-rate for the complex (Figure 39O) while the F659A mutant allowed the Kif-protein complex to dissociate (Figure 39P) and no binding response was detectable when dMNJ was used as ligand (Figure 39N). The E330Q, D463N and T688A mutants also formed stable non-dissociable complexes with Kif, similar to that observed for wild type enzyme, but not E599Q (data not show).

The D463N mutant revealed a surprising difference in binding characteristics between the $Man_9GlcNAc_2$-glycopeptide and dMNJ ligands. The binding affinity of dMNJ to the D463N mutant was reduced ~73-fold (Table 11), but binding to the $Man_9GlcNAc_2$-glycopeptide (Figure 39) as well as the disaccharide ligands (not shown) was virtually eliminated. Double mutations of D463N/E330Q or D463/E599Q also remained unable to form stable complexes with the $Man_9GlcNAc_2$-glycopeptide ligand. These data are consistent with a role for this latter residue in binding the substrate in the +1 subsite as we detected in our subsequent co-crystal structure with the thiodisaccharide (see below).

The binding constant for interaction of dMNJ with the T688A mutant was determined to be 8.17±1.68 μM compared to a value of 1.61±0.64 μM for the wild type enzyme as the result of the faster off-rate for the T688A mutant, while the K_D for $Man_9GlcNAc_2$ significantly decreased (Figure 33K). The increased binding affinity and slowed on- and off-rate for T688A to

$Man_9GlcNAc_2$ was similar to the increase in glycan affinity for the E330Q mutant, which allowed the measurement of both k_a and k_d for both mutant enzymes (Table 9). In both mutants the higher affinities likely result from a reduction in catalytic turnover allowing the uncleaved product to remain associated with the active site.

The binding analysis using SPR showed that R461L exhibited a poor affinity of binding to $Man_9GlcNAc_2$-glycopeptide that could not be measured. The binding dissociation (K_D) of R641A for $Man_9GlcNAc_2$-glycopeptide was measured to be 4.1 μM and that of R597A was 34 μM. Both R461A and R597A exhibited slower on/off rates compare to that of the wild type enzyme (data not shown).

3.12.2 Disaccharide binding to *Hs*ERManI — A thiodisaccharide of Man-α1,2-Man-*O*-CH_3 (methyl-2-S-(α-D-mannopyranosyl)-2-thio-α-D-mannopyranoside) was synthesized as a modification of a previously published method [147] and the structure was confirmed by NMR spectroscopy. Proton scalar couplings confirmed that both pyranose rings are in the conventional $^4C_1$ conformation in solution and qualitative analysis of NOEs and carbon-proton scalar couplings showed that the glycosidic bond adopts angles similar to an equivalent O-glycoside (data not shown).

The IC_{50} for the thiodisaccharide compound was determined to be about 200 μM using 2 ug/ml *Hs*ERManI with 50 uM $Man_9GlcNAc_2$-PA. The on- and off-rates of the thiodisaccharide and the equivalent *O*-glycoside for binding to wild type *Hs*ERManI (Figure 40) or the E330Q mutant (data not shown) were significantly slower than the equivalent values for the $Man_9GlcNAc_2$-peptide ligand and both disaccharide ligands had lower equilibrium binding affinities. The on- and off-rates were significantly different for the two disaccharides, but the

equilibrium binding affinity (K_D) was only ~5-fold higher for the thiodisaccharide over the *O*-glycoside. These data, in combination with the NMR data above, indicate that the solution behavior and binding of the thiodisaccharide to H*s*ERManI is likely to be similar to the *O*-glycoside substrate. The inability to cleave the thiodisaccharide may also account for the slightly increased binding affinity for the latter compound, since the binding affinity for the *O*-glycoside may reflect both binding and hydrolysis by the wild type enzyme.

3.13 Effect of Ca^{2+} on catalysis

The role of the protein-bound Ca^{2+} ion on catalysis was determined from the specific activity measured in buffers containing the metal chelator, EGTA, to control the free Ca^{2+} ion concentration in the reaction buffer at pH 7.0 using 20 μM $Man_9GlcNAc_2$ as substrate. The specific activity of the wild type and the T688A mutant were plotted against the concentration of free Ca^{2+} as shown in Figure 41. The curve of specific activity for both the wild type enzyme and the T688A mutant appeared to be sigmoidal with respect to pCa (-log [Ca^{2+}]) similar to data expected from common equilibrium dialysis experiments. Therefore, the affinity constant for Ca^{2+}, K_{Ca}, was determined by non-linear regression analysis using eq. 18 [126],

$$y = \frac{nK_{Ca}\left[Ca^{2+}\right]}{1 + K_{Ca}\left[Ca^{2+}\right]} \qquad \text{eq. 18}$$

where y is equal to the moles Ca^{2+} bound per mole of enzyme, which was redefined as the unit of α-mannosidase specific activity measured as the result of Ca^{2+} binding to the enzyme, n is the number of sites, which was redefined as the apparent specific activity per Ca^{2+} binding event per μg enzyme. As a result, the K_{Ca} for the wild type enzyme was determined to be 0.24 ±0.02 $\times 10^6$ M^{-1} and for T688A the K_{Ca} was determined to be 0.15±0.01 $\times 10^6$ M^{-1}, 1.6-fold lower than that of

wild type. The specific activity (*n*) of T688A was 15-fold different than that of wild type, which corresponded to 20-fold difference in catalytic efficiency (Table 10) rather than the 28-fold difference in catalytic rate alone. This result suggested that the T688A mutation affected both the catalytic rate and binding to substrate, but only minor change in Ca^{2+} affinity. The K_{Ca} for wild type *Hs*ERManI was similar to the affinity constants previously determined for the yeast ERManI [167] and rabbit liver GManIA [168].

3.14 Effect of Ca^{2+} on binding

The binding analysis for dMNJ to the wild type enzyme in the absence of Ca^{2+} (Figure 39I) resulted in ~340-fold higher K_D, ~100-fold slower for on-rate (k_a) and 2.7-fold faster off-rate (k_d) compared to those binding kinetic parameters of dMNJ to wild type enzyme in the presence of Ca^{2+} (Figure 39B). In contrast, the dissociation constants (K_D) for $Man_9GlcNAc_2$ to wild type enzyme in the presence and absence of calcium ion (Figure 33A and J) were determined to be less than 2-fold different. In Ca^{2+}-free buffer, the binding constant for $Man_9GlcNAc_2$ was affected by the absence of catalysis which allows $Man_9GlcNAc_2$ to remain bound to the wild type enzyme. As a result, the on-rate and the off-rate of binding of $Man_9GlcNAc_2$ to wild type enzyme in the absence of Ca^{2+} were be determined to be $18\pm0.16 \times 10^3$ $s^{-1}M^{-1}$ and $90.5\pm16.3 \times 10^{-3}$ s^{-1}, respectively. These results indicated that Ca^{2+} had much less effect on K_D for $Man_9GlcNAc_2$ than that of dMNJ and that the enzyme is able to bind the substrate and dMNJ to the active site even without the coordination of Ca^{2+} to the glycone binding site, although with lower affinity.

3.15 Co-crystal structure of a thiodisaccharide and *Hs*ERManI

3.15.1 Co-crystallization of thiodisaccharide and *Hs*ERManI — Since the crystals for *Hs*ERManI grown under the conditions previously reported (1.7 M ammonium sulfate) were unable to diffract at atomic resolution, the recombinant protein was subjected to a crystallization screening and optimization as well as additive screening prior to attempting co-crystallization with the thiodisaccharide substrate analogue. Initial sparse-matrix screening resulted in the identification of five conditions which generated split rod shape crystals (Figure 42A), but none of these conditions produced large single crystals. Further additive screening identified five additives which produced rod shape crystals and six additives which produced plate shape crystals. The addition of 1,4-butanediol was found to produce the best crystals (Figure 42B) and improved diffraction to beyond 1.35 Å. Since there was a limited supply of the thiodisaccharide substrate analogue, direct co-crystallization was attempted using the above conditions without further optimization. Although the single co-crystals grown by this method were considerably smaller in size than that of the native crystals, one of the crystals produced diffraction data that could be scaled to 1.41 Å (Figure 43) with good statistics and completeness (Table 12). Diffraction analysis indicates that both native and co-crystals belong to space group *P1* and the Matthews coefficients [169] indicate a single molecule per asymmetric unit. One of the unit cell constants (α) of the co-crystal was calculated to be significantly larger than that of the native crystal. Even though the difference in the unit cell constant suggests a significant impact of the presence of thiodisaccharide on crystal packing, there was no significant difference in overall protein structure between native crystal and co-complex structures (data not show).

3.15.2 Co-complex structure of *Hs*ERManI with the thiodisaccharide analog — Co-crystalization of recombinant *Hs*ERManI with the thiodisaccharide analog resulted in crystals that diffracted at 1.4Å and the structure of the co-complex was solved by molecular replacement using the structure of *Hs*ERManI (PDB 1FMI) as the probe. The structure revealed an $(\alpha\alpha)_7$ barrel with an extra density corresponding to the thiodisaccharide in the proposed –1 and +1 subsites (Figure 44A). As anticipated for the thiodisaccharide, the C-S bond lengths for the thiodisaccharide were both ~1.8Å, significantly greater than the standard ~1.4Å C-O bonds in a glycosidic linkage. Modeling of Man-α-*O*-CH_3 in the +1 subsite revealed an unambiguous $^4C_1$ chair conformation for the monosaccharide, whereas the conformation of the glycone in the –1 subsite was clearly distorted (Figures 44A and 44B). The hydroxyls associated with C3 and C4, as well as the C5-C6 linkage were in axial configurations, and the O2' hydroxyl was equatorial in identical positions compared to the $^1C_4$ chair conformation of the previously published dMNJ co-complex [14]. However, the positions of C1, O5 and C5 were clearly distorted from the $^1C_4$ chair into a $^3S_1$ skew-boat conformation (Figure 44). The altered position of C5 resulted in a corresponding change in the position of C6, however a rotation of the C5-C6 bond resulted in a nearly identical position of the O6' hydroxyl for hydrogen bonding to O-ε1 of E599 and NH1 of R597. Thus, C1, O5, C5, and C6 were the only atoms that were significantly altered in position from the $^1C_4$ chair of the DMJ co-complex structure [14] and none of these atoms directly interact with the enzyme in the –1 subsite. Comparison of the of the $^3S_1$ skew-boat conformation with the $^1C_4$ chair revealed that the transition between these two conformations results predominately from a twist at C5, the O5 ring oxygen, and the C1 carbon and the $^3H_4$ conformation is the planar intermediate between these two structures (Figures 13 anf 46). The movements for C5, O5, and C1 would be ~0.4 Å, ~1Å, and ~0.3Å, respectively, during the conformational switch.

3.15.3 Interactions between ERManI and the thiodisaccharide substrate analog — Interactions between the non-reducing terminal residue in the thiodisaccharide and the –1 subsite residues are stabilized by identical direct interactions as in the ERManI-dMNJ co-complex, including direct coordination of the Ca^{+2} ion to the O2' and O3' hydroxyls, hydrogen bonding to the O4' and O6' hydroxyls, and a hydrophobic stacking of F659 adjacent to the C4-C5-C6 region of the –1 residue (Figure 38). The predominant interactions with the +1 residue are a pair of hydrogen bonds between the two carboxylate oxygens of D463 and the O3' and O4' hydroxyls of the +1 sugar residue. Additional hydrogen bonds were found between the enzyme and the O4' and the O6' hydroxyls of the +1 residue.

3.16 Thermodynamic evaluation of catalysis and binding of wild type, E330Q and T688A mutants of *Hs*ERManI

3.16.1 Temperature dependence study of catalysis — The catalytic rate (k_{cat}) of the wild type and the E330Q and T688A mutants of H*s*ERManIA toward $Man_9GlcNAc_2$ were obtained from initial rates measured at different temperatures shown in Figure 47. The reflexion points were observed at 40ºC and 35ºC from the exponential rise of catalytic rates for wild type and E330Q respectively, but no reflexion point was observed for T688A over the range of temperature investigated. The reflexion point indicated the temperature of protein denaturation and the data beyond the reflexion point were not used for Arrhenius plot analysis (Figure 48). The activation energy (E_a) was calculated from the slope ($-E_a/R$) of Arrhenius plots and the thermodynamic activation parameters of the catalysis reaction were calculated at 25ºC as described in Chapter 2 and summarized in Table 13. Because of high error in the data, calculation of the values for E_a for the wild type enzyme made a comparison to the T688A mutant not particularly informative;

therefore it is only possible to conclude that the thermodynamics of catalysis for wild type, E330Q, and T688A were not significantly different.

3.16.2 Temperature-dependence of substrate binding —The binding properties for $Man_9GlcNAc_2$ to the wild type and mutant forms of H*s*ERManI were obtained from the SPR binding analyses at different temperatures as described in Chapter 2. The biosensor responses for wild type, E330Q and T688A shown in Figure 49 were representative of the biosensor responses using 50, 10 and 10 μM of $Man_9GlcNAc_2$ for the respective enzymes. The off-rate for the T688A mutant with the $Man_9GlcNAc_2$-glycopeptide ligand indicated that the binding responses significantly increase as the temperature increases, while the off-rate for E330Q binding responses remained unaffected. The temperature dependent binding response plots showed that lower temperature reduces the enzyme-$Man_9GlcNAc_2$ complex dissociation as observed with the wild type enzyme at 10-15ºC. As the temperature increases beyond 15ºC the SPR response decreases linearly, presumably as a result of enzymatic cleavage of the enzyme-glycan complex. In contrast, the T688A mutant showed an increase in binding response to maximum at 20ºC followed by and a decrease at higher temperature. The change of binding response can be explained by the effect of catalytic hydrolysis on the dissociation event at higher temperature. The catalytic rate would be predicted to increase as temperature increases and result in a faster off-rate as a result of increased rate of cleavage of $Man_9GlcNAc_2$ to $Man_8BGlcNAc_2$ (Figure 49A and C). Comparison of the catalytic rate of wild type and the T688A mutant toward $Man_9GlcNAc_2$ at 10ºC and 37ºC indicates that the wild type enzyme has 30-fold increase in activity over this temperature span whereas the T688A mutant increases 10-fold over the same temperature range (data not shown). Unlike wild type *Hs*ERManI or the T688 mutant, the binding response of the E330Q mutant increased as the temperature increased (Figure 49B).

These results suggest that there is little significant contribution of catalytic cleveage of the ligand by the mutant enzyme over this temperature range. The increase in binding response with temperature would therefore reflect only the binding event without catalysis. This conclusion was confirmed by the comparison of catalytic rate of E330Q at 10ºC and 37ºC at pH 7.0. The catalytic rate increased only by 2-fold over this span of temperature (data not shown). Additional support came from studies of varying pH in SPR studies with the E330Q mutant (Figure 50). The biosensor response for $Man_9GlcNAc_2$ binding to E330Q indicated that at pH 7.0 (Figure 42B) or higher (Figure 50A) there is high affinity binding and a significantly reduced off-rate resulting from minimal catalytic cleavage of the ligand, while at pH 5.0 (Figure 50C), the binding affinity reduced dramatically due to an increase of the off-rate in response to the increased catalytic rate of E330Q near its pH optimum. Therefore, the binding properties of E330Q at pH 7.0 reflect predominantely a binding interaction, and not catalysis. In such a case, increasing the temperature affected the binding response by predominately increasing the on-rate for E330Q and not the off-rate as shown in Eyring plots (Figure 52A). The van't Hoff analysis (Figure 51) demonstrates that the wild type enzyme and E330Q bind to $Man_9GlcNAc_2$ with similar thermodynamics consisting of lower enthalpy and unfavorable entropy compared to that of T688A whose binding energy was driven by higher enthalpy and a favorable entropy. The thermodynamic parameters at 25ºC for *Hs*ERManI and $Man_9GlcNAc_2$ substrate were summarized in Table 14. The thermodynamics of the transition state are summarized in Figure 53 and Table 15. Thermodynamic analyses of binding reveal profound differences between E330Q and T688A and the wild type enzyme. Even though T688A and E330Q allowed the observation of both on-rate and off-rate, the E330Q mutant is a better model for binding analysis than T688A because the binding kinetics of T688A contain both catalytic and binding components, while the binding kinetics of E330Q is mainly

comprised of a binding interaction without catalysis. The thermodynamics of binding for E330Q show the same trend as that of the wild type enzyme suggesting a similar binding mechanism.

3.17 Oligosaccharides and binding analysis — The E330Q mutant was used as a model to investigate the contribution of individual mannose residues to the binding interaction between ERManI and $Man_9GlcNAc_2$. Characterization of the binding parameters for various high mannose oligosaccharides to ERManI were performed and compared (Figure 45 and Table 16). The contribution of individual residues or groups of residues can be determined by a combination of difference calculations of binding ΔG values as shown in Table 17. For example, the contribution of residue M_{10} can be calculated in two ways: $\Delta G_{Man9GlcNAc2} - \Delta G_{Man1\alpha1,2Man}$ and $\Delta G_{Man9GlcNAc2} - \Delta G_{Man1\alpha1,2Man}$. The rationale for the various calculations are shown in Table 17 and the final values for the ΔG contributions for various residues are shown in Figure 55. These calculations indicate that the glycone residue contribute only (~7.0 kJ/mol) to the affinity of binding while residue M_7 contributes ~17.6 kJ/mol. Residues M_9, M_8 and M_{11} together contribute ~6.4 kJ/mol and the contribution of the remainder of the glycan structure to the affinity of binding is negligible (~2.5 kJ/mol). The conclusions of these studies, that the residue M_7 contributes binding interactions that account for approximately half of the binding energy for the substrate, is consistent with the mutagenesis data indicating that D463 plays a critical role in substrate binding affinity. Even a conservative mutation (D463N) in this residue eliminates detectable binding of $Man_9GlcNAc_2$ –glycopeptide ligands by SPR and results in a 800-fold drop on k_{cat}. Surprisingly, there was no change in K_m for the D463N mutant using the $Man_9GlcNAc_2$ substrate.

Figure 22: Time course of digestion of the $Man_9GlcNAc_2$-PA oligosaccharide substrate by recombinant *Hs*ERManI, recombinant murine *Mm*GManIA, or a mixture of the two recombinant enzymes. The recombinant fusion protein containing the *Hs*ERManI linked to protein A was expressed in COS cells, and the enzyme in the culture media was adsorbed to IgG-Sepharose and used in enzyme digestions containing the $Man_9GlcNAc_2$-PA substrate (left panels). Additional incubations were carried out containing either recombinant murine *Mm*GManIA (center panels) or a combination of the recombinant *Hs*ERManI and *Mm*GManIA at concentrations identical to the individual digestions (right panels). Aliquots from the reactions were removed at the times indicated at the right and were resolved by NH_2-HPLC as described in Chapter 2. The elution position of oligosaccharide size standards are indicated at the top: $Man_5GlcNAc_2$-PA (5), $Man_6GlcNAc_2$-PA (6), $Man_7GlcNAc_2$-PA (7), $Man_8GlcNAc_2$-PA (8), and $Man_9GlcNAc_2$-PA (9).

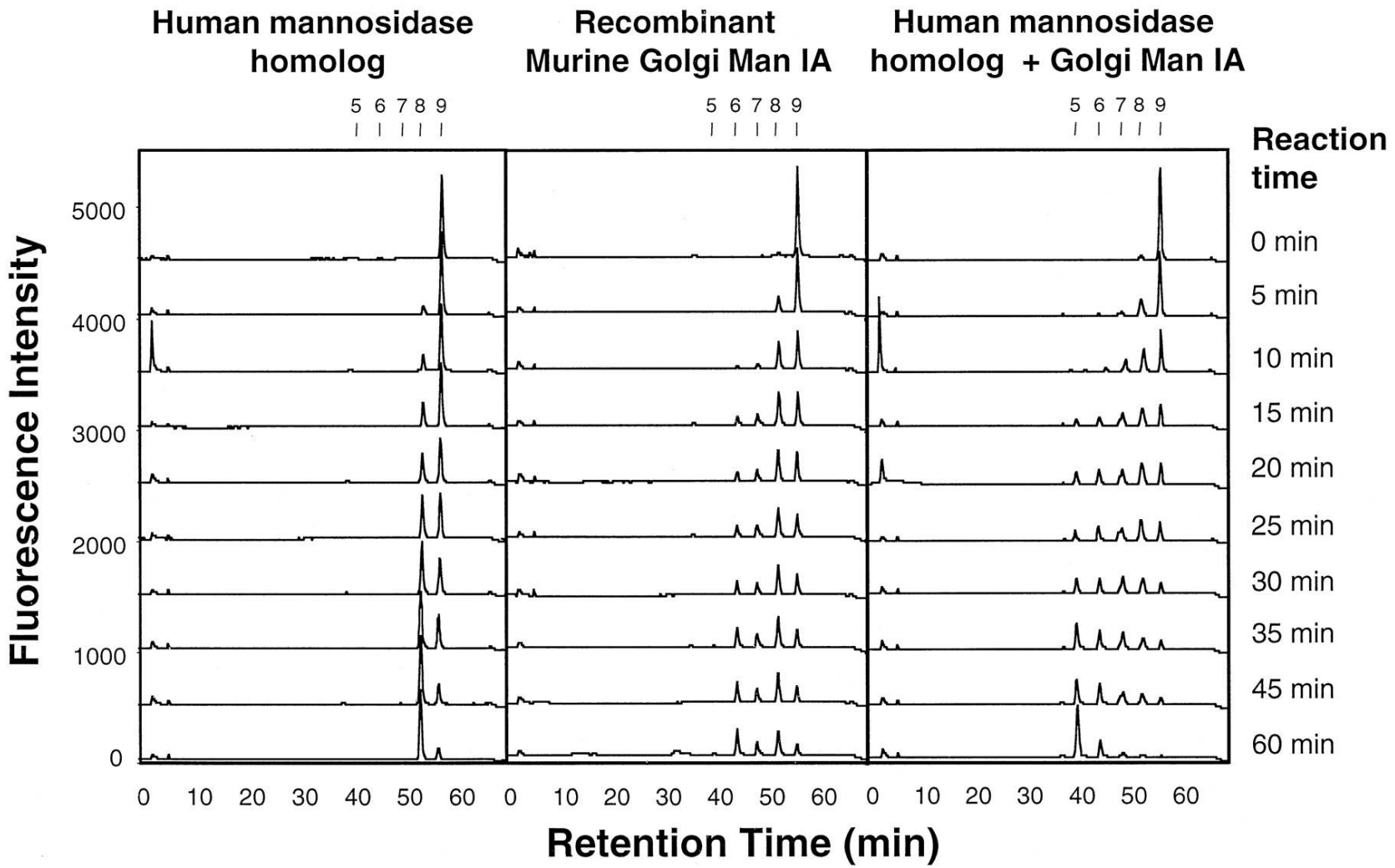

Taken from Gonzalez, D.S., K. Karaveg, *et al.* (1999) *J. Biol. Chem.* **274**: 21375-86.

Figure 23: Identification of $Man_8GlcNAc_2$ isomers generated during enzymatic digestions by *Hs*ERManI and by *Mm*GManIA. The peaks corresponding to $Man_8GlcNAc_2$-PA in the time course studies in Figure 22 were pooled and resolved by C_{18}-HPLC as described in Chapter 2. The three $Man_8GlcNAc_2$-PA isomer standards were generated as described previously [72] and are shown in A. The $Man_8GlcNAc_2$-PA isomer product of the *Hs*ERManI reaction (Man_8B) is shown in B. The $Man_8GlcNAc_2$-PA isomer products of *Mm*GManIA (Man_8A and Man_8C) are shown in C. The bottom axis is elution time (in min) from the C_{18}-HPLC column.

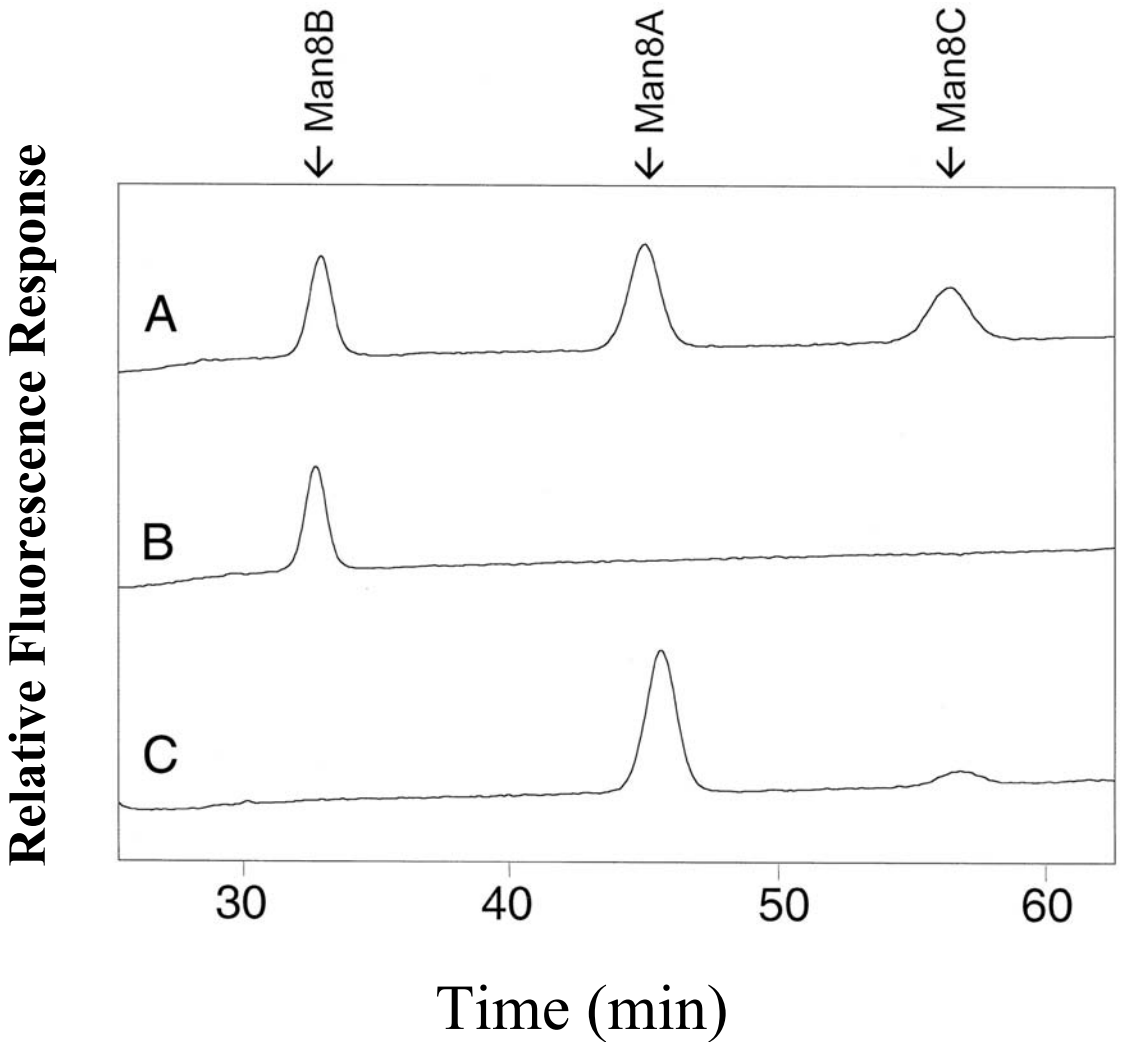

Taken from Gonzalez, D.S., K. Karaveg*, et al.* (1999) *J. Biol. Chem.* **274**: 21375-86.

Figure 24: Enzymatic properties of the recombinant *Hs*ERManI. Enzyme assays of the *Hs*ERManI were carried out using the recombinant fusion protein bound to IgG-Sepharose beads and $Man_9GlcNAc_2$-PA as substrate. A, pH profile of enzyme activity expressed as a percentage of maximal activity; B, kifunensine inhibition of the catalytic activity expressed as a percentage of control activity in the absence of inhibitors; C, dMNJ inhibition of the catalytic activity expressed as a percentage of control activity in the absence of inhibitors; D, EGTA inhibition expressed as a percentage of control activity in the absence of EGTA; E, recovery of mannosidase activity by the addition of $CaCl_2$ after prior incubation in the presence of 200 μM EGTA.

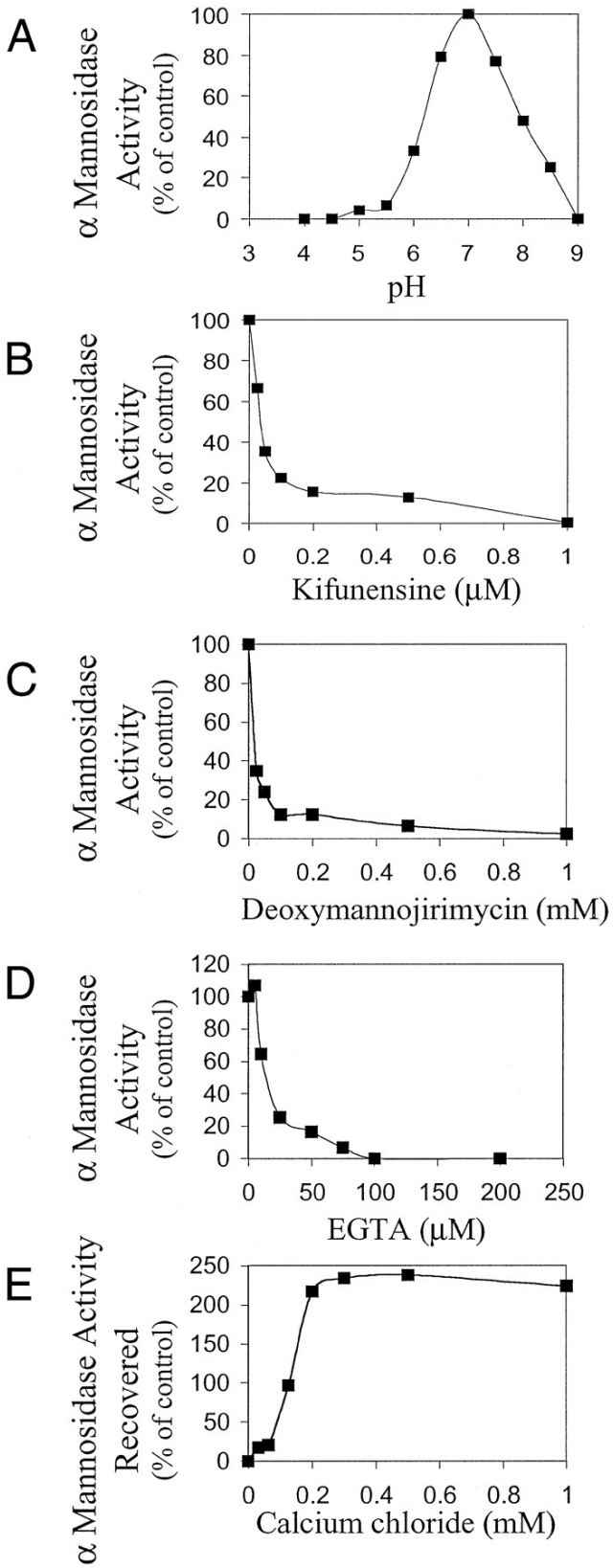

Taken from Gonzalez, D.S., K. Karaveg*, et al.* (1999) *J. Biol. Chem.* **274**: 21375-86.

Figure 25: The effect of cations on the activity of the *Hs*ERManI. The effects of the indicated cations on mannosidase activity are shown either before (open bars) or after (closed bars) preincubation with 200 μM EDTA. Enzyme activity is expressed as a percentage of the control activity in the absence of added cation. Cations were added as chloride or sulfate salts as indicated in Chapter 2 to a final concentration of 1 mM.

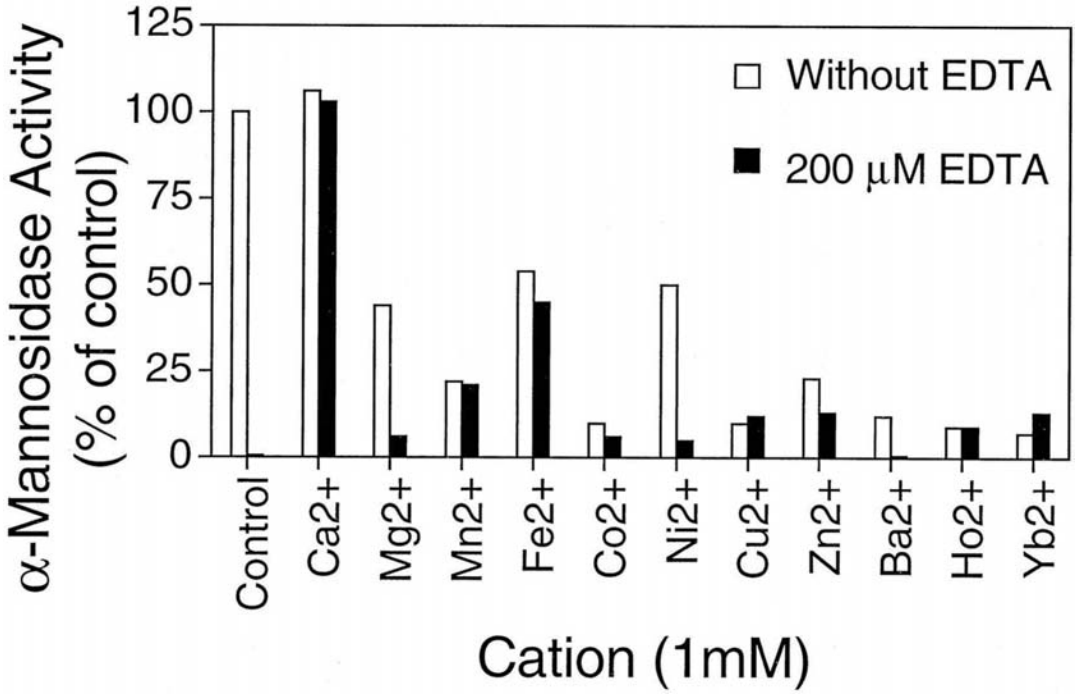

Taken from Gonzalez, D.S., K. Karaveg*, et al.* (1999) *J. Biol. Chem.* **274**: 21375-86.

Table 5. The effect of dMNJ on the relative activity of *Hs*ERManI and murine *Mm*GManIA in a mixed enzyme reaction. The relative sensitivity of recombinant *Hs*ERManI and murine *Mm*GManIA to inhibition by dMNJ was determined in an enzyme reaction containing both enzymes at an approximate ratio of 0.4:1 (*Hs*ERManI to *Mm*GManIA). Three reactions were prepared with the $Man_9GlcNAc_2$-PA substrate and incubated for the times indicated in the presence or absence of dMNJ. The $Man_8GlcNAc_2$-PA peak was isolated by NH_2-HPLC, as indicated by the arrow on the profiles, and the relative ratios of the $Man_8GlcNAc_2$-PA isomers were determined by C_{18}-HPLC as described in Chapter 2. The sizes of the individual oligosaccharide peaks on the NH_2-HPLC column are shown at the bottom of the table (M_5, $Man_5GlcNAc_2$-PA; M_6, Man6$GlcNAc_2$-PA; M_7, Man$GlcNAc_2$-PA; M_8, $Man_8GlcNAc_2$-PA; M_9, $Man_9GlcNAc_2$-PA). The presence of $Man_8GlcNAc_2$ isomer B is indicative of the *Hs*ERManI activity, and the presence of $Man_8GlcNAc_2$ isomers A and C are indicative of *Mm*GManIA activity. The ratio of the isomers ($Man_8B/(Man_8A + Man_8C)$ would represent the relative activity of the *Hs*ERManI versus *Mm*GManIA in the reaction. The dMNJ appeared to have a greater effect on inhibition of *Mm*GManIA as indicated by the increase in the ratio in response to the inhibitor.

Time of Digestion	dMNJ conc	NH_2-HPLC Column Profile	Percent distribution of the $Man_8GlcNAc_2$ isomer structures			
			Man8B	Man8A	Man8C	$\frac{\text{Man8B}}{\text{Man8A+Man8C}}$
5 min	0	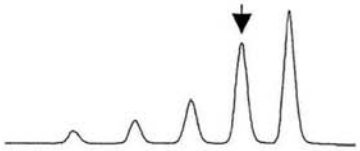	27.3	63	9.8	0.375
20 min	0	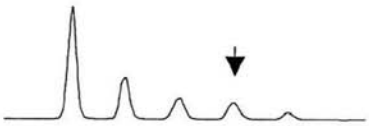	29.6	61.9	8.5	0.42
20 min	5 μM	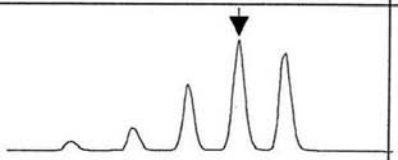	68.2	27.7	4.1	2.14

M5 M6 M7 M8 M9

Taken from Gonzalez, D.S., K. Karaveg*, et al.* (1999) *J. Biol. Chem.* **274**: 21375-86.

Figure 26: *P. pastoris* expression of *Hs*ERManI using the pPICZαA expression vector. (A) The culture media from an induced *Hs*ERManI expression culture was sampled daily following induction with methanol and 10 µl was resolved per lane by SDS-PAGE followed by immunobloting using an anti-*Hs*ERManI polyclonal antibody raised in rabbits as described under "Material and Methods". Each time point in panel A corresponds to α-mannosidase activity measurement shown in panel B.

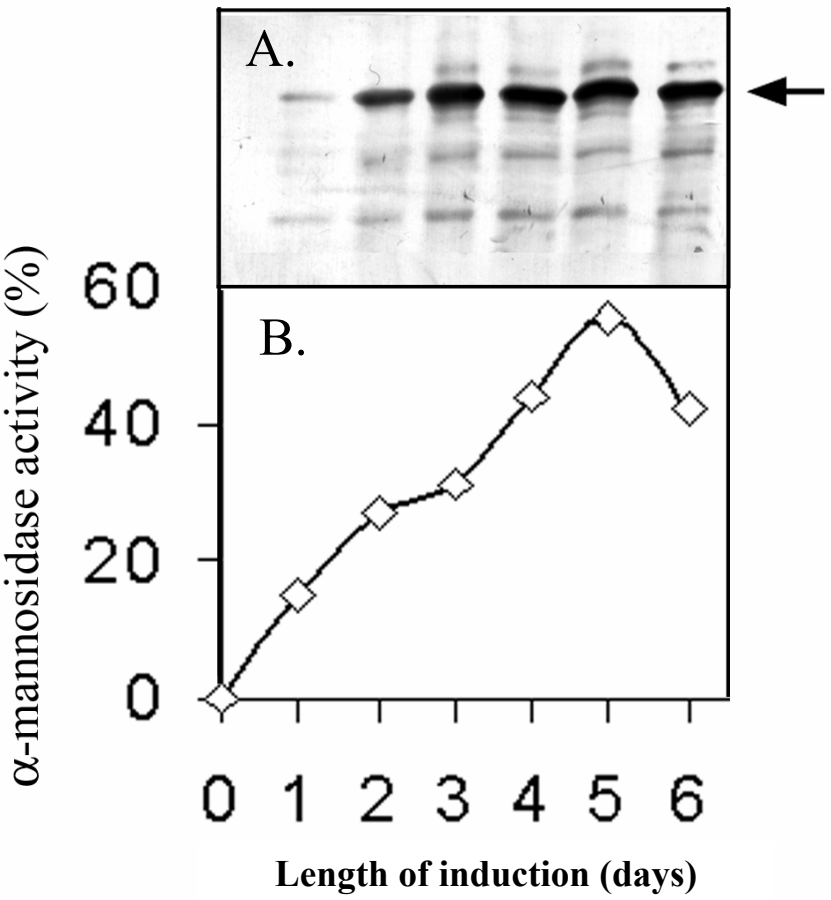
A.
B.
α-mannosidase activity (%)
60
40
20
0
0 1 2 3 4 5 6
Length of induction (days)

Figure 27: The elution profile of recombinant *Hs*ERManI using SP-Sepharose column (15 × 200 mm). The protein (—) was eluted under gradient of 0 – 500 mM NaCl as described in Chapter 2. The peak containing α-mannosidase activity (–◊–) appeared as a sharp peak at ~ 400 mM NaCl. The insert was a pool of eluted material at volume 60-85 ml and resolved by SDS-PAGE. The band corresponding to *Hs*ERManI appears as a band at 55 kDa.

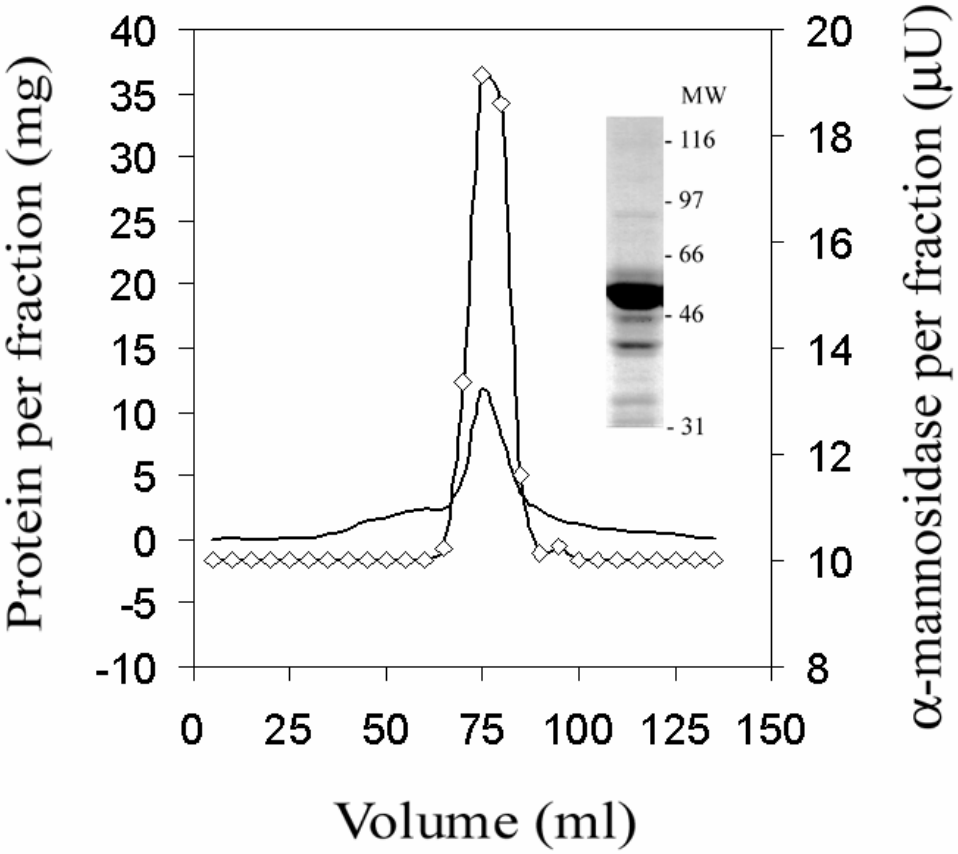
Protein per fraction (mg)
α-mannosidase per fraction (μU)
Volume (ml)
MW
116
97
66
46
31
40
35
30
25
20
15
10
5
0
-5
-10
20
18
16
14
12
10
8
0
25
50
75
100
125
150

Figure 28: The elution profile of recombinant *Hs*ERManI using a Superdex 75 gel filtration column (1.6 ×65 cm). (B) The protein (—) was eluted and α-mannosidase activity (–◊–) was monitored as described in Chapter 2. The content of the fractions (10 µl) were resolved on SDS-PAGE (A). An open arrowhead indicates the material of ~ 80 kDa was separated from the α-mannosidase containing fractions (fractions 15-19).

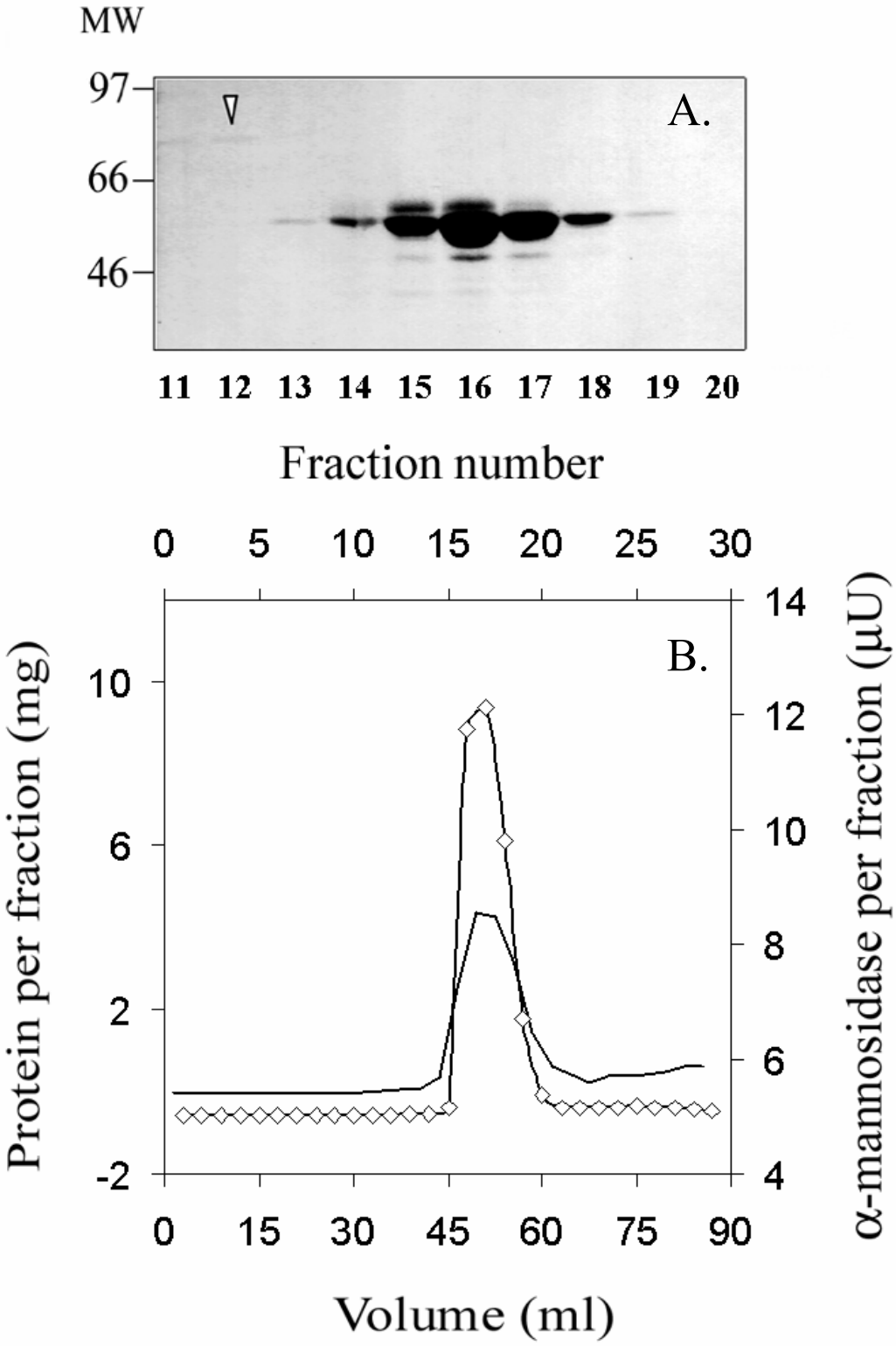
MW
97
66
46
A.
11 12 13 14 15 16 17 18 19 20
Fraction number
0 5 10 15 20 25 30
B.
Protein per fraction (mg)
10
6
2
-2
14
12
10
8
6
4
α-mannosidase per fraction (μU)
0 15 30 45 60 75 90
Volume (ml)

Table 6. Purification of recombinant *Hs*ERManI from the medium of a transformed *P. pastoris* culture.

Fraction	Volume (ml)	Total activity (µunits)	Total protein (mg)	Specific activity (µunits/mg)	Yield (%)	Purification (-fold)
Media	1000	23.7	6,467	0.004	100	1
Ultrafiltration	100	19.3	330	0.058	82	16
SP-Sepharose	25	17.9	12.3	1.455	76	398
Superdex-75	15	15.3	5.4	2.857	65	781

Figure 29: Solubility of purified recombinant *Hs*ERManI in the presence of additive agents. The SP-Sepharose purified protein was concentrated to ~ 4.0 mg/ml in the presence of various agents as described in Chapter 2. The histogram represents the percentage of total purified protein remaining soluble (▉) following the concentration, percentage of total purified protein remaining soluble material after storage for 9 days at 4ºC (▓), the α-mannosidase activity at day 9th (▒). The percentage values of the histograms (▉ and ▓) shown are the relative ratio of the quantity of measurment to that of the starting material prior to concentration. The percentage values of the histograms of enzyme activity (▒) shown are the relative enzyme specific activity of soluble enzyme after 9 days of storage at 4ºC in the presence of additive compared to that of orginal material prior to concentration.

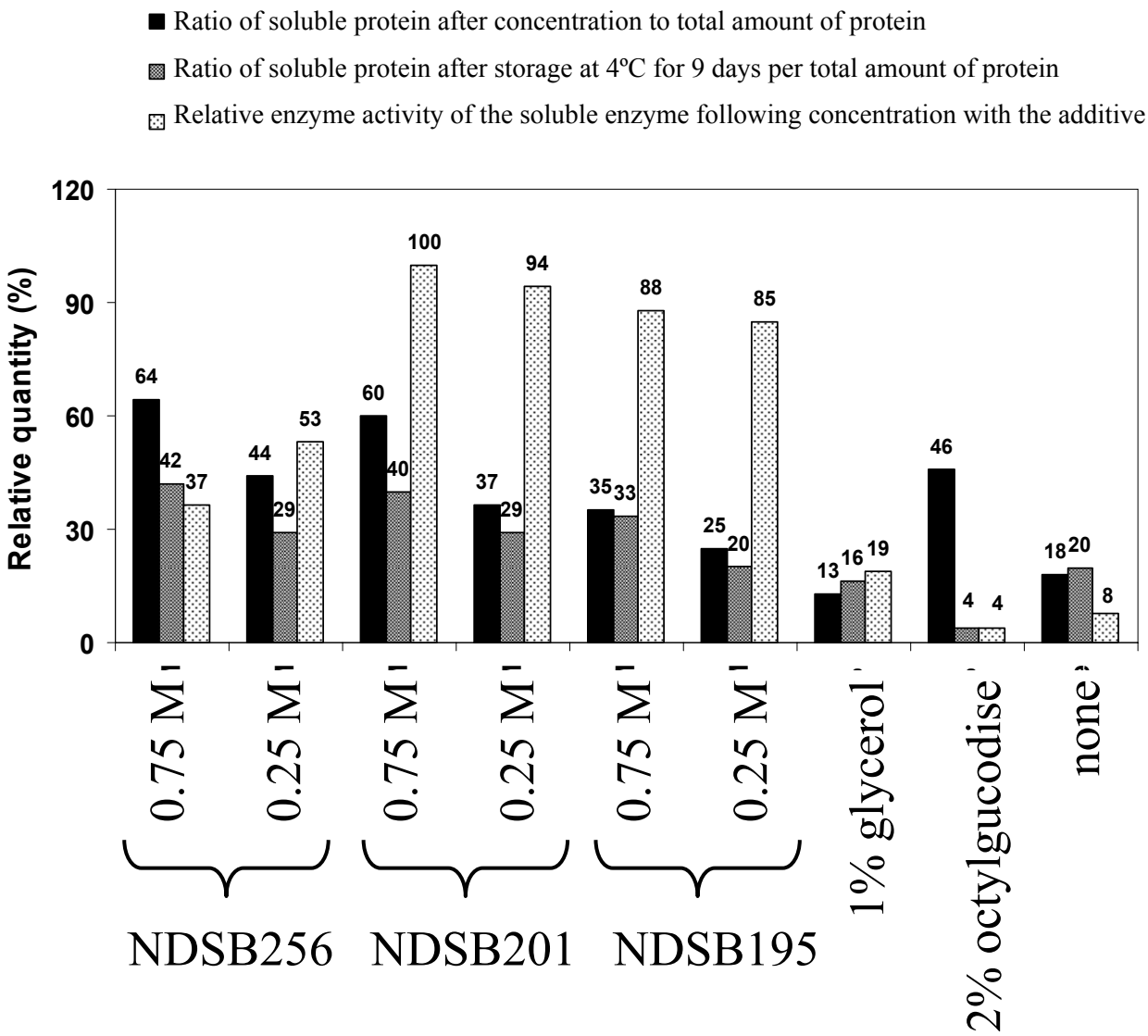
Ratio of soluble protein after concentration to total amount of protein
Ratio of soluble protein after storage at 4ºC for 9 days per total amount of protein
Relative enzyme activity of the soluble enzyme following concentration with the additive
Relative quantity (%)
120
90
60
30
0
64
42
37
44
29
53
60
40
100
37
29
94
35
33
88
25
20
85
13
16
19
46
4
4
18
20
8
0.75 M
0.25 M
0.75 M
0.25 M
0.75 M
0.25 M
1% glycerol
2% octylglucodise
none
NDSB256
NDSB201
NDSB195

Figure 30: Enzyme kinetic analysis for hydrolysis of α1,2 mannoside linkages by the *Hs*ERManI using various substrates; (a) $Man_9GlcNAc_2$-PA, (b) $Man_8GlcNAc_2$-PA isomer B, (c) Manα1,2Manα-O-CH_3, (d) Manα1,2Man. The product analysis and kinetic parameters are determined as described in Chapter 2.

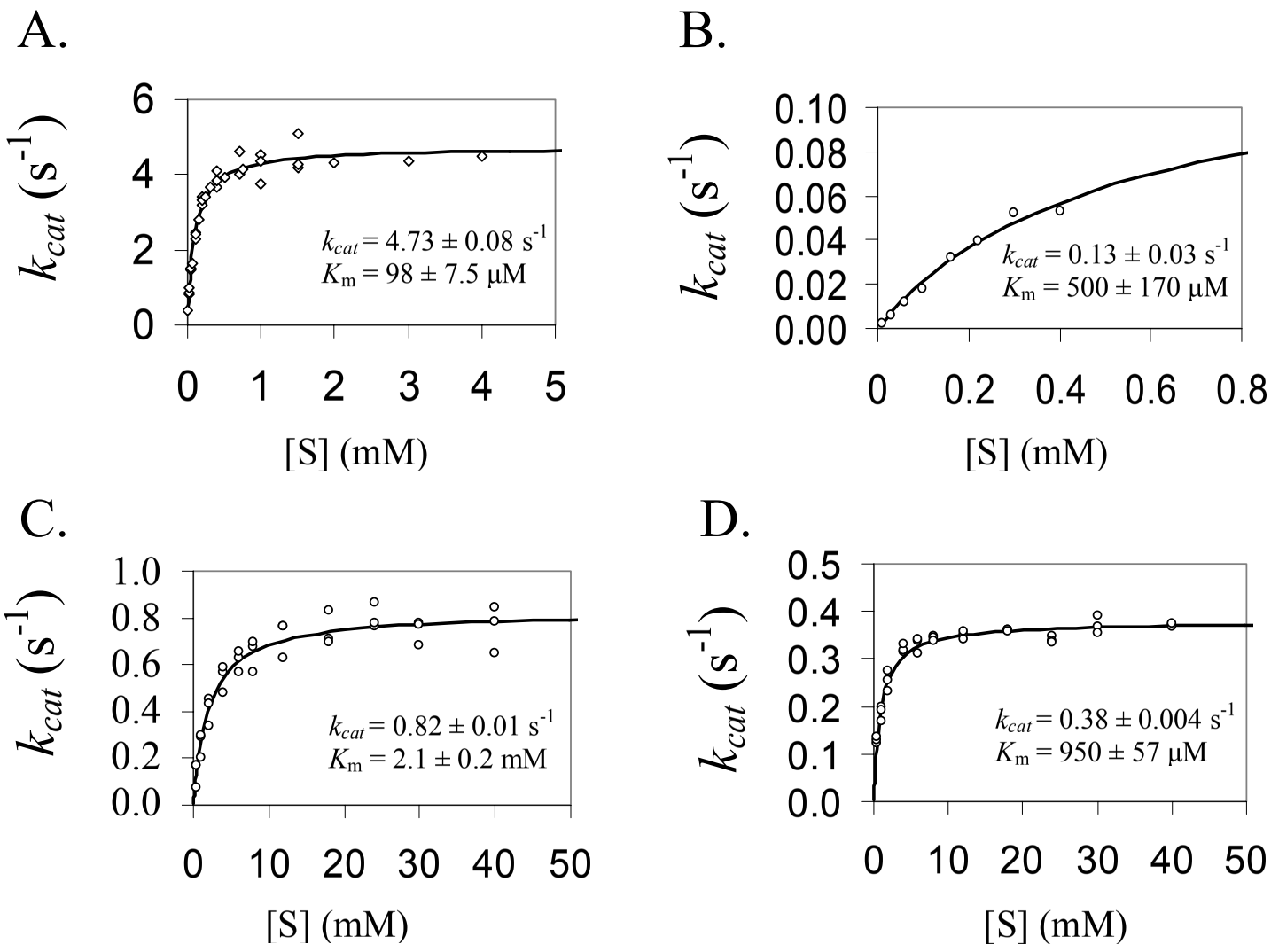
A.
k_{cat} (s^{-1})
k_{cat} = 4.73 ± 0.08 s^{-1}
K_m = 98 ± 7.5 µM
[S] (mM)
B.
k_{cat} (s^{-1})
k_{cat} = 0.13 ± 0.03 s^{-1}
K_m = 500 ± 170 µM
[S] (mM)
C.
k_{cat} (s^{-1})
k_{cat} = 0.82 ± 0.01 s^{-1}
K_m = 2.1 ± 0.2 mM
[S] (mM)
D.
k_{cat} (s^{-1})
k_{cat} = 0.38 ± 0.004 s^{-1}
K_m = 950 ± 57 µM
[S] (mM)

Figure 31: Chemical structures of mannosidases and glucosidases inhibitors; 1-deoxymannojirimycin and kifunensine, the class II α-mannosidase inhibitors swainsonine and 1,4-dideoxy-1,4-imino-D-mannitol, as well as the specific ER α-glucosidase I and II inhibitors castanospermine and 1-deoxynojirimycin are shown. Please note that to facilitate the comparison of different inhibitors and the discussion of the catalytic mechanism, all of the inhibitors have been numbered so that they have similar atom numbering relative to 1-deoxymannojirimycin and mannose. (This is not the standard IUPAC numbering.)

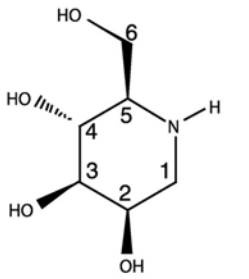

1-Deoxymannojirimycin

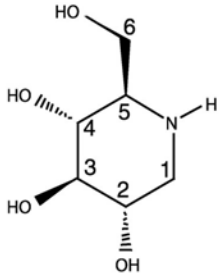

1-Deoxynojirimycin

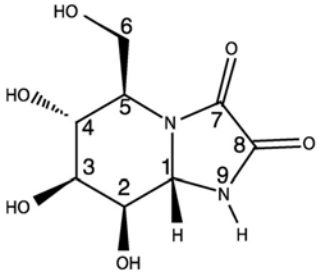

Kifunensine

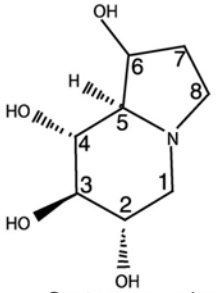

Castanospermine

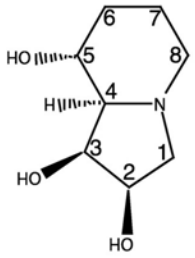

Swainsonine

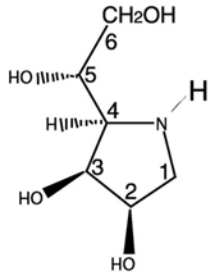

1,4-dideoxy-1,4-imino-D-mannitol

Taken from Vallee, F., K. Karaveg*, et al.* (2000) *J. Biol. Chem.* **275**: 41287-98.

Figure 32: The *Hs*ERManI inhibition analysis. The reciprocal plots of the initial rate of the recombinant enzyme (1 μg/ml) using various concentration of $Man_9GlcNAc_2$-PA as substrate in the presence of the inhibitors; (a) Kifunensine (0, 0.5, 1, 2 and 4 μM); (c) 1-deoxymannojirimycin (0, 5, 10, 20, 35 and 50 μM). The linear regression analysis of (a) and (c) yielded the apparent K_m/k_{cat},which were used to plot against inhibitor concentration [I] in (b) and (d) respectively. The K_i of the inhibitor was determined by non-linear regression fit to the apparent K_m/k_{cat} using eq. 11.

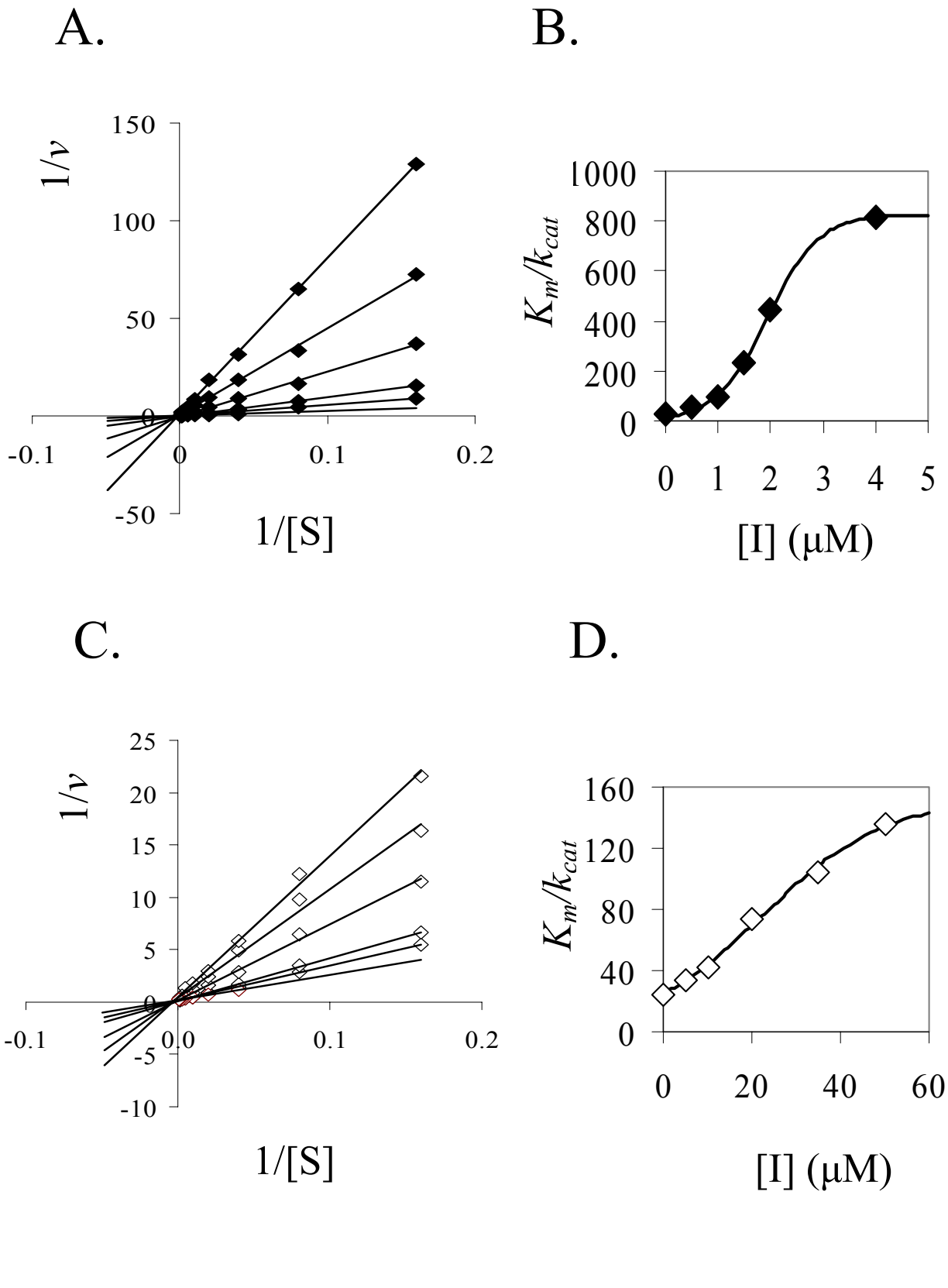
A.
B.
C.
D.
1/v
1/[S]
K_m/k_{cat}
[I] (μM)
150
100
50
0
-50
-0.1
0
0.1
0.2
1000
800
600
400
200
0
1
2
3
4
5
25
20
15
10
5
-5
-10
160
120
80
40
20
40
60

Figure 33: Calorimetric titration of wild type *Hs*ERManI with class 1 mannosidase inhibitors; 1-Deoxymannojirimycin (dMNJ) (A and B) and kifunensine (B and C) were injected into the calorimetry reaction cell containing 1-2 mg/ml wild type *Hs*ERManI**.** Shown in A and C are the integrated injection heat values for the calorimetric titration of dMNJ (0.4 mM) (B) and Kif (0.3 mM) (D), respectively. The titration was carried out at 25 ºC. Aliquots of the inhibitor solution (5 µl) were injected into the enzyme solution at a starting concentration of 0.017 mM for dMNJ and 0.010 mM for Kif. The titration parameters (n = binding stoichiometry, K_A = association constant, H = enthalpy) determined by curve fitting to the heat of binding are summarized below.

Parameters	**dMNJ**	**Kif**
n	1.39	1.22
K_A ($\times 10^6$ M)	0.12±0.02	13±7.5
H (kJ/mol)	-76±8.9	-91±5.1

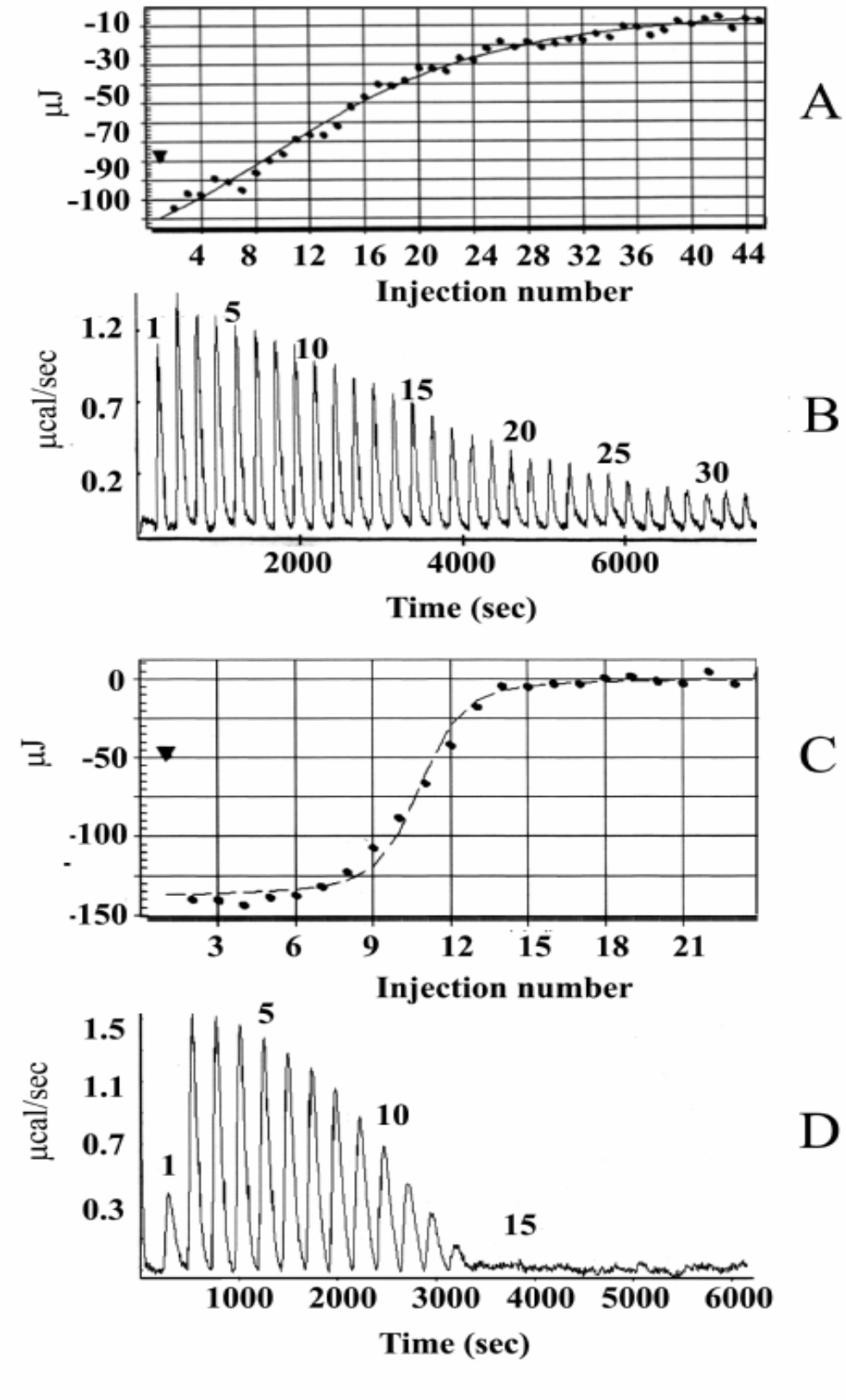
-10
-30
-50
-70
-90
-100
µJ
4 8 12 16 20 24 28 32 36 40 44
Injection number
A
1.2
0.7
0.2
µcal/sec
1
5
10
15
20
25
30
2000 4000 6000
Time (sec)
B
0
-50
-100
-150
µJ
3 6 9 12 15 18 21
Injection number
C
1.5
1.1
0.7
0.3
µcal/sec
1
5
10
15
1000 2000 3000 4000 5000 6000
Time (sec)
D

Table 7. The inhibition of human class 1 α1,2-mannosidase.

Inhibitor	IC_{50} [a] (μM)	K_i [b] (μM)	K_D [c] (μM)	
			SPR	ITC
Kifunensine	0.20	0.13 ± 0.01	< 0.03	0.08 ± 0.01
1-Deoxymannojirimycin	20	11 ± 0.2	1.6 ± 0.64	8.7 ± 2.0
1,4-Dideoxy-1,4-imino-D-mannitol	1,500	-	-	
Swainsonine	> 10,000	-	-	
1-Deoxynojirimycin	> 10,000	-	-	
Castanospermine	> 10,000	-	-	

[a] The IC_{50} values were determined as described under "Materials and Methods" using a constant 3 ng/μl enzyme and 4 μM $Man_9GlcNAc_2$-PA substrate and varying the concentrations of the inhibitor.
[b] The K_i values were determined from non-linear regression analysis as described in Figure 25.
[c] The K_D values were determined from SPR and ITC as described in "Materials and Methods".

Modified from Vallee, F., K. Karaveg*, et al.* (2000) *J. Biol. Chem.* **275**: 41287-98.

Figure 34: The effect of pD on the catalytic pH optimum of *Hs*ERManI. The deuterium buffer was prepared as described in Chapter 2. The reaction rate was measured using $Man_9GlcNAc_2$-PA (20 μM) as substrate and 1 μg/ml of enzyme in the deuterium buffer (–♦–), pD 4.0-9.9, and protium buffer (–◊–), pH 4.0-9.9.

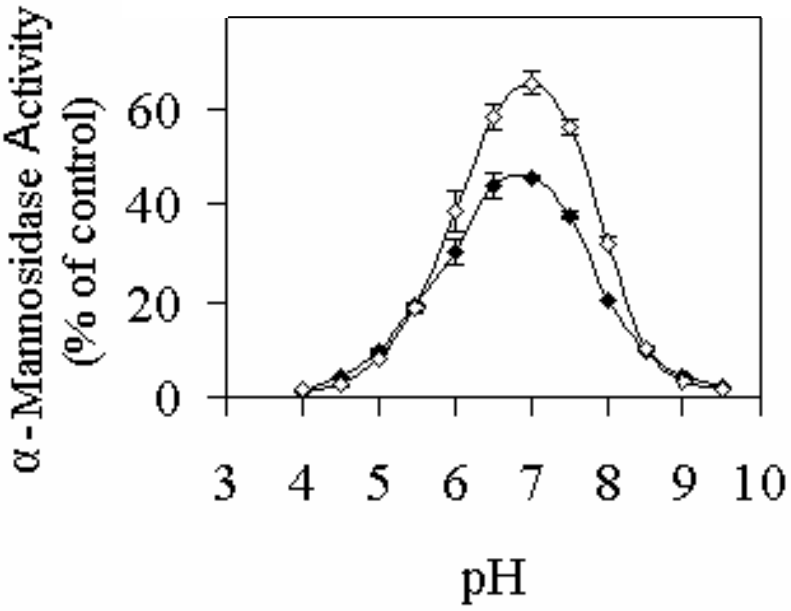
α-Mannosidase Activity
(% of control)
0
20
40
60
3
4
5
6
7
8
9
10
pH

Figure 35: Ratios [($k_{(\chi)}/k_{(0)}$] of the catalytic activity of *Hs*ERManI toward (A) Manα1,2Man and (B) $Man_9GlcNAc_2$-PA measured with different fractions D_2O (in 100% H_2O) are plotted as a function of the molar fraction D_2O (χ). The deuterium isotope effect (DIE) for Manα1,2Man and $Man_9GlcNAc_2$-PA were calculated to be 1.82 ± 0.03 and 1.76 ± 0.06 respectively. The solid lines were fit using the corresponding DIEs to various models to reflect the number of protons involved in transition-state formation for: (—, a) a single proton, eq. 9; (—, b) two protons, eq. 10; (—, c) many protons, eq. 11; (—, d) a single very tight reactant-state proton, eq. 12; (—, e) multiple protons contributing to a single reactant state and a transition state, using a polynomial function described in eq. 13 where $i \rightarrow n = 6$. The R^2 of fits to the polynomial functions were summarized in Table 8. The formulas of the fit were summarized in Table 9.

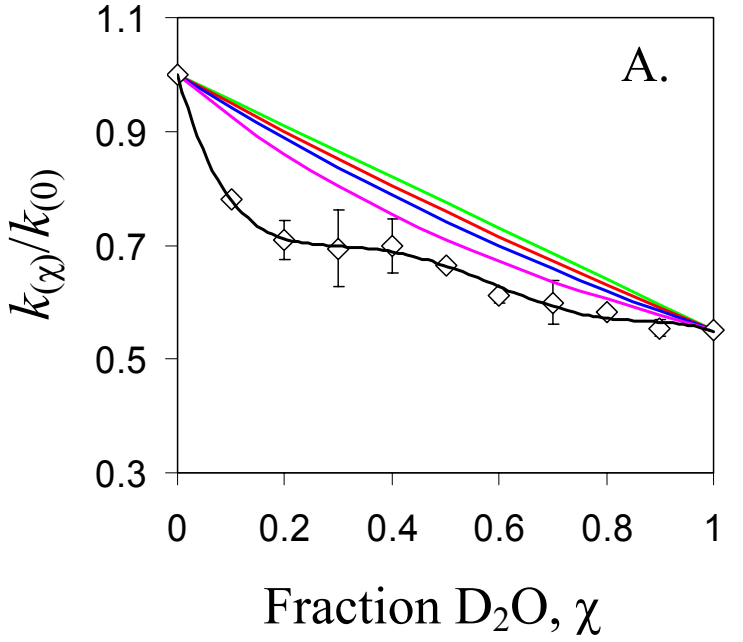
A.
1.1
0.9
0.7
0.5
0.3
0
0.2
0.4
0.6
0.8
1
$k_{(\chi)}/k_{(0)}$
Fraction D_2O, χ

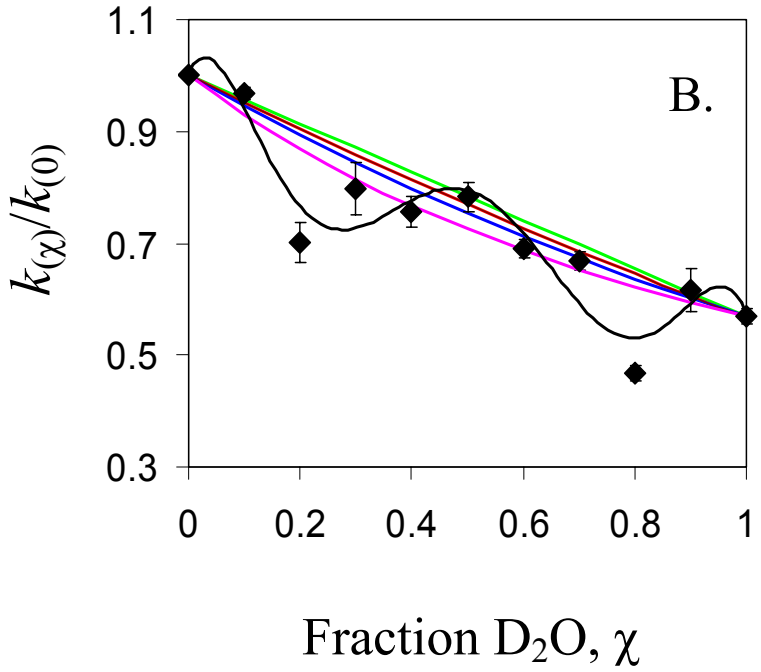
B.
1.1
0.9
0.7
0.5
0.3
0
0.2
0.4
0.6
0.8
1
$k_{(\chi)}/k_{(0)}$
Fraction D_2O, χ

Table 8. The R^2 values for the various proton-inventory curve fits to a polynomial function[a].

i*→ *n	**Manα1,2Man (A)**	**$Man_9GlcNAc_2$-PA (B)**
1	0.789	0.761
2	0.888	0.784
3	0.937	0.787
4	0.982	0.838
5	0.996	0.840
6	0.996	0.913

[a] $k_{(\chi)}/k_{(0)} = \prod_{i}^{n=6}(1 - \chi + \chi\phi_i^T)$;

k is catalytic rate constant;
χ is molar fraction of D_2O and H_2O;
n, i are number and/or order of protons;
ϕ^T is the fractionation factors of DIE in the transition-state.

Figure 36: The plot of reciprocal of $k_{(\chi)}/k_{(0)}$ (σ) from Figure 35 vs χ. The solid lines were linear regression fits of eq. 14, see Table 9. The linear regression coefficient (*m*) for Manα1,2Man (–◊–) and $Man_9GlcNAc_2$ (–♦–) were 0.71 ($R^2 = 0.916$) and 0.74 ($R^2 = 0.965$) respectively.

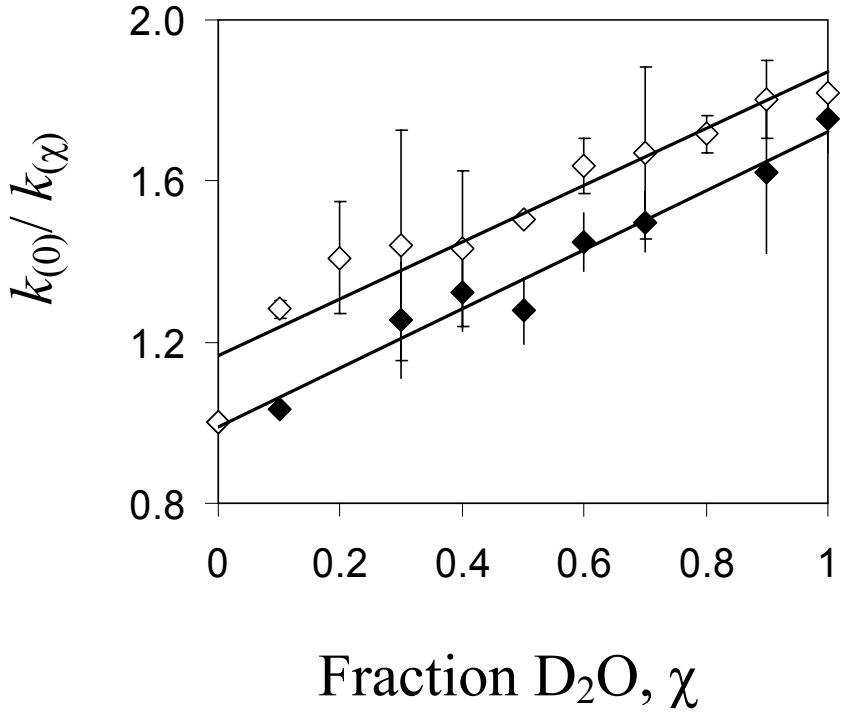
2.0
1.6
1.2
0.8
$k_{(0)}/\ k_{(\chi)}$
0
0.2
0.4
0.6
0.8
1
Fraction D_2O, χ

Table 9. Summary of the mathematical models used to investigate the proton inventory effect.

Model	Relationship[a]	Eq.
a	$k_{(\chi)}/k_{(0)} = 1 - \chi + \chi\sigma$	9
b	$k_{(\chi)}/k_{(0)} = (1 - \chi + \chi\sqrt{\sigma})^2$	10
c	$k_{(\chi)}/k_{(0)} = \sigma^{\chi}$	11
d	$k_{(\chi)}/k_{(0)} = 1/(1 - \chi + \chi\phi^R)$	12
e	$k_{(\chi)}/k_{(0)} = \prod_{i}^{n=6}(1 - \chi + \chi\phi_i^T)$	13
f	$k_{(0)}/k_{(\chi)} = 1 - \chi + \chi\phi^R$	14
DIE	$DIE = 1/\sigma$	15
Reverse DIE	$\sigma = k_{(1)}/k_{(0)}$	16
Isotropic fractionation factor	$k_D/k_H = \phi^T/\phi^R$	17

[a] The equations were modified from Ref. [122, 123]
k is catalytic rate constant.
χ is molar fraction of D_2O and H_2O.
n, i are number and/or order of protons
ϕ^T is the fractionation factors of DIE in the transition-state.
ϕ^R is the fractionation factors of DIE in the reaction-state.

Figure 37: Relative α1,2-mannosidase activities for *Hs*ERManI mutant enzymes. Amino acid changes in recombinant *Hs*ERManI were created by site directed mutagenesis using pPICZαA-ERManI as the template and expressed in *P. pastoris*. The purified recombinant enzymes, both wild type and mutant forms, were used to compare the specific activities of the recombinant enzymes toward $Man_9GlcNAc_2$-PA (20 μM) in MES buffer pH 7.0 at 37ºC. The product formation and protein concentrations were determined as described in Chapter 2.

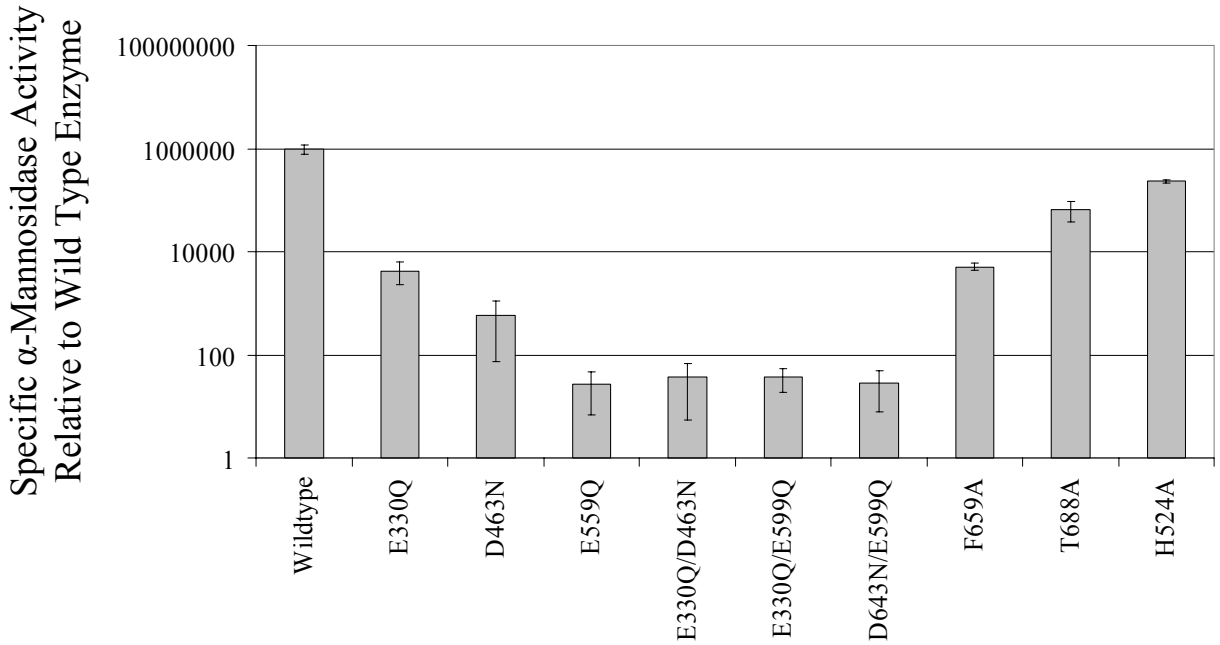
Specific α-Mannosidase Activity
Relative to Wild Type Enzyme
100000000
1000000
10000
100
1
Wildtype
E330Q
D463N
E559Q
E330Q/D463N
E330Q/E599Q
D643N/E599Q
F659A
T688A
H524A

Table 10: Kinetic constants for wild type and mutant *Hs*ERManI using $Man_9GlcNAc_2$ as substrate.

	pH Optimum[a]	K_m	k_{cat}	k_{cat}/K_m	$\frac{k_{cat}/K_m}{k_{cat}/K_m \text{ (wt)}}$
	(pH)	(μM)	($s^{-1} \times 0.001$)	($s^{-1} \cdot M^{-1}$)	(%)
Wild type (wt)	7.0	110 ± 8	3,700 ± 110	33,000 ± 1,600	100
T688A	6.5	19 ± 1.0	130 ± 3	6800 ± 490	20
F659A	6.8	120 ± 0	30± 1.4	250 ± 6	0.7
E330Q[b]	5.3 (7.1)	68 ± 1 (90 ± 7)	84 ± 3 (18 ± 3)	1,200 ± 48 (200 ± 37)	3.5 (0.6)
E330A	6.8	160±9	30±0.4	190±11	0.6
D463N	6.8	110 ± 1	4.6 ± 0.2	42 ± 2	0.1
E599Q	6.7	160 ± 22	0.026 ± 0.003	0.16 ± 0.03	0.0005
H524A	6.9	210±21	860±45	4100±460	12
R461A	6.5	510±130	600±100	1,200±360	3.6
R461L[c]	6.5	330±33	70±4	210±24	0.6
R597A	6.5	470±38	110±6	230±23	0.7
R334A	NA[d]	NA	NA	-	-

[a] Assay data were fit to generate a bell-shaped curve to yield a pH optimum with a standard error of less than 0.1 pH unit

[b] The pH optimum of the E330Q mutant is 5.3, but the kinetic constants for the enzyme assayed at pH 7.1 (pH optimum for wild type enzyme) are also shown in parenthesis.

[c] The enzyme exhibits the ability to readily hydrolyze $Man_9GlcNAc_2$-PA to $Man_6GlcNAc_2$-PA.

[d] Not available due to lack of recombinant enzyme expression in *P. pastoris*.

Figure 38: pH-rate analysis for wild type and E330Q mutant of *Hs*ERManI. Kinetic analyses of wild type and the E330Q mutant of ERManI were performed using $Man_9GlcNAc_2$-PA as substrate and initial rates of hydrolysis were determined by NH_2-HPLC. Values for K_m and k_{cat} were determined as described in Chapter 2 at 0.5 pH unit intervals as shown and plotted as log k_{cat}/K_m versus pH. The curves fit for the pair of macroscopic dissociation constants (Ka_2 and Ka_3, blue figures, upper left panel) are indicated by the dotted lines using the equation: $\log\left(\frac{k_{cat}}{K_m}\right)_{obs} = \log\left(\frac{k_{cat}}{K_m}\right)_{max} - \log\left(1+\frac{10^{-pH}}{10^{-pK_{a2}}}+\frac{10^{-pK_{a3}}}{10^{-pH}}\right)$. The curves fit for the set of four microscopic dissociation constants (Ka_1, Ka_2, Ka_3, and Ka_4, red figures, upper left panel) are indicated by the solid black lines using the equation: $\log\left(\frac{k_{cat}}{K_m}\right)_{obs} = \log\left(\frac{k_{cat}}{K_m}\right)_{max} - \log\left[\left(1+\frac{10^{-pH}}{10^{-pK_{a2}}}+\frac{10^{-pK_{a3}}}{10^{-pH}}\right)\left(1+\frac{10^{-pH}}{10^{-pK_{a1}}}\right)\left(1+\frac{10^{-pK_{a4}}}{10^{-pH}}\right)\right]$. The derived macroscopic and microscopic dissociation constants from the above equations are shown in the table at the bottom of the figure.

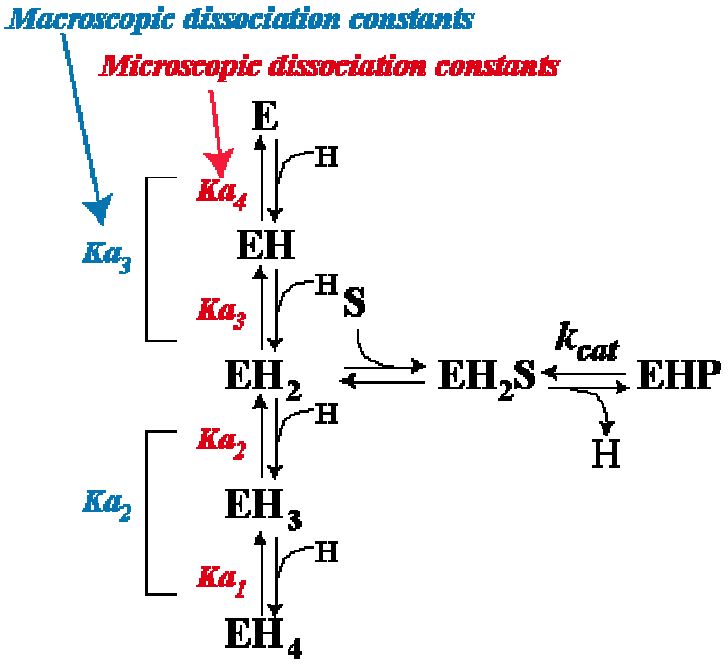

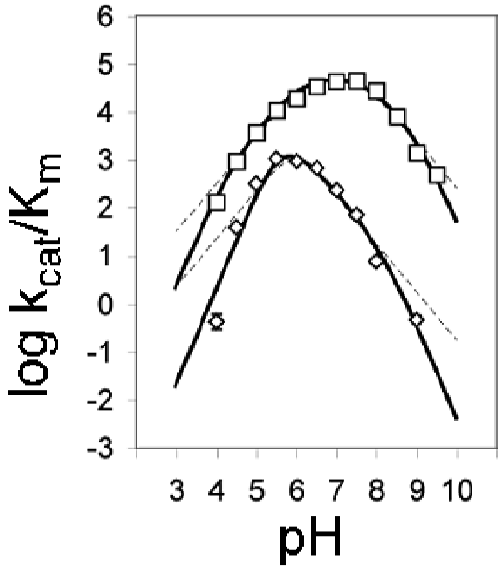

	Macroscopic dissociation			Microscopic dissociation				
	pKa2	pKa3	R	pKa1	pKa2	pKa3	pKa4	R
Wild type	6.3 ± 0.01	7.6 ± 0.01	0.98	4.29 ± 0.02	6.13 ± 0.03	7.82 ± 0.15	9.2 ± 0.35	0.99
E330Q	7.57 ± 0.84	4.29 ± 0.83	0.96	5.93 ± 0.04	7.02 ± 0.07	4.13 ± 0.01	8.26 ± 0.12	0.98

Figure 39: Binding of ligands to wild type and mutant *Hs*ERManI in surface plasmon resonance (SPR) studies. Wild type or mutant ERManI was immobilized on the SPR chip surface as described in Chapter 2 and various concentrations of either $Man_9GlcNAc_2$-glycopeptide, dMNJ, or Kif ligands were tested for binding. The data were collected in duplicate and representative SPR sensorgrams in the ligand concentration series are shown. For the binding studies with dMNJ, Kif, and some of the studies with $Man_9GlcNAc_2$-glycopeptide as ligand, the on- and off-rates were sufficiently slow to allow curve fitting of the sensorgrams using the 1:1 Langmuir binding algorithm model in the BIAevaluation 3.1 software suite to determine values for k_a, k_d, and K_D. In binding studies with wild type ERManI, the F659A mutant, and the E599Q mutant, the kinetics of binding for the $Man_9GlcNAc_2$-glycopeptide ligand were too rapid for curve fitting, so the equilibrium sensorgram values were used to plot a saturation curves (insets plots in the panels A, C, and M) and calculate values for K_D. Table 11 summarizes the SPR binding data obtained for wild type ERManI and all of the mutants using the $Man_9GlcNAc_2$-glycopeptide, dMNJ, and Kif as ligands.

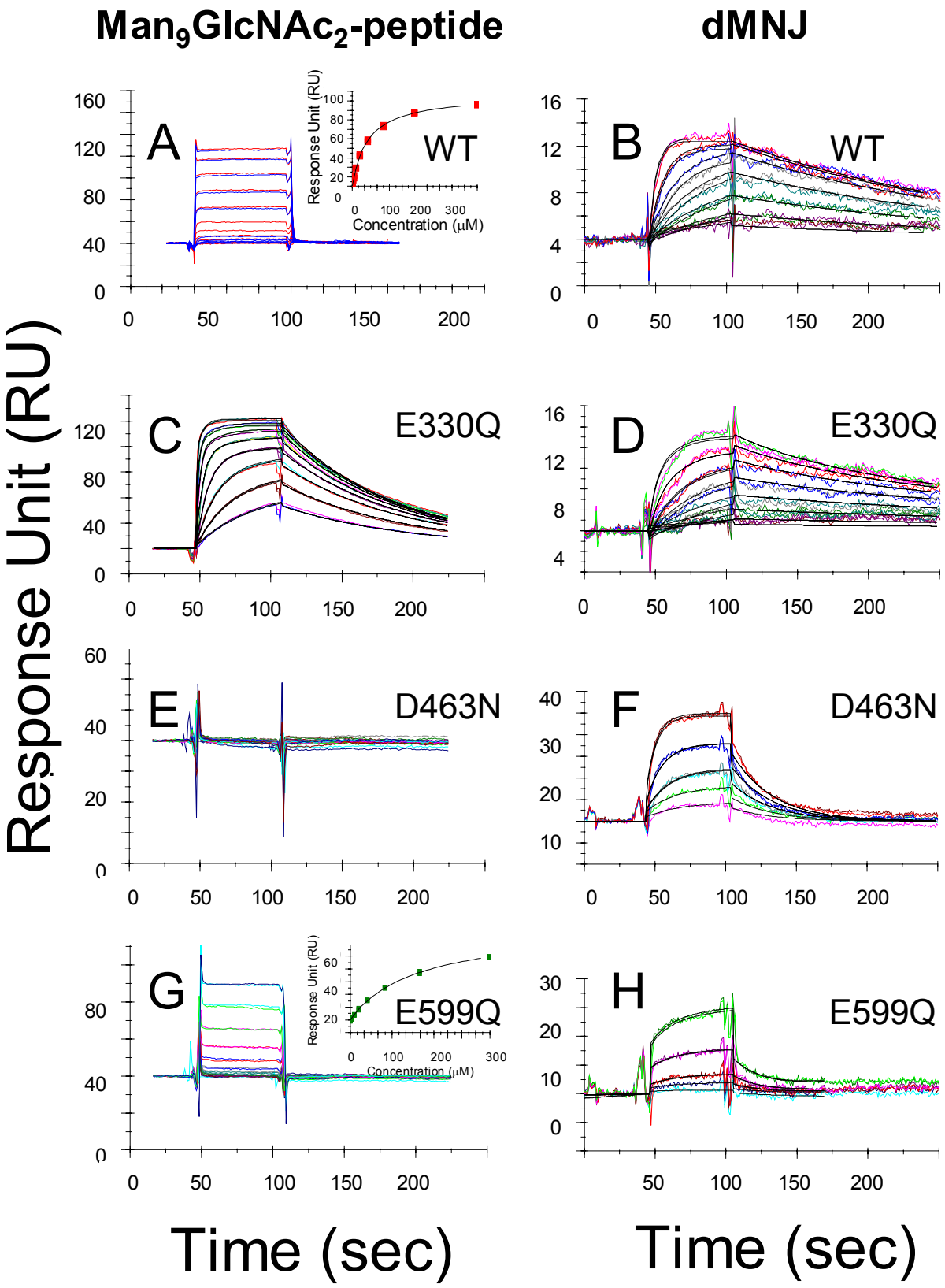
Man9GlcNAc2-peptide
dMNJ
A
WT
B
WT
C
E330Q
D
E330Q
E
D463N
F
D463N
G
E599Q
H
E599Q
Response Unit (RU)
Concentration (μM)
Time (sec)
Time (sec)

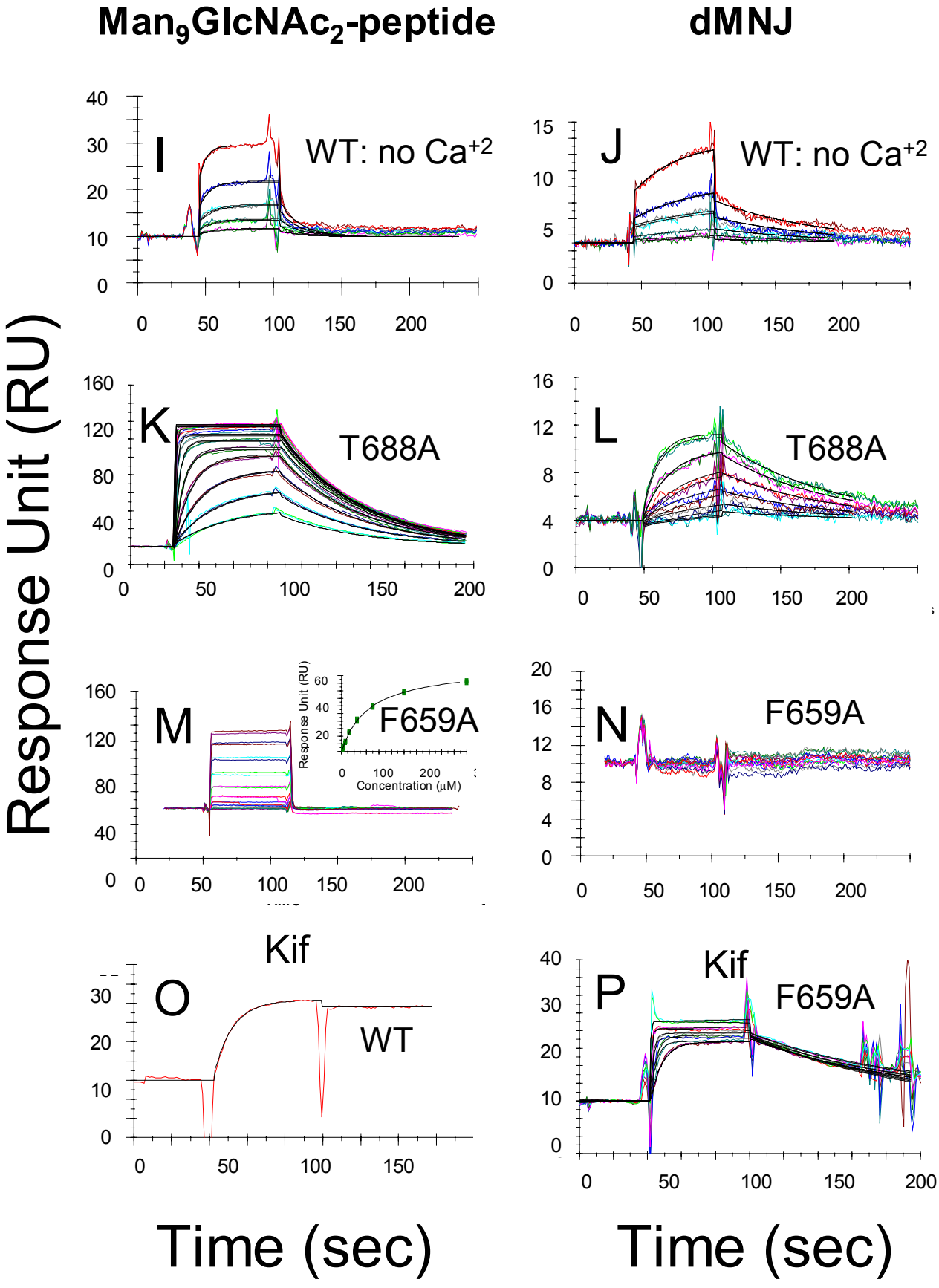
Man9GlcNAc2-peptide
dMNJ
Response Unit (RU)
I
WT: no Ca+2
J
WT: no Ca+2
K
T688A
L
T688A
M
F659A
Response Unit (RU)
Concentration (μM)
N
F659A
Kif
O
WT
Kif
P
F659A
Time (sec)
Time (sec)

Table 11. Summary of binding kinetic parameters.

Ligand	Figure	Concentration of ligand	Protein	Fitting type	k_a	k_d	K_D	$\frac{K_D}{K_D(wt)}$
		(μM)			($s^{-1}\cdot M^{-1}\times 1000$)	($s^{-1}\times 0.001$)	(μM)	-
dMNJ[a]	J	62.5-1000	Wild type[b]	1:1	0.023±0.000	12.8±0.71	553±25.5	343
	B	1.96-62.5	Wild type	1:1	2.94±0.73	4.74±1.47	1.61±0.64	1
	L	1.96-62.5	T688A	1:1	1.46±0.23	11.95±1.56	8.17±1.68	5.1
	N	62.5-1000	F659A	1:1	-	-	ND	-
	D	1.96-62.5	E330Q	1:1	1.06±0.56	2.62±1.63	2.47±2.02	1.5
	F	62.5-1000	D463N	1:1	0.33±0.15	38.3±9.0	117±62	73
	H	62.5-1000	E599Q	1:1	0.033±0.004	56.8±12.2	1730±440	1080
$Man_9GlcNAc_2$ Pentapeptide[a]	I	0.39-400	Wild type[b]	1:1	1.18±0.16	90.5±16.3	76.4±3.8	1.6
	A	0.39-400	Wild type	Steady state affinity	-	-	48.6±1.7	1
	K	0.39-400	T688A	1:1	14.0±3.9	13.1±3.5	0.94±0.36	0.02
	M	0.39-400	F659A	Steady state affinity	-	-	194±80.6	4.0
	C	0.39-50	E330Q	1:1	21.9±4.9	11.1±2.7	0.51±0.17	0.01
	E	0.39-400	D463N	1:1	-	-	ND	-
	I	0.39-400	E599Q	Steady state affinity	-	-	184±22	4
KIF[c]	O	25	Wild type	1:1	>4.05	<0.10	<0.025	1
	P	25-400	F659A	1:1	7.38±0.19	11±0.1	1.45±0.05	<58

[a] the binding analyses were performed at 10 ºC

[b] the immobilized surfaces were treated with EGTA overnight by continuous flow of running buffer containing 5 mM EGTA at 5 μl/min and the binding analyses were performed in buffer containing 200 μM EGTA.

[c] the binding analyses were performed at 25 ºC

Figure 40: Binding studies of *O*- or *S*-glycosides of Manα1,2Man-*O*-CH_3 to wild type *Hs*ERManI by surface plasmon resonance (SPR). Wild type ERManI was immobilized on the SPR chip surface as described in Methods and various concentrations of either the *O*-glycoside of Manα1,2Man-*O*-CH_3 or the equivalent thiodisaccharide were tested for binding to the enzyme. The data were collected in duplicate and representative SPR sensograms in the ligand concentration series are shown. The on- and off-rates were sufficiently slow to allow curve fitting of the sensograms using the 1:1 binding algorithim model in the Biaevaluation 3.1 software suite to determine values for k_a, k_d, and K_D indicated in the respective tables in the figure.

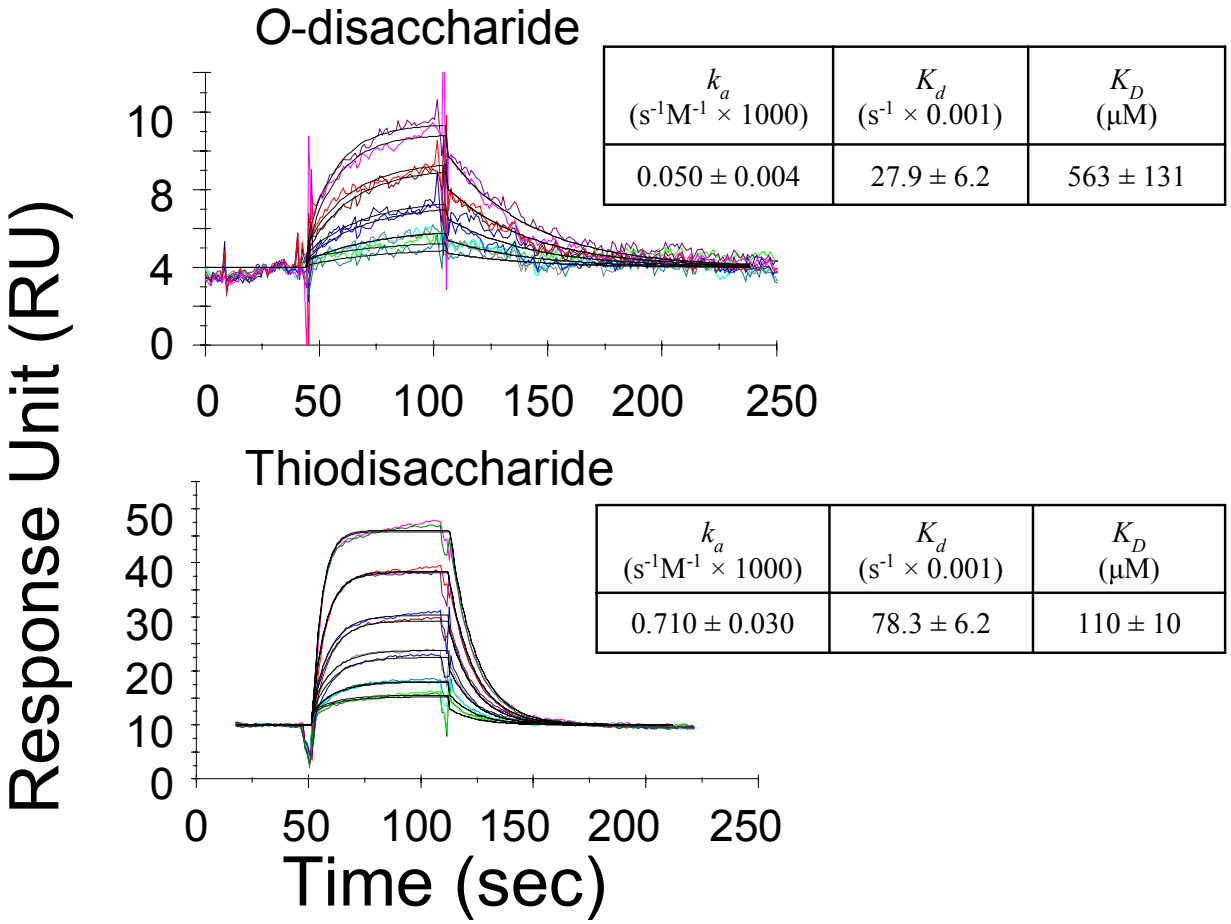

k_a ($s^{-1}M^{-1} \times 1000$)	K_d ($s^{-1} \times 0.001$)	K_D (μM)
0.050 ± 0.004	27.9 ± 6.2	563 ± 131

k_a ($s^{-1}M^{-1} \times 1000$)	K_d ($s^{-1} \times 0.001$)	K_D (μM)
0.710 ± 0.030	78.3 ± 6.2	110 ± 10

Figure 41: Comparison of the Ca^{+2} ion affinity for wild type and T688A mutant of *Hs*ERManI. The effect of Ca^{2+} on catalysis was determined from the specific activity measured in presence of the divalent cation chelator, EGTA, to control the free Ca^{2+} concentration in the reaction buffer at pH 7.0 using 20 mM $Man_9GlcNAc_2$ as substrate. The specific activity of wild type (–■–) and the T688A (–◊–) mutant of ERManI were plotted against concentration of free Ca^{2+} and appeared to have a sigmoidal relationship similar to that expected for a common equilibrium dialysis experiment. The affinity constant for Ca^{2+}, K_{Ca}, was determined by non-linear regression analysis as described in Chapter 2. The solid line and dashed line were the fit to equation 18 for wild type (K_{Ca} = 0.24 ± 0.02, and n = 10 ± 0.2) and T688A (K_{Ca} = 0.15 ± 0.01, and n = 0.66 ± 0.1) *Hs*ERManI, respectively.

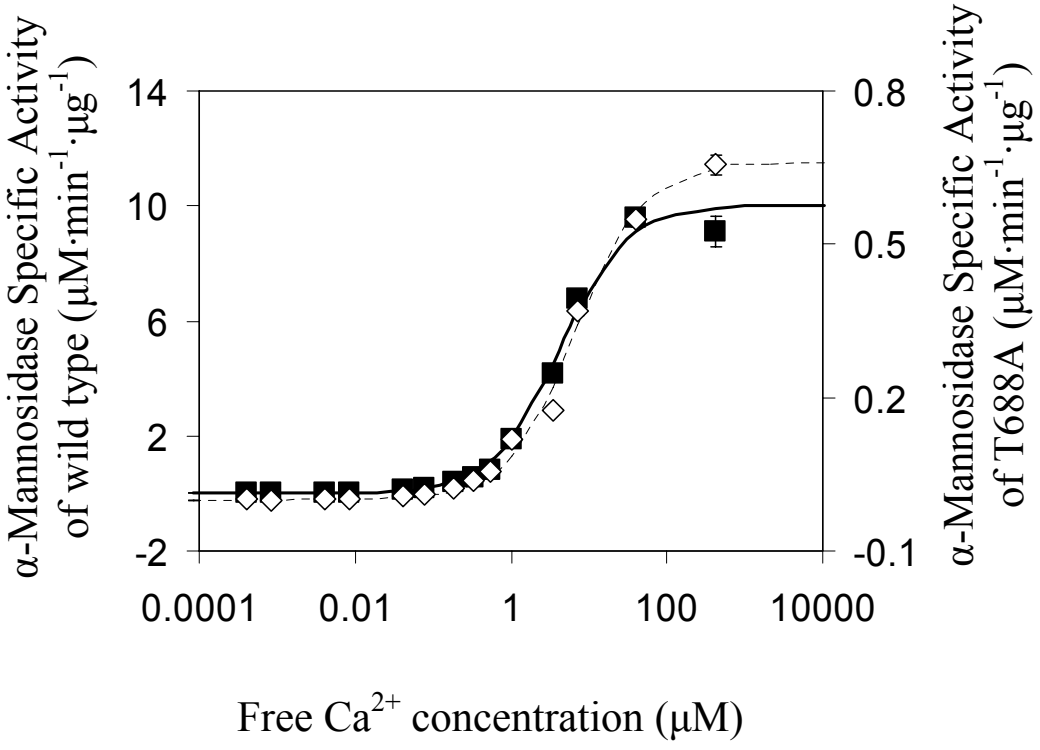
α-Mannosidase Specific Activity of wild type (μM·min-1·μg-1)
α-Mannosidase Specific Activity of T688A (μM·min-1·μg-1)
14
10
6
2
-2
0.8
0.5
0.2
-0.1
0.0001
0.01
1
100
10000
Free Ca2+ concentration (μM)

Figure 42: The best native crystals of *Hs*ERManI after sparse-matrix optimization (A) and additive screening (B). A) The crystals were grown in a hanging drop prepared over 1 ml of mother liquor containing 24% (*w*/*v*) PEG 4000, 100 mM MES/NaOH pH 6.0, 50 mM ammonium sulfate. B) The crystals were obtained from a hanging drop prepared over 1 ml of mother liquor containing 24% (*w*/*v*) PEG 4000, 100 mM MES/NaOH pH 6.0, 50 mM ammonium sulfate containing 10% (*v*/*v*) 1,4 butanediol. The crystal shown in B is ~80×80×20 μm in size.

A

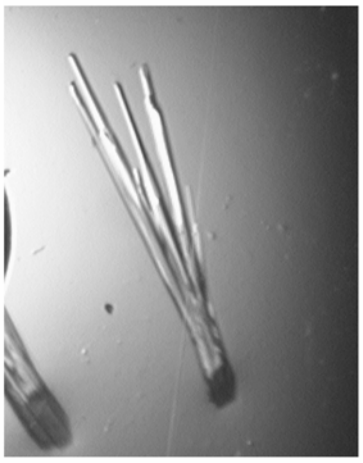

B

Figure 43: A diffraction image of the co-complex crystal of *Hs*ERMan1 and the thiodisaccharide substrate analogue. The red box in panel A marks the area that is shown in panel B. Brightness settings were adjusted in panel B to enhance the intensity of higher resolution reflections. The images were prepared using DTDISPLAY [170]**.**

A

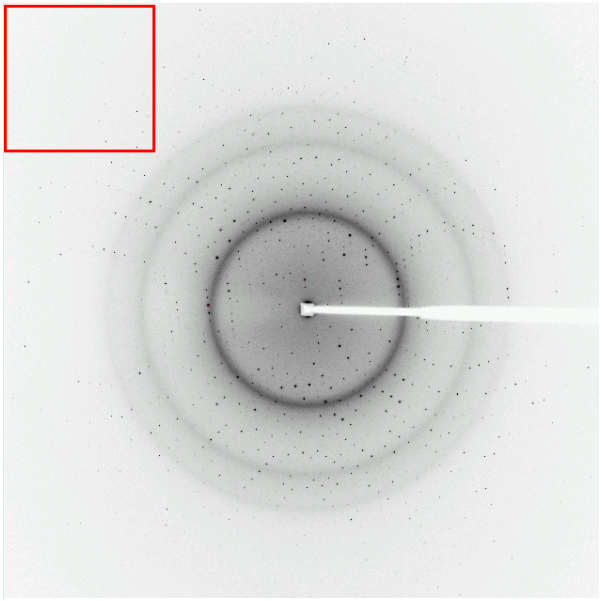

B

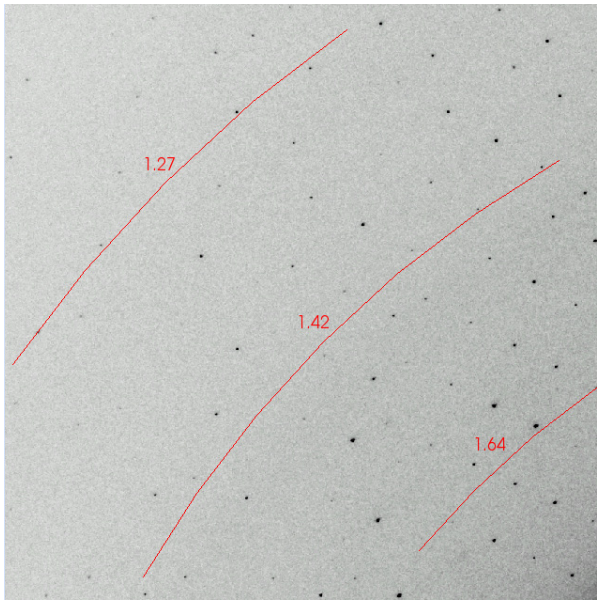

Table 12. X-ray diffraction data collection and refinement statistics

Parameter	Value
Data resolution (high resolution shell) Å	48.80-1.41 (1.45-1.41)[a]
Unique observed reflection	84600 (8225)
Completeness (%)	95.5 (93.2)
$\langle I \rangle / \langle \sigma(I) \rangle$	41.8 (13.0)
Average redundancy	4.0 (3.5)
Space group	*P1*
Unit cell lengths *a, b, c* (Å)	50.69, 53.88, 56.23
Unit cell angles α, β, γ (º)	89.50, 63.61, 62.61
Matthews coefficient ($Å^3 \cdot Da^{-1}$)	2.4
Solvent content (%, *v/w*)	4.7
Number of unique reflections used in refinement	76092 (5417)
Number of reflection in free set	8507 (631)
R_{cryst} (%)	14.4 (15.8)
R_{free} (%)	16.2 (19.3)
Number of non-hydrogen atoms refined	4097
r.m.s. deviation (Å) Bonds	0.014
r.m.s. deviation (º) Angles	1.34
Mean temperature factor ($Å^2$)	8.4
Wilson temperature factor ($Å^2$)	9.3

[a] The values in parenthesis corresponded to the parameter of the high resolution shell.

Figure 44: Normalized Fo-Fc electron density map for the disaccharide in the active site of *Hs*ERManI and comparison of the sugar ring conformations of dMNJ and the M7 glycone residue in the +1 site for *Sc*ERManI. Stereographic representation of the difference electron density for the omitted inhibitor in the ERManI-thiodisaccharide co-complex (Panel A). The inhibitor model is shown to aid in map interpretation. For map calculation, inhibitor atoms were deleted from the model. The remaining model atoms were displaced randomly by an average 0.3Å and their temperature factors were randomly altered by an average 3Å^2 with the program Moleman. Amplitudes and phases for the weighted difference map were calculated after ten cycles of REFMAC5 refinement. The reducing terminal Man-α-*O*-CH_3 is at the top of the figure, labeled as the +1 subsite residue, and the non-reducing terminal Man residue in the $^3S_1$ conformation is labeled as the –1 subsite residue. The electron density map was contoured at 3σ for the grey mesh and 10σ for the red mesh demonstrating the significant electron density at the glycosidic sulfur, the O3' and O4' hydroxyls of the +1 residue, and the O2', O3, and O4' hydroxyls of the –1 residue. (Panel B) The protein structure of the ERManI-thiodisaccharide co-complex was aligned with the corresponding protein structures of the ERManI-dMNJ co-complex and the co-complex of yeast ERManI containing a $Man_5GlcNAc_2$ glycan in the active site using Swiss-PdbViewer (version 3.7). Displayed in the figure are the structures of the thiodisaccharide (yellow stick figure), dMNJ (green stick figure) and the M7 residue of the $Man_5GlcNAc_2$ glycan in the +1 subsite (white stick figure). The M7 residue is in an identical conformation as the +1 residue of the thiodisaccharide and in a similar position except for an offset of 0.5-0.7Å resulting from the longer C-S bond lengths of the thio-disaccharide. The positioning of the –1 subsite residues (dMNJ versus the –1 residue of the thio-disaccharide) were virtually identical at the C2, C3 and C4 positions. The main differences in the two structures are the positions of C1, O5, C5,

and C6. The $^{1}C_{4}$ chair structure of dMNJ is distinguished from the $^{3}S_{1}$ skew boat of the –1 residue of the thiodisaccharide by a conformational twist at this latter side of the pyranose ring. This figure was rendered using using MacPymol (version 0.95) to generate the rasterized images.

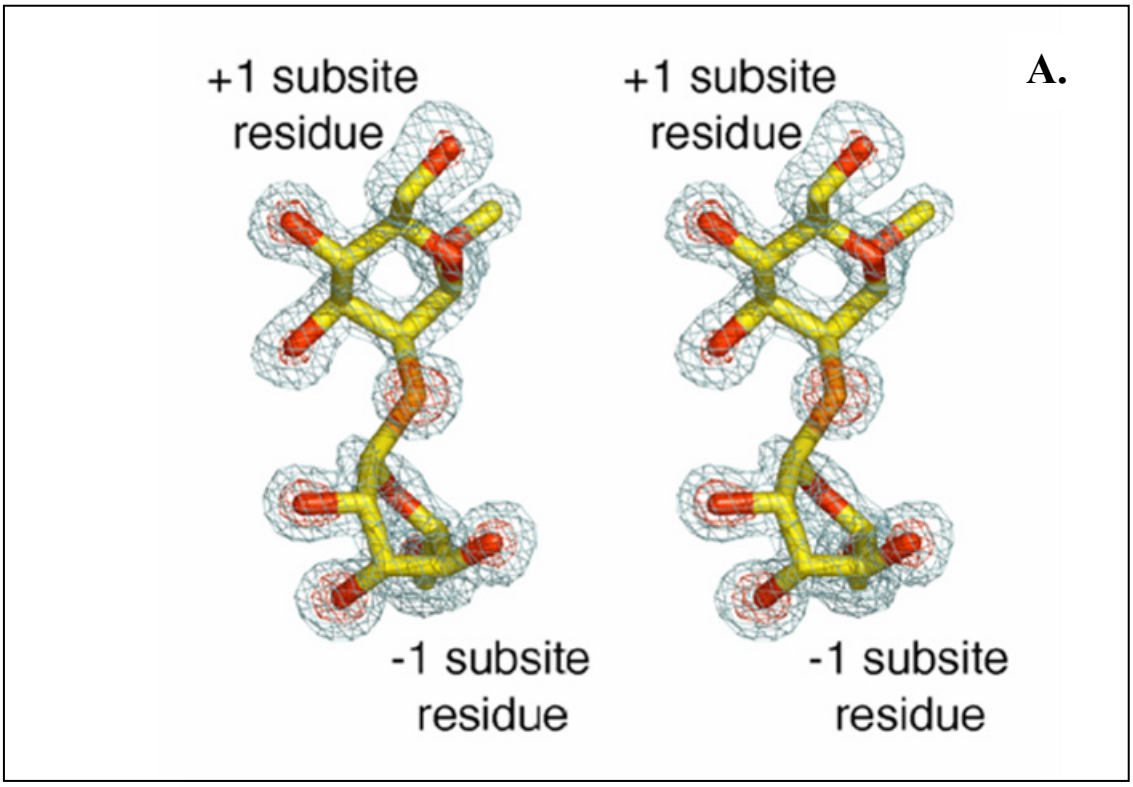
A.
+1 subsite residue
+1 subsite residue
-1 subsite residue
-1 subsite residue

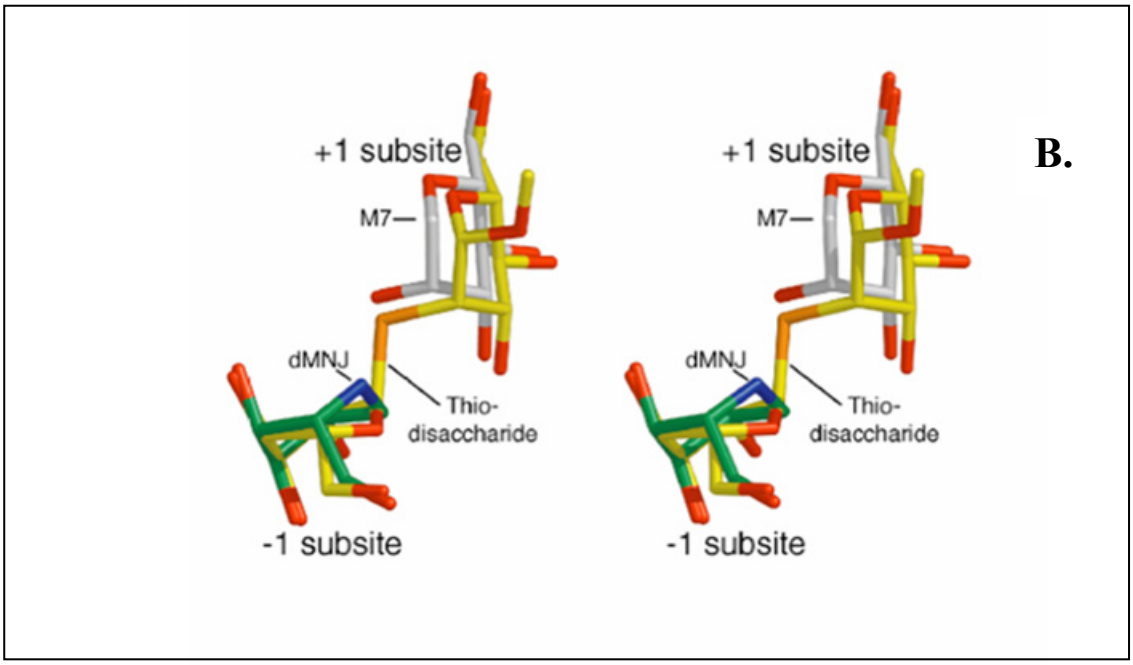
B.
+1 subsite
M7—
dMNJ
Thio-disaccharide
-1 subsite
+1 subsite
M7—
dMNJ
Thio-disaccharide
-1 subsite

Figure 45: Interactions between the thiodisaccharide and the +1 and -1 binding sites in *Hs*ERManI. A schematic diagram (left panel) of the interactions between the thiodisaccharide and ERManI in the –1 and +1 subsites demonstrating hydrogen bonding interactions (green dotted lines), direct coordination of the enzyme-associated Ca^{+2} ion, (blue dotted lines) and proposed acid-catalyzed protonation and attack by the water nucleophile (red dotted lines). Residue numbering of amino acid side chains in the respective subsites is indicated in the figure. The stereo view (center and right panels) illustrates the binding of the thiodisaccharide in the –1 and +1 subsites with direct hydrogen bonds (yellow dotted lines), coordination to the Ca^{+2} ion (blue dotted lines), and the proposed nucleophile trajectory and acid protonation of the glycosidic oxygen (red dotted lines). This figure was rendered using using MacPymol (version 0.95) to generate rasterized images.

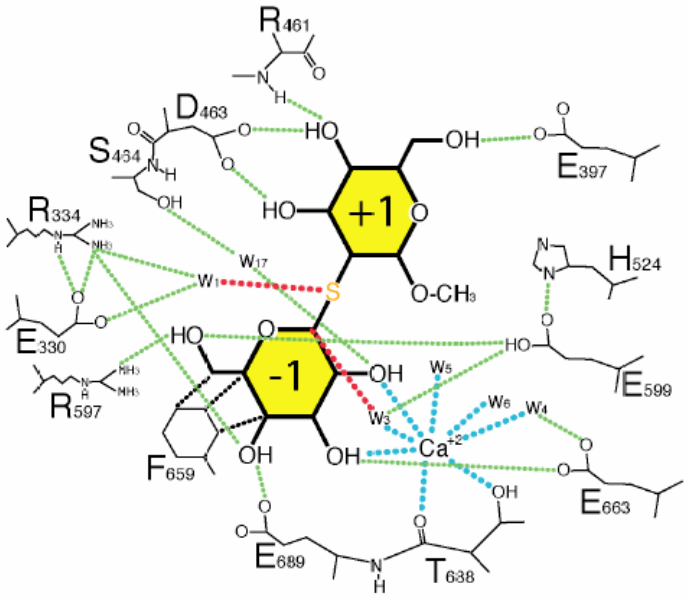
R461
D463
S464
R334
W17
W1
S
+1
O-CH3
H524
E330
HO
-1
OH
W5
W3
W6
W4
Ca+2
R597
F659
OH
OH
E397
E599
E663
E689
T638
N
H

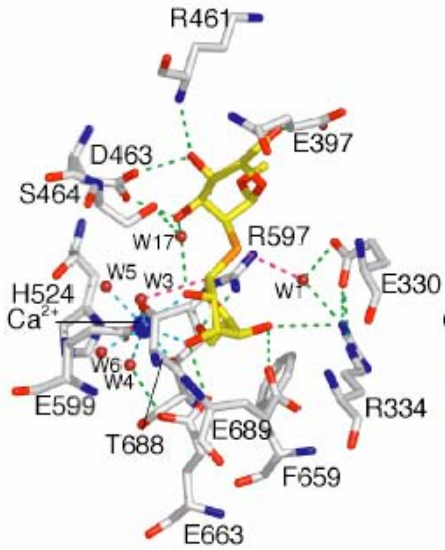
R461
E397
D463
S464
W17
R597
W5
W3
W1
E330
H524
Ca2+
W6
W4
E599
R334
T688
E689
F659
E663

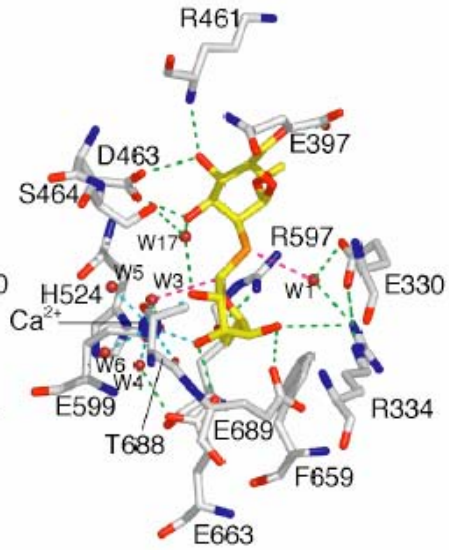
R461
E397
D463
S464
W17
R597
W5
W3
W1
E330
H524
Ca2+
W6
W4
E599
R334
T688
E689
F659
E663

Figure 46: Proposed mechanism for *Hs*ERManI—The model for the mechanism of ERManI **c**atalyzed hydrolysis of Manα1,2Man linkages based on kinetic analysis and substrate analog co-crystal structure**.** Substrate binding to the –1 subsite results in distortion of the glycone into a $^{3}S_{1}$ skew boat conformation by binding interactions in both the –1 and +1 subsites. E330 acts as the general acid in a through-water protonation of the glycosidic oxygen leading to the formation of the $^{3}H_{4}$ oxocarbenium ion transition state with ring planarity at C2-C1-O5-C5. Base-catalyzed (E599) proton abstraction from the water nucleophile (W3) results in the attack of the anomeric center and inversion of configuration to form a β-hydroxyl on the enzymatic product in a $^{1}C_{4}$ chair conformation.

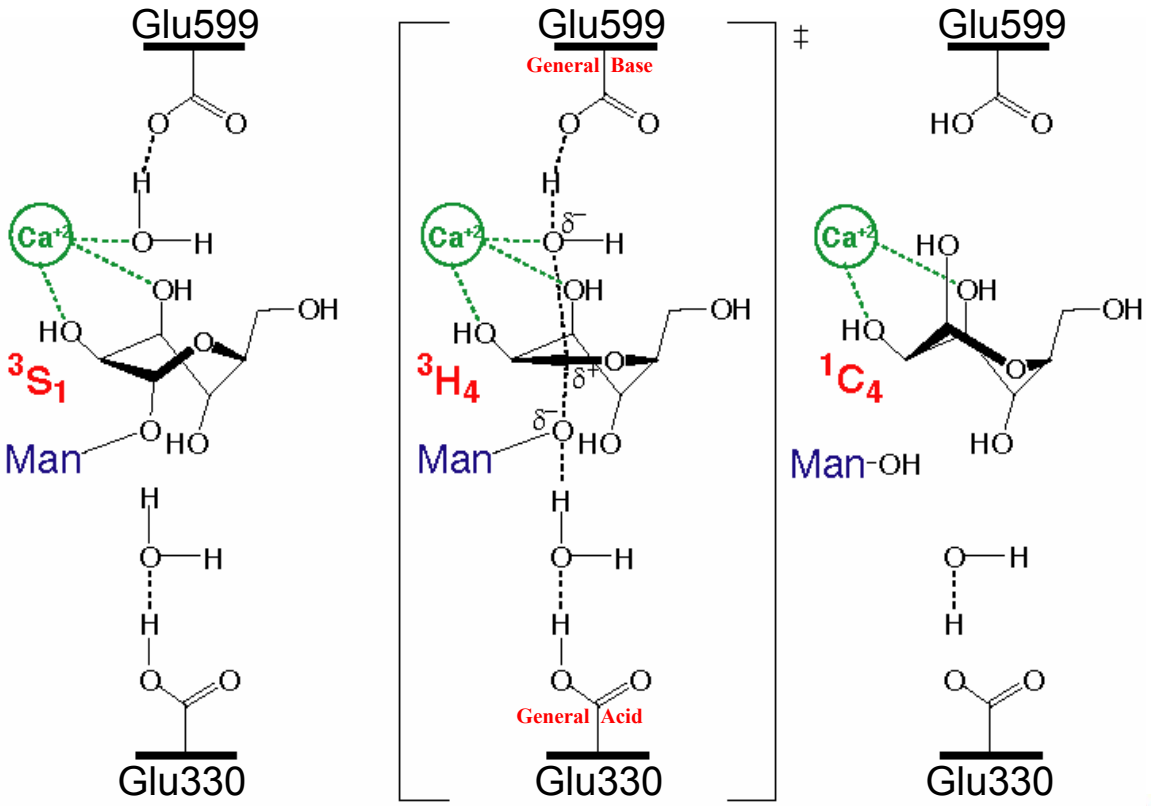

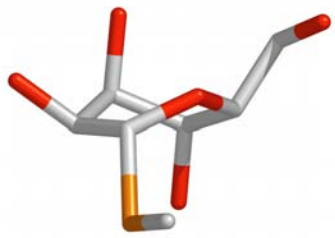

-1 residue from
the thio-disaccharide
co-crystal ($^3S_1$)

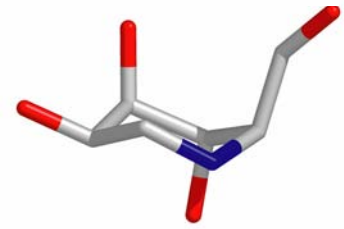

dMNJ in -1 site
($^1C_4$)

Figure 47: The temperature dependence of the catalytic rate (k_{cat}) for $Man_9GlcNAc_2$-PA by *Hs*ERManI. The catalytic rate of wild type (A), E330Q (B), and T688A (C) were determined from the initial rates measured at the optimal pHs of 7.0, 5.3 and 6.5 respectively. The enzyme assays were carried out as described in Chapter 2.

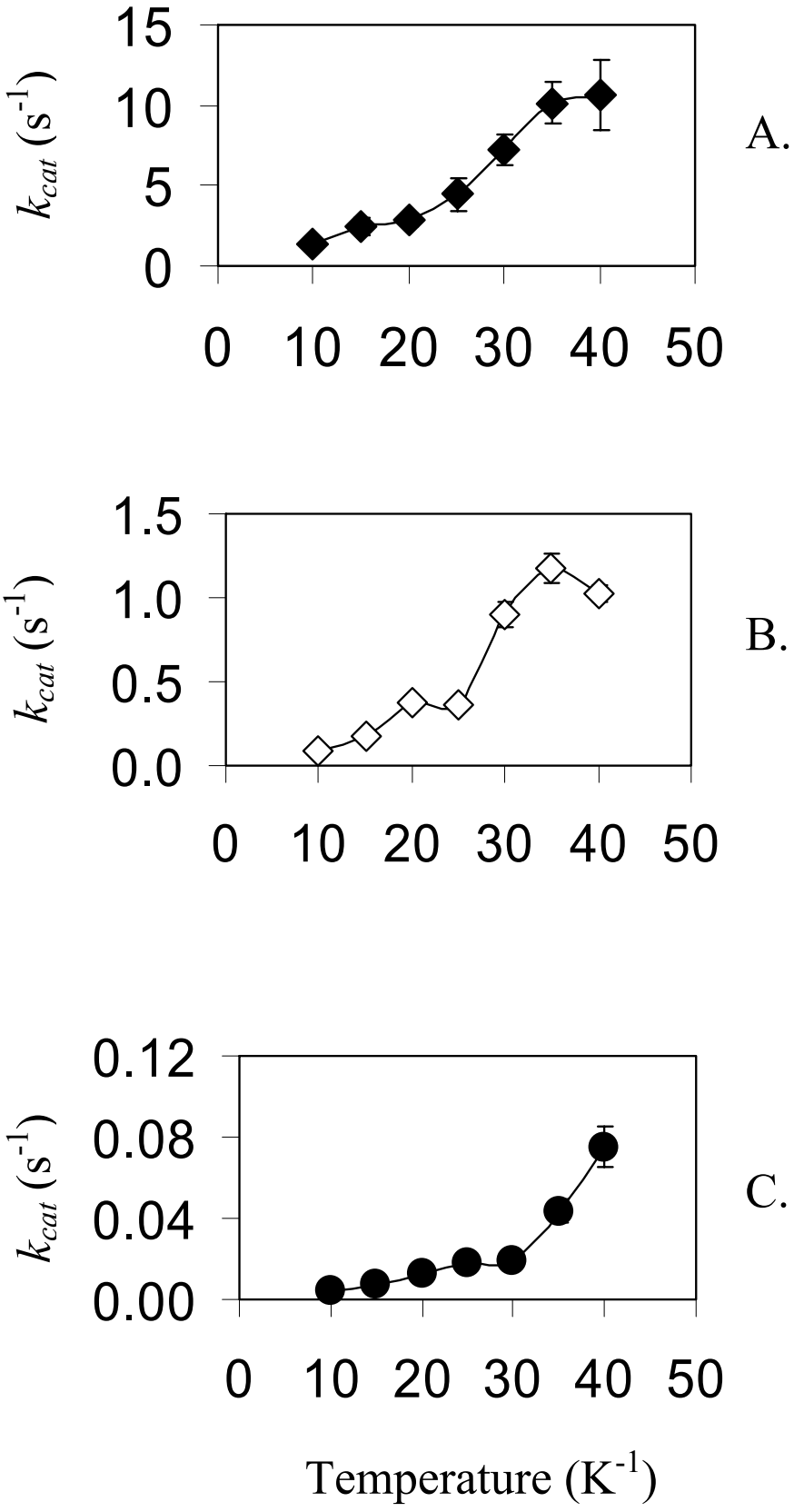
15
10
5
0
k_{cat} (s^{-1})
0 10 20 30 40 50
A.
1.5
1.0
0.5
0.0
k_{cat} (s^{-1})
0 10 20 30 40 50
B.
0.12
0.08
0.04
0.00
k_{cat} (s^{-1})
0 10 20 30 40 50
C.
Temperature (K^{-1})

Figure 48: The Arrhenius plots of catalytic rate (ln k_{cat} versus reciprocal absolute temperature) for catalysis of $Man_9GlcNAc_2$-PA by *Hs*ERManI. The solid lines correspond to linear regression of the experimental data shown in Figure 47. The fitting coefficient (*m*) for wild type (◆) is -7.495, $R^2 = 0.990$; E330Q (◇) is -8.832, $R^2 = 0.963$; T688A (●) is -6.988, $R^2 = 0.889$.

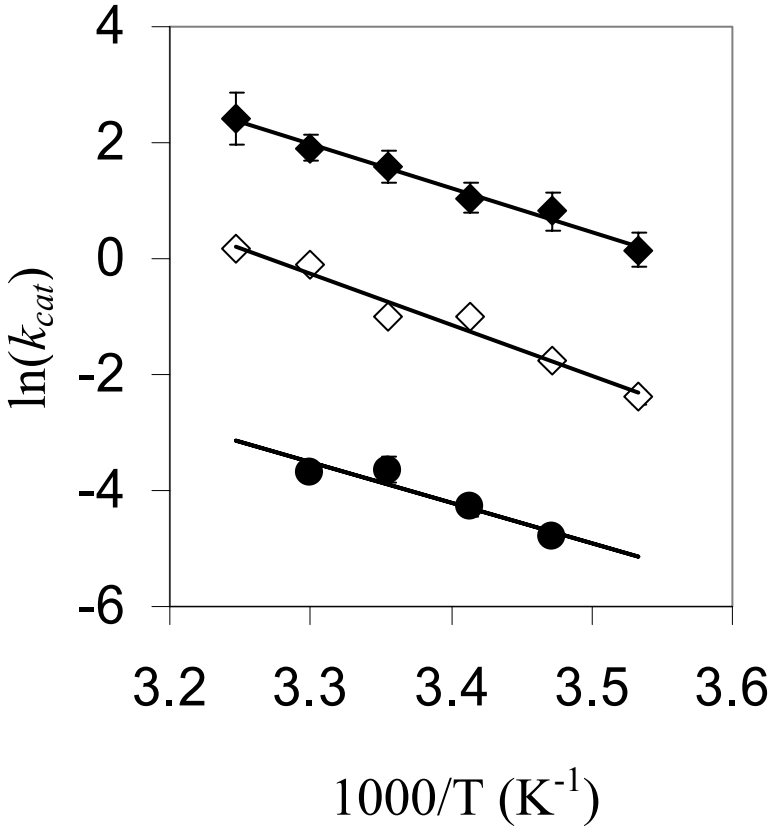
4
2
0
-2
-4
-6
ln(kcat)
3.2
3.3
3.4
3.5
3.6
1000/T (K-1)

Table 13. Thermodynamic activation parameters for *Hs*ERManI; wild type, E330Q and T688A at 25 ºC.

Parameters	**Wild type**	**E330Q**	**T688A**
k_{cat} (s^{-1}) at 25 ºC	4.5 ± 1.2	0.36 ± 0.02	0.02 ± 0.004
E_a ($kJ \cdot mol^{-1}$)	57 ± 8.6	73 ± 5.1	63 ± 5.9
$\Delta G^{\ddagger}$ ($kJ \cdot mol^{-1}$)	69 ± 0.7	76 ± 0.1	83 ± 0.5
$\Delta H^{\ddagger}$ ($kJ \cdot mol^{-1}$)	55 ± 8.7	71 ± 5.1	61 ± 5.9
$T\Delta S^{\ddagger}$ ($kJ \cdot mol^{-1}$)	-15 ± 8.7	-4.5 ± 5.1	-22 ± 5.9

Figure 49: The temperature dependence of *Hs*ERManI interactions with the $Man_9GlcNAc_2$-glycopeptide (Man_9) ligands. The biosensor binding responses shown on the left column are duplicate injections of a single concentration of Man_9GlcNA_2-glycopeptide recorded at 5, 10, 15, 20, 25, 30 and 35 ºC; (A) 50 μM of Man_9GlcNA_2-glycopeptide ligand concentration for wild type ERManI (A) and 10 μM for E330Q (B) and T688A (C). The arrowheads indicate the position on the sensorgram where the relative binding responses (%) were determined and plotted against the temperature as shown in the corresponding column. The arrows within the panels on the left side indicate the direction of changes in biosensor response as the effect of temperature change was being monitored.

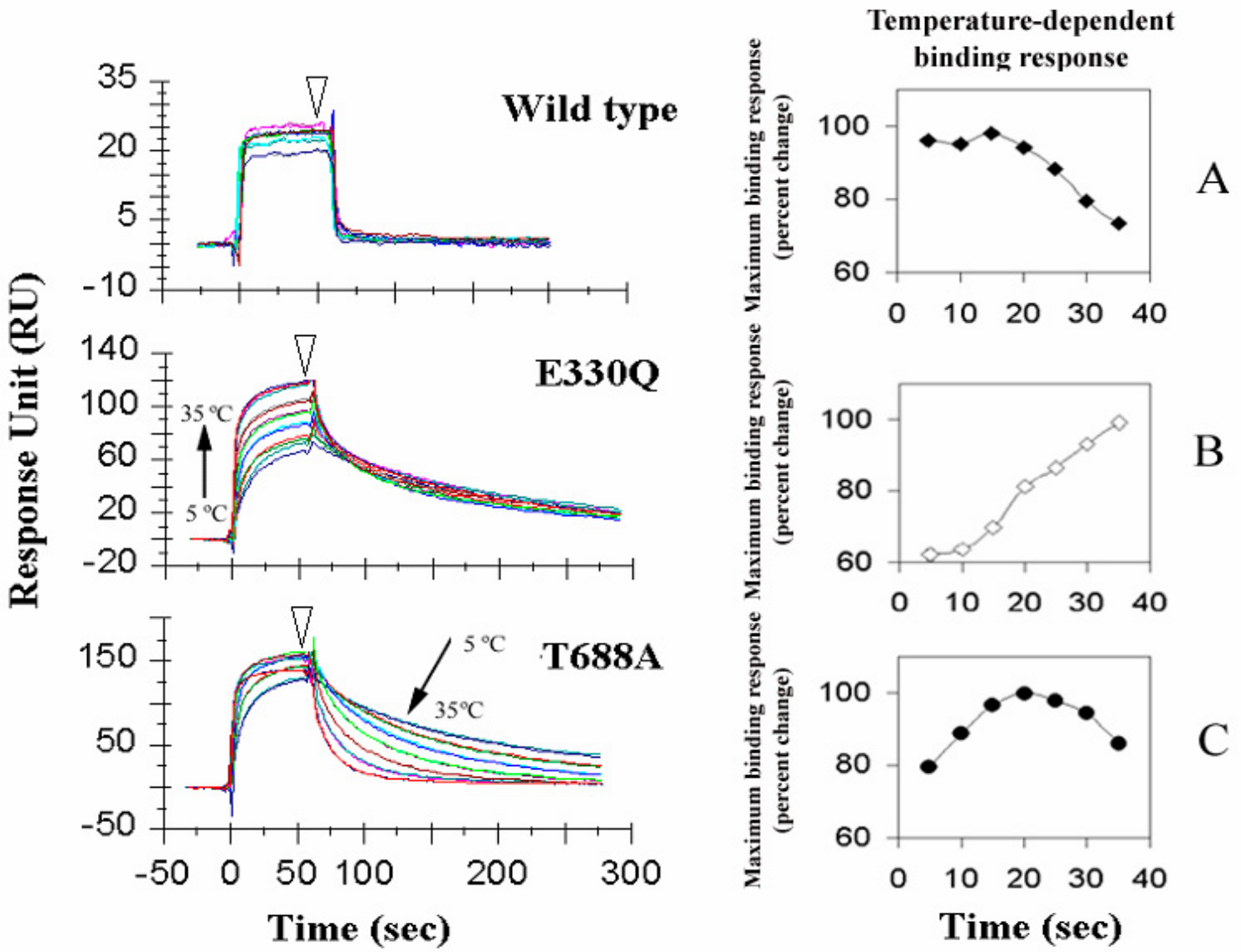
Wild type
E330Q
T688A
35 ℃
5 ℃
5 ℃
35℃
Response Unit (RU)
Time (sec)
Temperature-dependent binding response
Maximum binding response (percent change)
A
B
C
Time (sec)

Figure 50: The pH effect on binding of $Man_9GlcNAc_2$-glycopeptide to the E330Q mutant of *Hs*ERManI. The binding analysis were carried out in running buffer pH 8.0 (A), 7.0 (B), 6.0 (C) and 5.0 (D) at 10 ºC. The biosensor responses were obtained from duplicate injections of a concentration series from 3.25-400 μM $Man_9GlcNAc_2$-glycopeptide prepared in the running buffer of the respective pH that was being analyzed. The black lines represent global fits to a 1:1 Langmuir binding model in C, but not shown in A or B.

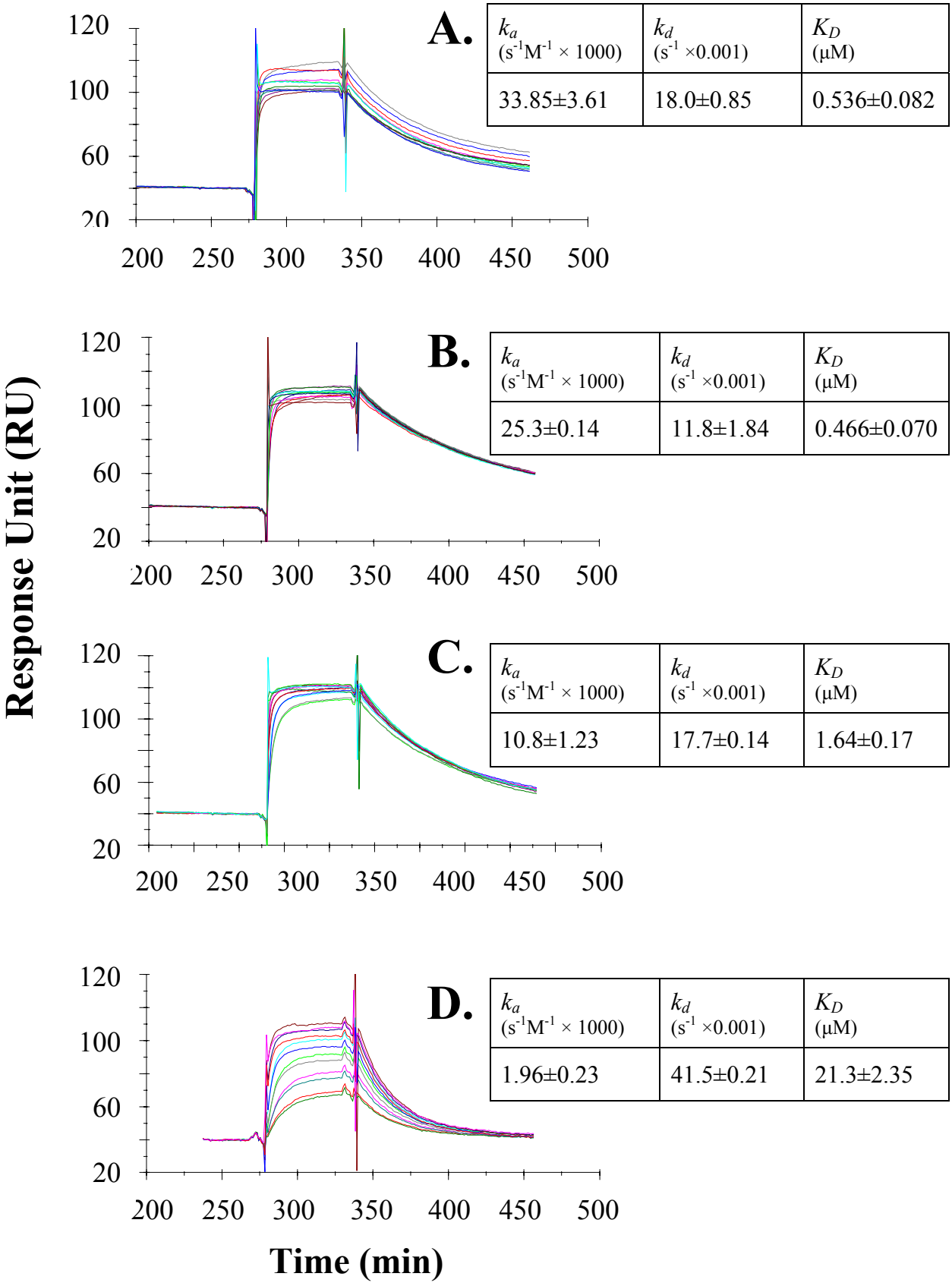

k_a ($s^{-1}M^{-1}$ × 1000)	k_d (s^{-1} ×0.001)	K_D (μM)
33.85±3.61	18.0±0.85	0.536±0.082

k_a ($s^{-1}M^{-1}$ × 1000)	k_d (s^{-1} ×0.001)	K_D (μM)
25.3±0.14	11.8±1.84	0.466±0.070

k_a ($s^{-1}M^{-1}$ × 1000)	k_d (s^{-1} ×0.001)	K_D (μM)
10.8±1.23	17.7±0.14	1.64±0.17

k_a ($s^{-1}M^{-1}$ × 1000)	k_d (s^{-1} ×0.001)	K_D (μM)
1.96±0.23	41.5±0.21	21.3±2.35

Figure 51: van't Hoff plots for the *Hs*ERManI and $Man_9GlcNAc_2$-glycopeptide (Man_9) interactions determined from SPR analyses performed at different temperatures. The binding constants (K_D) were derived from the global fitting to duplicate injections of concentration series of 6.5-100 μM Man_9 for wild type enzyme, and 0.65-10 μM Man_9 for E330Q and T688A. The solid lines are the linear fits to the experimental data with the correlation coefficients (R^2) of 0.899 for wild type enzyme (◆); 0.940 for E330Q (◇); and 0.876 for T688A (●). The error bars were included for all points, but in some instances they were very small.

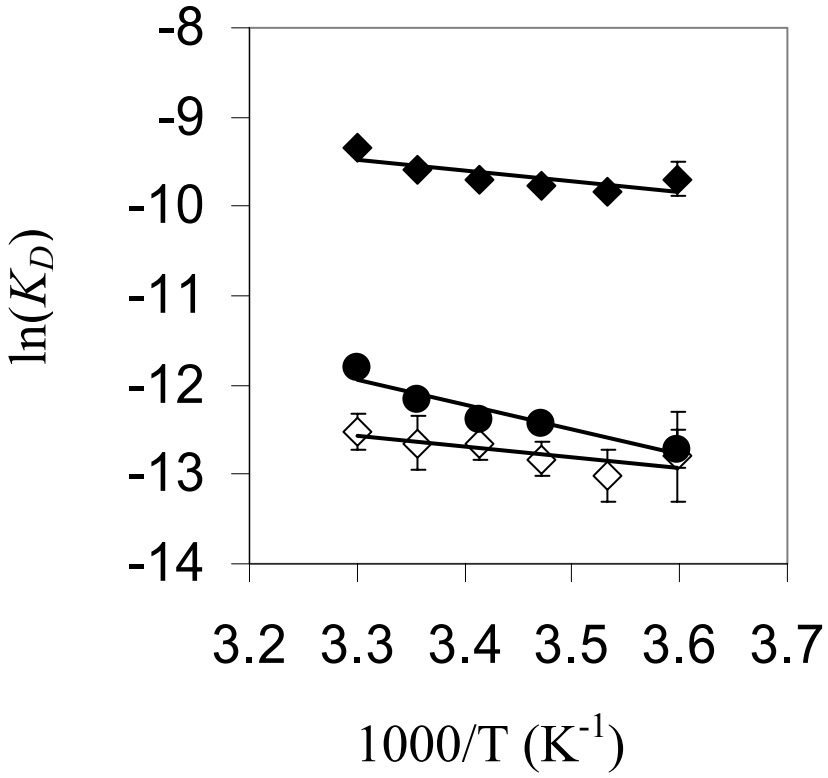
-8
-9
-10
-11
-12
-13
-14
ln(K_D)
3.2
3.3
3.4
3.5
3.6
3.7
1000/T (K^{-1})

Table 14. Summary of the thermodynamic parameters for the *Hs*ERManI and $Man_9GlcNAc_2$-glycopeptide at 25 ºC from the van't Hoff analysis in Figure 51.

Parameters	**Wild type**	**E330Q**	**T688A**
K_A ($\times 1000\ M^{-1}$)	12 ± 0.8	447 ± 93	607 ± 99
ΔG^o ($kJ \cdot mol^{-1}$)	-22 ± 0.2	-31 ± 0.5	-31 ± 0.4
ΔH^o ($kJ \cdot mol^{-1}$)	-18 ± 5.3	-16 ± 4.5	-47 ± 6.5
$T\Delta S^o$ ($J \cdot mol^{-1} \cdot K^{-1}$)	5.2 ± -5.1	14 ± -4.3	-16 ± -6.3

Figure 52: Eyring plots for the *Hs*ERManI and $Man_9GlcNAc_2$-glycopeptide interaction examining the contribution of (A) k_a or (B) k_d determined from SPR analyses for E330Q (◇) and T688A (●). The solid lines were the fits for E330Q with R^2 = 0.959 and 0.987; T688A with R^2 = 0.998 and 0.999, for k_a and k_d respectively.

A.

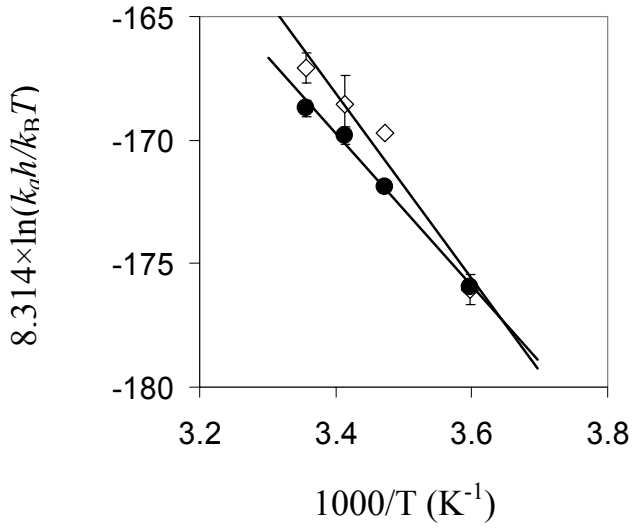
-165
-170
-175
-180
3.2
3.4
3.6
3.8
8.314×ln(k_a h/k_B T)
1000/T (K^-1)

B.

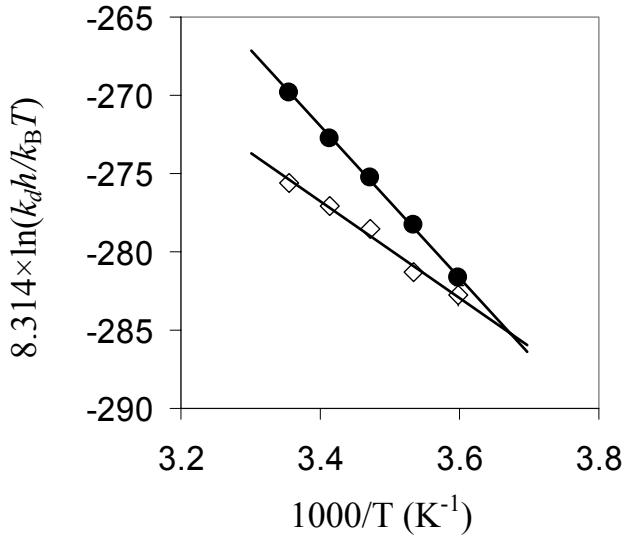
-265
-270
-275
-280
-285
-290
3.2
3.4
3.6
3.8
8.314×ln(k_d h/k_B T)
1000/T (K^-1)

Table 15. Theoretical activation parameters determined for $Man_9GlcNAc_2$-glycopeptide interactions with *Hs*ERManI.

Parameters[a]	**E330Q**		**T688A**	
	association	**dissociation**	**association**	**dissociation**
ΔG^o **(kJ·mol^{-1})**	50 ± 6.0	82 ± 3.6	50 ± 1.4	80 ± 1.6
ΔH^o **(kJ·mol^{-1})**	37 ± 1.4	31 ± 2.5	31 ± 0.9	48 ± 1.1
$T\Delta S^o$ **(kJ·mol^{-1}·K^{-1})**	-12 ± 1.7	-51 ± 2.5	-19 ± 1.0	-32 ± 1.2

[a] Parameters were derived from Eyring plots using the kinetic rate constants determined by SPR. The Gibbs free energy for activation at 25 ºC was derived from relationship $\Delta G = \Delta H - T\Delta S$

Figure 53: Free energy profiles for $Man_9GlcNAc_2$-glycopeptide interactions with E330Q (—) and T688A (—). ΔG^o, ΔH^o, and $-T\Delta S^o$ were derived from the van't Hoff and Eyring analysis. The reactants and products are indicated by R and P, respectively.

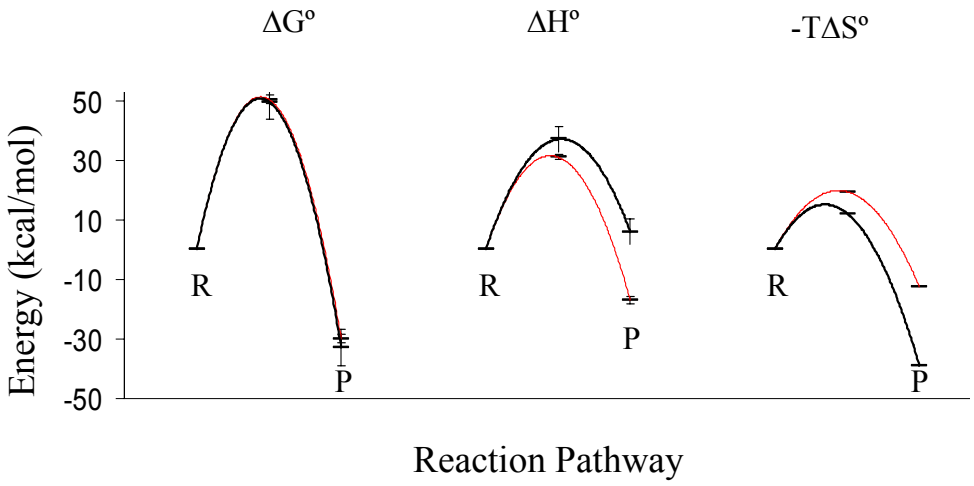
ΔGº
ΔHº
-TΔSº
50
30
10
-10
-30
-50
Energy (kcal/mol)
R
P
R
P
R
P
Reaction Pathway

Figure 54: The binding analysis of *Hs*ERManI and high mannose oligosaccharide-PA interactions using the E330Q mutant as a model system. The biosensor responses represent duplicate injections of 2-fold serial dilutions of (A) $Man_9GlcNAc_2$-PA (0.39-50 μM), (B) $Man_8BGlcNAc_2$-PA (6.25-100 μM), (C) $Man_6GlcNAc_2$-PA (12.5-400 μM), (D) $Man_5GlcNAc_2$-PA (12.5-400 μM) and (E) Manα1,2Man (15.6-500 μM). The binding kinetics parameters are summary in Table 16

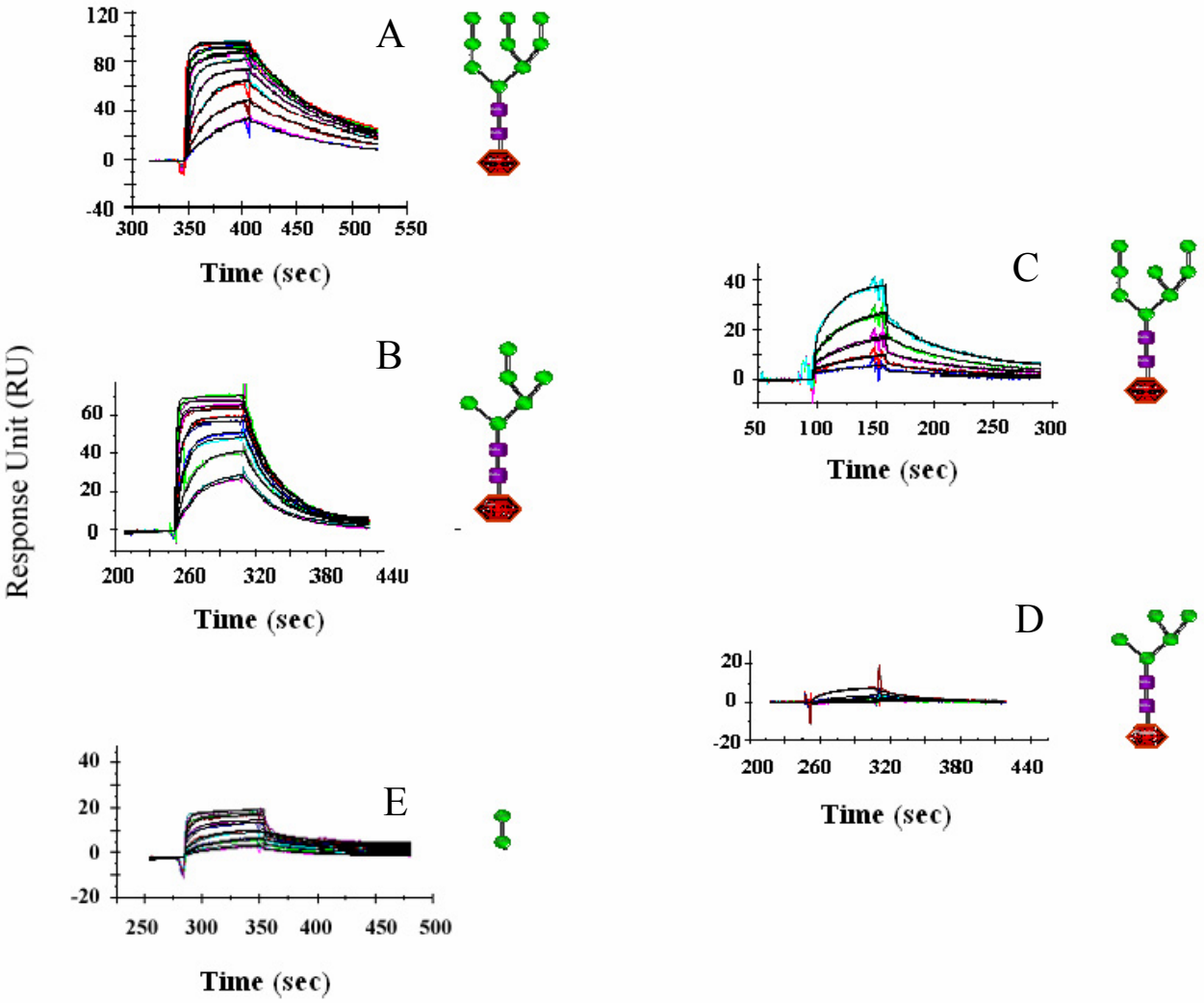
A
B
C
D
E
Response Unit (RU)
Time (sec)
Time (sec)
Time (sec)
Time (sec)
Time (sec)

Table 16. Summary of binding analysis of *Hs*ERManI and oligosaccharide-PA interactions using the E330Q mutant as a model for binding studies.

Ligand	k_a ($\times 1000$ $s^{-1}M^{-1}$)	k_d ($\times 0.001$ s^{-1})	K_D (μM)	$\Delta G^{283,\,a}$ (kJ/mol)
$Man_9GlcNAc_2$-Peptide	21.9 ± 4.9	11.1 ± 2.7	0.51 ± 0.17	-34.1 ± 0.82
$Man_9GlcNAc_2$-PA	21.5 ± 1.5	15.2 ± 0.14	0.710 ± 0.043	-33.3 ± -0.14
$Man_8BGlcNAc_2$-PA	0.591 ± 0.013	14.9 ± 0.566	25.2 ± 0.41	-24.9 ± -0.04
$Man_6GlcNAc_2$-PA	1.64 ± 0.06	31.9 ± 0.07	19.5 ± 0.80	-25.5 ± -0.10
$Man_5GlcNAc_2$-PA	0.139 ± 0.016	29.9 ± 5.6	214 ± 16.3	-19.9 ± -0.18
Manα1,2Man-*O*-CH_3	4.69 ± 0.21	163 ± 5.0	34.7 ± 2.58	-24.2 ± -0.19
Manα1,2Man	0.934 ± 0.250	26.1 ± 2.48	28.6 ± 4.99	-24.6 ± -0.41

[a] $\Delta G^{283} = -RT\ln(1/K_D)$, at 283 K and $R = 8.314$ $j \cdot mol^{-1} \cdot K^{-1}$.

Table 17. Calculation of the binding contribution of the oligosaccharide.

Residue(s) (x)	Calculation scheme $-\Delta G_X = \lvert\lvert\Delta G_A\rvert - \lvert\Delta G_B\rvert - \lvert\Delta G_C\rvert - \ldots\rvert$	$-\Delta G_X$	**Average** $-\Delta G_X$
-Asn/PA-	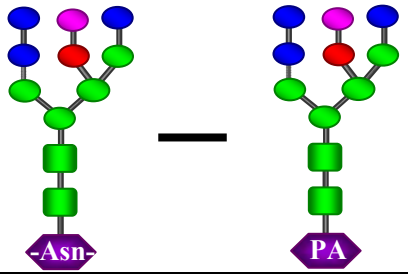	**34.0-33.3**	**0.7**
	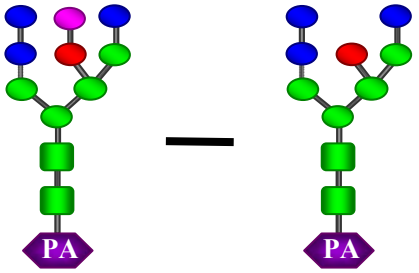	**33.3-24.9**	**7.0±1.4**
	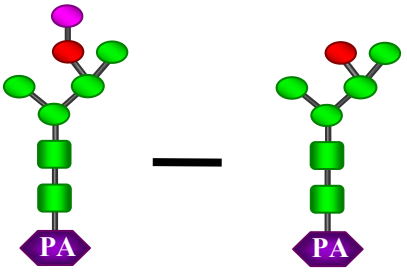	**25.5-19.9**	
3 × 	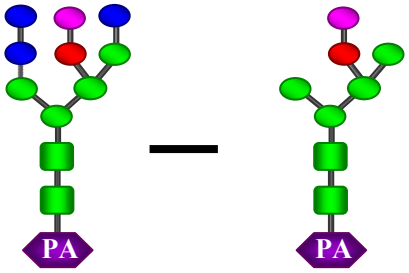	**33.3-25.5**	**6.4±1.4**
	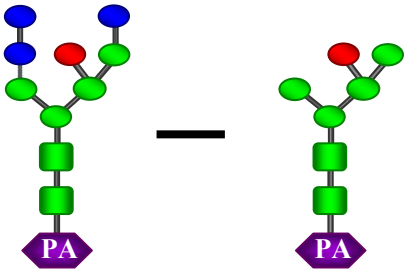	**24.9-19.9**	

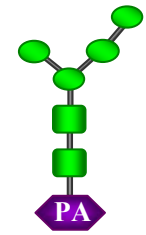 Or 4× +2×	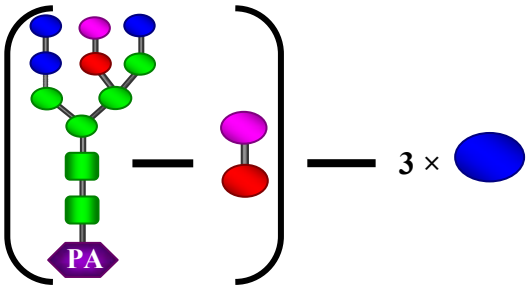	(33.3-24.6)-6.4	1.8 ±0.8
	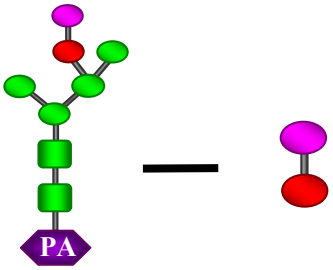	25.5-24.6	
	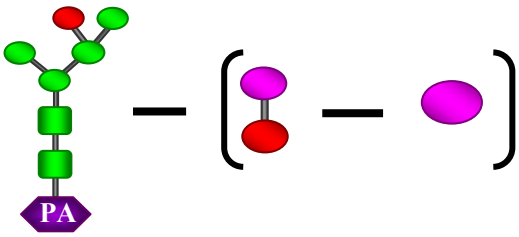	19.9 - (24.6-7)	
	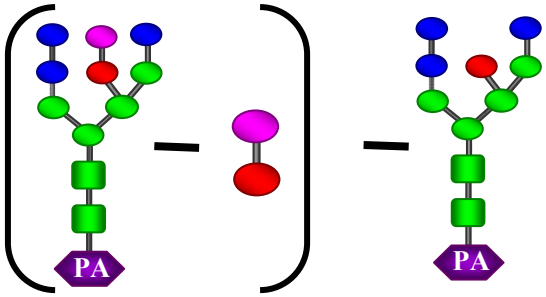	(33.3-24.6) -24.9	17.6±1.4
	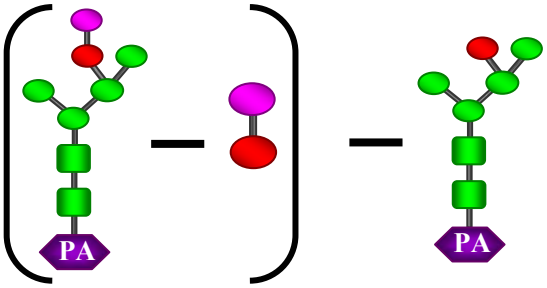	(25.5-24.6) -19.9	
	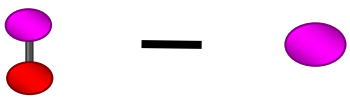	24.6-7.0	

Figure 55: Mapping the $Man_9GlcNAc_2$-PA and *Hs*ERManI interaction profile using free energy of binding.

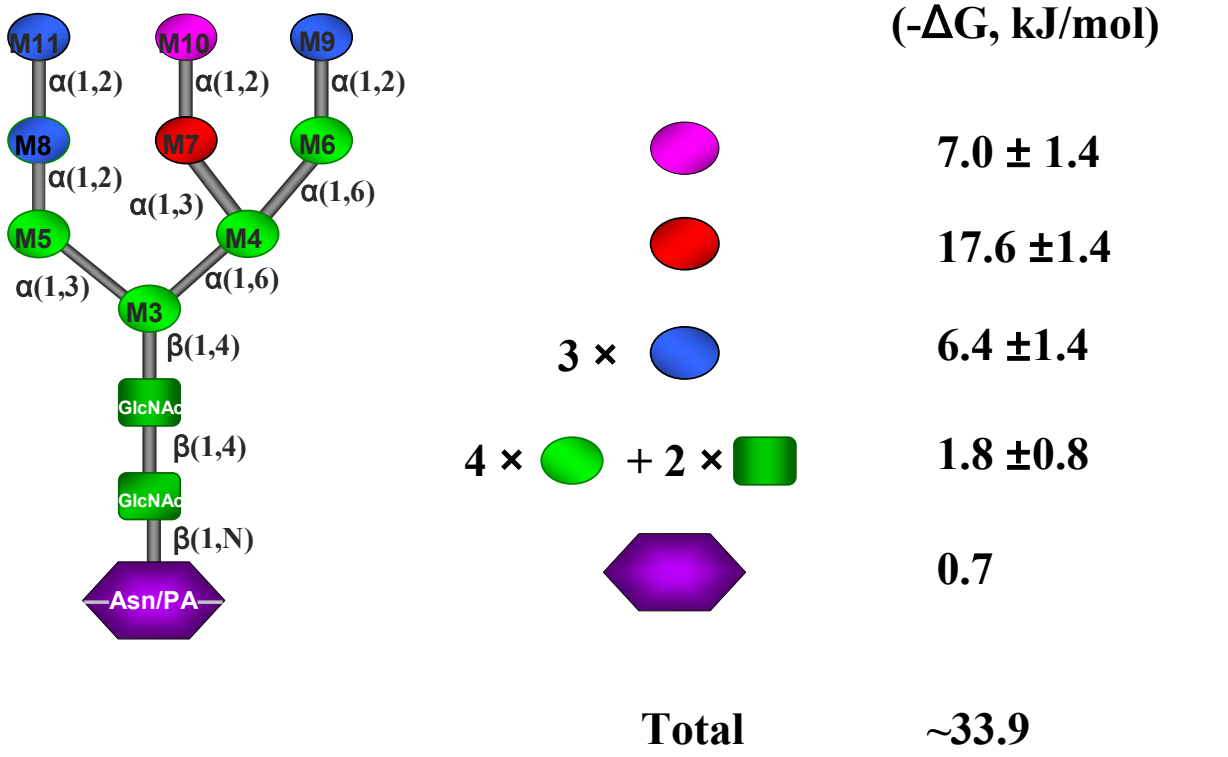

CHAPTER 4

DISCUSSION

The extent of α1,2-mannose trimming of Asn-linked oligosaccharides in the early secretory pathway varies in eukaryotic organisms from the removal of a single mannose residue in *S. cerevisiae* [3] to the removal of all four α1,2-mannose residues in metazoan organisms [23]. In all eukaryotic organisms examined, with the possible exception of the fission yeast *Schizosaccharomyces pombe* [171], mannose trimming is initiated in the ER by the removal of a single mannose residue from $Man_9GlcNAc_2$ to produce the Man8B structure. Further trimming of α1,2-mannose residues in animal and plant systems occurs through the action of multiple mannosidases in the ER and Golgi [23]. Primary sequence similarity between the *S. cerevisiae* processing mannosidase and the mammalian Golgi processing α1,2-mannosidases, along with their common requirement for Ca^{2+} for catalytic activity, their sensitivity to inhibition by dMNJ and kifunensine, and their common reaction mechanism [72, 172], has led to the classification of these enzymes as class 1 mannosidases [23]. This classification contrasts them with the more heterogeneous collection of processing and catabolic mannosidases, termed class 2 mannosidases [23], in the ER, Golgi, lysosomes, and cytosol, that do not require Ca^{2+}, are sensitive to a distinctive set of inhibitors, and have a different mechanism of action [173]. A similar separation of the mannosidases into two distinct families was made during the classification of glycosylhydrolases based on sequence similarities (Class 1 = Swiss-Prot glycosylhydrolase family 47; Class 2 = Swiss-Prot glycosylhydrolase family 38) [174-176].

Biochemical evidence for an ER mannosidase I-like activity in mammalian cells was originally described over 23 years ago [177, 178] and the proposed contribution of the enzyme to

the maturation of Asn-linked oligosaccharides has been described in several reviews [23, 86, 179]. Prior to our cloning and characterization of the human enzyme [10],very little was known about the enzyme from mammalian sources other than biochemical characteristics determined through enzyme assays in crude membrane extracts [26]. Previous attempts to clone the enzyme resulted in the isolation of cDNAs encoding either the rat cytosolic/ER mannosidase II [26, 177] or mouse Golgi Man IB [158].

4.1 Characterization of the catalytic domain encoded by the *Hs*ERManI cDNA

We anticipated that the mammalian ERManI would be a class 1 mannosidase based on two lines of evidence. First, *in vitro* assay data indicated that the mammalian ERManI was inhibited by dMNJ and kifunensine but not swainsonine, and the enzyme required Ca^{2+} for catalytic activity [26]. Second, the only known class 1 mannosidase in *S. cerevisiae* is an ER processing mannosidase that catalyzes the equivalent enzymatic reaction as the mammalian ERManI, cleaving $Man_9GlcNAc_2$ to the same Man8B isomer [180], indicating that the yeast enzyme may be an ortholog of the human enzyme.

Cloning and expression of a human homolog of the *S.cerevisiae* ERManI as a fusion with protein A demonstrated that the COOH-terminal 435 amino acids of the coding region, a sequence common with the other class 1 mannosidases, contains the catalytic domain of the enzyme and that the NH_2-terminal ~220 amino acids are not required for catalytic activity. The enzyme cleaved a single residue from $Man_9GlcNAc_2$ to produce the Man8B isomer with no further digestion of the substrate even after a prolonged incubation. The recombinant enzyme was inhibited by dMNJ and kifunensine but not swainsonine and could not cleave *p*NP-α-Man. The requirement for divalent cations in the enzyme reaction was demonstrated by the strong inhibition with either EDTA or EGTA and the recovery of the enzyme activity by the addition of Ca^{2+}.

These inhibition profiles, along with requirement for divalent cations and the inability to cleave *p*NP-α-Man, are hallmarks of class 1 mannosidases. In combination with the specificity for producing the Man8B isomer from $Man_9GlcNAc_2$, the catalytic characteristics indicate that the human cDNA that we isolated encodes an enzyme activity previously described for ERManI [181].

The accumulation of glycoproteins containing the Man8B structure in cultured cells incubated with low concentrations of dMNJ was among the first evidence suggesting the presence of a unique mannosidase activity in the ER [182]. These data demonstrated that ERManI was more resistant to inhibition by dMNJ than the Golgi enzymes, mannosidase IA, IB and IC [72]. Subsequent work indicated that the ER might also contain a distinctive dMNJ-sensitive mannosidase activity that would produce the Man8B isomer from $Man_9GlcNAc_2$ [182, 183]. Our data on the recombinant *Hs*ERManI have shown that the enzyme is sensitive to inhibition by dMNJ. In addition, our enzyme mixing experiments (Table 5) have shown that the ER enzyme was relatively less sensitive to inhibition than Golgi Man IA. These data indicate that treatment of cells with less than fully inhibitory concentrations of dMNJ would result in the production of oligosaccharides with the Man8B isomer structure. Higher dMNJ concentrations would be predicted to result in full ERManI inhibition and accumulation of $Man_9GlcNAc_2$ structures. It is noteworthy that the concentration of dMNJ used previously to demonstrate a dMNJ-resistant ER mannosidase activity in cultured cells (150 μM dMNJ [182]) would not be expected to fully inhibit ERManI. In contrast, when higher dMNJ concentrations (0.4-1 mM) were employed, a partial [182] or complete [183] inhibition of cleavage from $Man_9GlcNAc_2$ to Man8B was observed in cultured cells. An additional complexity arises from the fact that the early enzymology and biosynthetic labeling studies [177, 182-185] predated the biochemical identification of ER mannosidase II [26, 181], an enzyme that has been shown to produce the

Man8C isomer and potentially smaller structures from $Man_9GlcNAc_2$ in the ER of mammalian cells [26]. This latter enzyme is also sensitive to inhibition by dMNJ but not kifunensine. As a result of the action of these two enzymes, several factors could contribute to the variable oligosaccharide structures observed in dMNJ-treated cells [182, 183]. Although the absolute enzyme activity levels of ERManI and ERManII in different cell types are not known, the relative ratios of the two enzymes have been previously shown to vary widely in different cell types. Moreover, the capacity of different cell types [181] to transport dMNJ into the lumen of the ER is unknown and may also vary between cell types. Finally, the residence time of glycoprotein substrates in the ER is known to be quite variable [186] and may influence the degree of processing by ER mannosidases. Conclusions about the dMNJ-sensitivity of ERManI based on an examination of the effect of dMNJ treatment of cultured cells could, therefore, be misleading, and this enzyme could be responsible for both of the activities that have previously been termed dMNJ-sensitive or dMNJ-resistant ER mannosidases.

It is interesting to note that the substrate specificity of ERManI was found to be complementary to the substrate specificity of Golgi Man IA (Figure 22). The former enzyme cleaves a single α1,2-mannose from $Man_9GlcNAc_2$ to produce Man8B, while the latter enzyme will cleave the other three α1,2-mannose residues on $Man_9GlcNAc_2$, but recognizes the central branch mannose substrate for ERManI with at least 10-fold lower efficiency [72]. Enzyme mixing experiments confirmed the complementarity of ERManI activity with Golgi ManIA to result in the rapid and efficient cleavage of $Man_9GlcNAc_2$ to $Man_5GlcNAc_2$. The differences in substrate recognition by the two enzymes are striking considering their similarity in sequence. Structure determination of these two enzymes [15, 66] revealed that the differences in their substrate recognition was partially determined by structural steric hindrance in the selective binding of appropriate branches of the high mannose N-glycan structure.

ER mannosidase I-like activity, cleaving $Man_9GlcNAc_2$ to the Man8B structure, is the last step in oligosaccharide processing that is fully conserved from yeast to mammals. In *S. cerevisiae*, further extension of the oligosaccharide by mannose addition leads to the formation of mannans [3, 25]. In mammals, oligosaccharides are further processed by mannose trimming and extension into complex type structures [179]. As the last conserved step in eukaryotic oligosaccharide processing, ERManI presumably accomplishes a critical role in oligosaccharide maturation. In *S. cerevisiae*, the enzyme does not appear to be essential for growth [64] or extension of mannan structures [47], but the enzyme may contribute to the timing step in the quality control degradation of glycoproteins in the ER [45, 46]. A similar role for ERManI activity has been implicated in mammalian glycoprotein turnover in the ER [44, 187]. The availability of the mammalian cDNA encoding ERManI should allow a more direct testing of the hypothesis that the conserved role of the enzyme in eukaryotes is to target misfolded glycoproteins for quality control degradation.

4.2 Expression and Purification

The expression of the *Hs*ERManI cDNA in *P. pastoris* was used to generate sufficient quantities of purified recombinant enzyme necessary for antibody production and detailed enzyme kinetics analysis as well as crystal structure analysis [14]. The recombinant protein was purified using cation exchange chromatography and gel filtration with a yield ~5 mg per liter of rich culture media. The purified enzyme appeared to undergo NH_2-terminal degradation beyond the α-factor signal sequence. The NH_2-terminal sequence of the purified protein was AEVP. The molecular weight of purified protein was determined to be ~55 kDa, consistent with the NH-terminal sequence data indicating a cleavage of 54 amino acids from the NH_2 terminus and final size of 473 amino acid residues for the recombinant product.

Using the purified recombinant enzyme we were able to detect the hydrolysis of a disaccharide substrate as well as the further cleavage of $Man_8GlcNAc_2$-PA isomer B to smaller oligosaccharides with the catalytic rate 180-fold slower than the cleavage of the natural substrate $Man_9GlcNAc_2$-PA (Figure 36). The ability of yeast ERManI to hydrolyze Man8B has also been reported previously [31]. The steady-state kinetic parameters for $Man_9GlcNAc_2$-PA cleavage by *Hs*ERManI were in agreement with those reported for *Sc*ERManI [188]. The Michaelis-Menten constant (K_m) for Manα1,2Man and Manα1,2Manα-*O*-CH_3 by *Hs*ERManI were determined to be 1-2 mM, similar to equivalent values for *Mm*GManIA and IB [72].

4.3 The inhibition of class I mannosidase

Kinetic analysis of the K_i values for kifunensine and dMNJ were determined to be 130 nM and 11 μM, respectively (Table 7) for *Hs*ERManI using $Man_9GlcNAc_2$-PA as substrate**.** The inhibition effect for these two compounds did not follow either standard competitive or noncompetitive inhibition [166, 189]. It was worth noting that the K_i of dMNJ of *Hs*ERManI was determined to be slightly lower than that of *Mm*GManIA (18.3 μM) [72], even though it was shown earlier (Table 5) that the latter was more sensitive to dMNJ than the former enzyme. These results could indicated that the mode of action of dMNJ was different between the Golgi and ER α1,2-mannosidases.

*Hs*ERManI and *Mm*GManIA are not inhibited by 1-deoxynojirimycin, castanospermine, swainsonine, or 1,4-dideoxy-1,4-imino-D-mannitol. Since the only difference between 1-deoxymannojirimycin and 1-deoxynojirimycin is the orientation of the O-2' hydroxyl (Figure 30), the specificity of the enzyme for these inhibitors would appear to be influenced by the configuration of the O-2' hydroxyl [14]. Because the O-2' and O-3' hydroxyls of castanospermine

are in the same orientation as those of 1-deoxynojirimycin and they are also unable to bind the enzyme confirmed the critical role of the O-2' hydroxyl.

The lack of inhibition of class 1 α1,2-mannosidases by swainsonine and the poor inhibition by 1,4-dideoxy-1,4-imino-D-mannitol [26] (Table 7) could be explained by the ring conformation of these inhibitors. Swainsonine and 1,4-dideoxy-1,4-imino-D-mannitol are potent inhibitors of the class 2 mannosidases such as Golgi α-mannosidase II and lysosomal α-mannosidase [86]. In contrast to kifunensine, 1-deoxymannojirimycin, castanospermine, and 1-deoxynojirimycin, which are pyranose mannose and glucose substrate mimics, the class 2 mannosidase inhibitors, swainsonine and 1,4-dideoxy-1,4-imino-D-mannitol, are thought to mimic the ring-flattened transition state mannosyl cation of these retaining enzymes as furanose analogs of mannose [86] (Figure 30). The energy-minimized structures of swainsonine and 1,4-dideoxy-1,4-imino-D-mannitol show that although the furanose ring will have a different sugar ring conformation than the $^{1}C_{4}$ conformation of the pyranose ring of 1-deoxymannojirimycin and kifunensine, the O-2' and O-3' hydroxyls are in the same relative orientations in all four inhibitors (Figure 30). This suggests that both swainsonine and 1,4-dideoxy-1,4-imino-D-mannitol should be able to inhibit the class 1 mannosidase based on the O-2' and O-3' configurations alone. However, experimentaly, the enzyme can be inhibited poorly by 1,4-dideoxy-1,4-imino-D-mannitol [26] and is insensitive to swainsonine (Table 7). The poor inhibitory properties of 1,4-dideoxy-1,4-imino-D-mannitol indicated that this latter compound is conformationally more flexible in binding to the enzyme active site, while the conformation of swainsonine is more rigid and unable to fit in the active site of the class 1 mannosidases. The preference for 1-deoxymannojirimycin over 1-deoxynojirimycin and castanospermine, the lack of inhibition of the enzyme by swainsonine, and the weak inhibition by 1,4-dideoxy-1,4-imino-D-mannitol all point

to the critical role of correctly oriented O-2' and O-3' hydroxyls in a pyranose ring structure, not only for substrate specificity, but also for inhibitor specificity.

The pyranose rings of kifunensine and the protein-bound conformation of 1-deoxymannojirimycin are identical (Figure 30). However, kifunensine binds to α1,2-mannosidases with higher affinity than 1-deoxymannojirimycin, indicating that the five-membered ring and its substituents are also important components of inhibitor binding and likely lock the pyranose ring into a pre-formed $^{1}C_{4}$ conformation. The inhibitor structures presented in this study therefore provide the first structural data regarding the specificity of this class of enzymes for α1,2-mannose residues and a blueprint for future inhibitor design of novel therapeutic agents for the treatment of genetic diseases that are characterized by rapid degradation of misfolded glycoproteins.

4.4 Proton inventory study

In an attempt to verify the role of a second water residue in catalysis by *Hs*ERManI as had been proposed in Vallee *et al.* [14], a proton inventory study was investigated using either $Man_9GlcNAc_2$-PA or Manα1,2Man as substrate. The DIEs and fractionation factors for the reactant state (ϕ^R) determined at the pH optimum were 1.82 and 0.71 for Manα1,2Man and 1.76 and 0.74 for $Man_9GlcNAc_2$-PA, respectively (Figures 34 and 35). The DIE and ϕ^R for hydrolysis by *Hs*ERManI can be classified into the following types of functional groups in which hydrogen atoms are involved using the criteria suggested [122-124]: "1) Bonds from hydrogen to *sp* carbon, 2) bonds from hydrogen to positive oxygen, 3) hydrogen bonds to oxygen of high basicity in water solution, and 4) transition-state hydrogen bridges in "solvation catalysis". The 4th situation is more likely the case for an acid-base catalyzed reaction by ERManI which

involves the proton transfer via formation and fusion of bonds involving hydrogen atoms. The DIE and ϕ^R under these circumstances were expected to be small, in the range of 1.5-3.0 and 0.3-0.7, respectively [123]. Since there was no clear explanation for the cause of this type of isotope effect in acid-base catalysis, the experimental data were fit to different models as summarized in Table 9. As a result, the experimental data fit best using a polynomial function which suggested 5-6 protons involved in the transition and reactant states (Figure 34 and Table 9). This result and crystal structure for *Hs*ERManI suggest [14] that the 5 protons may be contributed from the 4 water residues which are coordinated with the Ca^{2+} ion and the one nucleophile water. The presence of the 6th proton does not seem to be necessary as it does not improve the fit significantly (Table 8) for Manα1,2Man, while it appeared to improve the fit significantly for $Man_9GlcNAc_2$-PA. However, the calculation based on the experimental data for $Man_9GlcNAc_2$-PA should be considered suspect since it contains a large error that might lead to misleading conclusions.

4.5 Mutagenesis analysis

The proposed mechanism for *Hs*ERManI from prior structural studies suggested that the enzyme has several unusual characteristics for an inverting glycosidase, including the involvement of an unusual high free energy $^1C_4$ sugar conformation, a through-water protonation of the glycosidic oxygen and a water nucleophile that was also directly coordinated to an enzyme-associated Ca^{+2} ion. In an effort to understand the mechanism for glycoside bond hydrolysis and possibly get insights into how the EDEM proteins are compromised in glycosidase activity, we generated mutations in the potential catalytic residues of *Hs*ERManI and examined

their effects on substrate binding and catalysis. In parallel studies we also examined the structure of a co-complex between *Hs*ERManI and an uncleavable thiodisaccharide substrate analog.

The proposed catalysts [14] E330, D463 and E599 were mutated to Gln, Asn and Gln respectively. The possible auxiliary amino acids for the general base (H524) and the general acid (R334) were also chosen and mutated to Ala. The single mutants and double mutants of these residues did not completely inactivate the enzyme and the residual α1,2-mannosidase specific activity that could be detected ranged from 10-10^5-fold lower than that of the wild type enzyme (Figure 37). These results indicated that these mutations did not prevent the recombinant enzymes from being expressed and functional with the exception of R334A. The mutation of R334 to Ala resulted in absence of expression of the protein in a secreted form indicating this residue also played a significant role in the structural folding and stabilization of the polypeptide and a change to Ala resulted in an unfavorable state for protein folding. The R597 is a conserved residue that forms a H-bond with the O-6′ hydroxyl of the inhibitor and stabilized the equatorial conformation of the C5-C6 linkage. Mutating this residue to an Ala residue resulted in reduction of the catalytic rate and higher K_m (Table 10). The substrate binding affinity for R597A was determined to be in the same range as the wild type enzyme even though its catalytic rate decreased by ~50-fold. These results indicate that R597A mutation results in a stable expression product, while the corresponding R334A mutation results in an unstable expression product.

4.5.1 The impact of R461 —R461 has been proposed to play a major role in substrate binding and recognition. [66]. This residue was mutated to Ala and Leu and resulted in a reduced catalytic rate (10- and 70-fold, respectively) (Table 10). Only the R461L mutant was found to readily catalyze the cleavage of $Man_9GlcNAc_2$-PA to $Man_{8\text{-}6}GlcNAc_2$-PA, similar to that previously reported in *Sc*ERManI [110]. The binding affinity of R461L was determined to be

significantly less than that of the R461A mutant indicating that R461 contributes to substrate binding affinity and substrate specificity for H*s*ERManI.

Our working hypothesis is that the R461L mutation eliminates specific hydrogen bonding interactions and creates extra empty space at the core of the glycan binding site that allows for the rotation of the linkages associated with the M3 mannose. The greater freedom of the flexibility of the glycan structure may be consistent with the more promiscuous cleavage specificity for the mutant. In contrast, the R461A mutant would be predicted to allow even greater flexibility for rotation of the glycan substrate linkages. The lack of broadened specificity for this mutant is contrasted with the R461L mutant and suggest that there maybe a positive role for the Leu residue in this position, as seen in the GManIA structure. Mutation to Ala may not provide the specific interactions necessary for the braod specificity binding pocket. These data suggest that a further study of the roles of protein residues in the glycan binding cleft will be required to come to any definitive conclusions on substrate specificity for these enzymes.

4.5.2 The impact of F659 —The SPR analysis showed that the F659A mutant lost its ability to bind to dMNJ (Figure 39N) and also lost its ability to form a stable complex with Kif (Figure 39P) compared with the wild type enzyme (Figure 39O). These results indicate that the presence of the aromatic sidechain of F659 is required for binding the $^{1}C_{4}$ conformer and/or stabilization via van der Waals interactiont with the C_4-C_5-C_6 region of dMNJ. The inability to stabilize the $^{1}C_{4}$ sugar conformation resulted in the reduction of catalytic rate (k_{cat}) by 120-fold, but not a reduction in the K_m with the $Man_9GlcNAc_2$-PA substrate. The overall oligosaccharide binding affinity showed only a 4-fold reduction.

4.5.3 The impact of T688 —The mutation of T688 to Ala resulted in a reduction in the catalytic rate and K_m. The calcium equilibrium analysis results showed that the T688A mutant was capable of binding to calcium with only 2-fold less efficiency than the wild type enzyme, while catalysis was reduced by 30-fold (Figure 41). These results indicate that the presence of T688 was not required for Ca^{2+} binding to the active site, but may require favorable coordination with its γ-O with the Ca^{2+} ion for efficient catalysis. The SPR analysis of the T688A mutant for dMNJ binding affinity showed that the absence of T688 side chain only reduces the binding of dMNJ by ~5-fold compared to the wild type enzyme or a loss of ~4 kJ/mol of binding energy. In contrast, the binding of dMNJ was reduced greatly in the absence of Ca^{2+}, which accounted for a loss of ~14 kJ/mol of binding energy for the wild type enzyme (Table 9) and E330Q and T688A mutants (data not shown). The binding energy of $Man_9GlcNAc_2$ in the absence of Ca^{2+} was reduced by ~10 kJ/mol for both E330Q and T688A, assuming there was no catalytic effects at 10ºC. The SPR analysis results indicated that the absence of the T688 side chain or Ca^{2+} did not prevent the binding of dMNJ or $Man_9GlcNAc_2$, but in the absence of Ca^{2+}, the enzyme completely lost its catalytic ability. Therefore, Ca^{2+} plays a major role in catalysis by coordinating the nucleophilic water and possibly lowering its pK_a. Ca^{2+} also plays a role in assisting in glycone binding and contributing to the binding energy.

4.5.4 The impact of E330 —Mutation of E330 to an isosteric amide (E330Q) caused a significant decrease in k_{cat} , a 1.8 pH unit drop in the pH optimum, and a ~3.3 pH unit drop in the calculated pKa of the macroscopic dissociation constant for the basic limb of the pH curve. These data confirm the role of this residue as the general acid in the catalytic mechanism. However, the distance between the carboxyl side chain and the sulfur in the thiodisaccharide co-complex, the equivalent of the glycosidic oxygen in this structure, is too long for direct protonation (Figure

45). The presence of a weak density for an intervening water molecule confirms that E330 acts indirectly in a through-water protonation of the glycosidic oxygen. An attempt to probe the role of an adjacent Arg residue that may influence the pKa of the general acid by mutagenesis (R334A) was unsuccessful, but the high calculated pKa for the catalytic acid (pH 7.6-7.8) is expected to reflect the local environment of E330 and the adjacent R334 residue.

4.5.5 The impact of E599 —Mutation of E599 to the isosteric amide (E599Q) resulted in a much more profound drop in k_{cat} (~10^5-fold) and a ~1000-fold loss in affinity for binding to dMNJ. Surprisingly, the drop in affinity of binding for the $Man_9GlcNAc_2$-glycopeptide ligand by SPR was only 4-fold, suggesting that the loss in catalytic turnover by the absence of the catalytic base predominately resulted from an unfavorable binding of the glycone residue in the -1 subsite rather than the docking of the >+1 residues in the glycan binding cleft. Mutagenesis of the His residue adjacent to the E599 catalytic base (H524A) reduced the k_{cat} by ~4-fold and slightly increased the K_m, but the effects were relatively minor by comparison to the conversion of the catalytic base to the isosteric amide. These data would indicate that E599 acts as the catalytic base and there is not a significant role of H524 in the catalytic mechanism of ERManI.

4.5.6 The impact of D463 —The role of D463 in the ERManI mechanism was tested by examining the kinetics and substrate binding of an isosteric amide mutant of the enzyme (D463N) and by examining the nature of the interactions between this residue and the substrate analog in the thiodisaccharide co-complex. The D463N mutant resulted in an ~800-fold drop in k_{cat}, and virtually eliminated binding of the $Man_9GlcNAc_2$-glycopeptide substrate to the enzyme by SPR. In the co-crystal, D463 clearly acted to coordinate the +1 residue by interacting with both the O3' and O4' hydroxyls of this residue. We anticipated that the isosteric amide

substitution at this position (D463N) would be able to maintain hydrogen bonding capability, but eliminate the potential role of this residue as a catalytic acid. Since this residue clearly is involved in stabilizing the interaction with the +1 residue and does not act as a general acid, we were surprised that the mutation would have such a profound effect on substrate binding. Precedent for a significant decrease in bond length and increase in hydrogen bond strength for carboxylate side chains over isosteric amides has been previously noted [190]. The critical role of the proposed higher affinity interactions for the carboxylate over the amide would be strongly indicated by the significant drop in k_{cat} and the total loss of measurable binding affinity for high mannose oligosaccharides in the D463 mutant.

4.6 Acid/base chemistry in the active site of GH family 47 mannosidases

The positions of the amino acid side chains in both the –1 and +1 subsites of ERManI are not significantly altered as a consequence of binding the thiodisaccharide. The position of the sulfur in the thiodisaccharide is ~4.2Å from O-ε2 of E330, indicating, as previously proposed [14], that there is likely not a direct protonation of the glycosidic oxygen by this enzyme carboxyl side chain. Both E330 and R334 are in similar positions compared to the ERManI-DMJ complex [14], and a weak electron density of a proposed water molecule, W1, is within proximity of the glycosidic sulfur (3.2Å) and hydrogen bonding distance from both carboxyl oxygens of E330 (2.6 Å and 3.0Å, respectively) as well as NH2 of R334 (2.7Å). A direct interaction between E330 and R334 is also indicated by the proximity of O-ε1 of E330 to both NH2 (3.0Å) and N–ε (2.9Å) of R334.

The positions of the proposed catalytic base, E599, and the water nucleophile, W3, as well as the protein associated Ca^{+2} ion are essentially unchanged from the free enzyme or the

ERManI-DMJ complex [14]. The distances from E599 to W3 (2.7Å) and from W3 to C1 of the sugar in the –1 site (3.2Å) would indicate that the water nucleophile could be activated by the E599 base for nucleophilic attack. The distance from W3 to the C1 of the glycone would be expected to be even less at the ring-flattened $^{3}H_{4}$ transition state.

Standard glycosidases mechanisms invoke a transition state where a partial positive charge is delocalized between the anomeric carbon and the ring oxygen to form an oxocarbenium ion with partial double bond character. Of the four potential sugar ring conformers that satisfy the criteria for co-planarity at C2-C1-O5'-C5 (Figure 13), only the $^{3}H_{4}$ half chair had not yet been identified as a potential glycosidase transition state conformation. The unusual $^{1}C_{4}$ conformation for dMNJ in the ERManI-dMNJ complex has led to the suggestion that the family 47 glycosidases may employ a $^{3}H_{4}$ transition state [95]. To confirm the use of the proposed transition state we determined the structure of the co-complex with a thiodisaccharide substrate analog and unambiguously demonstrated a $^{3}S_{1}$ skew boat conformation for the glycone in the -1 subsite. The similarity in the solution state binding affinities for the *S*- and *O*-glycosides suggest that the *S*-glycoside interacts with the enzyme in a similar mode as true *O*-glycoside substrates. In the itinerary of sugar ring conformational interconversions, the $^{1}C_{4}$ chair and $^{3}S_{1}$ skew boat conformations bracket the $^{3}H_{4}$ half chair conformation (Figure 13 and 46). A similar type of bracketing of ring flattened transition states has been used to identify the three other potential co-planar transition state conformations for inverting and retaining glycosidases [95].

The co-complex structure described here indicates that the Class 1 mannosidases bind to substrates constrained at the C3, C4, and C5 positions into an axial configuration for the respective hydroxyls in a high energy $^{3}S_{1}$ sugar conformation (Figures 13 and 46). Binding is mediated by direct interaction of the O2' and O3' hydroxyls of the -1 residue with the enzyme bound Ca^{+2} ion along with a matrix of hydrogen bonding interactions with the O4' and O6' sugar

hydroxyls and a hydrophobic stacking of F659 with the C4-C5-C6 region of the -1 residue (Figure 45). Additional interactions between the +1 residue and D463 play a critical role in positioning the glycosidic linkage in proximity to the active site residues. Constraining the -1 residue into the high free energy $^{3}S_{1}$ sugar conformation would be predicted to reduce the activation energy to form the co-planar $^{3}H_{4}$ transition state through a conformational twist at C5, O5 and C1. Through-water proton transfer from the E330 general acid to the glycosidic oxygen would result in glycoside bond cleavage and formation of the $^{3}H_{4}$ ring-flattened oxocarbenium ion transition state. Deprotonation of the water nucleophile by E599 will induce the nucleophilic attack of the C1 carbon to produce a $^{1}C_{4}$ chair configuration of the enzymatic product containing an inverted β-hydroxyl at the anomeric center. These data are consistent with a mechanism of glycoside bond cleavage in which a least motion effect of a conformational twist at the -1 subsite accounts for the formation of the novel exploded transition state.

4.7 Molecular basis of substrate binding and recognition

To date, there have been no significant structural differences detected between the known class 1 mannosidases in the –1 subsites or in the proposed catalytic residues, even though they hydrolyze different α1,2 mannoside linkages in $Man_{9\text{-}5}GlcNAc_2$ [31, 73, 191]. Therefore, the substrate recognition and binding events in the $\geq$ +1 subsites must define the branch specificities for the individual family members.

The structural analysis of class 1 α1,2-mannosidases [14, 15, 66, 68, 69] revealed several common features including a β-hairpin loop inserting into the core of the $(\alpha\alpha)_7$-barrel and a Ca^{2+} ion coordinated into a pentagonal bipyradimal geometry with 8 ligands, including 4 water residues and the carbonyl oxygen and O-γ atom of T688 located at the apex of the β-hairpin loop.

The Ca^{2+} ion also coordinates with 2′ and 3′ hydroxyl groups of -1 subsite mannose residue providing a significant electrostatic force for substrate-enzyme interaction, in addition to several hydrogen bonding interactions with the protein at several points throughout the oligosaccharide binding site.

Even though the C_α backbones of the known protein structures of class 1 α1,2-mannosidases can be overlaid with very close alignment, the amino acid sequence similarity is not very high [15], particularly in the region of the anti-parallel β sheets at the long connect side, where the branches of the oligosaccharide substrate interact with the enzyme to define the branch specificity of oligosaccharide cleavage. In order to avoid the complexity and complications of interpreting the effects structural changes contributed by altering the amino acid residues in the glycan binding pocket, the binding kinetics and affinities of different glycan oligomers and isomers of $Man_{9\text{-}5}GlcNAc_2$ were tested using the E330Q mutant of *Hs*ERManI as a model to investigate the interactions involved in oligosaccharide binding.

The isothermal titration calorimetry (ITC) has been previously used to investigate the substrate binding thermodynamics of several glycosylhydrolase enzymes [192-195]. Using ITC to study protein-ligand binding requires large amounts of protein and ligand solution (millimolar range) and presents several problems in investigating the binding properties of class 1 α-mannosidases due to the tendency of recombinant enzyme to precipitate at high concentration [14] and the prohibitively large amount of glycan structures required for the experiment. Surface plasmon resonance technology (SPR) is an alternative mean to access the binding kinetics and affinity measurements using much less material compared to ITC. SPR analysis at different temperature can also provide basic binding kinetics (K_A, k_a, and k_d) as well as thermodynamic (ΔG, ΔH, and ΔS) information [137, 140]. It was critical that a catalytically inactive enzyme was used to obtain the binding constant (K_A) at low temperature so that the measured enthalpy

contains a minimal contribution from the hydrolysis event. The ability to measure the on (k_a) and off (k_d) rate in the binding event also allowed the monitoring of the substrate binding event independently from catalysis

4.7.1 The thermodynamics of substrate binding to E330Q and T688A — In an attempt to understand the molecular basis for differences in substrate recognition and binding properties, fundamental information on catalysis, binding kinetics, and thermodynamics were first evaluated using the wild type enzyme and catalytically deficient mutant enzymes as tools to assess the molecular basis of substrate recognition and binding among class 1 mannosidases.

The mutation of E330 and T688 resulted in the reduction of catalytic rate, increased the glycan in binding affinity, and allowed the detailed observation of binding kinetics for the oligosaccharide substrate ($Man_9GlcNAc_2$) with minimal contribution of catalysis. The properties of these mutations are of interest as tools for assessing and understanding the substrate binding mechanism for the class 1 mannosidases. The E330Q and T688A were not significantly different in their thermodynamics of catalysis, but significantly different in thermodynamic of binding. Even though the free energies for $Man_9GlcNAc_2$ binding to E330Q and T688A were equal, Eyring analysis showed that E330Q binding was driven by higher enthalpy and higher entropy during the binding event compared to those of T688A. It was worth noting that the equilibrium analysis (the van't Hoff analysis using binding dissociation constant (K_D)) (Table 14) and transition state analysis (Eyring analysis using on/off-rates of binding) resulted in differences in net gain or loss of enthalpy and entropy, especially the net enthalpy of the E330Q mutant and the net entropy of the T688A mutant (Table 15). For the E330Q mutant, the former analysis indicated a favorable enthalpy, while the latter analysis resulted in unfavorable enthalpy. For the T688A, the former analysis indicated a favorable entropy, while the latter analysis resulted in an

unfavorable entropy. The difference in binding thermodynamic parameters of T688A and E330Q derived from equilibrium and transition state analysis indicated that the binding equilibrium of T688A and E330Q were the result of different mechanisms than those that yielded the on-rate (k_a) and the off-rate (k_{off}). Because of the complicated interpretation of the thermodynamic data and the limitation in data collection, there was no further attempt to verify the cause of the net enthalpy or entropy changes observed in E330Q or T688A. However, the implications of the thermodynamics of binding will be crucial factors for assessing future data on the E330Q and T688A mutants.

4.7.2 Oligosaccharides binding analysis — The catalytically inactive E330Q mutant was used as a model for the dissection of the binding interactions and affinity contributions from individual mannose residues of the high mannose substrate in its docking to the glycan binding cleft of *Hs*ERManI. The M10 residue which is buried in the -1 subsite, coordinated by Ca^{2+} and stabilized by the hydrophobic interaction with F659, contributed ~7.0 kJ/mol to the glycan binding energy. The M7 residue resulted in a ~17.6 kJ/mol contribution to binding energy. The core mannose residues M3-M6 resulted in only a ~1.8 kJ/mol contribution, while the peripheral mannose residues, M8, M9 and M11, resulted in a contribution of as much as ~6.4 kJ/mol binding energy. The total binding energy for $Man_9GlcNAc_2$ was calculated to be ~33.9 kJ/mol, both by summation of the individual binding energies of each component as well as by direct measurement. The on-rate of the oligosaccharide binding was most influenced by the addition of the +1 subsite component, although the off-rate was also influenced by the peripheral mannose residues.

In conclusion, the use of the E330Q mutant in SPR binding studies was shown to be an invaluable tool in assessing the binding contributions of each component of the substrate

allowing an identification of the key residues that are responsible for substrate binding. Applying a similar approach to map the contributions of oligosaccharide substrate residues for the other class 1 mannosidases should reveal the molecular basis of substrate recognition and specificity. More importantly, the ability to measure the detailed binding kinetics using the E330Q mutant should provide critical information in the analysis of new selective inhibitors for class I mannosidases as potential targets for human protein misfolding disorders.

4.8 Future studies

4.8.1 Mutagenesis — The inverting catalytic mechanism for glycosidases is a complex system that is commonly difficult to explain by simple mutagenesis studies [196]. In addition, the contributions of auxiliary amino acid residues is a common feature in a variety of glycosidases, including family 7, 10, 16 and 39 glycosidases, which are the retaining hydrolases [197, 198], and family 28 glycosidases, which is the inverting hydrolases [104, 199]. Therefore, it is of interest to explore different mutagenesis strategies in order to investigate the contributions and impacts of auxiliary amino acids in catalysis, especially H524, which is not conserved in the non-hydrolytic EDEM family members. In addition, R334 should be further investigated as well in its potential contribution to the acid protonation of the glycosidic oxygen.

4.8.2 Crystal structures —The T688A mutant resulted in interesting changes in enzyme kinetics and substrate binding. Without an X-ray structure of the substrate-analog co-complex with this mutant enzyme it is difficult to speculate on the implications of this mutation and its structural effect on catalysis and binding. Therefore, obtaining the crystal structure for this mutant in a co-complex with the thiodisaccharide may provide an explanation for the effects of this mutation on enzyme kinetics and substrate binding.

The E330Q mutant is almost catalytically inactive at pH 7.0 or higher when incubated with substrate at 10ºC or less. Therefore, it may be possible that this mutant could provide a structure for the co-complex of the enzyme with the natural substrate rather than the use of the un-clevable thiodisaccharide described in this dissertation.

The F659 residue was shown to have a major role in stabilization of the $^{1}C_{4}$ glycone conformation. The co-complex crystal of F659A with a high concentration of dMNJ could provide structural evidence supporting this conclusion. In addition, wild type enzyme in the absence of Ca^{2+} could be used to form a co-complex with dMNJ or the high mannose substrate to further address the mechanism of substrate binding.

4.8.3 Binding analysis using SPR —A combination of SPR and mutagenesis is a powerful tool for investigating the enzyme substrate interactions as well as the structural analysis of protein-glycan complexes. It is important to mutate the enzyme so that the catalytic rate is reduced to less than 0.02 s^{-1} as this is the detection limit for the off-rate by SPR, however this mutation must not result in a reduction in binding affinity. This dissertation showed that the general acid is an appropriate residue to be mutated for class 1 α-mannosidases. In addition to the preparation of a library of mutant enzymes, the availability of a high quality oligosaccharide library for binding analyses is also essential for mapping the glycan-protein interaction of class 1 α-mannosidases, especially the Golgi α-mannosidase subfamily. This dissertation provided the strategy for generating both enzyme mutants and glycan structures and isomers that will allow future studies on members of this enzyme family.

4.8.4 Isotope effect —Catalysis by family 47 glycosyl hydrolases involve several water residues which form a H-bonding matrix with the Ca^{+2} ion, the glycone, and aglycone residues as well as serving as the nucleophile. Analysis of the isotope effect by deuterated water revealed that a large number of protons contributed to catalysis and made the proton inventory study difficult to interpret. Therefore, an examination of secondary or tertiary proton effects could be an alternative approach to answer the questions of the number of protons and their specific contributions during catalysis for these enzymes.

REFFERENCES

1. Coutinho, P.M. and B. Henrissat, *Carbohydrate-active enzymes: an integrated database approach*, in *Recent Advances in Carbohydrate Bioengineering*, H.J. Gilbert, et al., Editors. 1999, The Royal Society of Chemistry: Cambridge. p. 3-12.

2. Moremen, K., *alpha-Mannosidases in Asparagine-linked Oligosaccharide Processing and Catabolism: Biology of Saccharides Part II*, in *A Comprehensive Handbook: Carbohydrates in Chemistry and Biology*, B. Ernst, G. Hart, and P. Sinay, Editors. 2000, John Wiley and Sons, Inc.: New York. p. 81-117.

3. Herscovics, A., *Processing glycosidases of Saccharomyces cerevisiae.* Biochim Biophys Acta, 1999. **1426**(2): p. 275-85.

4. Herscovics, A., *Importance of glycosidases in mammalian glycoprotein biosynthesis.* Biochim Biophys Acta, 1999. **1473**(1): p. 96-107.

5. Wu, Y., M.T. Swulius, K.W. Moremen, and R.N. Sifers, *Elucidation of the molecular logic by which misfolded alpha 1-antitrypsin is preferentially selected for degradation.* Proc Natl Acad Sci U S A, 2003. **100**(14): p. 8229-34.

6. Cabral, C.M., Y. Liu, and R.N. Sifers, *Dissecting glycoprotein quality control in the secretory pathway.* Trends Biochem Sci, 2001. **26**(10): p. 619-24.

7. Perlmutter, D.H., *Alpha-1-antitrypsin deficiency: biochemistry and clinical manifestations.* Ann Med, 1996. **28**(5): p. 385-94.

8. Teckman, J.H. and D.H. Perlmutter, *Retention of mutant alpha(1)-antitrypsin Z in endoplasmic reticulum is associated with an autophagic response.* American Journal of Physiology - Gastrointestinal and Liver Physiology, 2000. **279**(5): p. G961-74.

9. Kopito, R.R., *Biosynthesis and degradation of CFTR.* Physiol Rev, 1999. **79**(1 Suppl): p. S167-73.

10. Gonzalez, D.S., K. Karaveg, A.S. Vandersall-Nairn, A. Lal, and K.W. Moremen, *Identification, expression, and characterization of a cDNA encoding human endoplasmic reticulum mannosidase I, the enzyme that catalyzes the first mannose trimming step in mammalian Asn-linked oligosaccharide biosynthesis.* J Biol Chem, 1999. **274**(30): p. 21375-86.

11. Lal, A., J.S. Schutzbach, W.T. Forsee, P.J. Neame, and K.W. Moremen, *Isolation and expression of murine and rabbit cDNAs encoding an alpha 1,2-mannosidase involved in the processing of asparagine-linked oligosaccharides.* J Biol Chem, 1994. **269**(13): p. 9872-81.

12. Mast, S., *Discovery of the EDEM subfamily in the family 47 glycosyl hydrolases*, in *Biochemistry and Molecular Biology*. 2004, University of Georgia: Athens.

13. Mast, S.W., K. Diekman, K. Karaveg, A. Davis, R.N. Sifers, and K.W. Moremen, *Human EDEM2, a novel homolog of family 47 glycosidases, is involved in ER-associated degradation of glycoproteins.* Glycobiology, 2004.

14. Vallee, F., K. Karaveg, A. Herscovics, K.W. Moremen, and P.L. Howell, *Structural basis for catalysis and inhibition of N-glycan processing class I alpha 1,2-mannosidases.* J Biol Chem, 2000. **275**(52): p. 41287-98.

15. Tempel, W., K. Karaveg, Z.J. Liu, J. Rose, B.C. Wang, and K.W. Moremen, *Structure of mouse Golgi alpha-mannosidase IA reveals the molecular basis for substrate specificity among class 1 (family 47 glycosylhydrolase) alpha1,2-mannosidases.* J Biol Chem, 2004. **279**(28): p. 29774-86.

16. Apweiler, R., H. Hermjakob, and N. Sharon, *On the frequency of protein glycosylation, as deduced from analysis of the SWISS-PROT database.* Biochim Biophys Acta, 1999. **1473**(1): p. 4-8.

17. Hirschberg, C.B. and M.D. Snider, *Topography of glycosylation in the rough endoplasmic reticulum and Golgi apparatus.* Annu Rev Biochem, 1987. **56**: p. 63-87.

18. Burda, P. and M. Aebi, *The dolichol pathway of N-linked glycosylation.* Biochim Biophys Acta, 1999. **1426**(2): p. 239-57.

19. Knauer, R. and L. Lehle, *The oligosaccharyltransferase complex from yeast.* Biochim Biophys Acta, 1999. **1426**(2): p. 259-73.

20. Dempski, R.E., Jr. and B. Imperiali, *Oligosaccharyl transferase: gatekeeper to the secretory pathway.* Curr Opin Chem Biol, 2002. **6**(6): p. 844-50.

21. Helenius, A. and M. Aebi, *Roles of N-linked glycans in the endoplasmic reticulum.* Annu Rev Biochem, 2004. **73**: p. 1019-1049.

22. Weng, S. and R.G. Spiro, *Evaluation of the early processing routes of N-linked oligosaccharides of glycoproteins through the characterization of Man8GlcNAc2 isomers: evidence that endomannosidase functions in vivo in the absence of a glucosidase blockade.* Glycobiology, 1996. **6**(8): p. 861-8.

23. Moremen, K.W., R.B. Trimble, and A. Herscovics, *Glycosidases of the asparagine-linked oligosaccharide processing pathway.* Glycobiology, 1994. **4**(2): p. 113-25.

24. Dairaku, K. and R.G. Spiro, *Phylogenetic survey of endomannosidase indicates late evolutionary appearance of this N-linked oligosaccharide processing enzyme.* Glycobiology, 1997. **7**(4): p. 579-86.

25. Herscovics, A. and P. Orlean, *Glycoprotein biosynthesis in yeast.* Faseb J, 1993. **7**(6): p. 540-50.

26. Weng, S. and R.G. Spiro, *Endoplasmic reticulum kifunensine-resistant alpha-mannosidase is enzymatically and immunologically related to the cytosolic alpha-mannosidase.* Arch Biochem Biophys, 1996. **325**(1): p. 113-23.

27. Molinari, M., V. Calanca, C. Galli, P. Lucca, and P. Paganetti, *Role of EDEM in the release of misfolded glycoproteins from the calnexin cycle.* Science, 2003. **299**(5611): p. 1397-400.

28. Hosokawa, N., I. Wada, K. Hasegawa, T. Yorihuzi, L.O. Tremblay, A. Herscovics, and K. Nagata, *A novel ER alpha-mannosidase-like protein accelerates ER-associated degradation.* EMBO Rep, 2001. **2**(5): p. 415-22.

29. Grinna, L.S. and P.W. Robbins, *Substrate specificities of rat liver microsomal glucosidases which process glycoproteins.* J Biol Chem, 1980. **255**(6): p. 2255-8.

30. Sousa, M.C., M.A. Ferrero-Garcia, and A.J. Parodi, *Recognition of the oligosaccharide and protein moieties of glycoproteins by the UDP-Glc:glycoprotein glucosyltransferase.* Biochemistry, 1992. **31**(1): p. 97-105.

31. Herscovics, A., P.A. Romero, and L.O. Tremblay, *The specificity of the yeast and human class I ER alpha 1,2-mannosidases involved in ER quality control is not as strict previously reported.* Glycobiology, 2002. **12**(4): p. 14G-15G.

32. Jakob, C.A., E. Chevet, D.Y. Thomas, and J.J. Bergeron, *Lectins of the ER quality control machinery.* Results Probl Cell Differ, 2001. **33**: p. 1-17.

33. Ellgaard, L. and A. Helenius, *ER quality control: towards an understanding at the molecular level.* Curr Opin Cell Biol, 2001. **13**(4): p. 431-7.

34. Trombetta, E.S. and A. Helenius, *Lectins as chaperones in glycoprotein folding.* Curr Opin Struct Biol, 1998. **8**(5): p. 587-92.

35. Chevet, E., C.A. Jakob, D.Y. Thomas, and J.J. Bergeron, *Calnexin family members as modulators of genetic diseases.* Semin Cell Dev Biol, 1999. **10**(5): p. 473-80.

36. Zapun, A., N.J. Darby, D.C. Tessier, M. Michalak, J.J. Bergeron, and D.Y. Thomas, *Enhanced catalysis of ribonuclease B folding by the interaction of calnexin or calreticulin with ERp57.* J Biol Chem, 1998. **273**(11): p. 6009-12.

37. Moussalli, M., S.W. Pipe, H.P. Hauri, W.C. Nichols, D. Ginsburg, and R.J. Kaufman, *Mannose-dependent endoplasmic reticulum (ER)-Golgi intermediate compartment-53-mediated ER to Golgi trafficking of coagulation factors V and VIII.* J Biol Chem, 1999. **274**(46): p. 32539-42.

38. Scales, S.J., R. Pepperkok, and T.E. Kreis, *Visualization of ER-to-Golgi transport in living cells reveals a sequential mode of action for COPII and COPI.* Cell, 1997. **90**(6): p. 1137-48.

39. Presley, J.F., N.B. Cole, T.A. Schroer, K. Hirschberg, K.J. Zaal, and J. Lippincott-Schwartz, *ER-to-Golgi transport visualized in living cells.* Nature, 1997. **389**(6646): p. 81-5.

40. Paulsson, K.M. and P. Wang, *Quality control of MHC class I maturation.* Faseb J, 2004. **18**(1): p. 31-8.

41. Wang, Y. and M.J. Androlewicz, *Oligosaccharide trimming plays a role in the endoplasmic reticulum-associated degradation of tyrosinase.* Biochem Biophys Res Commun, 2000. **271**(1): p. 22-7.

42. McCracken, A.A. and J.L. Brodsky, *Assembly of ER-associated protein degradation in vitro: dependence on cytosol, calnexin, and ATP.* J Cell Biol, 1996. **132**(3): p. 291-8.

43. Liu, Y., P. Choudhury, C.M. Cabral, and R.N. Sifers, *Intracellular disposal of incompletely folded human alpha1-antitrypsin involves release from calnexin and post-translational trimming of asparagine-linked oligosaccharides.* J Biol Chem, 1997. **272**(12): p. 7946-51.

44. Liu, Y., P. Choudhury, C.M. Cabral, and R.N. Sifers, *Oligosaccharide modification in the early secretory pathway directs the selection of a misfolded glycoprotein for degradation by the proteasome.* J Biol Chem, 1999. **274**(9): p. 5861-7.

45. Jakob, C.A., P. Burda, J. Roth, and M. Aebi, *Degradation of misfolded endoplasmic reticulum glycoproteins in Saccharomyces cerevisiae is determined by a specific oligosaccharide structure.* J Cell Biol, 1998. **142**(5): p. 1223-33.

46. Knop, M., N. Hauser, and D.H. Wolf, *N-Glycosylation affects endoplasmic reticulum degradation of a mutated derivative of carboxypeptidase yscY in yeast.* Yeast, 1996. **12**(12): p. 1229-38.

47. Puccia, R., B. Grondin, and A. Herscovics, *Disruption of the processing alpha-mannosidase gene does not prevent outer chain synthesis in Saccharomyces cerevisiae.* Biochem J, 1993. **290 (Pt 1)**: p. 21-6.

48. Wiertz, E.J., D. Tortorella, M. Bogyo, J. Yu, W. Mothes, T.R. Jones, T.A. Rapoport, and H.L. Ploegh, *Sec61-mediated transfer of a membrane protein from the endoplasmic reticulum to the proteasome for destruction.* Nature, 1996. **384**(6608): p. 432-8.

49. McCracken, A.A. and J.L. Brodsky, *Evolving questions and paradigm shifts in endoplasmic-reticulum-associated degradation (ERAD).* Bioessays, 2003. **25**(9): p. 868-77.

50. Molinari, M. and A. Helenius, *Chaperone selection during glycoprotein translocation into the endoplasmic reticulum.* Science, 2000. **288**(5464): p. 331-3.

51. Oda, Y., N. Hosokawa, I. Wada, and K. Nagata, *EDEM as an acceptor of terminally misfolded glycoproteins released from calnexin.* Science, 2003. **299**(5611): p. 1394-7.

52. Pilon, M., R. Schekman, and K. Romisch, *Sec61p mediates export of a misfolded secretory protein from the endoplasmic reticulum to the cytosol for degradation.* Embo J, 1997. **16**(15): p. 4540-8.

53. Bays, N.W. and R.Y. Hampton, *Cdc48-Ufd1-Npl4: stuck in the middle with Ub.* Curr Biol, 2002. **12**(10): p. R366-71.

54. Verma, R., S. Chen, R. Feldman, D. Schieltz, J. Yates, J. Dohmen, and R.J. Deshaies, *Proteasomal proteomics: identification of nucleotide-sensitive proteasome-interacting proteins by mass spectrometric analysis of affinity-purified proteasomes.* Mol Biol Cell, 2000. **11**(10): p. 3425-39.

55. Voges, D., P. Zwickl, and W. Baumeister, *The 26S proteasome: a molecular machine designed for controlled proteolysis.* Annu Rev Biochem, 1999. **68**: p. 1015-68.

56. Hirsch, C., D. Blom, and H.L. Ploegh, *A role for N-glycanase in the cytosolic turnover of glycoproteins.* Embo J, 2003. **22**(5): p. 1036-46.

57. Hirsch, C., S. Misaghi, D. Blom, M.E. Pacold, and H.L. Ploegh, *Yeast N-glycanase distinguishes between native and non-native glycoproteins.* EMBO Rep, 2004. **5**(2): p. 201-6.

58. Yamagishi, M., T. Ishimizu, S. Natsuka, and S. Hase, *Co(II)-regulated substrate specificity of cytosolic alpha-mannosidase.* J Biochem (Tokyo), 2002. **132**(2): p. 253-6.

59. Ma, J., R. Wollmann, and S. Lindquist, *Neurotoxicity and neurodegeneration when PrP accumulates in the cytosol.* Science, 2002. **298**(5599): p. 1781-5.

60. Chapple, J.P., C. Grayson, A.J. Hardcastle, R.S. Saliba, J. van der Spuy, and M.E. Cheetham, *Unfolding retinal dystrophies: a role for molecular chaperones?* Trends Mol Med, 2001. **7**(9): p. 414-21.

61. Brodsky, J.L., *Chaperoning the maturation of the cystic fibrosis transmembrane conductance regulator.* Am J Physiol Lung Cell Mol Physiol, 2001. **281**(1): p. L39-42.

62. Lomas, D.A. and R. Mahadeva, *Alpha1-antitrypsin polymerization and the serpinopathies: pathobiology and prospects for therapy.* J Clin Invest, 2002. **110**(11): p. 1585-90.

63. Wu, Y., I. Whitman, E. Molmenti, K. Moore, P. Hippenmeyer, and D.H. Perlmutter, *A lag in intracellular degradation of mutant alpha 1-antitrypsin correlates with the liver disease phenotype in homozygous PiZZ alpha 1-antitrypsin deficiency.* Proc Natl Acad Sci U S A, 1994. **91**(19): p. 9014-8.

64. Camirand, A., A. Heysen, B. Grondin, and A. Herscovics, *Glycoprotein biosynthesis in Saccharomyces cerevisiae. Isolation and characterization of the gene encoding a specific processing alpha-mannosidase.* J Biol Chem, 1991. **266**(23): p. 15120-7.

65. Grondin, B. and A. Herscovics, *Topology of ER processing alpha-mannosidase of Saccharomyces cerevisiae.* Glycobiology, 1992. **2**(4): p. 369-72.

66. Vallee, F., F. Lipari, P. Yip, B. Sleno, A. Herscovics, and P.L. Howell, *Crystal structure of a class I alpha1,2-mannosidase involved in N-glycan processing and endoplasmic reticulum quality control.* Embo J, 2000. **19**(4): p. 581-8.

67. Tremblay, L.O. and A. Herscovics, *Cloning and expression of a specific human alpha 1,2-mannosidase that trims Man9GlcNAc2 to Man8GlcNAc2 isomer B during N-glycan biosynthesis.* Glycobiology, 1999. **9**(10): p. 1073-8.

68. Van Petegem, F., H. Contreras, R. Contreras, and J. Van Beeumen, *Trichoderma reesei alpha-1,2-mannosidase: structural basis for the cleavage of four consecutive mannose residues.* J Mol Biol, 2001. **312**(1): p. 157-65.

69. Lobsanov, Y.D., F. Vallee, A. Imberty, T. Yoshida, P. Yip, A. Herscovics, and P.L. Howell, *Structure of Penicillium citrinum alpha 1,2-mannosidase reveals the basis for differences in specificity of the endoplasmic reticulum and Golgi class I enzymes.* J Biol Chem, 2002. **277**(7): p. 5620-30.

70. Yoshida, T., Y. Kato, Y. Asada, and T. Nakajima, *Filamentous fungus Aspergillus oryzae has two types of alpha-1,2-mannosidases, one of which is a microsomal enzyme that removes a single mannose residue from Man9GlcNAc2.* Glycoconj J, 2000. **17**(11): p. 745-8.

71. Martinez-Perez, F., A. Becerra, J. Valdes, S. Zinker, and H. Arechiga, *A possible molecular ancestor for mollusk APGWamide, insect adipokinetic hormone, and crustacean red pigment concentrating hormone.* J Mol Evol, 2002. **54**(6): p. 703-14.

72. Lal, A., P. Pang, S. Kalelkar, P.A. Romero, A. Herscovics, and K.W. Moremen, *Substrate specificities of recombinant murine Golgi alpha1, 2-mannosidases IA and IB and comparison with endoplasmic reticulum and Golgi processing alpha1,2-mannosidases.* Glycobiology, 1998. **8**(10): p. 981-95.

73. Herscovics, A., *Structure and function of Class I alpha 1,2-mannosidases involved in glycoprotein synthesis and endoplasmic reticulum quality control.* Biochimie, 2001. **83**(8): p. 757-62.

74. Tremblay, L.O. and A. Herscovics, *Characterization of a cDNA encoding a novel human Golgi alpha 1, 2-mannosidase (IC) involved in N-glycan biosynthesis.* J Biol Chem, 2000. **275**(41): p. 31655-60.

75. Tremblay, L.O., N. Campbell Dyke, and A. Herscovics, *Molecular cloning, chromosomal mapping and tissue-specific expression of a novel human alpha1,2-mannosidase gene involved in N-glycan maturation.* Glycobiology, 1998. **8**(6): p. 585-95.

76. Gonzalez, D.S. and I.K. Jordan, *The alpha-mannosidases: phylogeny and adaptive diversification.* Mol Biol Evol, 2000. **17**(2): p. 292-300.

77. Inoue, T., T. Yoshida, and E. Ichishima, *Molecular cloning and nucleotide sequence of the 1,2-alpha-D-mannosidase gene, msdS, from Aspergillus saitoi and expression of the gene in yeast cells.* Biochim Biophys Acta, 1995. **1253**(2): p. 141-5.

78. Yoshida, T. and E. Ichishima, *Molecular cloning and nucleotide sequence of the genomic DNA for 1,2-alpha-D-mannosidase gene, msdC from Penicillium citrinum.* Biochim Biophys Acta, 1995. **1263**(2): p. 159-62.

79. Maras, M., N. Callewaert, K. Piens, M. Claeyssens, W. Martinet, S. Dewaele, H. Contreras, I. Dewerte, M. Penttila, and R. Contreras, *Molecular cloning and enzymatic characterization of a Trichoderma reesei 1,2-alpha-D-mannosidase.* J Biotechnol, 2000. **77**(2-3): p. 255-63.

80. Yoshida, T., T. Inoue, and E. Ichishima, *1,2-alpha-D-mannosidase from Penicillium citrinum: molecular and enzymic properties of two isoenzymes.* Biochem J, 1993. **290 (Pt 2)**: p. 349-54.

81. Hosokawa, N., L.O. Tremblay, Z. You, A. Herscovics, I. Wada, and K. Nagata, *Enhancement of endoplasmic reticulum (ER) degradation of misfolded Null Hong Kong alpha1-antitrypsin by human ER mannosidase I.* J Biol Chem, 2003. **278**(28): p. 26287-94.

82. Shah, N., D.A. Kuntz, and D.R. Rose, *Comparison of kifunensine and 1-deoxymannojirimycin binding to class I and II alpha-mannosidases demonstrates different saccharide distortions in inverting and retaining catalytic mechanisms.* Biochemistry, 2003. **42**(47): p. 13812-6.

83. Harpaz, N. and H. Schachter, *Control of glycoprotein synthesis. Processing of asparagine-linked oligosaccharides by one or more rat liver Golgi alpha-D-mannosidases dependent on the prior action of UDP-N-acetylglucosamine: alpha-D-mannoside beta 2-N-acetylglucosaminyltransferase I.* J Biol Chem, 1980. **255**(10): p. 4894-902.

84. Misago, M., Y.F. Liao, S. Kudo, S. Eto, M.G. Mattei, K.W. Moremen, and M.N. Fukuda, *Molecular cloning and expression of cDNAs encoding human alpha-mannosidase II and a previously unrecognized alpha-mannosidase IIx isozyme.* Proc Natl Acad Sci U S A, 1995. **92**(25): p. 11766-70.

85. Fukuda, M.N. and T.O. Akama, *The in vivo role of alpha-mannosidase IIx and its role in processing of N-glycans in spermatogenesis.* Cell Mol Life Sci, 2003. **60**(7): p. 1351-5.

86. Daniel, P.F., B. Winchester, and C.D. Warren, *Mammalian alpha-mannosidases--multiple forms but a common purpose?* Glycobiology, 1994. **4**(5): p. 551-66.

87. van den Elsen, J.M., D.A. Kuntz, and D.R. Rose, *Structure of Golgi alpha-mannosidase II: a target for inhibition of growth and metastasis of cancer cells.* Embo J, 2001. **20**(12): p. 3008-17.

88. Heikinheimo, P., R. Helland, H.K. Leiros, I. Leiros, S. Karlsen, G. Evjen, R. Ravelli, G. Schoehn, R. Ruigrok, O.K. Tollersrud, S. McSweeney, and E. Hough, *The structure of bovine lysosomal alpha-mannosidase suggests a novel mechanism for low-pH activation.* J Mol Biol, 2003. **327**(3): p. 631-44.

89. Wolfenden, R. and M.J. Snider, *The depth of chemical time and the power of enzymes as catalysts.* Acc Chem Res, 2001. **34**(12): p. 938-45.

90. Henrissat, B., I. Callebaut, S. Fabrega, P. Lehn, J.P. Mornon, and G. Davies, *Conserved catalytic machinery and the prediction of a common fold for several families of glycosyl hydrolases.* Proc Natl Acad Sci U S A, 1995. **92**(15): p. 7090-4.

91. Davies, G., M.L. Sinnott, and S.G. Withers, *Glyosyl transfer*, in *Comprehensive Biological Catalysis*, M.L. Sinnott, Editor. 1998, Academic Press. p. 119-208.

92. Davies, G. and B. Henrissat, *Structures and mechanisms of glycosyl hydrolases.* Structure, 1995. **3**(9): p. 853-9.

93. Davies, G.J., K.S. Wilson, and B. Henrissat, *Nomenclature for sugar-binding subsites in glycosyl hydrolases.* Biochem J, 1997. **321 (Pt 2)**: p. 557-9.

94. Rye, C.S. and S.G. Withers, *Glycosidase mechanisms.* Curr Opin Chem Biol, 2000. **4**(5): p. 573-80.

95. Davies, G.J., V.M. Ducros, A. Varrot, and D.L. Zechel, *Mapping the conformational itinerary of beta-glycosidases by X-ray crystallography.* Biochem Soc Trans, 2003. **31**(Pt 3): p. 523-7.

96. Zechel, D.L. and S.G. Withers, *Glycosidase mechanisms: anatomy of a finely tuned catalyst.* Acc Chem Res, 2000. **33**(1): p. 11-18.

97. Zechel, D.L. and S.G. Withers, *Dissection of nucleophilic and acid-base catalysis in glycosidases.* Curr Opin Chem Biol, 2001. **5**(6): p. 643-649.

98. Davies, G.J., L. Mackenzie, A. Varrot, M. Dauter, A.M. Brzozowski, M. Schulein, and S.G. Withers, *Snapshots along an enzymatic reaction coordinate: analysis of a retaining beta-glycoside hydrolase.* Biochemistry, 1998. **37**(34): p. 11707-13.

99. Golan, G., D. Shallom, A. Teplitsky, G. Zaide, S. Shulami, T. Baasov, V. Stojanoff, A. Thompson, Y. Shoham, and G. Shoham, *Crystal structures of Geobacillus stearothermophilus alpha-glucuronidase complexed with its substrate and products: mechanistic implications.* J Biol Chem, 2004. **279**(4): p. 3014-24.

100. Guerin, D.M., M.B. Lascombe, M. Costabel, H. Souchon, V. Lamzin, P. Beguin, and P.M. Alzari, *Atomic (0.94 A) resolution structure of an inverting glycosidase in complex with substrate.* J Mol Biol, 2002. **316**(5): p. 1061-9.

101. Guimaraes, B.G., H. Souchon, B.L. Lytle, J.H. David Wu, and P.M. Alzari, *The crystal structure and catalytic mechanism of cellobiohydrolase CelS, the major enzymatic component of the Clostridium thermocellum Cellulosome.* J Mol Biol, 2002. **320**(3): p. 587-96.

102. Miyake, H., G. Kurisu, M. Kusunoki, S. Nishimura, S. Kitamura, and Y. Nitta, *Crystal structure of a catalytic site mutant of beta-amylase from Bacillus cereus var. mycoides cocrystallized with maltopentaose.* Biochemistry, 2003. **42**(19): p. 5574-81.

103. Sidhu, G., S.G. Withers, N.T. Nguyen, L.P. McIntosh, L. Ziser, and G.D. Brayer, *Sugar ring distortion in the glycosyl-enzyme intermediate of a family G/11 xylanase.* Biochemistry, 1999. **38**(17): p. 5346-54.

104. Shimizu, T., T. Nakatsu, K. Miyairi, T. Okuno, and H. Kato, *Active-site architecture of endopolygalacturonase I from Stereum purpureum revealed by crystal structures in native and ligand-bound forms at atomic resolution.* Biochemistry, 2002. **41**(21): p. 6651-9.

105. Sabini, E., G. Sulzenbacher, M. Dauter, Z. Dauter, P.L. Jorgensen, M. Schulein, C. Dupont, G.J. Davies, and K.S. Wilson, *Catalysis and specificity in enzymatic glycoside hydrolysis: a 2,5B conformation for the glycosyl-enzyme intermediate revealed by the structure of the Bacillus agaradhaerens family 11 xylanase.* Chem Biol, 1999. **6**(7): p. 483-92.

106. Varrot, A., J. Macdonald, R.V. Stick, G. Pell, H.J. Gilbert, and G.J. Davies, *Distortion of a cellobio-derived isofagomine highlights the potential conformational itinerary of inverting beta-glucosidases.* Chem Commun (Camb), 2003(8): p. 946-7.

107. Zou, J., G.J. Kleywegt, J. Stahlberg, H. Driguez, W. Nerinckx, M. Claeyssens, A. Koivula, T.T. Teeri, and T.A. Jones, *Crystallographic evidence for substrate ring distortion and protein conformational changes during catalysis in cellobiohydrolase Ce16A from trichoderma reesei.* Structure Fold Des, 1999. **7**(9): p. 1035-45.

108. Herscovics, A., *Glycosidases of the asparagine-linked oligosaccharide processing pathway*, in *Comprehensive Natural Products Chemistry*, B.M. Pinto, Editor. 1999, Elsevier: New York. p. 13-35.

109. Mulakala, C. and P.J. Reilly, *Understanding protein structure-function relationships in Family 47 alpha-1,2-mannosidases through computational docking of ligands.* Proteins, 2002. **49**(1): p. 125-34.

110. Romero, P.A., F. Vallee, P.L. Howell, and A. Herscovics, *Mutation of Arg(273) to Leu alters the specificity of the yeast N-glycan processing class I alpha1,2-mannosidase.* J Biol Chem, 2000. **275**(15): p. 11071-4.

111. Stoddard, J.F., *Sterochemistry of carbohydrates*. 1971, New York, N.Y.: Wyley-interscience. 47-122.

112. Laemmli, U.K., *Cleavage of structural proteins during the assembly of the head of bacteriophage T4.* Nature, 1970. **227**(259): p. 680-5.

113. Liao, Y.F., A. Lal, and K.W. Moremen, *Cloning, expression, purification, and characterization of the human broad specificity lysosomal acid alpha-mannosidase.* J Biol Chem, 1996. **271**(45): p. 28348-58.

114. Vuillard, L., T. Rabilloud, R. Leberman, C. Berthet-Colominas, and S. Cusack, *A new additive for protein crystallization.* FEBS Lett, 1994. **353**(3): p. 294-6.

115. Blisnick, T., M.E. Morales-Betoulle, L. Vuillard, T. Rabilloud, and C. Braun Breton, *Non-detergent sulphobetaines enhance the recovery of membrane and/or cytoskeleton-associated proteins and active proteases from erythrocytes infected by Plasmodium falciparum.* Eur J Biochem, 1998. **252**(3): p. 537-41.

116. Scaman, C.H., F. Lipari, and A. Herscovics, *A spectrophotometric assay for alpha-mannosidase activity.* Glycobiology, 1996. **6**(3): p. 265-70.

117. Tomiya, N., Y.C. Lee, T. Yoshida, Y. Wada, J. Awaya, M. Kurono, and N. Takahashi, *Calculated two-dimensional sugar map of pyridylaminated oligosaccharides: elucidation of the jack bean alpha-mannosidase digestion pathway of Man9GlcNAc2.* Anal Biochem, 1991. **193**(1): p. 90-100.

118. Saha, S.K. and C.F. Brewer, *Determination of the concentrations of oligosaccharides, complex type carbohydrates, and glycoproteins using the phenol-sulfuric acid method.* Carbohydr Res, 1994. **254**: p. 157-67.

119. Cleland, W.W., *Statistical analysis of enzyme kinetic data.* Methods Enzymol, 1979. **63**: p. 103-38.

120. Lonhienne, T., E. Baise, G. Feller, V. Bouriotis, and C. Gerday, *Enzyme activity determination on macromolecular substrates by isothermal titration calorimetry: application to mesophilic and psychrophilic chitinases.* Biochim Biophys Acta, 2001. **1545**(1-2): p. 349-56.

121. Lonhienne, T., C. Gerday, and G. Feller, *Psychrophilic enzymes: revisiting the thermodynamic parameters of activation may explain local flexibility.* Biochim Biophys Acta, 2000. **1543**(1): p. 1-10.

122. Schowen, K.B. and R.L. Schowen, *Solvent isotope effects of enzyme systems.* Methods Enzymol, 1982. **87**: p. 551-606.

123. Venkatasubban, K.S. and R.L. Schowen, *The proton inventory technique.* CRC Crit Rev Biochem, 1984. **17**(1): p. 1-44.

124. Schowen, K.B., H.H. Limbach, G.S. Denisov, and R.L. Schowen, *Hydrogen bonds and proton transfer in general-catalytic transition-state stabilization in enzyme catalysis.* Biochim Biophys Acta, 2000. **1458**(1): p. 43-62.

125. Bers, D.M., C.W. Patton, and R. Nuccitelli, *A practical guide to the preparation of Ca2+ buffers.* Methods Cell Biol, 1994. **40**: p. 3-29.

126. Potter, J.D., P. Strang-Brown, P.L. Walker, and S. Iida, *Ca2+ binding to calmodulin.* Methods Enzymol, 1983. **102**: p. 135-43.

127. Lis, H., N. Sharon, and E. Katchalski, *Soybean hemagglutinin, a plant glycoprotein. I. Isolation of a glycopeptide.* J Biol Chem, 1966. **241**(3): p. 684-9.

128. Lis, H. and N. Sharon, *Soybean agglutinin--a plant glycoprotein. Structure of the carboxydrate unit.* J Biol Chem, 1978. **253**(10): p. 3468-76.

129. Evers, D.L., R.L. Hung, V.H. Thomas, and K.G. Rice, *Preparative purification of a high-mannose type N-glycan from soy bean agglutinin by hydrazinolysis and tyrosinamide derivatization.* Anal Biochem, 1998. **265**(2): p. 313-6.

130. Rice, K.G., N.B. Rao, and Y.C. Lee, *Large-scale preparation and characterization of N-linked glycopeptides from bovine fetuin.* Anal Biochem, 1990. **184**(2): p. 249-58.

131. Deras, I.L., M. Sano, I. Kato, and Y.C. Lee, *Assay of glycoamidases and endo-beta-N-acetylglucosaminidases by lectin capture and dissociation-enhanced lanthanide fluorescence immunoassay.* Anal Biochem, 2000. **278**(2): p. 213-20.

132. Sutton, C.W. and J.A. O'Neill, *Preparation of glycopeptides.* Methods Mol Biol, 1997. **64**: p. 73-9.

133. Deras, I.L., N. Kawasaki, and Y.C. Lee, *Quantitative recovery of Man9GlcNAc2Asn derivatives from concanavalin A.* Carbohydr Res, 1998. **306**(4): p. 469-71.

134. Hase, S., *High-performance liquid chromatography of pyridylaminated saccharides.* Methods Enzymol, 1994. **230**: p. 225-37.

135. Hase, S., *Analysis of sugar chains by pyridylamination.* Methods Mol Biol, 1993. **14**: p. 69-80.

136. Tokugawa, K., S. Oguri, and M. Takeuchi, *Large scale preparation of PA-oligosaccharides from glycoproteins using an improved extraction method.* Glycoconj J, 1996. **13**(1): p. 53-6.

137. Myszka, D.G., *Kinetic, equilibrium, and thermodynamic analysis of macromolecular interactions with BIACORE.* Methods Enzymol, 2000. **323**: p. 325-40.

138. Myszka, D.G., *Improving biosensor analysis.* J Mol Recognit, 1999. **12**(5): p. 279-84.

139. AB, B., *Biaevaluation 3.1 manual*.

140. Day, Y.S., C.L. Baird, R.L. Rich, and D.G. Myszka, *Direct comparison of binding equilibrium, thermodynamic, and rate constants determined by surface- and solution-based biophysical methods.* Protein Sci, 2002. **11**(5): p. 1017-25.

141. Pierce, M.M., C.S. Raman, and B.T. Nall, *Isothermal titration calorimetry of protein-protein interactions.* Methods, 1999. **19**(2): p. 213-21.

142. Wiseman, T., S. Williston, J.F. Brandts, and L.N. Lin, *Rapid measurement of binding constants and heats of binding using a new titration calorimeter.* Anal Biochem, 1989. **179**(1): p. 131-7.

143. Ku, H., *Notes on the Use of Propagation of Error Formulas.* J Research of National Bureau of Standards-C. Engineering and Instrumentation, 1966. **70C**(4): p. 263-273.

144. Jancarik, J. and S.H. Kim, *Sparse matrix sampling: a screening method for crystallization of proteins.* J. Appl. Cryst., 1991. **24**(4): p. 409-11.

145. D'Arcy, A., C. Elmore, M. Stihle, and J.E. Johnston, *A novel approach to crystallizing proteins under oil.* J. Cryst. Growth,, 1996. **168**: p. 175-180.

146. Chayen, N.E., P.D. Shaw Stewart, D.L. Maeder, and D.M. Blow, *An automated system for micro-batch protein crystallization and screening.* J. Appl. Cryst., 1990. **23**(4): p. 297-302.

147. Johnston, B.D. and B.M. Pinto, *Synthesis of heteroanalogues of disaccharides as potential inhibitors of the processing mannosidase Class I enzymes.* Carbohydrate Research, 1998. **310**(1-2): p. 17-25.

148. Hope, H., *Cryocrystallography of biological macromolecules: a generally applicable method.* Acta Cryst, 1988. **B44**: p. 22-6.

149. Teng, T.-Y., *Mounting of crystals for macromolecular crystallography in a free-standing thin film.* J. Appl. Cryst., 1990. **23**: p. 387-391.

150. Otwinowski, Z. and W. Minor, *Processing of x-ray diffraction data collected in oscillation mode.* Methods Enzymol, 1997. **276**: p. 307-326.

151. Kissinger, C.R., D.K. Gehlhaar, and D.B. Fogel, *Rapid automated molecular replacement by evolutionary search.* Acta Crystallogr D Biol Crystallogr, 1999. **55**(Pt 2): p. 484-91.

152. McRee, D.E., *XtalView/Xfit--A versatile program for manipulating atomic coordinates and electron density.* J Struct Biol, 1999. **125**(2-3): p. 156-165.

153. Potterton, E., P. Briggs, M. Turkenburg, and E. Dodson, *A graphical user interface to the CCP4 program suite.* Acta Crystallogr D Biol Crystallogr, 2003. **59**(Pt 7): p. 1131-7.

154. Murshudov, G.N., *Refinement of macromolecular structures by the maximum-likelihood method.* Acta Crystallogr D Biol Crystallogr, 1997. **53**(Pt 3): p. 240-55.

155. Winn, M.D., *An overview of the CCP4 project in protein crystallography: an example of a collaborative project.* J Synchrotron Radiat, 2003. **10**(Pt 1): p. 23-5.

156. Davis, I.W., L.W. Murray, J.S. Richardson, and D.C. Richardson, *MOLPROBITY: structure validation and all-atom contact analysis for nucleic acids and their complexes.* Nucleic Acids Res, 2004. **32**(Web Server issue): p. W615-9.

157. Sanchez-Lopez, R., R. Nicholson, M.C. Gesnel, L.M. Matrisian, and R. Breathnach, *Structure-function relationships in the collagenase family member transin.* J Biol Chem, 1988. **263**(24): p. 11892-9.

158. Herscovics, A., J. Schneikert, A. Athanassiadis, and K.W. Moremen, *Isolation of a mouse Golgi mannosidase cDNA, a member of a gene family conserved from yeast to mammals.* J Biol Chem, 1994. **269**(13): p. 9864-71.

159. Schneikert, J. and A. Herscovics, *Two naturally occurring mouse alpha-1,2-mannosidase IB cDNA clones differ in three point mutations. Mutation of Phe592 to Ser592 is sufficient to abolish enzyme activity.* J Biol Chem, 1995. **270**(30): p. 17736-40.

160. Schneikert, J. and A. Herscovics, *Characterization of a novel mouse recombinant processing alpha-mannosidase.* Glycobiology, 1994. **4**(4): p. 445-50.

161. Lowe, J.B., J.F. Kukowska-Latallo, R.P. Nair, R.D. Larsen, R.M. Marks, B.A. Macher, R.J. Kelly, and L.K. Ernst, *Molecular cloning of a human fucosyltransferase gene that determines expression of the Lewis x and VIM-2 epitopes but not ELAM-1-dependent cell adhesion.* J Biol Chem, 1991. **266**(26): p. 17467-77.

162. Larsen, R.D., V.P. Rajan, M.M. Ruff, J. Kukowska-Latallo, R.D. Cummings, and J.B. Lowe, *Isolation of a cDNA encoding a murine UDPgalactose:beta-D-galactosyl- 1,4-N-acetyl-D-glucosaminide alpha-1,3-galactosyltransferase: expression cloning by gene transfer.* Proc Natl Acad Sci U S A, 1989. **86**(21): p. 8227-31.

163. Larsen, R.D., L.K. Ernst, R.P. Nair, and J.B. Lowe, *Molecular cloning, sequence, and expression of a human GDP-L-fucose:beta-D-galactoside 2-alpha-L-fucosyltransferase cDNA that can form the H blood group antigen.* Proc Natl Acad Sci U S A, 1990. **87**(17): p. 6674-8.

164. Kukowska-Latallo, J.F., R.D. Larsen, R.P. Nair, and J.B. Lowe, *A cloned human cDNA determines expression of a mouse stage-specific embryonic antigen and the Lewis blood group alpha(1,3/1,4)fucosyltransferase.* Genes Dev, 1990. **4**(8): p. 1288-303.

165. Rajan, V.P., R.D. Larsen, S. Ajmera, L.K. Ernst, and J.B. Lowe, *A cloned human DNA restriction fragment determines expression of a GDP-L-fucose: beta-D-galactoside 2-alpha-L-fucosyltransferase in transfected cells. Evidence for isolation and transfer of the human H blood group locus.* J Biol Chem, 1989. **264**(19): p. 11158-67.

166. Kuzmic, P., S. Sideris, L.M. Cregar, K.C. Elrod, K.D. Rice, and J.W. Janc, *High-throughput screening of enzyme inhibitors: automatic determination of tight-binding inhibition constants.* Anal Biochem, 2000. **281**(1): p. 62-7.

167. Ziegler, F.D. and R.B. Trimble, *Glycoprotein biosynthesis in yeast: purification and characterization of the endoplasmic reticulum Man9 processing alpha-mannosidase.* Glycobiology, 1991. **1**(6): p. 605-14.

168. Schutzbach, J.S. and W.T. Forsee, *Calcium ion activation of rabbit liver alpha 1,2-mannosidase.* J Biol Chem, 1990. **265**(5): p. 2546-9.

169. Matthews, B.W., *Solvent content of protein crystals.* J. Mol. Biol., 1968. **33**(2): p. 491-7.

170. Pflugrath, J.W., *The finer things in X-ray diffraction data collection.* Acta Crystallogr D Biol Crystallogr, 1999. **55 (Pt 10)**: p. 1718-25.

171. Ziegler, F.D., T.R. Gemmill, and R.B. Trimble, *Glycoprotein synthesis in yeast. Early events in N-linked oligosaccharide processing in Schizosaccharomyces pombe.* J Biol Chem, 1994. **269**(17): p. 12527-35.

172. Lipari, F., B.J. Gour-Salin, and A. Herscovics, *The Saccharomyces cerevisiae processing alpha 1,2-mannosidase is an inverting glycosidase.* Biochem Biophys Res Commun, 1995. **209**(1): p. 322-6.

173. Howard, S., C. Braun, J. McCarter, K.W. Moremen, Y.F. Liao, and S.G. Withers, *Human lysosomal and jack bean alpha-mannosidases are retaining glycosidases.* Biochem Biophys Res Commun, 1997. **238**(3): p. 896-8.

174. Henrissat, B., *Glycosidase families.* Biochem Soc Trans, 1998. **26**(2): p. 153-6.

175. Henrissat, B. and A. Bairoch, *Updating the sequence-based classification of glycosyl hydrolases.* Biochem J, 1996. **316 (Pt 2)**: p. 695-6.

176. Henrissat, B. and G. Davies, *Structural and sequence-based classification of glycoside hydrolases.* Curr Opin Struct Biol, 1997. **7**(5): p. 637-44.

177. Bischoff, J., K. Moremen, and H.F. Lodish, *Isolation, characterization, and expression of cDNA encoding a rat liver endoplasmic reticulum alpha-mannosidase.* J. Biol. Chem., 1990. **265**(28): p. 17110-7.

178. Godelaine, D., M.J. Spiro, and R.G. Spiro, *Processing of the carbohydrate units of thyroglobulin.* J Biol Chem, 1981. **256**(19): p. 10161-8.

179. Kornfeld, R. and S. Kornfeld, *Assembly of asparagine-linked oligosaccharides.* Annu Rev Biochem, 1985. **54**: p. 631-64.

180. Jelinek-Kelly, S., T. Akiyama, B. Saunier, J.S. Tkacz, and A. Herscovics, *Characterization of a specific alpha-mannosidase involved in oligosaccharide processing in Saccharomyces cerevisiae.* J Biol Chem, 1985. **260**(4): p. 2253-7.

181. Weng, S. and R.G. Spiro, *Demonstration that a kifunensine-resistant alpha-mannosidase with a unique processing action on N-linked oligosaccharides occurs in rat liver endoplasmic reticulum and various cultured cells.* J Biol Chem, 1993. **268**(34): p. 25656-63.

182. Bischoff, J., L. Liscum, and R. Kornfeld, *The use of 1-deoxymannojirimycin to evaluate the role of various alpha-mannosidases in oligosaccharide processing in intact cells.* J Biol Chem, 1986. **261**(10): p. 4766-74.

183. Rizzolo, L.J. and R. Kornfeld, *Post-translational protein modification in the endoplasmic reticulum. Demonstration of fatty acylase and deoxymannojirimycin-sensitive alpha-mannosidase activities.* J Biol Chem, 1988. **263**(19): p. 9520-5.

184. Bischoff, J. and R. Kornfeld, *The effect of 1-deoxymannojirimycin on rat liver alpha-mannosidases.* Biochem Biophys Res Commun, 1984. **125**(1): p. 324-31.

185. Bischoff, J. and R. Kornfeld, *Evidence for an alpha-mannosidase in endoplasmic reticulum of rat liver.* J Biol Chem, 1983. **258**(13): p. 7907-10.

186. Lodish, H.F., N. Kong, M. Snider, and G.J. Strous, *Hepatoma secretory proteins migrate from rough endoplasmic reticulum to Golgi at characteristic rates.* Nature, 1983. **304**(5921): p. 80-3.

187. Yang, M., S. Omura, J.S. Bonifacino, and A.M. Weissman, *Novel aspects of degradation of T cell receptor subunits from the endoplasmic reticulum (ER) in T cells: importance of oligosaccharide processing, ubiquitination, and proteasome-dependent removal from ER membranes.* J Exp Med, 1998. **187**(6): p. 835-46.

188. Lipari, F. and A. Herscovics, *Calcium binding to the class I alpha-1,2-mannosidase from Saccharomyces cerevisiae occurs outside the EF hand motif.* Biochemistry, 1999. **38**(3): p. 1111-8.

189. Copeland, R.A., D. Lombardo, j. Giannaras, and c. decicco, *estimating K_I values for tight binding inhibitors from dose-response plots.* Bioorganic and Medicinal Chemistry Letters, 1995. **5**(17): p. 1947-1952.

190. Taylor, R. and O. Kennard, *Hydrogen-bond geometry in organic crystals.* Acc. Chems. Res., 1984. **17**: p. 320-326.

191. Moremen, K.W., *Golgi alpha-mannosidase II deficiency in vertebrate systems: implications for asparagine-linked oligosaccharide processing in mammals.* Biochim Biophys Acta, 2002. **1573**(3): p. 225-35.

192. Zolotnitsky, G., U. Cogan, N. Adir, V. Solomon, G. Shoham, and Y. Shoham, *Mapping glycoside hydrolase substrate subsites by isothermal titration calorimetry.* Proc Natl Acad Sci U S A, 2004. **101**(31): p. 11275-80.

193. Sakka, K., M. Nakanishi, M. Sogabe, T. Arai, H. Ohara, A. Tanaka, T. Kimura, and K. Ohmiya, *Isothermal titration calorimetric studies on the binding of a family 6 carbohydrate-binding module of Clostridium thermocellum xynA with xylooligosaccharides.* Biosci Biotechnol Biochem, 2003. **67**(2): p. 406-9.

194. Dias, F.M., F. Vincent, G. Pell, J.A. Prates, M.S. Centeno, L.E. Tailford, L.M. Ferreira, C.M. Fontes, G.J. Davies, and H.J. Gilbert, *Insights into the molecular determinants of substrate specificity in glycoside hydrolase family 5 revealed by the crystal structure and kinetics of Cellvibrio mixtus mannosidase 5A.* J Biol Chem, 2004. **279**(24): p. 25517-26.

195. Lammerts van Bueren, A. and A.B. Boraston, *Binding sub-site dissection of a carbohydrate-binding module reveals the contribution of entropy to oligosaccharide recognition at "non-primary" binding subsites.* J Mol Biol, 2004. **340**(4): p. 869-79.

196. Armand, S., M.J. Wagemaker, P. Sanchez-Torres, H.C. Kester, Y. van Santen, B.W. Dijkstra, J. Visser, and J.A. Benen, *The active site topology of Aspergillus niger endopolygalacturonase II as studied by site-directed mutagenesis.* J Biol Chem, 2000. **275**(1): p. 691-6.

197. Olivera-Nappa, A., B.A. Andrews, and J.A. Asenjo, *A mixed mechanistic-electrostatic model to explain pH dependence of glycosyl hydrolase enzyme activity.* Biotechnol Bioeng, 2004. **86**(5): p. 573-86.

198. Yang, J.K., H.J. Yoon, H.J. Ahn, B.I. Lee, J.D. Pedelacq, E.C. Liong, J. Berendzen, M. Laivenieks, C. Vieille, G.J. Zeikus, D.J. Vocadlo, S.G. Withers, and S.W. Suh, *Crystal structure of beta-D-xylosidase from Thermoanaerobacterium saccharolyticum, a family 39 glycoside hydrolase.* J Mol Biol, 2004. **335**(1): p. 155-65.

199. van Santen, Y., J.A. Benen, K.H. Schroter, K.H. Kalk, S. Armand, J. Visser, and B.W. Dijkstra, *1.68-A crystal structure of endopolygalacturonase II from Aspergillus niger and identification of active site residues by site-directed mutagenesis.* J Biol Chem, 1999. **274**(43): p. 30474-80.